

4. SITE 648¹

Shipboard Scientific Party^{2, 3}

HOLE 648A

Date occupied: 6 November 1985, 2020 L

Date departed: 11 November 1985, 1200 L

Time on hole: 4 days, 15 hr, 40 min (includes television/sonar survey time)

Position: 22°55.310'N, 44°56.830'W

Water depth (sea level; corrected m, echo-sounding): 3323

¹ Detrick, R. B., Honnorez, J., Bryan, W. B., Juteau, T., et al., 1988. *Proc. ODP, Init. Repts. (Pt. A)*, 106/109: College Station, TX (Ocean Drilling Program).

² Robert S. Detrick (Co-Chief Scientist), Graduate School of Oceanography, University of Rhode Island, Kingston, RI 02881; Jose Honnorez (Co-Chief Scientist), Rosenstiel School of Marine and Atmospheric Sciences, University of Miami, 4600 Rickenbacker Causeway, Miami, FL 33149 (current address: Institut de Géologie, Université Louis Pasteur, 1 Rue Blessig, 67084 Strasbourg, France; Andrew C. Adamson (Staff Scientist), Ocean Drilling Program, Texas A&M University, College Station, TX 77843; Garrett W. Brass, Ocean Drilling Program, National Science Foundation, 1800 G Street NW, Washington, DC 20550; Kathryn M. Gillis, Department of Geology, Dalhousie University, Halifax, Nova Scotia B3H 3J5, Canada (current address: Département de Géologie, Université de Montréal, C.P. 6128, Succursale A, Montréal, Québec H3C 3J7, Canada); Susan E. Humphris, Department of Chemistry, Woods Hole Oceanographic Institution, Woods Hole, MA 02543; Catherine Mevel, Laboratoire de Pétrologie Métamorphique, Université Pierre et Marie Curie, 4 Place Jussieu, 75230 Paris 05, France; Peter S. Meyer, Department of Geology and Geophysics, Woods Hole Oceanographic Institution, Woods Hole, MA 02543; Nikolai Petersen, Institute für Geophysik, Universität München, Theresienstrasse 41, D-8000 München 2, Federal Republic of Germany; Martina Rautenschlein, Max-Planck-Institut für Chemie, Abteilung Geochemie, Postfach 3060, D-6500 Mainz, Federal Republic of Germany; Tsugio Shibata, Faculty of Science, Okayama University, 3-1-1 Tshishimanaka, Okayama 700, Japan; Hubert Staudigel, Geological Research Division, Scripps Institution of Oceanography, University of California, San Diego, La Jolla, CA 92093; Anita L. Wooldridge, Marine Geology and Geophysics, University of Miami, 4600 Rickenbacker Causeway, Miami, FL 33149; Kiyohiko Yamamoto, Faculty of Science, Tohoku University, Sendai, Miyagi Pref, 980, Japan.

³ Wilfred B. Bryan (Co-Chief Scientist), Department of Geology and Geophysics, Woods Hole Oceanographic Institution, Woods Hole, MA 02543; Thierry Juteau (Co-Chief Scientist), Laboratoire de Pétrologie, Université de Bretagne Occidentale, 6 Avenue Le Gorgeu, 29287 Brest, France; Andrew C. Adamson (ODP Staff Scientist), Ocean Drilling Program, Texas A&M University, College Station, TX 77843; Laurie K. Autio, Department of Geology and Geography, Morrill Science Center, University of Massachusetts, Amherst, MA 01003; Keir Becker, Rosenstiel School of Marine and Atmospheric Sciences, University of Miami, 4600 Rickenbacker Causeway, Miami, FL 33149; M. Mansour Bina, Laboratoire de Géomagnétisme, Université Pierre et Marie Curie, 4, Avenue de Neptune, 94107 St. Maur des Fosses, France; Jean-Philippe Eissen, O.R.S.T.O.M., B.P. A5, Noumea, New Caledonia (current address: O.R.S.T.O.M., IFREMER, BP 337, 2273 Brest Cedex, France); Toshitsugu Fujii, Earthquake Research Institute, University of Tokyo, 1-1-1 Yayoi, Bunkyo-ku, Tokyo 113, Japan; Timothy L. Grove, Department of Earth, Atmospheric and Planetary Sciences, Massachusetts Institute of Technology, Cambridge, MA 02139; Yozo Hamano, Earthquake Research Institute, University of Tokyo, 1-1-1 Yayoi, Bunkyo-ku, Tokyo 113, Japan; Rejean Hebert, Département de Géologie, Université Laval, Québec G1K 7P4, Canada; Stephen C. Komor, Bureau of Mines, Avondale Research Center, 4900 LaSalle Road, Avondale, MD 20782 (current address: Department of Geology and Geophysics, University of Wisconsin, Madison, WI 53706); Johannes Kopietz, Bundesanstalt für Geowissenschaften und Rohstoffe, Stilleweg 2, D-3000 Hannover 51, Federal Republic of Germany; Kristian Krammer, Institut für Geophysik, Universität München, Theresienstrasse 41, D-8000 München 2, Federal Republic of Germany; Michel Loubet, Laboratoire de Mineralogie, Université Paul Sabatier, 38 Rue des 36 Ponts, 31400 Toulouse, France; Daniel Moos, Borehole Research Group, Lamont-Doherty Geological Observatory, Columbia University, Palisades, NY 10964; Hugh G. Richards, Department of Geology, The University, Newcastle upon Tyne NE1 7RU, United Kingdom.

Water depth (rig floor; corrected m, echo-sounding): 3334

Bottom felt (m, drill pipe): 3310.5

Distance between rig floor and sea level (m): 11.1

Total depth (rig floor; m): 3315

Penetration (m): 4.5

Number of cores: 1

Total length of cored section (m): 4.5

Total core recovered (m): 0.07

Core recovery (%): 1.6

Sediment: none—bare-rock site

Basement:

Depth sub-bottom (m): 0

Nature: basalt pillows

Age: Quaternary

Velocity range (km/s): not measured

HOLE 648B

Date occupied: 11 November 1985, 1200 L

Date departed: 12 December 1985, 0300 L

Time on hole: 24 days, 21 hr (starting when hard-rock guidebase hit sea-floor)

Position: 22°55.320'N, 44°56.825'W

Water depth (sea level; corrected m, echo-sounding): 3325.9

Water depth (rig floor; corrected m, echo-sounding): 3337.0

Bottom felt (m, drill pipe): 3344.4

Distance between rig floor and sea level (m): 11.1

Total depth (rig floor; m): 3377.8

Penetration (m): 33.3

Number of cores: 6

Total length of cored section (m): 40.8 (includes 26.7 m of cored *in-situ* basalts (new hole (6.6–33.3 mbsf)) and 14.1 m cored basalt rubble filling previously drilled hole)

Total core recovered (m): 6.2

Core recovery (%): 15.2 (calculated from 40.8 m of cored hole)

Sediment: none—bare-rock site

Basement:

Depth sub-bottom (m): 0.0

Nature: basalt pillows

Age: Quaternary

Velocity range (km/s): 5.4–6.1

HOLE 648B

Date reoccupied: 29 April 1986, 0400 L

Date departed: 31 May 1986, 0430 L

Time on hole: 32 days, 30 min

Position: 22°55.320'N, 44°56.825'W

Water depth (sea level; corrected m; echo-sounding): 3325.9

Water depth (rig floor; corrected m; echo-sounding): 3337.0

Bottom felt (m, drill pipe): 3341.0

Distance between rig floor and sea level (m): 11.1

Total depth (rig floor; m): 3391.5

Penetration (m): Leg 109 = 17.2; total, Legs 106 and 109 = 50.5

Number of cores: 14

Total length of cored section (m): 66.2 (includes 17.2 m of cored *in-situ* basalts (new hole (33.3–50.5 mbsf) and 49 m of basalt rubble filling previously drilled hole. Total cement cored, 39.3 m)

Total core recovered (m): basalt, 5.15; cement, 12.45

Core recovery (%): 7.8 (calculated from 66.2 m of cored hole)

Sediment: none—bare-rock site

Basement:

Depth sub-bottom (m): 0

Nature: basalt pillows and flows

Age: Quaternary

Velocity range (km/s): 4.9–5.6

Principal results: *JOIDES Resolution* occupied Site 648 in the rift valley of the Mid-Atlantic Ridge about 70 km south of the Kane Fracture Zone. The site is in a shallow part of the inner rift valley (in a water depth of 3300 m) on the smooth rim of the summit plateau of a small axial volcano (Serocki Volcano). Sea Beam maps, SeaMARC I data, and a shipboard television-sonar survey were used to choose this site as the first for bare-rock drilling in zero-age oceanic crust.

Hole 648A, drilled at 22°55.310'N, 44°56.830'W, in a water depth of 3323 m was a first attempt to drill an unsupported hole in hard rock, using the Navidrill drilling motor. A total penetration of 4.5 m resulted in recovery of three pieces of sparsely plagioclase phryic basalt.

Hole 648B, at 22°55.320'N, 44°56.825'W in 3326 m of water was drilled following the successful deployment of the new hard-rock guidebase. During Leg 106, a total penetration of 33.3 mbsf resulted in the recovery of 6.2 m of sparsely to moderately olivine-plagioclase phryic basalt. During Leg 109, drilling operations extended Hole 648B by 17.2 m to a total depth of 50.5 mbsf and recovered 5.15 m of similar basalt. The total recovery was 15.2% during Leg 106 and 7.8% during Leg 109.

Site 648 provided a unique view of the internal structure of an axial rift valley volcano. The uppermost 30 m consists of pillow lavas, which built the volcanic edifice. The lower lithologic units consist of a vesicular basalt underlain by a massive holocrystalline basalt. These lower units probably represent massive flows that ponded inside Serocki Volcano.

Site 648 basalts are moderately evolved normal mid-ocean ridge basalt, saturated with olivine and plagioclase, which are geochemically similar to basalts from the 22°–25°N region. All basalts recovered at Site 648 are fresh; incipient alteration occurs along fractures. Alteration minerals are smectite and amorphous iron-hydroxyoxide.

BACKGROUND AND OBJECTIVES

The specific location selected for Site 648 depended, as always, on both scientific requirements and logistic considerations. Scientific objectives required that we drill on or extremely near the zero-age volcanic axis, while at the same time deploy the guidebase on a relatively flat, smooth area. The eastern side of the summit plateau of Serocki Volcano satisfied both requirements. Initial interpretation of Sea Beam bathymetry, SeaMARC I side-scan sonar images, and seismic-reflection data had suggested that Serocki Volcano marked an eruptive volcanic vent, which was on the volcanic axis and was also above the major centers of magmatic upwelling in this section of the median valley. Thus, this site held the possibility of drilling into and through a recently active hydrothermal vent system, through dikes or sills marking passages by which the latest extrusive units had been ejected, and perhaps, into the top of the chamber that had been the source of these eruptions.

GEOLOGIC AND TECTONIC SETTING

The following criteria, developed in consultation with ODP engineers, were used to choose a specific site within the MARK area for the first bare-rock hole:

1. The site should be in the Mid-Atlantic Ridge (MAR) rift valley, preferably on as young crust as possible.
2. The site should be an area having a minimum diameter of 7 m with a slope of $<20^\circ$ and a small-scale relief of <1 m.
3. The site should be free of surficial rubble, faults, or other potentially structurally incompetent material.
4. Topographic relief near the site should be as low as possible.

According to the results of the Sea Beam and SeaMARC I surveys, three areas identified by the site-survey team appeared to satisfy these criteria (Detrick et al., 1985). These sites were marked with acoustic navigation beacons during the SeaMARC I leg, and seafloor photographs were obtained in each area. After discussions among the site-survey scientists, ODP engineers, and the Legs 106 and 109 co-chief scientists, beacon site 2, in the rift valley about 70 km south of the Kane Transform, was chosen as the primary drilling target for Leg 106 (Fig. 1).

This site, now known as Site 648, is in the summit plateau of a small axial volcano, which we named Serocki Volcano after the senior ODP engineer in charge of the bare-rock drilling project. Serocki Volcano is one of a string of small, valley-parallel, axial volcanoes, most having collapsed summit craters, identified on the SeaMARC I records (Fig. 2). The volcano is about 800 m in diameter and stands about 50 m above the rift valley floor (Fig. 3). The western side of the volcano has been disrupted by several north-south-trending faults or fissures, which have been partly buried by later flows. Seafloor photographs show the summit plateau to consist predominately of bulbous and tubular pillow lavas with a light to moderate sediment cover.

This site was considered to be an attractive drilling target because it has a relatively simple tectonic setting in the middle of the rift valley, far from the Kane Fracture Zone (KFZ) in an area with easily identifiable, symmetric magnetic anomalies. The summit plateau is also an exceptionally flat area with a relief of only a few meters. Dredge samples from this area show the basalts to be typical mid-ocean ridge basalts (MORB). This site also offered the possibility of submersible sampling of the uppermost 50 m of the section (from which little core is expected), in the walls of the central crater, and along the outer rim of the summit plateau. The main drawback of this site is the extensive faulting and fissuring the area has undergone since the last major eruptive event.

Pre-Drilling Site Survey

Instrumentation

Although excellent site-survey data are available from this area, we recognized that additional, extremely high-resolution surveying would be necessary on Leg 106 to find a location meeting the aforementioned engineering specifications. Two tools were acquired for this purpose. The first is a high-resolution, low-light television camera manufactured by Colmek Systems Engineering. This state-of-the-art silicon intensified tube camera and its associated television telemetry system produces real-time black-and-white video images at extremely low light levels (0.001 candlepower) with a dynamic range of $>5,000,000:1$. The second tool is a color-imaging sonar manufactured by Mesotech Systems Ltd. Operating at 675 kHz, the Mesotech sonar

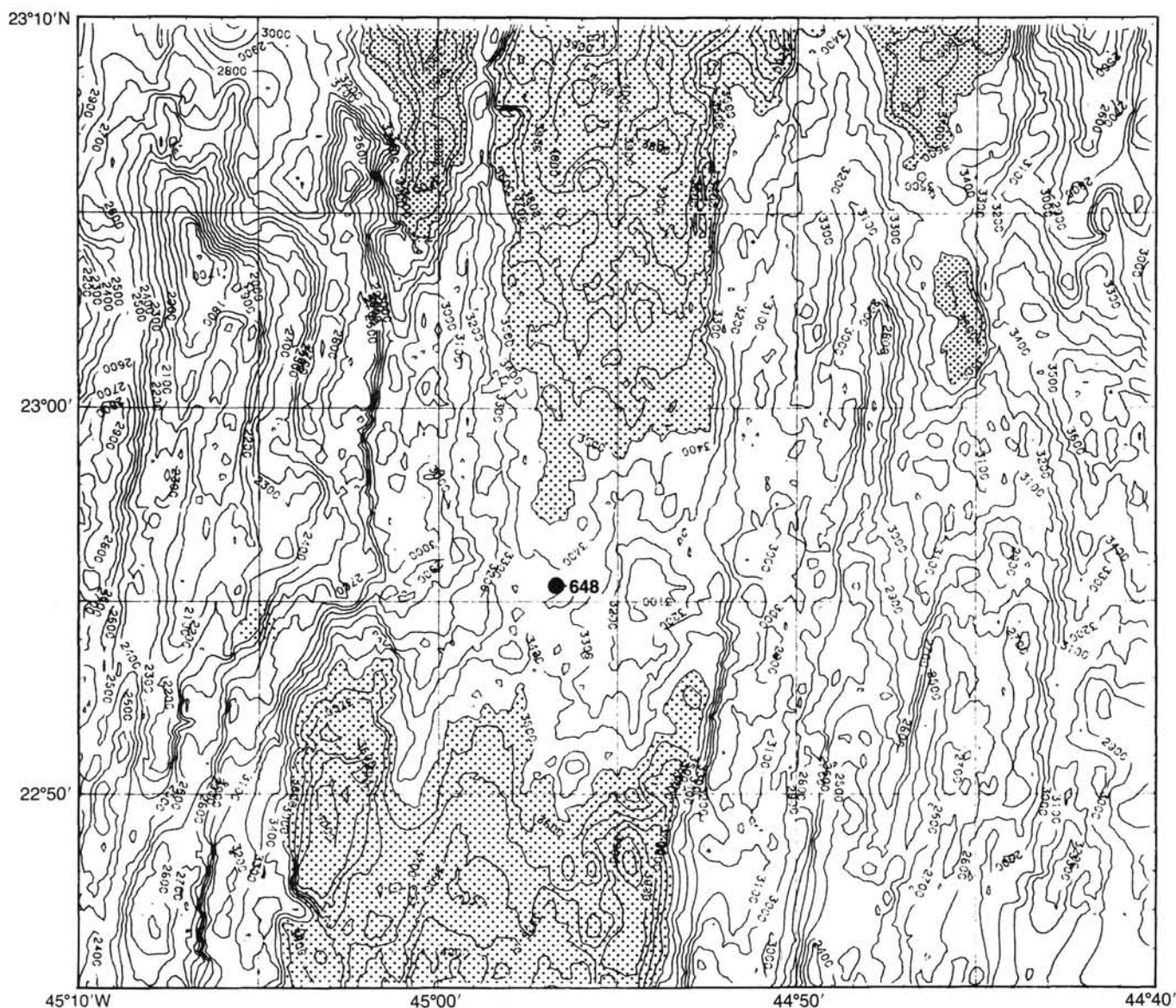
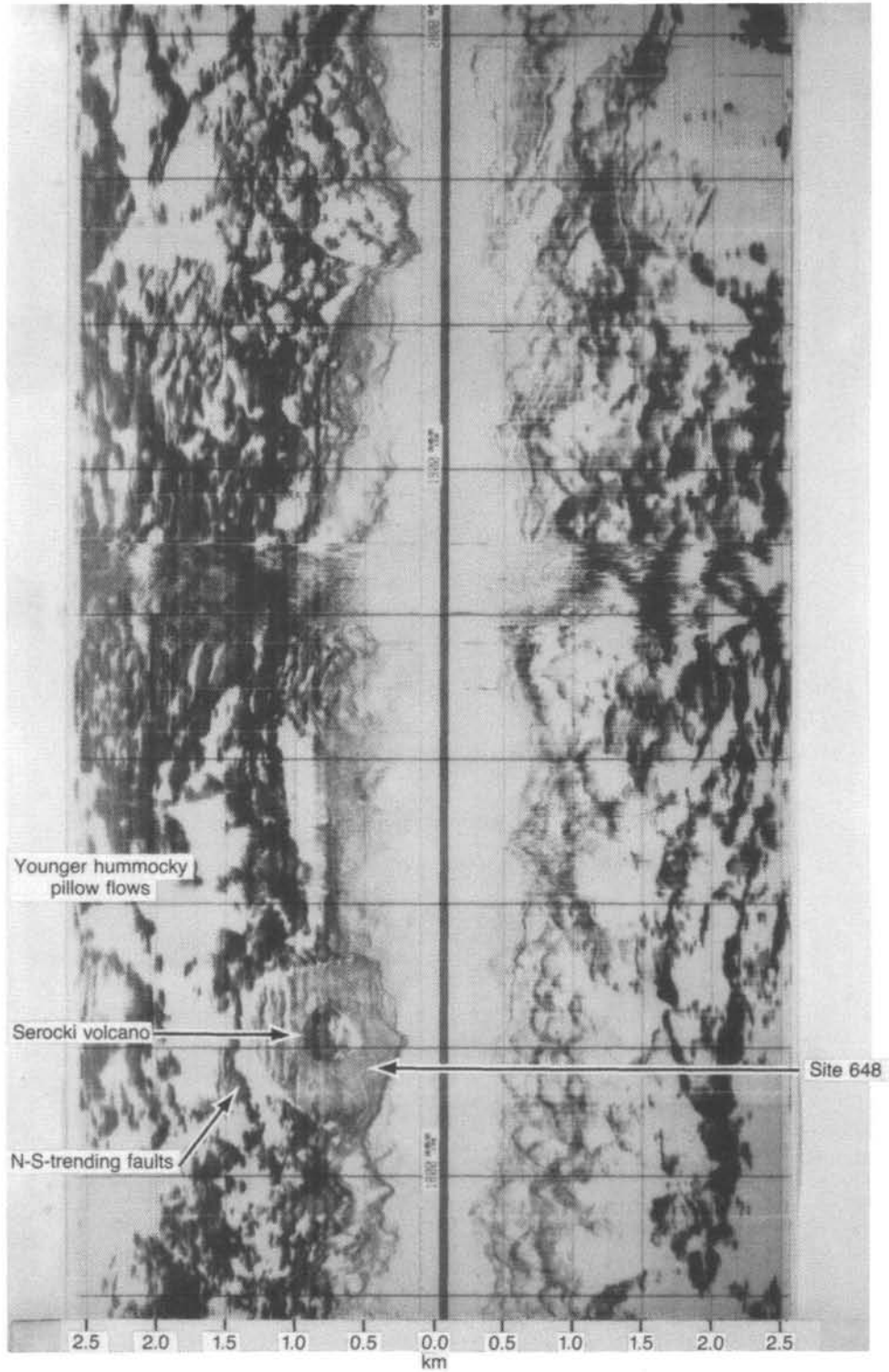


Figure 1. Sea Beam bathymetry map of the Mid-Atlantic Ridge rift valley south of the Kane Fracture Zone, showing location of Site 648 (beacon site 2). Contour interval, 100 m. Depths >3500 m are stippled.

tool provides a high-resolution, color sonar image, which indicates the distance and azimuth of a reflector (e.g., a fault scarp or fissure) from the tool and represents the intensity of the reflection by a range of colors. Objects can be detected at ranges of as much as 100 m, although because of the sonar's 90° beam width, the height of objects is difficult to determine. Both the camera and sonar were mounted on a vibration isolation tool (VIT), which is run up and down the outside of the drill string. Ideally, the camera provides real-time images of areas of the seafloor as wide as 5–10 m, while the Mesotechinsonifies an area as much as 100 m in diameter.

Using these tools and the drill ship's dynamic-positioning system to offset from the navigation beacon, we conducted a 24-hour survey of the eastern summit plateau of Serocki Volcano (Fig. 4). The first attempt to lower the television-sonar system down the outside of the drill string had to be aborted when the telemetry coaxial cable became wrapped around the drill pipe. The television-sonar system was redeployed by suspending it on the coaxial cable without the drill pipe, initially to de-

torque the cable. In this mode, however, the system worked well and throughout the rest of the survey the television-sonar system was used without the drill string. One major advantage of this configuration is that obstacle avoidance is much easier without the drill string, making it feasible to survey much closer to the seafloor and in areas of more rugged relief. We found that the best results were obtained by keeping the television-sonar system 6–8 m above the bottom, moving the ship at speeds of about 2 m/min, and waiting occasionally to let the cable equilibrate. At this height, the video presentation was of very high quality, providing some remarkable images of the seafloor (Fig. 5). The Mesotech sonar effectively maintained the proper height of the television-sonar system above the seafloor, resolving major changes in seafloor roughness (e.g., sedimented vs. un-sedimented) and detecting major tectonic features (e.g., scarps; see Fig. 6). However, the sonar could not resolve smaller scale features such as small fissures, lava-flow fronts, or individual pillows. We suspended a compass below the camera to provide directional information.



SeaMARC 1/85-01: O.D.P./Kane Fracture Zone survey
Hudson 85-010
Processed side-scan/1:50,000 scale

Figure 2. SeaMARC I record across Serocki Volcano, 5-km swath width. Note the evidence of extensive fissuring of the western summit plateau and younger, hummocky pillow flows that have partly buried the flanks of the volcano.

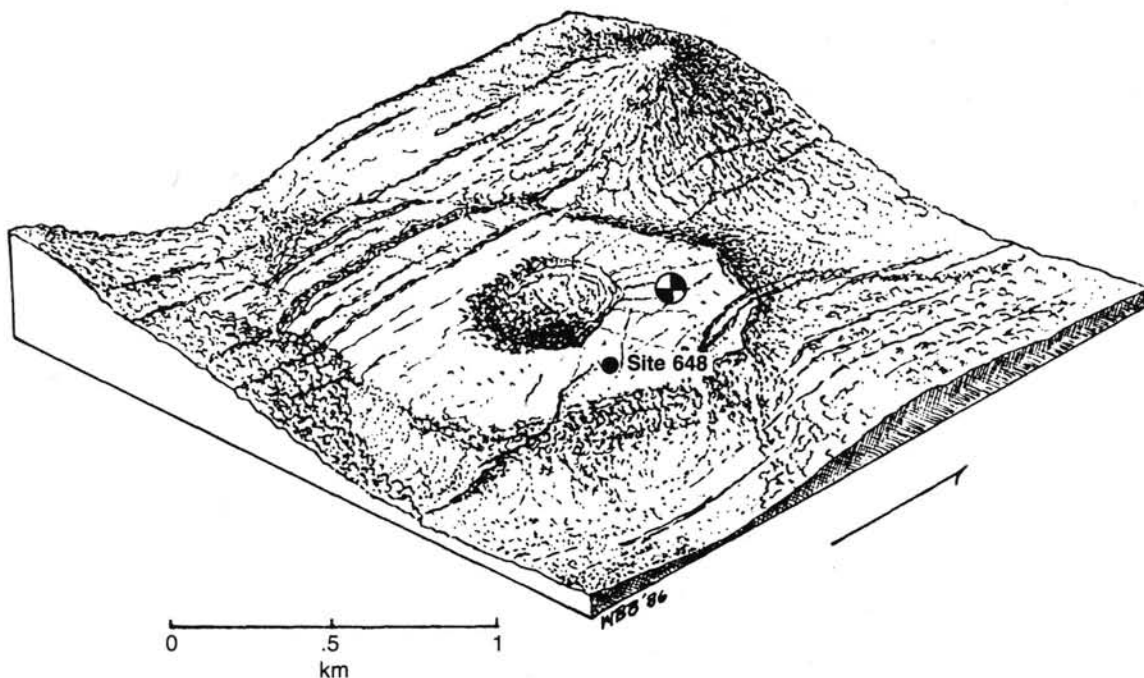


Figure 3. Artist's conception of Serocki volcano based on available Sea Beam and SeaMARC I data. The quartered circle shows the location of beacon 2. Site 648 is on the summit plateau, about halfway between the summit crater and the eastern edge of the summit plateau.

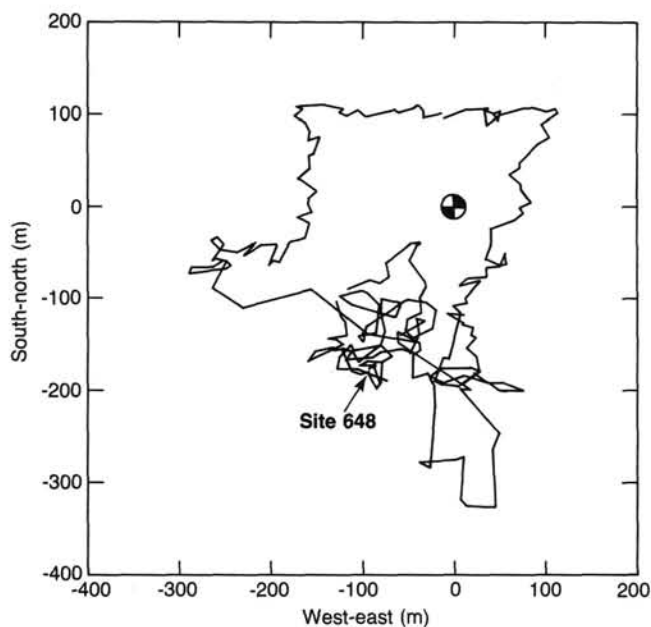


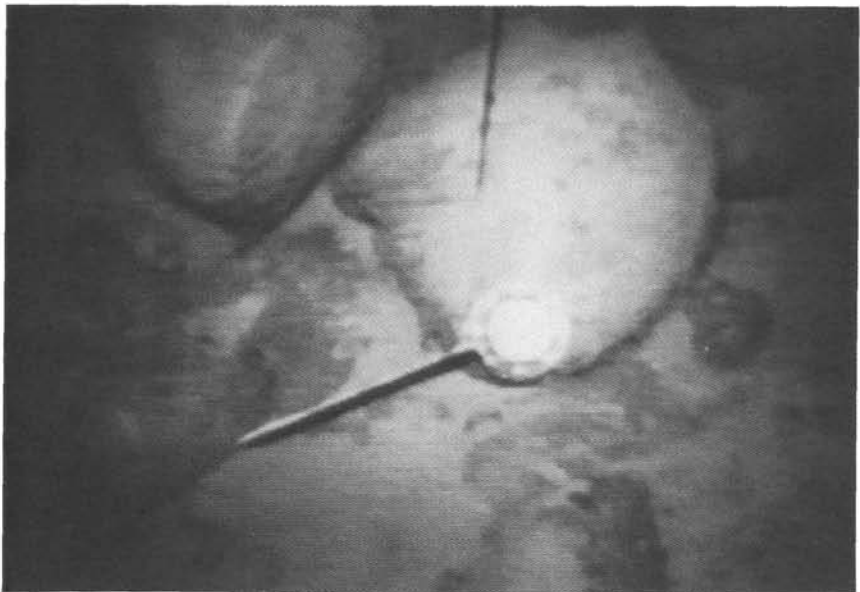
Figure 4. Location of video and sonar coverage obtained during 24-hr survey of the eastern summit plateau of Serocki Volcano before deployment of the hard-rock guidebase. Position of beacon 2 is indicated by quartered circle.

Results

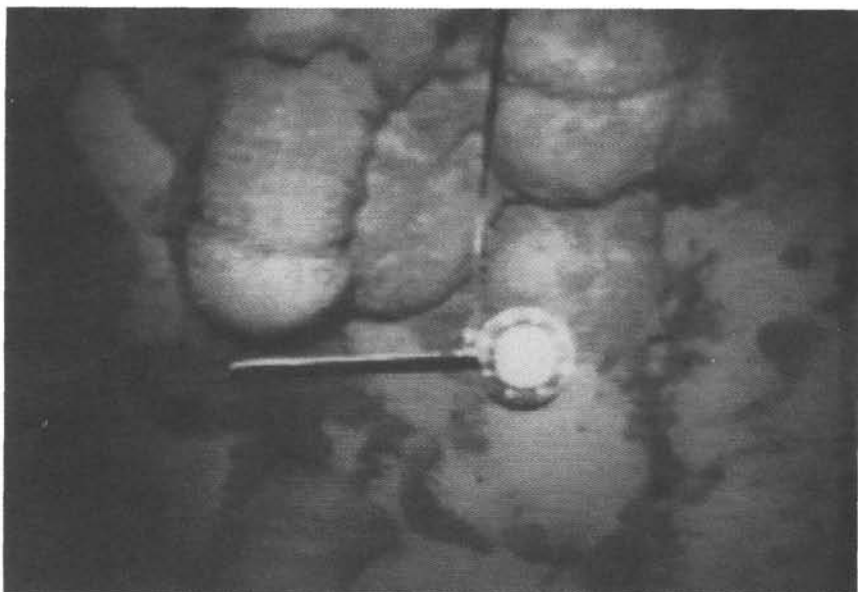
Figure 7 shows a geological map of Serocki Volcano made on the basis of survey results. The summit plateau is extremely flat (<4 m of relief) and consists almost entirely of bulbous and

elongate pillow lavas as high as 1–2 m with a light to moderate sediment cover (Figs. 5A and 5B). In a few places, the pillows are almost completely buried by sediment (Fig. 5C). Sheet flows were found in only one location near the northeastern crater rim (Fig. 5D). Significant amounts of surficial rubble are present near the rim of the central crater, within the crater itself, and near the base of the eastern plateau scarp. The walls of the crater and the eastern edge of the summit plateau are precipitous (Fig. 5E). Post-eruptive north-south fissuring is common throughout the eastern summit plateau, although most of the fissures are relatively minor (Fig. 5F). The amount of fissuring was surprising given the smooth character of the eastern summit plateau on the SeaMARC I records, and presented a problem in terms of choosing a site for deployment of the hard-rock guidebase (HRGB).

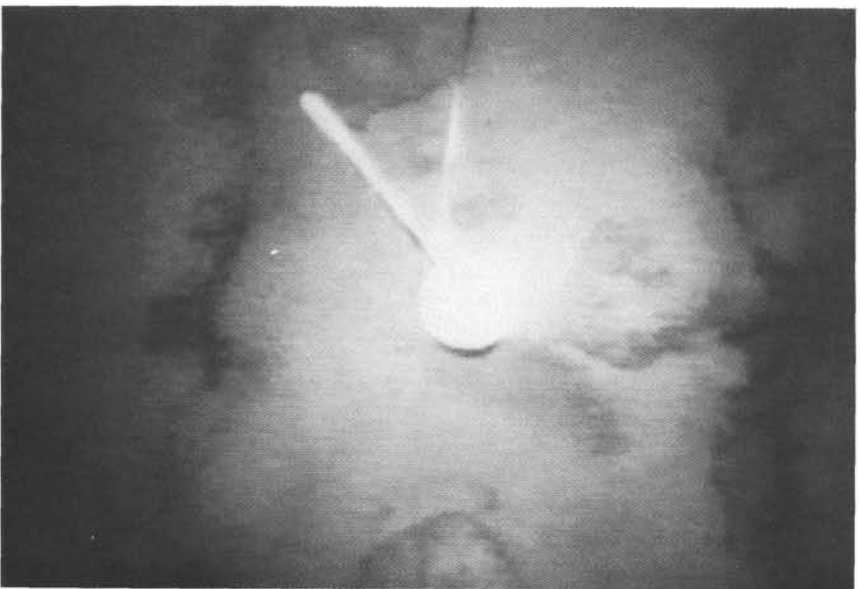
The observations made during this survey are generally consistent with the interpretation of the aforementioned Sea Beam and SeaMARC I records. Serocki Volcano is the product of an earlier, but very recent, eruption and has been disrupted by an ongoing extensional phase. A younger flow is observed burying older pillow lavas east of the summit plateau, which is consistent with the SeaMARC I evidence of some post-tectonic volcanism in this area (Fig. 5G). The age of Serocki Volcano is difficult to estimate precisely. The volcano is in the middle of the rift valley within the central magnetic anomaly, so an age of >700,000 yr is unlikely. As much as 1 m of sediment has buried pillow lavas on some parts of the summit plateau. If this sediment were entirely pelagic, we could think that the volcano is on the order of 10^5 yr old (assuming a pelagic sedimentation rate of 1–10 mm/k.y.). However, in many areas, seafloor photographs show darker sediment either at the surface or buried just below the surface. This dark sediment may have either a hydrothermal or a volcanogenic origin with only a thin dusting of pelagic sediment. If this is true, the age of the volcano could be extremely young, perhaps on the order of a few tens of thousands of years.



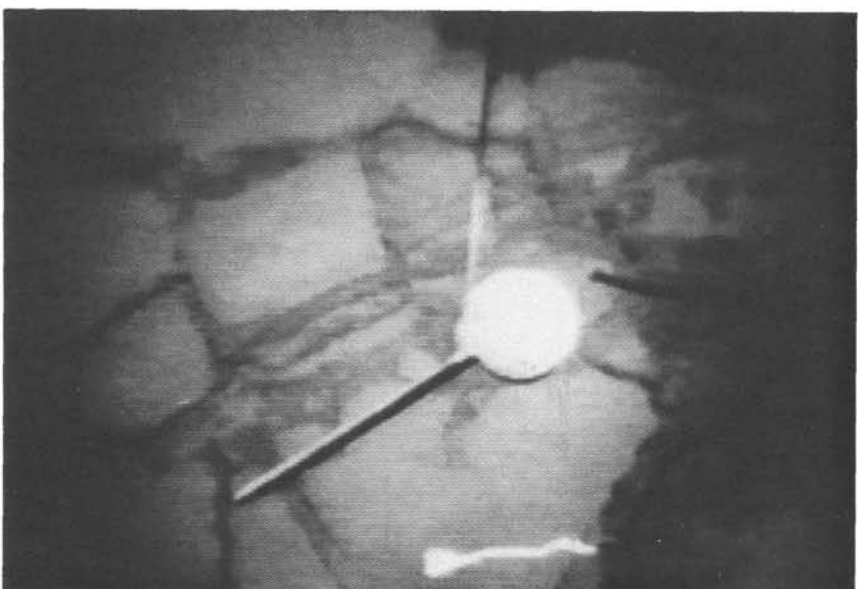
A



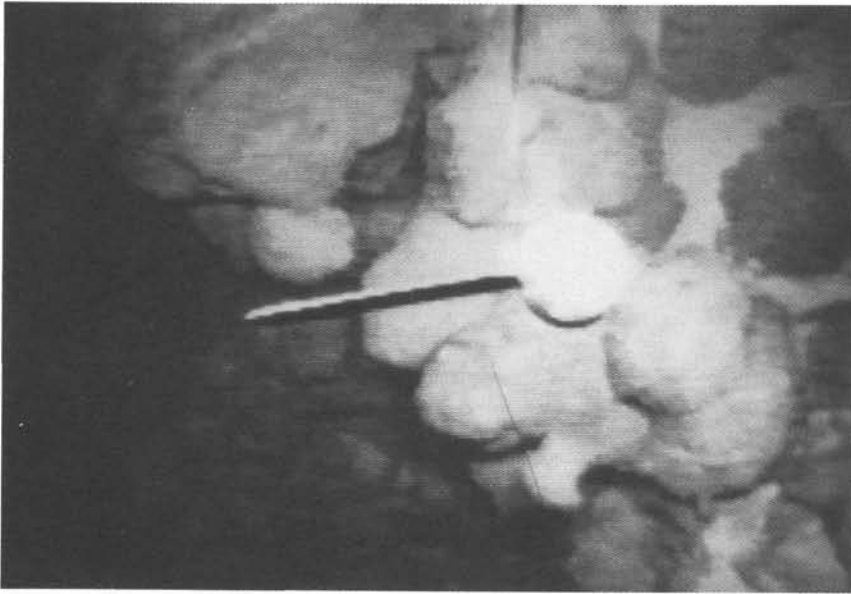
B



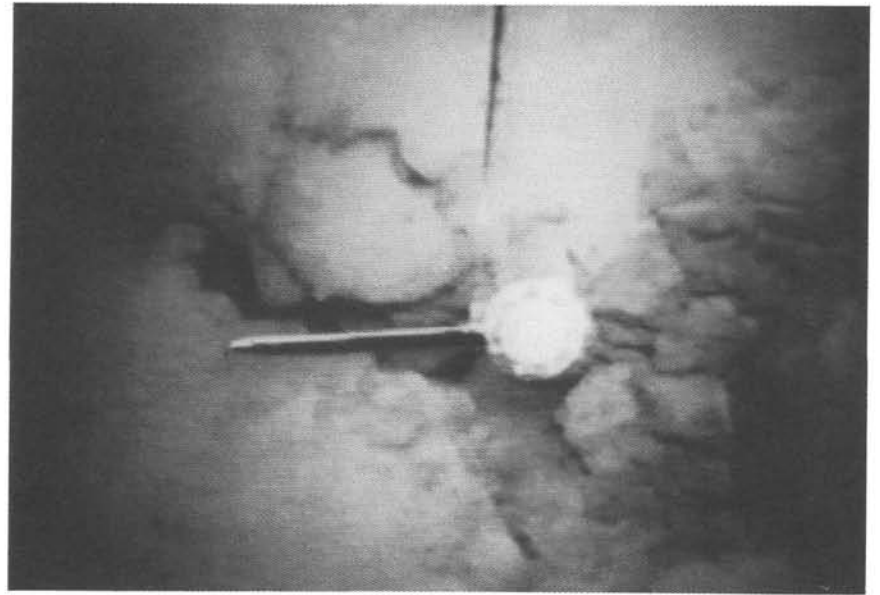
C



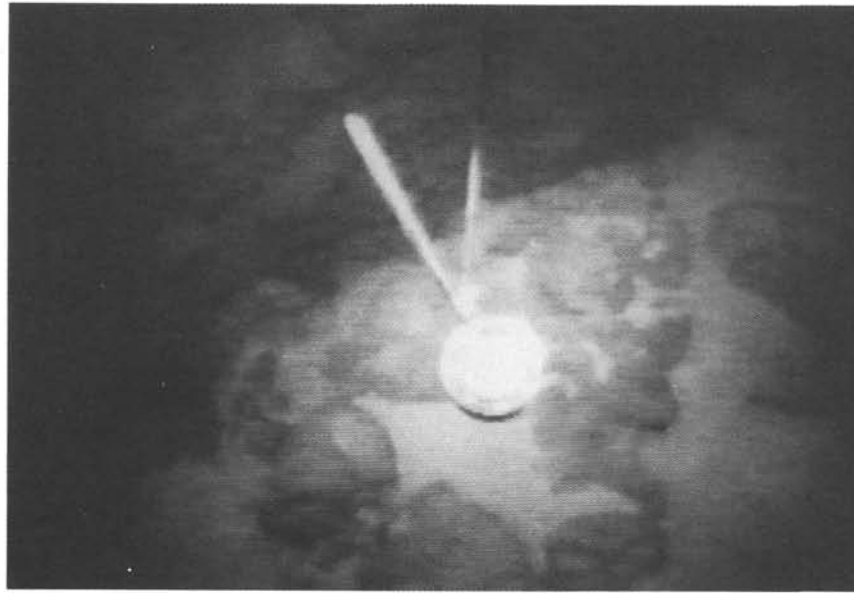
D



E



F



G

Figure 5. Photographs from the Colmek television-sonar system obtained during the survey: A. and B. Bulbous and elongate pillows that cover almost the entire summit plateau. C. Pillows almost completely buried by sediment. D. Sheet flows near the northeastern rim of central crater. E. Scarp at eastern edge of summit plateau. F. One of the many small fissures cutting the summit plateau. G. Younger flow burying older pillows east of the summit plateau.

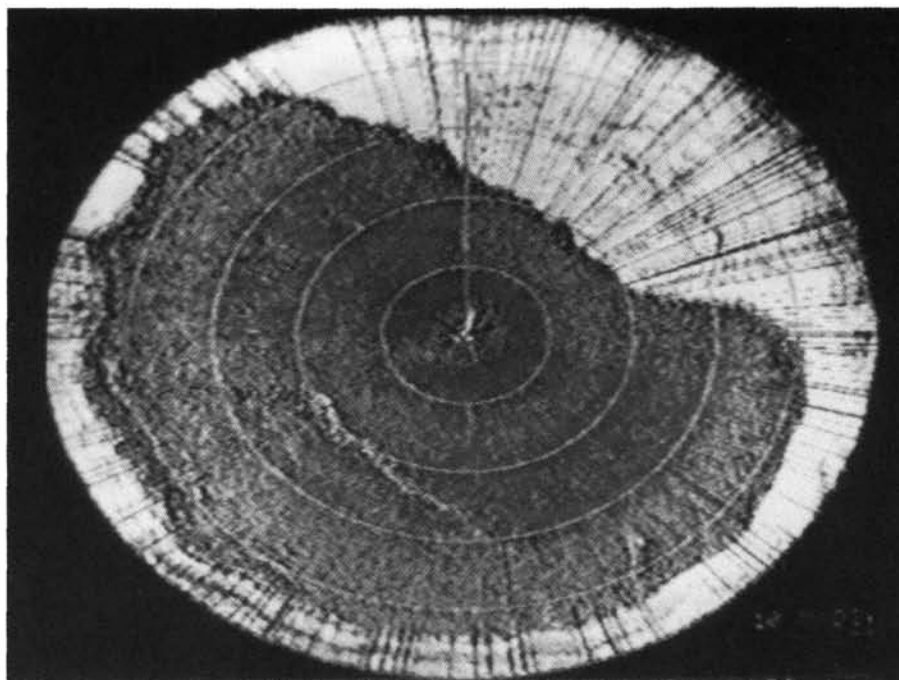


Figure 6. Mesotech sonar image showing the wall of the central crater (white) and the deeper water within the crater itself (dark). The Mesotech was useful in maintaining the television-sonar frame at a safe height above the seafloor and in avoiding obstacles like major fault scarps.

Site of the Hard-Rock Guidebase

A site was chosen for deployment of the HRGB approximately 206 m south-southeast of beacon 2, about halfway between the central crater and the edge of the summit plateau (22°55.3'N; 44°56.8'W; see Fig. 7). On the basis of this survey, this area is characterized by flat, moderately sedimented pillow lavas with no evidence of surficial rubble. Several small north-south-trending fissures, but no major ones, occur in the area and have an average separation of about 20 m. We would have preferred an area with no fissures, but from the survey and SeaMARC I results, it appears as though the entire summit plateau has experienced some degree of extensional disruption. We therefore chose to try to land the HRGB on the undisturbed seafloor lying between these small fissures.

Constructed from video tapes recorded after HRGB deployment, Figure 8 shows a map of the area surrounding the HRGB. The base landed successfully with an initial tilt of 5°. Subsequent shifting increased the tilt to about 10° . One of the legs appears to be suspended above a small fissure, while the other legs are standing on moderately sedimented basalt. Several large bulbous pillows crop out nearby, whereas a larger, north-south-trending fissure is about 6 m east of the HRGB.

We were, naturally, disappointed that the guidebase landed on a small fissure, especially after the careful and detailed site survey. There were three main reasons for this failure. First, during the survey, we were unable to monitor the position of the camera frame relative to the ship. Significant offsets of at least 20–60 m are likely, which lead to inaccuracies in our maps. Second, the dynamic-positioning system of the drill ship can nominally hold position only to within 1% of the water depth (30 m in this case), although 0.25% of water depth is possible under favorable conditions. The weather conditions were poor between the conclusion of the survey and the deployment of the HRGB, and we were unable to maintain the position chosen during the site survey for the guidebase deployment. Finally, because the camera was located above the HRGB during the deployment op-

eration, we had to land it “blind,” without being able to see the seafloor.

Summary

The feasibility of performing a high-resolution survey from the drill ship to find a guidebase deployment site was demonstrated at Site 648. The Colmek real-time television-sonar system provided a photographic image of the seafloor of exceptional quality, while the Mesotech sonar was essential for maintaining the television frame at the proper height above the seafloor and for avoiding major obstacles like fault scarps. When combined with the dynamic-positioning capabilities of the drill ship, these tools were shown to be a very powerful surveying system that promises to revolutionize the precise positioning of drill holes relative to seafloor geologic features.

Our experiences at Site 648, however, suggest that several modifications are needed to improve significantly the capabilities of this system for future legs. These include (1) a digital compass and a continuous time and date display on the real-time video screen, (2) electronic pan and tilt capabilities for the Colmek camera, (3) a navigation beacon on the camera frame to monitor its position relative to the ship during the survey and the HRGB deployment, (4) a method for imaging the seafloor below the guidebase during the deployment operation, and (5) 35-mm still cameras mounted on the frame to take color pictures every 60 s.

OPERATIONS

Leg 106

Leg 106 was selected for the operational testing of a hard-rock spud system designed to allow drilling into bare, fractured ocean-floor basalts at depth, a capability not previously available.

Work on the subsystems began in mid-January 1985 and was completed in time for the departure of Leg 106 from St. Johns, Newfoundland, on 1 November 1985.

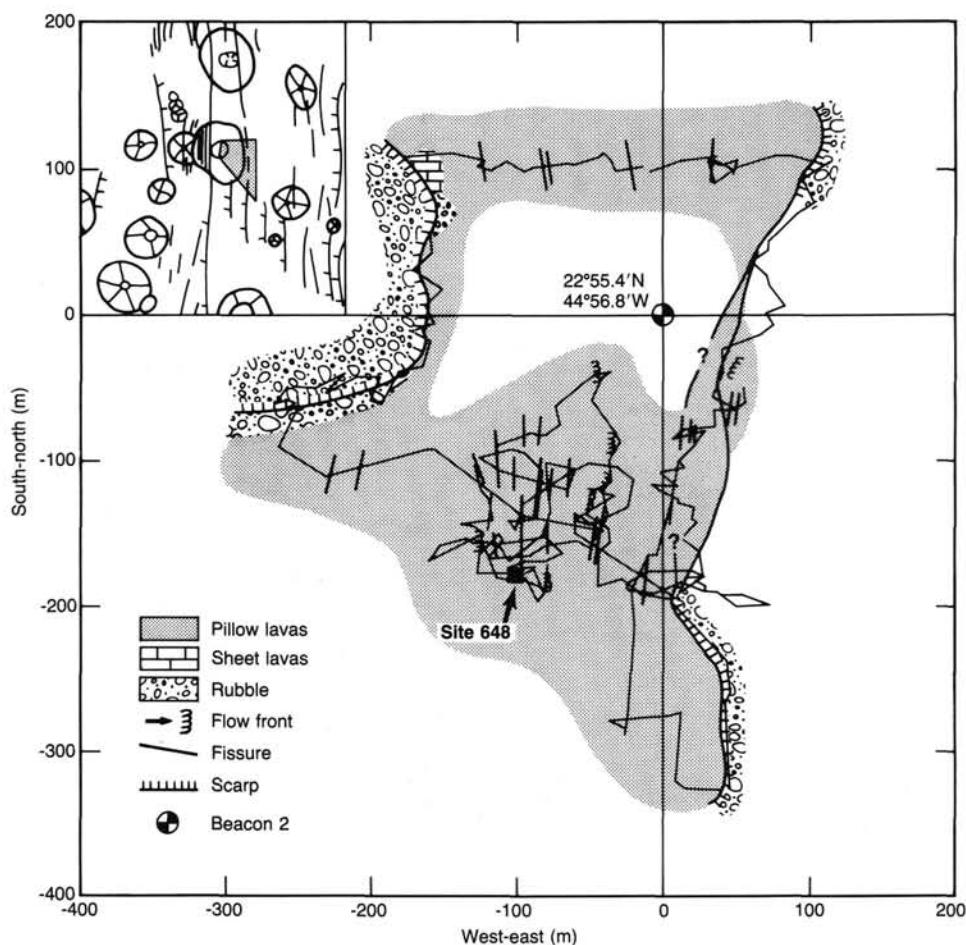


Figure 7. Geologic map of Serocki Volcano constructed from the video-survey results. Inset shows tectonic interpretation of the area immediately surrounding Serocki Volcano, based on available Sea Beam and SeaMARC I data.

The principal subsystems developed during Leg 106 preparations were as follows:

1. A gravity HRGB structure 5.2 m square and 3.3 m high, with the means to suspend the HRGB beneath the ship and to lower it to the seafloor, cement it in place, and release it. The HRGB is designed to be set over boulders and on slopes of as much as 20°. The structure receives a reentry cone and casing after drilling of the rock beneath the base.

2. Positive-displacement coring motors (PDCM), 9½ in. in diameter, for 10½-in. and 14½-in. bits, capable of providing 2¼-in. nominal wireline cores. The coring motors are driven by seawater pumped under high pressure from the ship. The drill string remains stable during use of the motors, since only the bottom 12.8 m of the drill string rotates.

3. A television-sonar system comprising a low-light-level television camera, capable of functioning at a depth of 6100 m, and a Mesotech sonar system for detailed site surveys and for monitoring reentry and other operations.

Major Port Activity

Two HRGB's were loaded aboard the *JOIDES Resolution* in St. John's, Newfoundland. The crew made a practice HRGB dry run, moving the two halves of the HRGB into position in the moonpool area. The base was assembled, and the hydraulic system was tested. The HRGB was then disassembled and stored.

The television winch with 6100 m of coaxial cable was set in the moonpool area, and the mezzanine was modified to accept the winch. Installation was completed at sea.

Site 648

The *JOIDES Resolution* left St. Johns, Newfoundland on 1 November 1985 for Leg 106 after taking on supplies and equipment. After 5.5 days of cruising, the vessel arrived at beacon site 2 (Site 648) located at the MAR, 70 km south of the KFZ on 6 November 1985. The site beacon was turned on and located at a range of 3 km.

Preparations were made for a seafloor site survey, using the television-sonar system. The drill string was made up with a core barrel driven by a 9½-in. PDCM. The drill pipe was lowered to 3121.5 m. Water depth was 3334.3 m. (The system incorporates a sleeve that is latched around the drill pipe. The frame can be pulled up or lowered, using the coaxial cable, while the drill pipe acts as a "track" or guide.) When the drill pipe was at 3121.5 m, we found that the frame could not be raised or lowered. It took 12 hr to retrieve the drill pipe, together with the television-sonar system; the coaxial cable needed to be unwrapped from the pipe by turning the drill pipe as it surfaced.

The system took about 18 wraps around the lower 1000 m of the pipe. When the cable head was removed, considerable torque was found in the cable. The frame was deployed again but without the drill pipe to allow the cable suspending the frame to de-

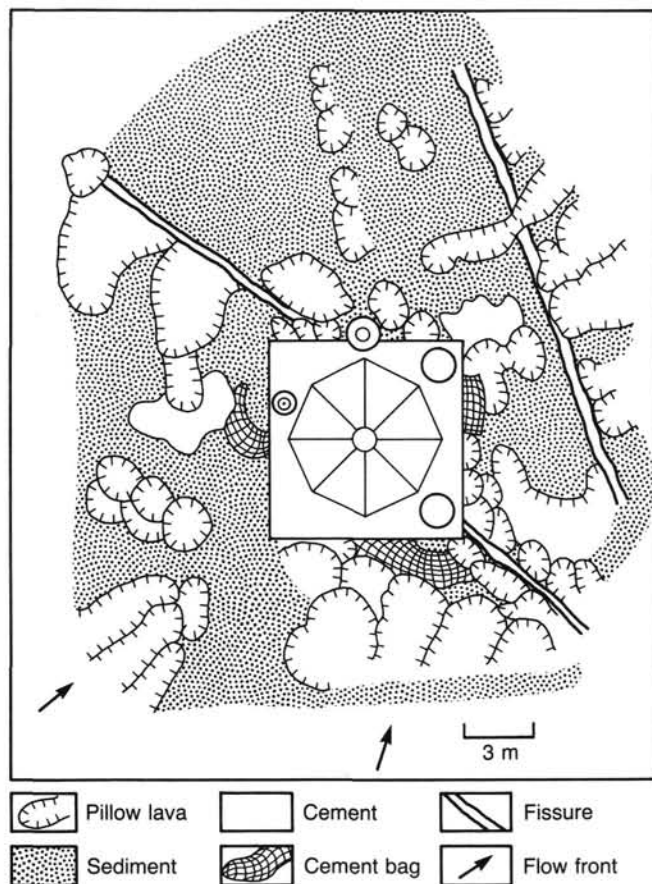


Figure 8. Sketch of the area around the hard-rock guidebase, constructed from video tapes recorded after the guidebase was deployed.

torque. While approaching bottom, the television camera sighted the floats from the site beacon at a water depth of about 3210 mbrf. The seafloor was sighted at water depth 3334 m. The site survey continued with the dynamically positioned (DP) vessel taking offsets to view the seafloor. Video and sonar presentations were high quality. The surveys were continued with the frame 6–8 m above seafloor. The sonar effectively helped maintain a “safe” elevation of the frame above seafloor and detected nearby potentially hazardous changes in relief.

After 28 hr of continuous site surveying and mapping, a site was chosen for deployment of the guidebase. The site was locally flat, consisting of pillow lavas 1–2 m in diameter.

After a somewhat unpromising start and cable torquing problems, the television-sonar system proved in subsequent tests to be rugged, dependable, and able to provide high-resolution black-and-white television coverage. Particle backscatter was minor, and sometimes the seafloor or reentry cone could be viewed at ranges of as much as 18 m.

Hole 648A

System tests were continued to determine if a hole could be drilled on bare rock without any guide structure or bit containment. For this test, a 9 $\frac{7}{8}$ -in. bit and standard rotary core barrel were made up to a drilling motor and bottom-hole assembly. This configuration did not allow for wireline coring, but a limited penetration with the standard barrel was acceptable.

The television-sonar system was deployed on the drill pipe to observe the bit. The drill pipe was lowered and found the seafloor at 3310.5 mbrf. After verifying the bit position, we raised the television-sonar system 100 m before resuming drilling to

protect the frame from excessive vibration. The 9 $\frac{7}{8}$ -in. bit cored from 0 to 4.5 mbsf. We used the television to check the spudding at 1.5, 3.0, and 4.5 mbsf and then recovered the frame and tripped the drill pipe back to surface.

Though this was a limited test, results showed that a hole could be drilled on hard rock without any lateral support. The pipe remained stable when only the lowermost 9–12 m rotated. The motor cored 4.5 m in 8.62 hr, drilling in fresh pillow basalt. Recovery was 7 cm of pillow basalt and glass.

Hard-Rock Guidebase Use in Hole 648B

Assembly of the HRGB was started at noon, 11 November. The lower half of the HRGB was secured in the moonpool area, and the upper section was landed and made up to the lower half. Lowering slings were attached, the release system tested, and the cementing hose made up to the HRGB. Weather deteriorated, swells reached 3–4 m, and the moonpool surged 2–5 m. An unusually strong Bermuda high-pressure area produced strong northeasterly winds and swells. The swells were forecast to moderate to <2 m in 96 hr. Weather conditions eventually moderated to 2–3-m swells, when the HRGB was deployed to the seafloor at 0435 hr, 17 November. The television-sonar system was deployed to monitor HRGB “landing,” which occurred successfully at 3344.4 mbrf.

An 18 $\frac{1}{2}$ -in. bit and a 9 $\frac{1}{2}$ -in. drilling motor were made up to a bottom hole assembly to initiate drilling. The bit was run down to 3334 m and the hole was reentered at 0915 hours, 18 November. The television-sonar system was deployed, allowing the driller to position the bit above the HRGB and to stab in for reentry using a television monitor at the drillers’ station. The reentry was made during winds of 30–35 kt, seas of 2–3 m, and easterly swells of 3.5–5 m, indicating that downhole reentry operations can continue in adverse weather conditions. We continued drilling the 18 $\frac{1}{2}$ -in.-diameter hole from 0 to 3.1 mbsf. The drill string was pulled out of the hole, and a new 9 $\frac{1}{2}$ -in. drilling motor and a 12 $\frac{1}{4}$ -in. bit were picked up. The smaller bit was selected in an attempt to increase the drilling rate.

We ran the 12 $\frac{1}{4}$ -in. bit to the top of the guidebase and positioned the ship for reentry, using the television-sonar system. After the reentry, the guidebase was checked using the television-sonar system and found to be in good condition. The 12 $\frac{1}{4}$ -in. bit drilled from 3.1 to 4.1 mbsf. We swept the hole with 30 bbl of high-viscosity mud to flush out cuttings. Drilling and reaming the 12 $\frac{1}{4}$ -in. hole continued to 4.2 mbsf. Hole conditions worsened while we worked pipe to uninstall the drilling motor. Three high-viscosity⁴ (100–200 s/qt) mud sweeps, 50 bbl each, were used to clear the hole. A maximum overpull of 40,000 lb freed the stalled drilling motor. We attempted to drill a 12 $\frac{1}{4}$ -in. hole at 4.2 mbsf; however, the motor was stalling, and the bit was barely able to get back to 4.2 mbsf through rubble fill.

The 12 $\frac{1}{4}$ -in. bit was pulled out of the hole, the drill motor laid down, and the first drill motor picked up. The jet on the rotor was plugged to increase motor torque, and a 9 $\frac{7}{8}$ -in. core bit was selected for coring the pilot hole. The bit reentered the guidebase, again finding 0.1 m of rubble fill, and the 9 $\frac{7}{8}$ -in. hole was drilled from 4.1 to 13.9 mbsf. Seven high-viscosity mud sweeps were spotted (100–115 s/qt, weighing 9.5–11.5 lb/gal). The drill motor stalled, but we freed it with a 70,000-lb overpull and pulled the 9 $\frac{7}{8}$ -in. bit with core barrel and drill motor out of the hole. Recovery was 3.2 m of basalt. Drilling had destroyed the bit and severely abraded the bit body.

The drill rig ran at the contract “breakdown” rate for 21 hr while we made crown sheave repairs. The rig crew serviced and refit the unit to proper alignment.

⁴ Viscosity determined using Marsh funnel.

A television survey found the guidebase sitting on moderately cemented pillows and the southeast leg wedged in a small fissure passing under the guidebase. A second fissure was located northeast of the guidebase. Two small cement ponds could be seen on the east and west sides of the guidebase.

An 18½-in. bit and a BHA were made up and run for reentry. The hole was opened up from 3.1 to 8.8 mbsf, and 50 bbl of high-viscosity mud was circulated to clean the hole. We then pulled the bit to the top of the HRGB and washed out the cone. The 18½-in. bit was pulled out of the hole.

A 14¾-in. bit was made up to a 9½-in. outer-diameter drilling motor. The top drive and heavy wall drilling joints ("knob-bies") were picked up, and the HRGB reentered again. Only 1 m of fill was found. The 14¾-in. bit opened up the 9¾-in. hole from 8.8 to 9.3 mbsf. A 50-bbl and a 15-bbl slug of high-viscosity (100–520 s/qt) mud were spotted. Drilling the 14¾-in. hole continued, enlarging the 9¾-in. hole in the interval from 9.3 to 13.3 mbsf. Seven 15-bbl pills of mud were used to clear the hole. Maximum overpull was 50,000 lb. Opening of the 9¾-in. hole continued from 13.3 to 15.3 mbsf, where preparations started for pulling in the 14¾-in. bit.

An 18½-in. bit was picked up, without a mud motor, to drill using the top drive for rotation. The drill string made a television-assisted reentry, and hole bottom was tagged at 8.8 mbsf. The 14¾-in. hole was reamed to 18½ in. from 8.8 to 12.6 mbsf, using top drive for torque. The hole was swept seven times with highly viscous mud to clear the cuttings. Maximum overpulls of as much as 50,000 lb. were required to free the stalled top drive.

Hole conditions worsened in the interval from 12.6 to 14.1 mbsf. Seven highly viscous mud sweeps (500+ s/qt) were pumped to clean the hole. Maximum overpull was 70,000 lb.

A positioning beacon was deployed, replacing the site survey beacon, which was weakening after 22 days of operation. The guidebase tilt beacon started to fail after 11 days use.

Hole instability continued to hinder drilling operations. Reaming the 14¾-in. hole to 18½ in. continued to 15.3 mbsf, where the hole was advanced to 16.1 mbsf. Five high-viscosity mud sweeps were pumped to ease hole problems. The drill pipe required overpulls of as much as 70,000 lb.

The open hole was cemented with 170 sacks of cement. We pulled the bit out of the hole and checked the guidebase. The hole was reentered with the 18½-in. bit, which encountered cement at 0.6 mbsf and drilled to 5.1 mbsf.

The 18½-in. bit was then pulled out of the hole, and a rerun 18½-in. bit was made up for a television-assisted reentry. The cement was drilled out to 18½ in. from 5.1 to 14.6 mbsf. The hole was swept four times with viscous mud slugs, but 2.5 m of rubble collected in the bottom of the hole. A 30-bbl slug of high-viscosity drilling fluid was circulated to clean the hole. The 18½-bit was pulled up in preparation for running 16-in. casing and a reentry cone into the guidebase.

We welded the casing shoe and moved the cone into the moonpool area where the gimbal was welded. Next, we made up the double "J" landing and releasing tool, assembled the cementing stinger, and laid it out on the pipe racker, and made up the hangar and casing. The 16-in. casing hangar was latched into the reentry cone. The running assembly was jayed into a 16-in. hangar, and the cone was deployed on 1 December. The assembly completed the trip to 3337 mbrf. Pipe was spaced out for reentry, the cementing assembly rigged up, and the cone landed in the guidebase. Cementing was aborted because of apparent blockage. The cementing stinger assembly was released from the 16-in. hangar. The valve on the cementing head was found partly closed, apparently by impact from elevator bails during heave.

The drill string was tripped out of the hole, the television-sonar system removed, and a cementing stinger assembly picked

up. We lowered the drill string and stinger below the ship, the television-sonar system was clamped to the drill pipe, and the string continued the trip to the reentry cone. After the drill pipe was spaced out for reentry, the vessel was repositioned and reentry occurred. The casing was cemented through the stinger with 34.4 bbl of 15.8-lb/gal cement. The cementing stinger stuck briefly in the cone, possibly because of a slight vessel offset. When the stinger came out, the reentry cone inadvertently picked up about 2 m and landed back at the original elevation. A check with the television camera showed the cone and guidebase in the proper attitude. The assembly was pulled free, and the cementing head was laid down. The drill pipe and stinger were then pulled to 3337 mbrf, and the drill string was flushed. After re-surveying the site with the drill pipe at 3337 mbrf, we pulled the drill string to the surface with a stop to remove the television-sonar system. The trip out continued to the surface and the stinger was laid down.

The ship ran at breakdown status for 12 hr while we repaired the top drive. The top-drive drilling-motor armature was grounded. Insulation broke down when windings blew at the junction to the commutator. The top-drive motor was replaced and rewired. Brake, air, and hydraulic system lines were installed, and stress points were magnafluxed.

A 14¾-in. bit assembly for top-drive operation was run in the hole and cement was tagged at 4.6 mbsf. The bit was pulled back to 1.6 mbsf; the television-sonar system was pulled to the main deck and secured. In a top-drive operation, the system is removed from the drill string because the entire string is rotated and possibly could damage the system.

The cementing shoe (at 5.6 mbsf) and fill were drilled from 4.6 to 14.6 mbsf. The hole was swept twice with 20-bbl sweeps of high-viscosity drilling fluid in an attempt to clear accumulated debris from the hole.

The television-sonar system was installed and run down the drill string to observe the bit being pulled from the HRGB and cone and look for junk. The 14¾-in. bit was pulled out of the hole, the system removed, and a new BHA run in the hole with a 13¾-in. concave junk mill. The top drive and "knobbie" joints were picked up for spacing-out on reentry. After reentry, the television-sonar system was pulled to main deck and secured. The drill string was run in hole to 11.6 mbsf (3 m of fill). Milling with top drive and the 13¾-in. concave mill continued from 11.6 to 16.6 mbsf. The hole was unstable; torque was high, and the motor was stalling. Four 20-bbl sweeps of high-viscosity mud were pumped. The maximum overpull was 115,000 lb (top drive in use). Bounce and vibration were noted from 14.1 to 15.1 mbsf. From 15.1 to 16.6 mbsf, drilling was smooth, indicating the junk had been milled through. The mill, however, after being lifted off the bottom, could not be worked past 15.6 mbsf because of the sloughing of 1 m of rubble fill. High-viscosity mud was circulated to clear the hole of cuttings. The drill pipe was pulled to the surface where the mill was found to be 95% expended, with little cutting life left.

Next, a 9¾-in. core bit was run in the hole with a top-drive bottom hole assembly and standard core barrel. A television-sonar-assisted reentry was made. Bottom was tagged at 13.3 mbsf; 3.3 m of fill was in the hole. Three cores were taken in the interval from 13.3 to 25.7 mbsf (Table 1). The drill string was then pulled to the surface, a new 9¾-in. bit was picked up, and the drill was run back in the hole to continue coring. A television-sonar-assisted reentry was completed. Bottom was tagged at 14.6 mbsf; 11.1 m of fill was in the hole. Two more cores were taken in the interval from 14.6 to 33.3 mbsf, the deepest depth reached at Hole 648B during Leg 106. An 85,000-lb drag was noted when we pulled out of the hole.

The 9¾-in. bit was brought to the surface and exchanged for a 14¾-in. bit (top-drive operations). Plans were to ream the

Table 1. Coring summary, Site 648.

Hole, Core no. ^a	Date	Time on deck	Total depth (m)		Depth (mbsf)	Length			Recovery (%) ^b	
			Top	Bottom		Advanced (m)	Cored (m)	Recovered (m)		
648A										
1R	11 Nov 85	0515	3310.5	3315	0.0-4.5	4.5	4.5	0.07	1.6	
648B										
			^c 3344.4	3351	0.0-6.6	6.6	0.0	0.00		
1R	22 Nov 85	2230	3351	3360.7	6.6-16.3	9.7	9.7	3.20	33	
^d 2R	6 Dec 85	1330	3357.7	3358.7	13.3-14.3	0.0	1.0	0.17	17	
^e 3R	6 Dec 85	1730	3358.7	3365.5	14.3-21.1	4.8	6.8	0.78	11.5	
4R	7 Dec 85	0037	3365.5	3370.1	21.1-25.7	4.6	4.6	0.52	11.3	
^d 5R	7 Dec 85	2015	3359	3370.1	14.6-25.7	0.0	11.1	0.43		
6R	8 Dec 85	0445	3370.1	3377.7	25.7-33.3	7.6	7.6	1.10	14.5	
^{d,f} 7R	12 May 86	0800	3356	3365	15-24	0.0	9.0	1.64		
^d 8R	12 May 86	1200	3365	3369	24-28	0.0	4.0	0.99	24.8	
^d 9R	13 May 86	1615	3369	3373.4	28-32.4	0.0	4.4	0.50	11.4	
^{d,g} 10R	13 May 86	2015	3369	3373.4	28-32.4	0.0	4.4	0.22	5	
^{d,h} 11R	14 May 86	2315	3355.8	3365.2	14.8-24.2	0.0	9.4	4.80		
^{d,h} 12R	15 May 86	0700	3356	3367	15-26	0.0	11.0	5.09		
^d 13R	16 May 86	1500	3364	3374	23-33	0.0	10.0	0.23	2.3	
^{d,h} 14R	17 May 86	1745	3355	3365	14-24	0.0	10.0	0.92		
ⁱ 15R	17 May 86	2330	3365	3375.8	24-34.8	1.5	10.8	1.22	11.3	
^{d,j} 16R	18 May 86	0315	3374.3	3375.8	33.3-34.8	0.0	1.5	0.81	54	
^d 17R	19 May 86	1015	3362.5	3375.8	21.5-34.8	0.0	13.3	0.29		
18R	19 May 86	2015	3375.8	3385.2	34.8-44.2	9.4	9.4	0.43	4.6	
19R	20 May 86	0115	3385.2	3390	44.2-49	4.8	4.8	0.19	4	
^{d,k} 20R	29 May 86	2000	3388	3391.5	47-50.5	1.5	3.5	0.27	7.7	

Notes: ^a Cores 1R-6R recovered during Leg 106, Cores 7R-20R recovered during Leg 109.

^b All recovery consists of basalt unless otherwise stated.

^c Water depth for Leg 106 = 3344.4 m; water depth for Leg 109 = 3341.0 m.

^d Cored through rubble and/or cement filling previously drilled hole—recovered basalt and/or cement.

^e Upper 2 m cored through rubble fill, lower 4.8 m cored in new hole.

^f Core composed of 1.54 m of cement and 0.10 m of basalt rubble.

^g Core composed of 0.10 m of cement and 0.12 m of basalt rubble.

^h Core composed entirely of cement.

ⁱ Upper 9.3 m cored through rubble/cement fill, lower 1.5 m cored in new hole.

^j Depths indicate cored through rubble fill; massive nature of basalts suggest cored *in-situ*.

^k Upper 2 m cored through rubble fill, lower 1.5 m cored in new hole.

Depths are arbitrary due to excessive fill being repeatedly drilled out of hole.

9 $\frac{3}{8}$ -in. hole to 14 $\frac{3}{4}$ in. so that the 14 $\frac{1}{2}$ -in. bit coring motors could continue the hole. Reaming the 14 $\frac{3}{4}$ -in. hole continued to 26.1 mbsf. Hole conditions were deteriorating, and the 14 $\frac{3}{4}$ -in. bit was pulled to the surface during reaming. Seventy-five barrels of high-viscosity mud were pumped in the hole to clear cuttings, while overpulls as great as 100,000 lb were required to clear the sticking pipe. The pipe reentered the hole and at 25.6 mbsf, an additional 140 bbl of high-viscosity drilling fluid was circulated to clear cuttings. The hole continued to be unstable, and overpulls of as much as 160,000 lb were required to free pipe. The 14 $\frac{3}{4}$ -in. bit was pulled out of the hole.

At this point, the rig crew made repairs to the top drive. The shaft was removed, inspected, and reinstalled, and the unit shimmed to alignment. The saver sub was found to be nonconcentric and was taken out of the string, further improving top-drive concentricity.

A 14 $\frac{3}{4}$ -in. bit was then run in the hole (top-drive operations) with a television-sonar-assisted reentry. The hole continued to be unstable, and maximum overpulls to 160,000 lb were required to unstick the drill pipe. Again, we used high-viscosity drilling fluid flushes. In an attempt to stabilize the hole, we filled the open hole with 31 bbl (100% excess) of cement. Cement was tagged at 14.6 mbsf on reentry and drilled out with a 14 $\frac{3}{4}$ -in. bit from 14.6 to 18.6 mbsf.

Drilling conditions were considered too severe to continue operations without drilling jars. Two hydraulic jars had been placed aboard the ship, but both had been bent at the mandrel and were not functioning. Because of the lack of jars to combat

stuck pipe, the unstable hole conditions, and the high priority assigned to keeping Hole 648B open, the ship moved to a new site (Site 649) 25 km south of the KFZ.

Site 648B reached a total depth of 33.3 mbsf. However, a total of 94.3 m was drilled, which consisted of fill and hole that was either reamed or cored. This is three times the actual penetration of 33.3 m. The hole was left with cement drilled out to 18.6 mbsf.

Leg 109

JOIDES Resolution returned to Hole 648B during Leg 109 to continue the development of the unsupported drilling and coring operations started on Leg 106. The primary objective of Leg 109 was to demonstrate the capability of drilling and coring young fractured basalt and to obtain core samples in Hole 648B to a target depth of 200-250 mbsf. Secondary coring and drilling objectives included the evaluation of reduced hole sizes, specialized cementing techniques for improving hole stability, and new bit design (12 $\frac{1}{4}$ -in. drill bits and 9 $\frac{3}{8}$ -in. core bits).

Leg 109 encountered many operational difficulties. Two bottom-hole assemblies were successfully fished out of Hole 648B, one of which protruded several meters above the top of the reentry cone.

Dakar Port Call

Leg 109 commenced at 0645 hr on 17 April 1986 in Dakar, Senegal. A major port task was to replace one of the main piston rods in the heave compensator. Other major activities in-

cluded repair of a reduction gear and the steering system, inspection/alignment of guide rails, and loading of SEDCO and ODP freight. A considerable amount of hardware critical to drilling operations was loaded: positive-displacement drilling and coring motors, drilling jars (two types), prototype 9/8-in. coring bits, prototype 12¼-in. drill bits, a special 10¾-in. casing string, and television-sonar system reentry equipment.

Under Way to Hole 648B

JOIDES Resolution departed Dakar at 1800 hr on 23 April 1986. The ship averaged 12.3 kt during transit. Light easterly winds and seas with partly cloudy to clear skies prevailed throughout the cruise. While the vessel was under way, preparations were made for the start of drilling operations at Hole 648B. A cementing stand pipe and manifold system were installed on the rig floor, and modifications were made to the cementing pumps to enhance operation of the equipment.

Hole 648B

JOIDES Resolution approached Site 648 during a global positioning system (GPS) satellite window; the beacon on the guidebase reentry cone was turned on, and the ship was established in dynamic-positioning mode. After a noncommandable beacon had been dropped, the beacon on the guidebase reentry cone was turned off.

We observed during Leg 106 that drilling and coring smaller hole sizes resulted in increased penetration rates and hole stability. Consequently in Leg 109, in an effort to reduce hole sizes, we stipulated 10¾-in. casing with special flush joint connections to be run in place of the 11¾-in. casing originally proposed. This allowed a reduction in hole diameter from 14¾ in. to 12¼ in. Drill collars 9½ in. in diameter were run with the 12¼-in. drill bits to reduce the size of the hole annulus. The reduction in annulus size was observed to increase hole stability and to improve hole cleaning with the limited volume of viscous bentonite and XP polymer sweeps that could be pumped. The reduced hole annulus also helped to prevent rubble from falling in the hole on top of the bit.

Though improvements were produced by the 12¼-in. bits and 9½-in. drill collars when compared with Leg 106 operations, considerable torque was still required to effect and maintain rotation to the bit. To minimize the chance of backing off part of the BHA or drill string caused by backlash torque, a maximum of 12,000 lb of drilling torque from the top drive was applied to the drill string. The sticky hole conditions encountered prevented effective rotation of the bit with the torque available for safe operation. We thought that increasing bit speed would help to some extent. The bit stalled continuously at 40–60 rpm, but when speed was increased to 120–180 rpm, the momentum of the large-diameter drill collars helped to maintain rotation of the bit, and a drilling rate of 1.2 m/hr was realized. Good progress was made using this drilling technique; however, a low-cycle fatigue failure of the hydraulic drilling jars resulted in the loss of the BHA.

Using a conventional 9½-in. outer-diameter Bowen slim-hole overshot with an 8-in. spiral grapple, we successfully fished out the damaged jar and BHA. The drilling-jar failure may be attributed to rotation of the partly unsupported BHA. It was necessary to drill with partly unsupported jars until the hole was deep enough to provide complete and adequate support. The jars would have been adequately supported in the hole if problems had not been encountered with rubble backfill. Jars were located two drill collars (20 m) above the bit.

In an effort to minimize the risk of running drilling jars, a mechanical jar intended for use with the rotary-coring system was run. The McCullough Torque Jar is considerably shorter than the hydraulic jar and was thought to withstand better the

stresses induced while drilling with the BHA partly unsupported. To maintain effective rotation, drilling continued with high bit speeds (120–180 rpm). After working in the hole with the BHA still partly unsupported, the jars again failed, resulting in three 9½-in. drill collars and the jar mandrel (fish) being left in the hole. The top of the jar mandrel protruded 3–4 m above the top of the reentry cone.

A 1-m-diameter cone was welded to the bottom of a 9½-in. Bowen slim-hole overshot lip guide to attempt a "reverse reentry" (Fig. 9). That is, instead of lowering the BHA into the reentry cone, a reentry cone (95% smaller in area than a standard reentry cone) was lowered onto the top of the BHA protruding from the hole. The 1-m-diameter cone guided the overshot and grapple, allowing capture of the top of the fish (Fig. 9). This was accomplished with the help of the television-sonar system coupled with precise manipulation of the fishing/reentry funnel using the dynamic-positioning system of the ship.

Though several reverse reentries were made on top of the fish, no positive engagement was accomplished using the 9½-in. overshot, and the grapple was destroyed. A double "J" fishing tool was manufactured that would engage the two loading dogs on the jar mandrel, and the 1-m-diameter fishing/reentry funnel was welded to the bottom of the double "J" fishing tool. The first trip was unsuccessful in retrieving the fish from the hole. Numerous reverse reentries were made on top of the fish, but the double "J" slots in the fishing tool would not engage with the loading dogs. The drill pipe was tripped out to examine the fishing tool. Modifications were made to the "J" slots, and the tool was run back into the hole for a second fishing attempt. This time the loading dogs successfully engaged in the two "J"

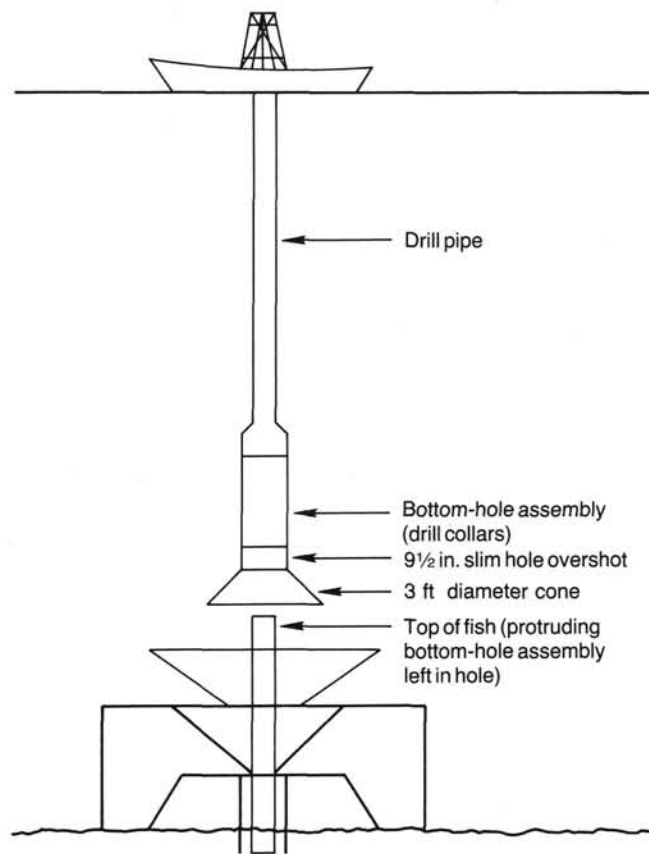


Figure 9. Equipment used in reversed reentry technique.

slots of the fishing tool. The parted BHA (fish) was then pulled out of the hole and retrieved to the surface.

We decided to evaluate the feasibility of working in the hole for an extended period (30 days) without setting the 10 $\frac{3}{4}$ -in. casing. Owing to the high risk of drilling with the 12 $\frac{1}{4}$ -in. bits, it was desirable to retrieve some core before attempting to set the casing. We also needed to verify that there were no large pieces of metal in the hole that might suspend drilling operations. This meant drilling and coring 1–2 m past the point in the hole where the jar failure had occurred. One mill and six core-bit runs were required to reach that point. Progress was hindered significantly by rubble backfill after each bit run. Most of the coring was done through rubble or with rubble in the hole, which limited core recovery significantly.

During these six core-bit runs, approximately 63 m of basalt and basaltic rubble and 39 m of cement were cored, from which 4.9 m of basalt and 12.45 m of cement were recovered. A depth of 49.5 mbsf was reached, which represents a penetration of approximately 16 m of new hole. Eventually, the time required to drill and core the rubble zone to get back to bottom was approaching that of the rotating life for the 9 $\frac{1}{2}$ -in. core bits. At this point, we decided to set casing because we could no longer make substantial progress with the 9 $\frac{1}{2}$ -in. coring strategy. We ran a 12 $\frac{1}{4}$ -in. bit to clean out the existing 12 $\frac{1}{4}$ -in. hole to a depth of 29 mbsf. The hole was filled with cement from 26 to 15 mbsf. A second 12 $\frac{1}{4}$ -in. bit run was made with a 12 $\frac{1}{4}$ -in. roller-reamer assembly to remove any ledges in the hole that might prevent the casing from being run to the bottom of the hole. An increase in torque downhole was an indication that the reamers were cutting a ledge away. We cleaned out the hole to a depth of 34 mbsf. The bit was tripped from the casing shoe to the bottom of the hole several times to ensure that the hole was open.

The 10 $\frac{3}{4}$ -in. casing string was made up to a 11 $\frac{3}{4}$ -in. casing hanger and running assembly. The special Hydril Tripleseal connections on the casing made up very easily. Each joint was drifted after being made up to ensure that the light-weight casing was not crushed while being tightened to the specified make up torque of 12,000 lb. All casing connections were locked with a thread adhesive and were tack welded. The hex kelly running tool and stinger assembly (the bumper sub/drill-pipe assembly that is run inside the casing to allow cement to be pumped out of the casing shoe and up around the casing) was made up and latched into place.

For this reentry, the television system was used without the sonar system, because of the limited amount of casing to be run. With longer casing strings, the driller can see a loss in the string-weight indicator as being an indication that the casing assembly is released, however, this was not possible with the light-weight string used in Hole 648B. A television centralizing sleeve was installed on top of the hex kelly landing-tool nut to facilitate passage of the television system frame over the casing hanger assembly and down onto the casing to position the television low enough (12–15 m off bottom) to be in camera range during reentry.

The casing assembly and television-centralizing sub were lowered 300 m below the keel, and the television system frame with a 27-in. inner-diameter running sleeve was run down the drill pipe to ensure that the television system frame passed freely over the hanger assembly. The television system was pulled back to the surface, and the casing run to the seafloor. The system was picked up and run down over the casing hanger and positioned for reentry on the casing. After reentry was made, the casing was slowly lowered into the hole. We encountered a restriction at 28 mbsf. The casing was picked up and slowly worked past the restriction. The casing shoe was lowered to a depth of

28 mbsf, the casing hanger was latched into the throat of the reentry cone, and the casing hanger was released from the drill pipe.

Television was used to visually verify that the casing hanger was properly latched in and released. Visual monitoring also minimized the chances of crushing or bending the casing during the reentry operation. When making a sonar reentry the drill pipe is lowered rapidly, which for this maneuver could have damaged the light-weight casing. The faster the casing is lowered into the hole the more likely that damage might result. Excellent television visibility, coupled with precise movements using the ship's dynamic-positioning system, allowed the casing to be run into the hole and be released safely and efficiently.

After the casing had been cemented in place, a 9 $\frac{1}{2}$ -in. tri-cone bit was used to drill out the casing shoe and to clean out the hole to a depth of 47 mbsf. Several check trips were made to examine the area from the bottom of the casing to the bottom of the hole. No fill or rubble was encountered. It appeared that the zone between 13 and 28 mbsf had been the major source of rubble that had repeatedly filled the hole after each core-bit run. Running casing to 28 mbsf isolated the major source of rubble and made it possible to continue coring operations. The 10 $\frac{3}{4}$ -in. casing string also vastly improved hole-cleaning capabilities by isolating the large-diameter hole sections in the upper part of the hole.

A 9 $\frac{1}{2}$ -in. core bit and a coring BHA were picked up and run into the hole. The hole was reamed several times between 42 and 47 mbsf after a tight spot was encountered at 42 mbsf. Again, there was no evidence of rubble falling into the hole, and a core was cut to a depth of 50.5 mbsf, making 1 m of new hole (Fig. 10). The cone lost on core bit run 6 was assumed to have been either milled or drilled up.

At 50.5 mbsf, the bit stalled out on the bottom, and when it was picked up to reestablish rotation, we noted an overpull of 100,000 lb. We exerted an increased overpull of 250,000 lb on the pipe, but the bit remained stuck in the hole. The pipe was continually worked for 31 hr to 44 mbsf with as much as 250,000-lb overpull exerted on the drill string. It seemed that a rock or possibly the core-bit cone in the hole had wedged between the bit and the side of the hole. This was evidenced by the fact that as much as 1000 gal/min of fluid could be circulated past the bit. If large amounts of rubble had been packed off around the bit, the flow rate would have been restricted.

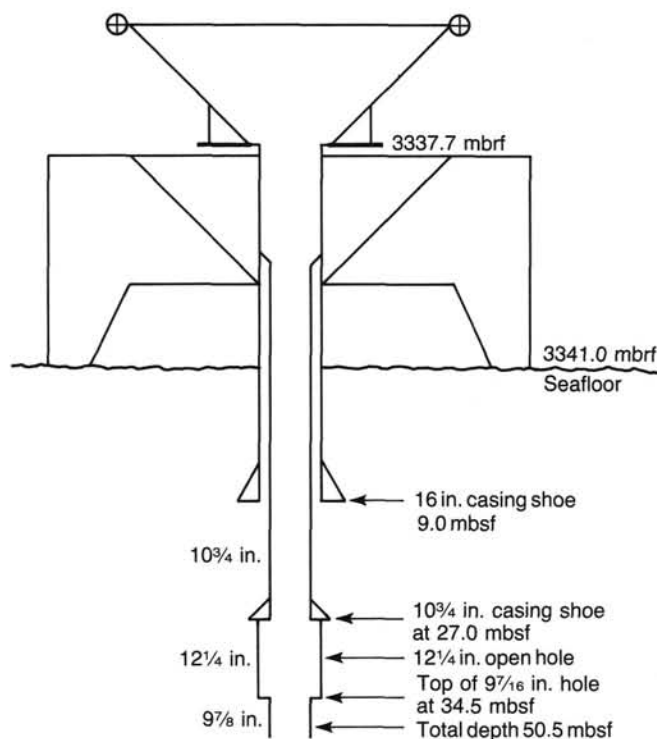
Because of the lack of progress made in freeing the pipe using conventional techniques, we decided to run an explosive charge out of the end of the bit and to detonate it, in hopes that the concussion from the explosion would free the stuck pipe. Thus, an explosive charge (a severing tool rigged up on a core barrel) was run down the drill pipe and was carefully run out of the bit and positioned 2 m below the bit. The charge was detonated while pulling a 250,000-lb overpull on the drill string. No immediate movement of the pipe was noted after detonation. The pipe was continually worked for approximately 2 hr. It gradually came free with an overpull of 250,000 lb.

Drilling operations were suspended at Hole 648B after the pipe had been freed. The current configuration of the hole is shown in Figure 10. To continue operations in Hole 648B, it will be necessary to make a mill run to remove the cone from the hole, after which coring operations may be resumed cautiously with the use of drilling jars.

Conclusions and Recommendations

Borehole Considerations

Reduced hole sizes and hole annuli considerably improve hole stability and hole-cleaning capability.



Note: Cone left in hole came from 9 $\frac{7}{8}$ in. core bit CC-7.

Figure 10. Present configuration of Hole 648B.

Drilling and Core Bits

The two 9 $\frac{7}{8}$ -in. core-bit designs resulted in a considerable increase in bit life. Core bits run on Leg 106 had an average bit life of 6 hr. The new core bits designed for use on Leg 109 were calculated to have a bit life > 12 hr.

Both the type 7 conical and type 75 chisel structures held up well under the adverse drilling conditions. The tungsten carbide wear buttons and the hardfacing applied to the shirttail area and along the leading edge of the bit legs provide considerable wear resistance. The increase in bit life can most likely be attributed to the wear-protection design features. Penetration rates for both core-bit designs (type 7 and type 75) averaged 2 m/hr.

The 12 $\frac{1}{4}$ -in. Q7JSL tricone bits also held up well in the hole. The tungsten carbide wear pads and wear buttons in the shirttail area and along the leading edge of bit legs provided considerable wear resistance. Penetration rate for the 12 $\frac{1}{4}$ -in. core bits was 1.2 m/hr.

The limiting factors for both the 9 $\frac{7}{8}$ -in. core bits and the 12 $\frac{1}{4}$ -in. hard-formation drill bits were the lack of adequate drilling weight and the limited torque that could be applied to the bit while drilling unstable hole intervals.

12 $\frac{1}{4}$ -in. Packed-Hole Drilling/Reaming Assembly

The 12 $\frac{1}{4}$ -in. reamer assembly run with the 9 $\frac{1}{2}$ -in. drill collars and the 12 $\frac{1}{2}$ -in. Q7JSL drill bit appeared to help minimize hole disturbance and to allow the bit to run smoothly while reaming the existing 12 $\frac{1}{4}$ -in. hole and while drilling out the cement. However, when the bit-reamer assembly encountered new hole, excessive torque was required to maintain bit rotation. It is therefore questionable whether this type of drilling assembly could be safely used for a making new hole without having the BHA adequately supported.

Specialized Cementing Techniques

Unstable hole conditions were experienced to varying degrees during all phases of drilling and coring operations. In an effort to enhance hole stability, open-hole cement plugs were pumped frequently at the end of selected bit runs. The cement plugs prevented the hole from caving in when the bits were pulled from the hole and cemented together fractures in the hole wall. The cement plugs provided enough stabilization to the upper part of the hole to allow limited coring operations. The cement plugs also provided enough temporary hole stability to allow casing to be successfully run to 28 mbsf. Had the special cementing techniques not been used, drilling operations would have been suspended before running the casing.

10 $\frac{3}{4}$ -in. Casing Hardware

The 10 $\frac{3}{4}$ -in. casing string worked well with the 11 $\frac{3}{4}$ -in. casing hanger. The limited clearance between the inside diameter of the casing and the 9 $\frac{7}{8}$ -in. bit (0.040 in. radially) was found to be adequate.

Prototype Television-Sonar System Running Hardware For Casing Reentry

The prototype centralizing sleeve for the 11 $\frac{3}{4}$ -in. casing hanger and the 27-in. inner-diameter running sleeve for the television-sonar system worked as designed. The frame passed freely in both directions over the casing-hanger assembly and enabled the system to be positioned down on the 10 $\frac{3}{4}$ -in. casing at the desired depth to make a safe and effective reentry.

Explosive Charges in Well Bore to Free Stuck Pipe

The technique of using an explosive charge outside the bit appears to be a viable measure if no other jarring force is available. It should be noted that this type of technique should only be used as a last resort before severing a drill pipe that is stuck in the hole.

Drilling Jars

Both the mechanical and hydraulic drilling jars had insufficient strength for aggressive drilling when unsupported above the seafloor. A hydraulic jar and a mechanical torque jar failed in the hole, resulting in two time-consuming fishing operations. The jars are of proven designs and have been used in the oil industry for many years. Development of a special set of drill jars will be required for future unsupported drilling. It should be noted that the mechanical and hydraulic jars were used successfully numerous times during supported downhole drilling in Hole 648B.

Special Fishing and Reentry Techniques

The 1-m-diameter funnel attached to the bottom of the fishing tools was a highly effective guide for making "reverse reentries" onto the jar mandrel protruding above the reentry cone. The television-sonar system and the ship's dynamic-positioning system were used during such operations.

The 1-m-diameter guide funnel represents a reentry target area that is approximately 95% smaller than that of a standard reentry cone. The scale of making a reentry into a 1-m-diameter target in 3341 m of water could be compared to standing on the top of a 43-m-tall derrick and trying to thread the 1-mm-diameter eye of a needle at the foot of the derrick.

Drilling Fluids

The viscous slugs of bentonite (gel) and XP polymer were pumped in individual volumes of 25–100 bbl in an effort to improve hole cleaning in Hole 648B. Although the results were

variable, the overall effectiveness of this technique, as on Leg 106, was at best marginal. Owing to the large-diameter hole sections in the upper hole, effective annular velocities were degraded below the effective slip velocities of cuttings that were being swept from the hole. Table 2 presents statistics on the coring and drilling operations at Hole 648B. The low core recovery rate can be attributed to the large amount of rubble that had to be redrilled on each core bit run.

Considerations for Future Unsupported Hard Rock Drilling

The following comments are intended to reflect current thoughts about drilling hard rock and are based on the recent drilling and coring operations conducted in Hole 648B during Leg 109.

To continue drilling operations in Hole 648B, or possibly to drill other sites with similar geological features, emphasis must be placed on drilling smaller diameter holes. Significant improvements were noted when the hole size was reduced from 12¼ in. to 9¾ in. in diameter. It can be expected that reducing the hole size further would result in continued improvement in drilling conditions. This would necessitate developing specially sized drill bits, drill collars, and casing not currently in the suite of tools utilized by the Ocean Drilling Program. The use of high-speed, small-diameter diamond bits powered by downhole motors and turbines capable of being run down inside the drill string in a manner similar to that of the current ODP coring systems (HPC, APC, XCB) should be considered. A system of this type is now in preliminary stages of development.

The guidebase has proven effective in spudding a hole on hard rock with only minimal support for the BHA. The drilling techniques used to date have provided reasonable penetration rates. However, the pacing factor in drilling young, fractured basalt formations is the lack of hole stability. Early emphasis needs to be placed on a means of addressing the unstable hole conditions and on establishing the upper strings of casing. If this can be accomplished, realistic progress in terms of hole cored could be realized on a single leg of drilling at future hard-rock drilling sites.

Table 2. Statistics for coring and drilling operations, Hole 648B, Leg 109.

Basalt/basalt rubble cored	66.25 m
Basalt recovered	5.15 m
Cement cored	39.0 m
Cement recovered	12.45 m
Rubble and cement drilled with 12¼-in. Q7JSL bits	60.0 m
Milled with 12¼-in. and 9¾-in. junk mills	13.2 m
Total meters drilled and cored, includes drilling fill and rubble. Does not include redrilling intervals on same bit run.	165.3 m
Rotating time: four 12¼-in. tricone bits Q7JSL Smith one 9¾-in. tricone bit FDGH Smith one 12¼-in. concave junk mill one 9¾-in. concave junk mill	87.5 hr
Coring time: five 9¾-in. RBI type 75 core bits two 9¾-in. RBI type 7 core bits	57 hr
Miscellaneous:	
> 112 km of pipe were tripped during operations at Hole 648B, Leg 109.	
175 bbl of cement were pumped to enhance hole stability.	
3256 bbl of gel and XP polymer were pumped to clean the hole.	
Average penetration rate of 9¾-in. core bits = 2.2 m/hr in cement/basalt rubble.	
Average penetration rate of 9¾-in. core bits = 2 m/hr in basalt (new hole).	
Average penetration rate of 12¼-in. Q7JSL bits = 1.2 m/hr in cement/basalt rubble.	

LITHOSTRATIGRAPHY

Two holes were drilled at Site 648 on the summit plateau of Serocki Volcano. Most of the area is covered by a very thin layer of sediment on the order of a few tens of centimeters thick; generally, the tops of pillow lavas and fresh flows are completely bare. The exposed basement consists of pillow basalts of varying size with rare sheet flows. Several north-south-trending fissures dissect the area.

Hole 648A was drilled between several large pillow lavas (about 1.5 m high) adjacent to a small fissure. A total penetration of 4.5 mbsf resulted in the recovery of three small pieces of basalt rubble equivalent to a recovery rate of 1.6% (Table 1). Low recovery was probably due to the "walking" action of the unsupported Navidrill, which created a pit several meters across.

Hole 648B, drilled following the successful deployment of the new hard-rock guidebase is in an area of pillow lavas dissected by several small fissures, one of which passed under the guidebase. The basement was extremely difficult to drill; the hole collapsed repeatedly, requiring occasional cleaning and re-drilling. A total penetration of 50.5 mbsf resulted in the recovery of 11.35 m of basalt rubble and oriented core (Table 1). The first 6.6 m of basement was deliberately not cored so as to maximize the chances of successfully establishing a hole under difficult drilling conditions.

Most of the basalts recovered on both legs represent cored rubble, although Cores 109-648B-15R, 109-648B-16R, and 109-648B-18R contain long pieces of massive basalt (as long as 30 cm) that could have been cored *in-situ*.

Hole 648A

Three pieces of sparsely plagioclase phyric basalt, two of which contain fresh glass, were recovered from this hole. The recovery represents pieces of unaltered pillow basalt belonging to a single lithologic unit (Fig. 11).

Hole 648B

Three lithological types were identified in the rocks recovered from Hole 648B. These are (1) aphyric to sparsely olivine-plagioclase phyric basalt with a fine-grained groundmass and <1% vesicles; (2) vesicular, sparsely olivine-plagioclase phyric basalt with as much as 10% empty vesicles; some pieces have a glassy margin and smaller and fewer vesicles; and, (3) massive holo-

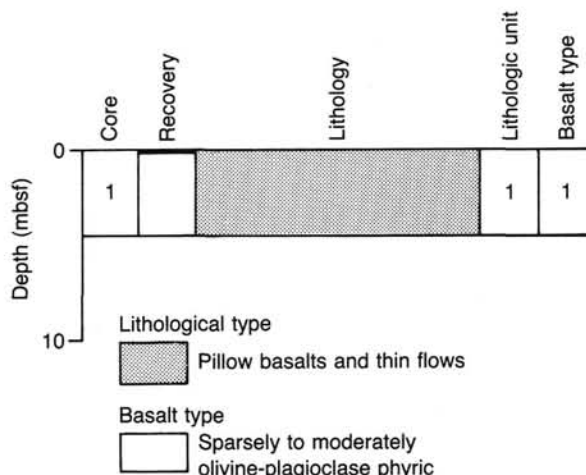


Figure 11. Proposed lithostratigraphy of Hole 648A.

crystalline, sparsely olivine-plagioclase phyric basalt with <1% vesicles.

The three lithological types appear in this order in the hole from top to bottom although pieces from types 1 and 2 are frequently found in the deeper cores as a result of coring rubble that fell into the hole. It is extremely difficult to establish a precise lithological sequence because of repeated sloughing of material into the hole between pipe trips. We cannot define cooling units in the material recovered since most of it represents rubble. However, a careful comparison of basalts recovered from the different cores from both legs allows us to propose a succession (Fig. 12). The constraint on the depth and thickness of the vesicular unit was determined by comparing Cores 106-648B-6R and 109-648B-15R which both contain the same vesicular basalt. We exclude the existence of two vesicular units because the vesicle content and size and the phenocryst content and size in Cores 106-648B-6R and 109-648B-15R overlap completely (Fig. 13). Moreover, the textural characteristics of the units that lie above and below the vesicular unit are comparable.

If we are correct, the lithological succession in Hole 648B could be as follows, from top to bottom:

1. The upper 30 m are interpreted as being pillow lavas, as evidenced by television surveys of the seafloor and by the glassy to variolitic margins recovered in the basalt pieces from this interval. Moreover, observations made by submersible in the central caldera of Serocki Volcano confirm that at least the upper

30 m of the section is composed of pillow lavas. Talus obscures the section below this depth.

2. The vesicular basalt that was assigned a thickness of about 3 m has no definable relationship with the overlying pillow basalts and probably represents the top of a massive flow or ponded lava. In Core 106-648B-6R, the vesicular basalt shows a progressive textural transition to the underlying massive holocrystalline basalts. Magnetic data, however, indicate a systematic difference in angle of about 30° for the magnetic vector between the vesicular basalt (three measurements) and the holocrystalline massive basalt (four measurements). If we accept the textural evidence that both facies were erupted as a single flow unit, the magnetic data indicate that at least some magmatic or tectonic event disturbed the initial continuity between both facies.

3. The holocrystalline basalt probably makes up the lower 17.5 m of the hole, although recovery from this section was very poor.

As bathymetric charts indicate, the height of Serocki Volcano is about 50–60 m above the surrounding floor of the rift valley; we infer that Hole 648B must have penetrated virtually through the volcano. This is confirmed by submersible dives into the central caldera of the volcano, the bottom of which is about 60 m below its rim. Talus obscures the walls below 30 mbsf, but where exposed, the floor consists of basalt flows. The massive basalts recovered by drilling could represent either ponded

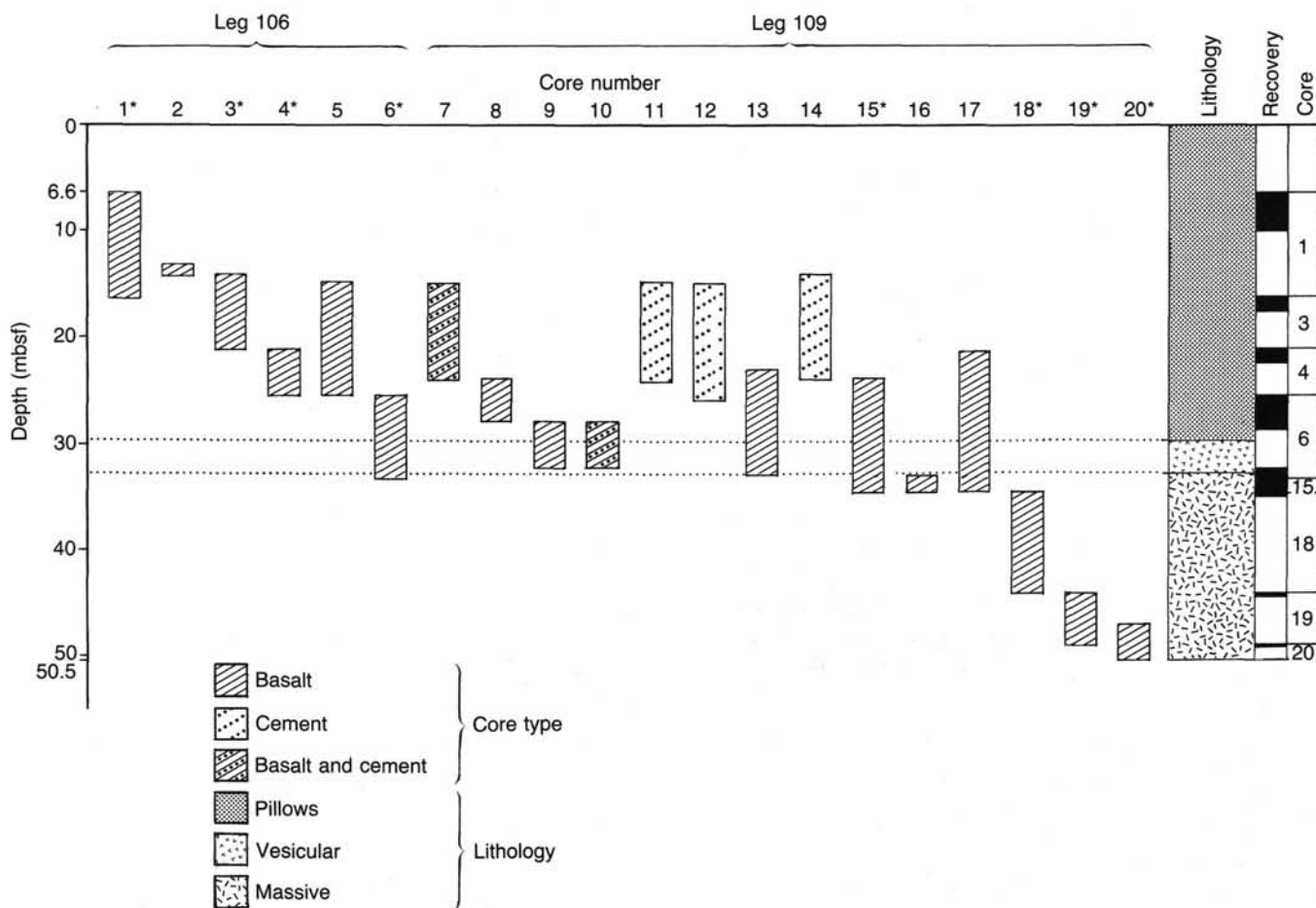


Figure 12. Proposed lithostratigraphy of Hole 648B. The stratigraphic position of each core is shown. Cores marked by an asterisk denote recovery from *in-situ* basement. Shaded intervals in the "Recovery" column show total recovery from corresponding section of hole. Cores that advanced the hole are numbered in the "Core" column.

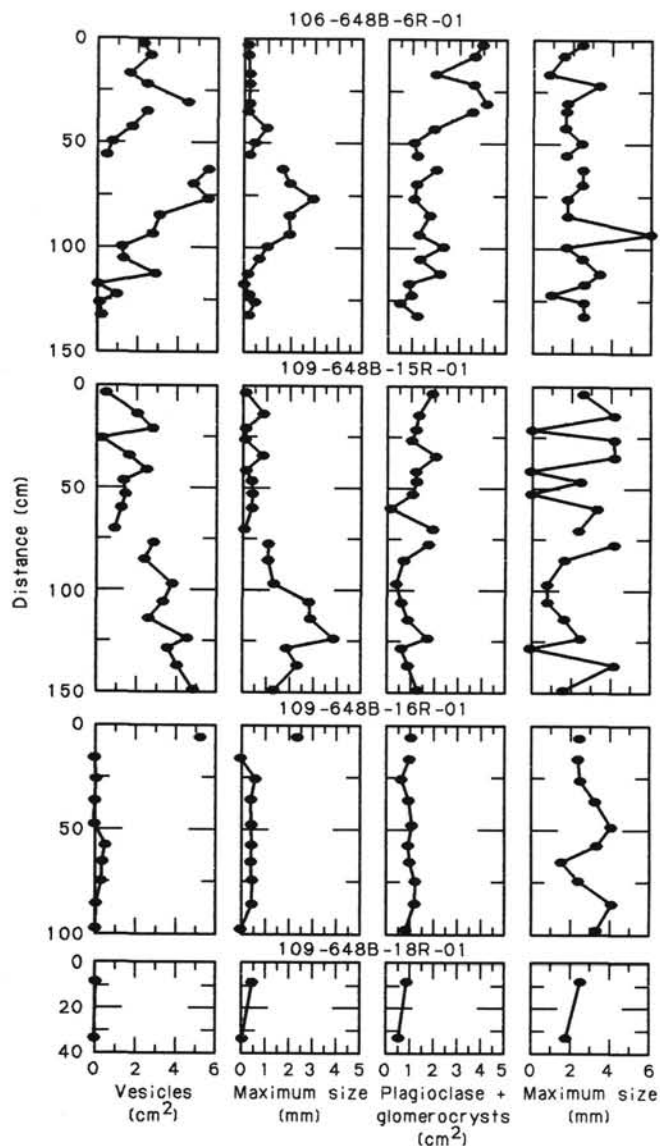


Figure 13. Variation in macroscopic textural characteristics of lavas in Hole 648B cores that sampled the vesicular and underlying massive lithologic units. Concentrations of vesicles and plagioclase glomerocrysts per unit area were obtained by counting all vesicles and glomerocrysts + phenocrysts on the sawed core surface and dividing the totals by the surface area. The maximum plagioclase dimension was always represented by the length of glomerocrystic aggregates. Solid lines connect textural characteristics of samples assigned to the same stratigraphic unit in the visual core-descriptions forms. In both Core 106-648B-6R and Cores 109-648B-15R through 109-648B-18R, the vesicle and plagioclase textures of the vesicular unit and the units that lie directly below and above it are similar.

lava or an intrusive body. (Note: The units shown on the visual core-description forms were defined by changes in grain size, occurrence of glassy margins, and/or variation in phenocryst percentage and assemblages. Because a large proportion of the basalts recovered from the hole represents cored rubble, the units have only limited lithological meaning.)

PETROGRAPHY

All basalts recovered from Site 648 are of one petrographic type: sparsely to moderately plagioclase-olivine phyric basalt.

The groundmass ranges from cryptocrystalline to fine grained. Textures are intergranular to subophitic, the intergranular and variolitic textures being most abundant.

Phenocrysts

Phenocryst abundances average 4% in plagioclase (range = <1%–10%) and 1% in olivine (range = 0%–5%; Table 3). Clinopyroxene occurs only rarely as a phenocryst phase in glomerocrysts with plagioclase and olivine and is anhedral with an average size of 0.35 mm. Spinel is absent in these basalts.

Plagioclase and olivine phenocrysts may occur singly, but more often they occur in glomerocrysts (Fig. 14). Phase proportions in glomerocrysts typically are plagioclase/olivine = 3/1. Present also are plagioclase-rich glomerocrysts, which include only minor amounts of olivine (Fig. 15) and olivine-rich glomerocrysts containing plagioclase and olivine in subequal proportions. None of the observed phenocrysts show evidence of internal deformation that would suggest they are xenolithic fragments of tectonized cumulates.

Plagioclase is the only phenocryst phase that is clearly visible in hand specimen. It occurs both as isolated phenocrysts and in glomerocrysts with olivine (average 1.5 mm measured perpendicular to (010)). The crystals range as large as 5 mm and are subhedral to euhedral with core compositions of approximately An_{80} (on the basis of combined Carlsbad-albite twins). Plagioclase phenocrysts exhibit complex morphologies and compositional zoning (see, for example, Fig. 16). Well-developed sector zoning in plagioclase (Fig. 17) is observed in some subvariolic samples and is typical of rapidly cooled pillow lavas (Bryan, 1974). Phenocrysts in individual samples exhibit a variety of zoning patterns, including (1) unzoned cores that may be euhedral or rounded and embayed and surrounded by oscillatory zones and/or a narrow normally zoned rim, (2) skeletal cores that enclose cryptocrystalline melt inclusions and often show patchy zoning surrounded by a normally zoned rim, and (3) euhedral or rounded and embayed cores (Fig. 18) surrounded by a skeletal zone enclosing trapped patches of groundmass. Such variability in zoning patterns has previously been interpreted as evidence of mixing of two or more magmas (Dungan et al., 1978).

Olivine phenocrysts are less common (typically about 1% by volume) and mostly occur in glomerocrysts with plagioclase, although in some samples (e.g., Samples 106-648A-1R-1, 2–4 cm, and 106-648B-1R-2, 37–40 cm) isolated phenocrysts are present. They are all euhedral to subhedral and range in size from 0.1 to 1.0 mm (average 0.5 mm), cryptocrystalline melt inclusions being present in some of the larger phenocrysts (e.g., Sample 106-648B-3R-1, 3–6 cm). X-ray-diffraction analysis of two olivine phyric samples suggests that olivine phenocryst compositions are approximately Fo_{80} (Yoder and Sahama, 1957).

Groundmass

In the groundmass of intergranular-textured samples, average modal abundances are 45% plagioclase, 42% clinopyroxene, 6% opaque minerals, \pm 1% olivine (Table 3 and Fig. 19). Plagioclase is acicular to lath-shaped and euhedral, grain sizes being 0.01–0.5 mm. Hopper and swallowtail plagioclase is observed but not as frequently as in variolitic samples. Clinopyroxene is subequant or acicular to dendritic. Certain samples have groundmass textures grading from intergranular to interstitial. In parts of these samples, interstitial areas are filled by small pools of dark-brown glass containing tiny needles of plagioclase, clinopyroxene, and opaque minerals.

The groundmass of rocks with subvariolic to variolitic textures consists primarily (72%–84%) of a micro- to cryptocrystalline mixture of acicular plagioclase (0.01–0.03 mm), dendritic to plumose clinopyroxene, small pools of glass, and granular

Table 3. Modal proportions of phenocryst and groundmass phases.

Sample	Texture	Phenocryst			Groundmass					Secondary mineral	
		Plag	Ol	Cpx	Plag	Ol	Cpx	Opaq	Mesostasis		Vesicles
106-648B-1R-1, 02-04, cm	SV	1	<1	0	—	—	—	—	—	S	tr.
106-648B-1R-1, 20-23, cm	GP-IS-IG	4	1	0	43	2	39	8	2	^a S	—
106-648B-1R-1, 30-33, cm	GP-IS-IG	4	1	0	43	1	43	4	4	S	—
106-648B-1R-1, 59-62, cm	GP-SV-IS	3	1	0	—	—	—	—	—	S	—
106-648B-1R-2, 37-40, cm	GP-SV	3	1	tr.	—	—	—	—	—	S	—
106-648B-1R-2, 114-117, cm	GP-IS-IG	4	1	0	—	—	—	—	—	^a S	<1
106-648B-1R-2, 117-120, cm	GP-SV	4	1	0	—	—	—	—	—	^a S	—
106-648B-1R-3, 26-29, cm	GP-SV	3	<1	0	—	—	—	—	—	^a S	tr.
106-648B-2R-1, 14-16, cm	GP-SV	1	1	0	—	—	—	—	—	S	<1
106-648B-3R-1, 03-06, cm	GP-SV	4	2	0	—	—	—	—	—	S	tr.
106-648B-3R-1, 31-34, cm	GP-IG	5	1	0	—	—	—	—	—	S	tr.
106-648B-3R-1, 74-77, cm	P-SV	4	<1	0	—	—	—	—	—	S	—
106-648B-4R-1, 40-42, cm	GP-SV	7	<1	0	—	—	—	—	—	^a S	—
106-648B-4R-1, 53-55, cm	IS-IG	10	1	0	—	—	—	—	—	S	—
106-648B-6R-1, 57-60, cm	GP-IG	7	<1	0	38	1	44	7	3	S	—
106-648B-6R-1, 78-81, cm	IG	4	<1	0	—	—	—	—	—	A	—
106-648B-6R-1, 129-131, cm	IG	4	1	0	—	—	—	—	—	—	—
106-648B-6R-1, 132-135, cm	IG	4	1	0	47	5	31	5	8	S	—
109-648B-8R-1, 68-70, cm	IG-GP	8	2	0	32	0	47	10	<1	S	2
109-648B-9R-1, 17-22, cm	SV	2	<1	0	14	0	0	0	84	S	—
109-648B-9R-1, 69-71, cm	SV-GP	3	<1	0	15	0	21	10	51	M	<2
109-648B-9R-1, 80-82, cm	IG-SV	2	<1	0	44	0	50	3	0	M	—
109-648B-13R-1, 00-03, cm	SV	2	1	0	19	0	0	0	79	S	—
109-648B-13R-1, 11-13, cm	IG-SV	2	<1	0	42	<1	47	8	<1	S	—
109-648B-15R-1, 33-37, cm	SV-GP	7	1	0	17	0	0	0	76	S	—
109-648B-15R-1, 111-113, cm	IG-SV	5	<1	0	39	<1	46	8	2	^a A	—
109-648B-15R-1, 120-123, cm	IG-SV	<1	<1	0	52	<1	42	5	0	M	—
109-648B-16R-1, 02-05, cm	IG-GP	2	<1	0	34	0	39	1	24	^a A	2
109-648B-16R-1, 48-50, cm	IG	3	2	0	55	1	37	8	0	S	—
109-648B-17R-1, 22-24, cm	IG-GP	3	1	0	47	1	42	6	0	0	—
109-648B-18R-1, 00-02, cm	SO-SR	3	<1	0	46	7	26	6	12	S	tr.
109-648B-18R-1, 38-40, cm	IG-IS-HC	2	<1	0	44	2	39	8	^b 4	0	—
109-648B-19R-1, 13-15, cm	IG-IS	1	0	0	44	2	43	7	^b 3	0	—
109-648B-20R-1, 48-50, cm	TR-PT	3	<1	0	41	1	15	0	39	0	—

Textures: GL = glomeroporphyritic, HC = hypocrySTALLINE, IG = intergranular, IS = intersertal, P = porphyritic, PT = pylotaxitic, SO = subophitic, SR = seriate, SV = subvariolic, TR = trachytic.

Vesicles: S—sparse, <1-2%; M—moderate, 3-5%; A—abundant, 6-10%.

Modes are based on 1500 points (samples 1R-1 to 6R-1) or 1000 points (samples 8R-1 to 20R-1), counted on 0.5-mm grid spacing.

^a presence of segregation vesicles.

^b glass.

Plag—plagioclase; Ol—olivine; Cpx—clinopyroxene; Opaq—opaques (general abundance of opaque minerals is titanomagnetite > ilmenite >> sulfide); tr—trace.

Phenocryst category includes phenocrysts and xenocrysts obviously larger than groundmass phases. Typical size ranges are Plag, 0.5-2.5 mm; Ol, 0.1-0.8 mm. Groundmass Plag includes microphenocrysts, typically 0.05-0.3 mm.

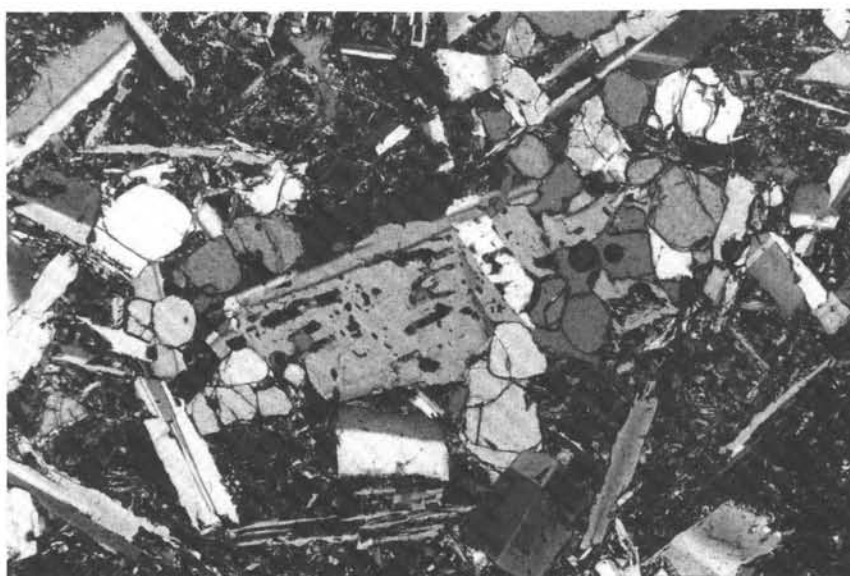


Figure 14. Typical glomerocryst composed of equant olivine grains (gray) and plagioclase laths (twinned). Crossed polars. Field of view = 3 mm. Sample 109-648B-8R-1, 68-70 cm.

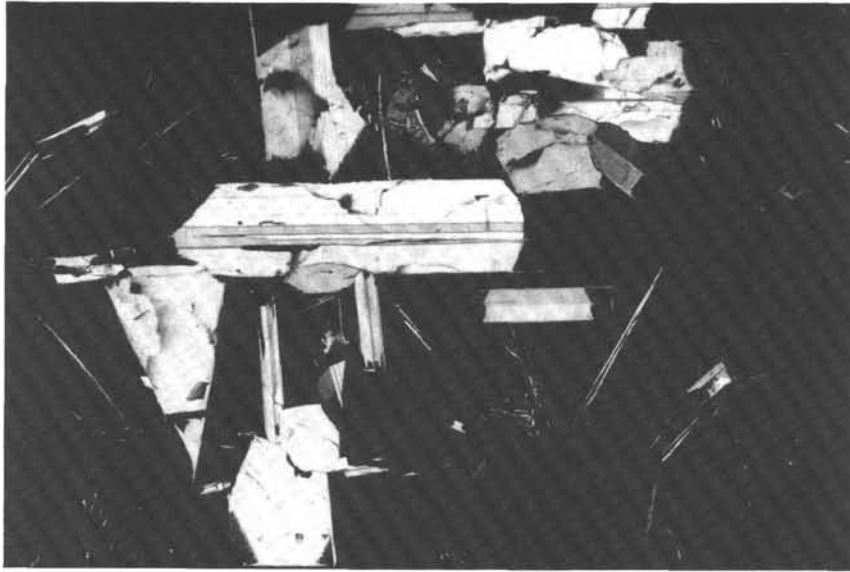


Figure 15. Plagioclase-rich glomerocryst. A small olivine fragment is present below the large plagioclase lath. Crossed polars. Field of view = 3 mm. Sample 109-648B-15R-1, 33-37 cm.



Figure 16. Complexly zoned plagioclase phenocryst. Crossed polars. Field of view = 3 mm. Sample 109-648B-16R-1, 48-50 cm.

opaque minerals (Fig. 20). Plagioclase microphenocrysts, commonly with hopper, swallowtail, or acicular shapes, compose 14%–19% of the variolitic samples. Many of the latter two types are very elongate (length-to-width ratios of 10:1–40:1) and some display a consistent dimensional orientation. The pilotaxitic groundmass texture in Sample 109-648B-20R-1, 48–50 cm, appears to be a variant of variolitic texture. In this sample, mesostasis and dendritic clinopyroxene fill interstices between small (0.01–0.07 mm) subaligned plagioclase laths. Plagioclase phenocrysts have the same orientation as the groundmass feldspars. One sample (109-648B-18R-1, 0–2 cm) has a subophitic texture. In this fine- to medium-grained sample, the groundmass contains large (0.4–2.0 mm), optically continuous clinopyroxene

and olivine grains that fill interstices and partly enclose subhedral plagioclase laths (0.1–2.0 mm). This sample contains 7% groundmass olivine (Table 3), the most observed in the sample suite.

Opaque phases in the Hole 648B basalts are 0.001–0.10 mm in size and compose 1%–8% of the volume. They include euhedral to skeletal titanomagnetite, laths and blades of ilmenite, and small blebs of sulfide minerals (Figs. 21 through 23). The general order of abundance of these phases is titanomagnetite > ilmenite >> sulfide minerals.

Both the hand specimens and thin sections contain vesicles and miarolitic voids. Vesicles typically compose <1% of the samples but in some samples make up to 10%, with no correla-

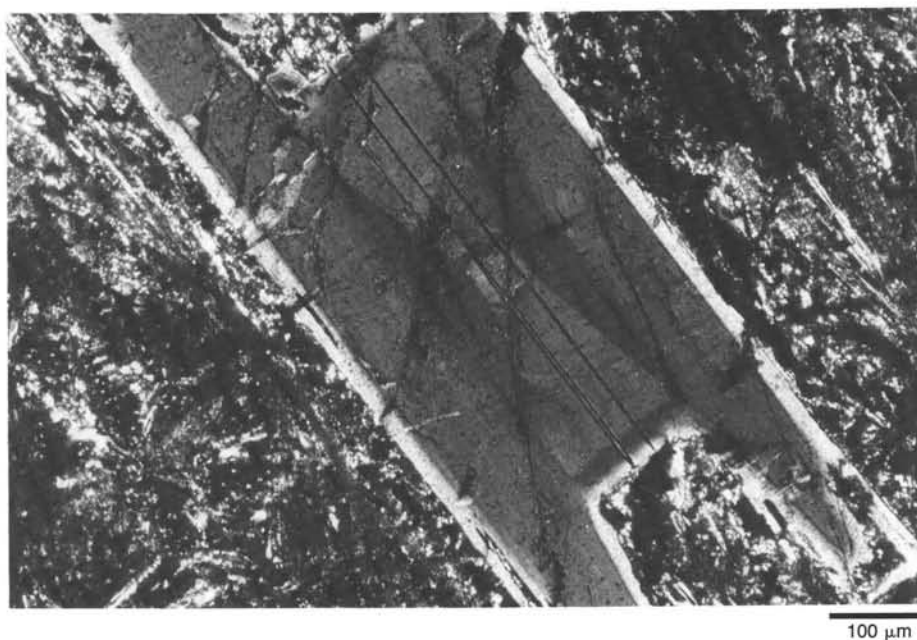


Figure 17. Sector zoning in plagioclase phenocryst with a narrow homogeneous rim in Sample 106-648B-1R-2, 37-40 cm. Crossed polars.

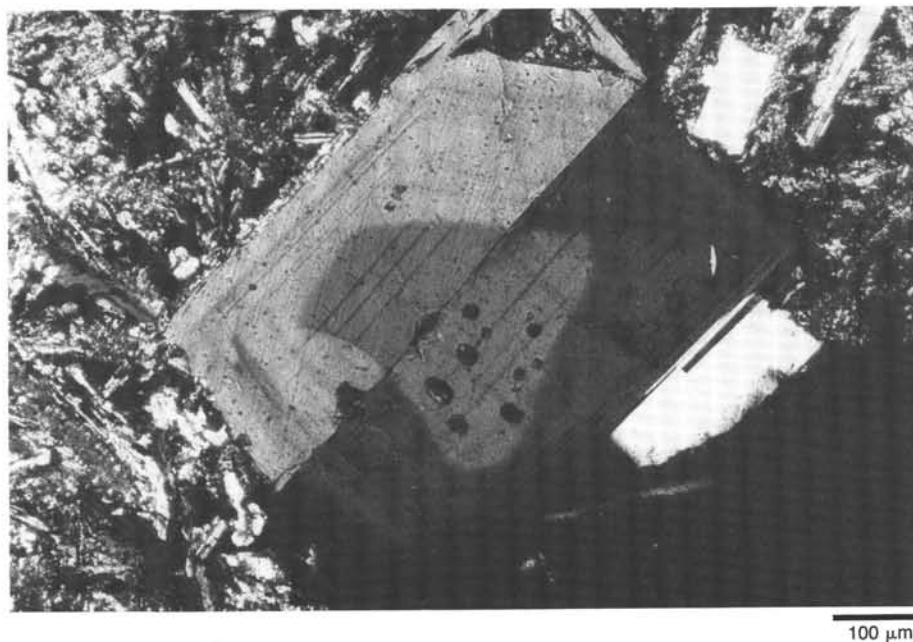


Figure 18. Plagioclase phenocryst showing resorbed core surrounded by fine-scale oscillatory zoning in Sample 106-648B-1R-2, 37-40 cm. Crossed polars.

tion apparent between vesicle abundance and groundmass texture. They range in size from 0.1 to 2.0 mm, and are generally round and empty (Fig. 24). However, the vesicles that are within alteration halos are sometimes lined with clay minerals. The interiors of some vesicles are lined with euhedral groundmass minerals that may project into the vesicle cavity (Fig. 25).

Partly or completely filled segregation vesicles (Fig. 26) make up < 1% of the groundmass volume and vary in size from 0.3 to

1.2 mm (mean = 1.0 mm). Crescents of fine-grained groundmass are seen in partly filled segregation vesicles. In individual thin sections, they commonly occur in a consistent orientation that probably indicates the gravity field in which the basalts cooled. Totally filled segregation vesicles are recognized by their darker color and finer grain size, compared with the surrounding groundmass, and are similar to those observed in Australian pillow lavas (Smith, 1968), in Leg 37 basalts (Baragar et al.,



Figure 19. Intergranular texture. Clinopyroxene (darker gray) fills interstices between plagioclase laths. Plain light. Field of view = 0.7 mm. Sample 109-648B-18R-1, 38–40 cm.



Figure 20. Subvolcanitic texture consisting of radiating sheaths of clinopyroxene with interstitial plagioclase and olivine in Sample 106-648B-1R-2, 117–120 cm. Plain light.

1977), and in Leg 46 basalts (Sato, 1978). They appear to have formed late in the crystallization history of a lava by infiltration of residual melt into vesicles that were previously filled with volatiles. According to Sato's broad-beam ($10\ \mu\text{m}$) microprobe analyses, segregation vesicles are enriched in FeO and TiO_2 compared with quenched glass and formed after 40%–60% crystallization.

Miarolitic voids are present in some Hole 648B basalts, where they typically compose < 25% of all voids. Faceted crystal faces can be seen projecting into void interiors in hand samples but are not observed in thin sections.

PETROLOGY AND GEOCHEMISTRY

Compositions of Hole 648B Basalts

In this section, chemical data on basalts recovered from Hole 648B on Legs 106 and 109 are presented. As discussed in the "Lithostratigraphy" section (this chapter), some of the same units probably were sampled by drilling operations on the two legs. Available analyses include major-element data on 11 glasses (Table 4) and major- and trace-element data on 19 whole-rock samples (Table 5). Averages and standard deviation of the analyses and some selected petrogenetic parameters are listed in Table 6.



Figure 21. Opaque phases viewed in reflected light. Three small, round, highly reflective sulfide blebs are near the center of the photograph. The other reflective phases are titanomagnetites. No ilmenite is visible in this view. Field of view = 0.5 mm. Sample 109-648B-19R-1, 13-15 cm.

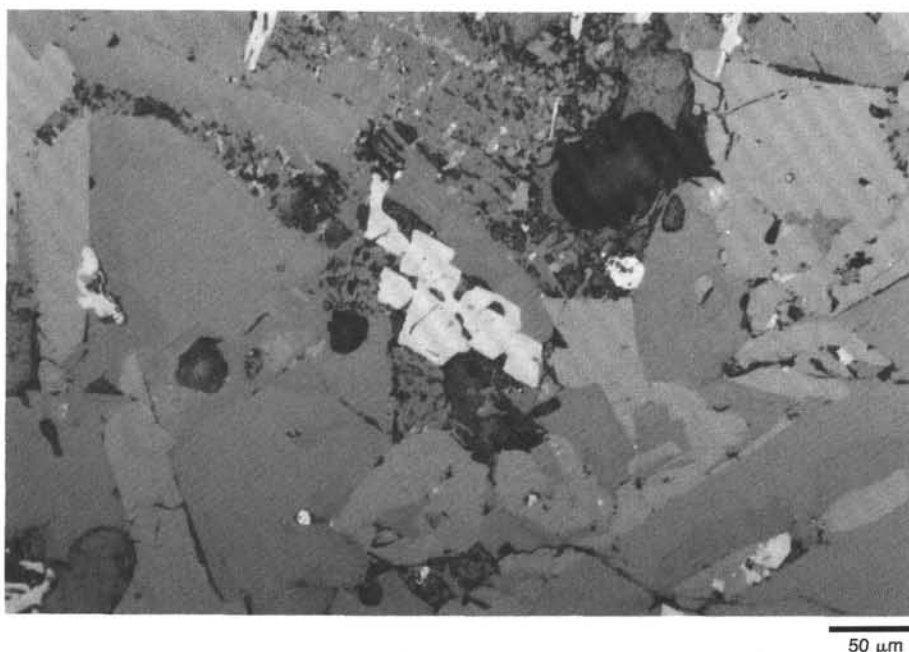


Figure 22. Grain of homogeneous titanomagnetite (center, light gray) in Sample 106-648B-6R-1, 129-131 cm. A spherule of iron sulfide (presumably pyrrhotite) is seen to the right of titanomagnetite grain (white). Reflected light.

Shown also are the composition of WHOI (Woods Hole Oceanographic Institution) sample A1192-29 and the average analyses for basalts collected in and around the KFZ and adjacent ridge axes (Bryan et al., 1981). Sample A1192-29 was collected at 23°N, on the west wall of the median valley south of the MAR-KFZ intersection. This sampling station is approximately 9 km north along strike of Hole 648B on a prominent ridge that parallels the axial valley trend (Bryan et al., 1981; Detrick et al., 1985). The KFZ averages represent the regional basalt composition near the KFZ and are useful for placing Hole 648B basalt compositions in a regional context. Compared with the KFZ av-

erage glass, Hole 648B mean glass has a slightly lower magnesium value and a higher TiO₂ content. Lower nickel and higher zirconium concentrations are present in the Hole 648B average whole rock relative to the KFZ average whole rock. The compositions of the Hole 648B average whole rock and A1192-29 are extremely similar.

The average loss on ignition (LOI) measured during preparation of XRF disks from Hole 648B whole rocks is 0.23 wt% (Table 6). For these fresh basalts, this value gives an estimate of their volatile content. The Hole 648B average falls in range of water contents (0.1-0.3 wt%) measured for other MAR basalts

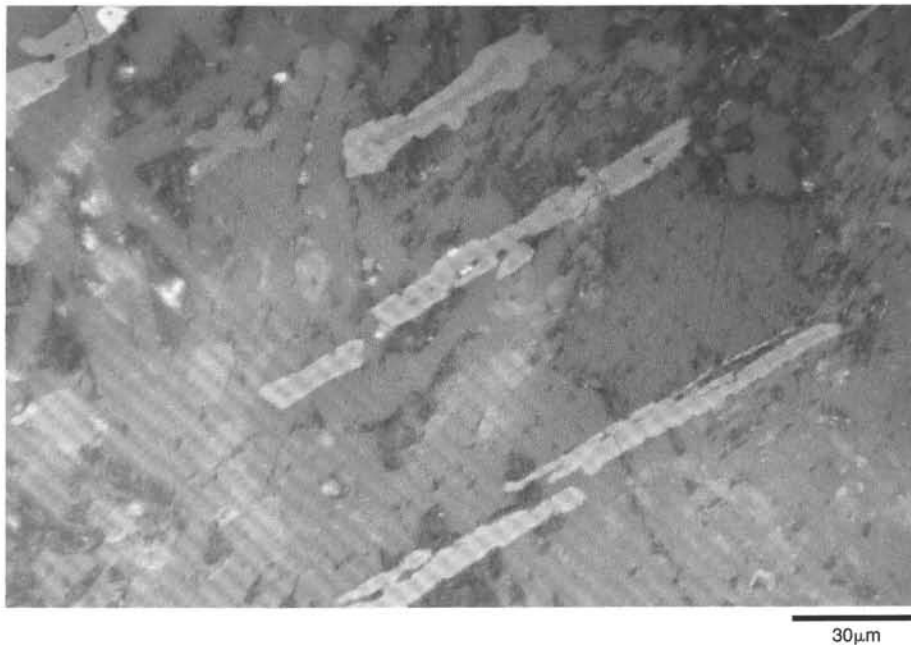


Figure 23. Laths of ilmenite/titanomagnetite in Sample 106-648B-6R-1, 129-131 cm. The central part of each lath is titanomagnetite (gray); the rim is ilmenite (light gray). Reflected light.

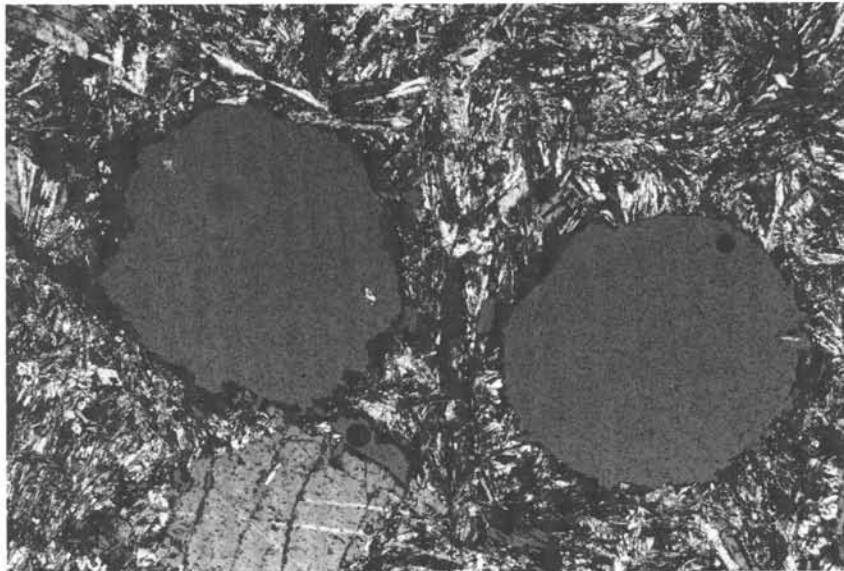


Figure 24. Round vesicles in an intergranular-textured basalt. Sample 109-648B-9R-1, 80-82 cm. Partly crossed polars. Field of view = 3 mm.

(Delaney et al., 1978). Some Hole 648B basalts contain as much as 10% vesicles, probably reflecting early CO_2 outgassing. The water depth at Hole 648B (3341 m) indicates that volatile exsolution occurred under a confining pressure of approximately 330 bar.

Coherent chemical variations are present within the Hole 648B suite. Whole-rock concentrations of TiO_2 and zirconium are positively correlated (Fig. 27). Samples recovered at the top of the pillow unit in Core 106-648B-1R (see "Lithostratigraphy" section, this chapter) are enriched in incompatible elements relative to the other samples. The massive unit sample has the lowest zirconium and TiO_2 contents. A negative correlation exists between magnesium values and TiO_2 concentrations (Fig. 28).

Glasses contain the most TiO_2 and have low magnesium values. The pillow unit basalts span the entire compositional range present in the data set, whereas massive unit basalt compositions are restricted to low TiO_2 and higher magnesium values.

In a plagioclase-clinopyroxene-quartz (PLAG-CPX-QTZ) subprojection from olivine (OL) in the pseudoquaternary OL-PLAG-CPX-QTZ system, the Hole 648B basalts plot in a tight cluster in the OL + PLAG + liquid (LIQ) field (Fig. 29). These basalts are well removed from the experimentally determined 1 atmosphere OL + PLAG + LIQ multiple-saturation boundary, which is consistent with the absence of clinopyroxene phenocrysts in the lavas. Comparison of the experimentally determined phase boundary and the Hole 648B data cluster indicates



Figure 25. Scanning electron microscope image of the interior of a vesicle in Sample 109-648B-15R-1, 120–122 cm. The large, girderlike grains are plagioclase, the hollow diamond-shaped grains are clinopyroxene. The parallel fine dendrites are intergrown plagioclase and clinopyroxene. Lighter colored, equant, euhedral plates intergrown with the dendrites are ilmenite and/or magnetite. Field of view = 50 μm .



Figure 26. Segregation vesicle with disrupted wall. Note flow of groundmass into vesicle. Sample 106-648B-1R-3, 26–29 cm. Plain light.

that approximately 20% crystallization is required to drive the basalts to three-phase saturation at 1 atmosphere.

An equilibrium olivine composition of $\text{Fo}_{81.5}$ can be calculated from the Hole 648B average glass composition and $K_D = 0.3$ ($K_D = (X_{\text{FeO}}/X_{\text{MgO}})^{\text{ol}} \times (X_{\text{MgO}}/X_{\text{FeO}})^{\text{glass}}$; Roeder and Emshie, 1970). This value agrees well with estimates of olivine phe-

nocryst compositions noted in the "Petrography" section (this chapter), suggesting that the Hole 648B olivines are in equilibrium with their host lavas. Equilibrium plagioclase compositions of An_{71-73} are calculated from the average Hole 648B glass and whole rock and $K_D = 1.2$ ($K_D = (X_{\text{Ca}}/X_{\text{Na}})^{\text{plag}} \times (X_{\text{Na}}/X_{\text{Ca}})^{\text{liq}}$; Grove and Bryan, 1983). Although these values lie within

Table 4. Microprobe analyses of Site 648 glasses and standards^a.

wt %	Hole 648A		Hole 648B									Reference standards			
	1R-1 10-11 cm	1R-1 12-13 cm	1R-1 37-38 cm	1R-1 50 cm	1R-3 92 cm	3R-1 84 cm	4R-1 65 cm	6R-1 25 cm	8R-1 34-37 cm	17R-1 30-31 cm	17R-1 15-16 cm	USNM 113716	VGA 99		
^b n	5	3	3	3	3	3	4	3	14	12	13	3	^c N 3	^c N 3	
SiO ₂	50.29	50.23	50.20	50.67	50.20	50.29	50.15	50.48	50.0	50.4	50.1	51.6	51.52	51.2	50.94
TiO ₂	1.82	1.80	1.81	1.81	1.80	1.73	1.70	1.76	1.63	1.65	1.67	1.26	1.30	3.92	4.06
Al ₂ O ₃	15.58	15.62	15.65	15.87	15.65	15.73	15.81	15.84	15.9	16.1	16.0	15.5	15.39	12.7	12.49
^d FeO	10.00	10.10	10.11	9.97	10.02	10.02	9.79	10.18	10.1	10.1	9.99	9.14	9.13	13.6	13.30
MnO	0.18	0.18	0.18	0.15	0.19	0.24	0.21	0.21	0.19	0.16	0.18	0.13	0.17	0.19	0.15
MgO	7.62	7.49	7.55	7.62	7.64	7.57	7.64	7.56	7.75	7.83	7.75	8.33	8.21	5.31	5.08
CaO	11.16	11.32	11.07	11.04	11.26	10.88	11.14	11.29	11.0	11.0	11.1	11.4	11.31	9.30	9.30
Na ₂ O	3.02	3.14	3.06	2.91	2.98	3.05	3.05	2.96	2.82	2.81	2.79	2.46	2.48	2.52	2.66
K ₂ O	0.15	0.14	0.14	0.12	0.15	0.15	0.15	0.13	0.12	0.13	0.14	0.09	0.09	0.86	0.82
P ₂ O ₅	0.17	0.16	0.17	0.17	0.16	0.17	0.16	0.15	0.14	0.15	0.15	0.10	0.12	0.43	0.38
Total	99.99	100.18	99.94	100.33	100.05	99.83	99.80	100.56	99.65	100.33	99.81	100.04	99.72	100.03	99.18

^a Analyses done on JEOL 733 superprobe at Massachusetts Institute of Technology.

^b Number of analyses.

^c As reported by Jarosewich, et al. (1979).

^d Total iron as FeO.

the range of optically determined compositions of Hole 648B plagioclase phenocrysts, plagioclase phenocrysts in many samples have distinctly higher anorthite contents (An_{80-85}). These anorthitic phenocrysts have crystallized from liquids having higher CaO/Na₂O than do the Hole 648B lavas and may be inherited from an earlier fractionation stage.

Average glass and whole-rock compositions are similar in the Hole 648B samples, as expected for these sparsely phyric basalts. However, some small but systematic differences appear

between the major-element concentrations in whole rocks and glasses. Figure 30 shows that normative forsterite (Fo) and anorthite (An) are positively correlated in the samples. This trend may be produced by fractional crystallization of olivine and plagioclase. Note that normative anorthite contents in whole rocks are systematically higher than in the coexisting glasses. Concentrations of MgO and Al₂O₃ are plotted in Figure 31, along with a 1-atmosphere liquid line of descent experimentally determined for WHOI sample AII96-18-1 from the KFZ (Tormey et al., in

Table 5. Whole-rock analyses, Site 648.

Hole Lithology ^a Core-section Interval (cm) Analyst ^c	648A P 1R-1 2-4		648B P 1R-1 17-20		648B P 1R-1 59-62		648B P 1R-2 37-40		648B P 1R-2 114-117		648B P 3R-1 31-34		648B P 3R-1 74-77	
	WHOI	Ship	WHOI	Ship	WHOI	Ship	WHOI	Ship	WHOI	Ship	WHOI	Ship	WHOI	Ship
SiO ₂	49.60		49.56	49.30	49.31	49.40	49.57	48.85	49.49	48.97	49.24	49.27	49.41	49.20
TiO ₂	1.78		1.73	1.71	1.72	1.70	1.74	1.73	1.69	1.70	1.65	1.63	1.68	1.66
Al ₂ O ₃	15.44		15.75	15.84	15.92	15.97	15.73	15.69	16.04	16.08	16.07	16.12	15.98	16.05
^d Fe ₂ O ₃	11.22		10.99	11.11	10.91	10.63	11.04	11.24	10.79	10.76	10.60	10.65	10.93	10.82
MnO	0.18		0.18	0.18	0.18	0.18	0.18	0.18	0.18	0.18	0.17	0.17	0.18	0.18
MgO	7.40		7.49	7.69	7.42	7.59	7.50	7.68	7.55	7.70	7.63	7.86	7.44	7.60
CaO	11.03		11.09	11.17	11.16	11.38	11.09	11.46	11.17	11.46	11.06	11.24	11.13	11.42
Na ₂ O	2.74		2.78	2.83	2.79	2.75	2.87	2.92	2.68	2.80	2.83	2.84	2.79	2.71
K ₂ O	0.15		0.17	0.21	0.17	0.19	0.15	0.22	0.15	0.19	0.17	0.20	0.18	0.19
P ₂ O ₅	0.17		0.17	0.17	0.18	0.17	0.18	0.18	0.18	0.17	0.18	0.16	0.17	0.16
Total	99.71		99.90	100.21	99.75	99.96	100.05	^e 100.00	99.93	^e 100.00	99.60	100.14	99.87	99.99
LOI	0.38		0.27		0.31		0.33		0.20		0.16		0.29	
^f Mg'-value	0.592		0.600	0.604	0.599	0.611	0.599	0.601	0.606	0.612	0.613	0.619	0.600	0.607
Rb	1.5	1.2	2.2	1.3	2.4	1.4	0.6	1.8	2.0	1.9	1.8	1.4	2.4	1.4
Sr	140	157	143	151	143	149	141	151	143	152	145	153	142	152
Y	42	28	42	35	41	35	42	35	40	35	41	34	40	34
Zr	134	138	130	134	129	132	131	136	128	132	125	127	126	130
Nb	3.3	3.7	3.0	3.4	3.8	3.2	3.6	3.6	3.8	3.4	3.8	3.2	3.4	3.6
Ni	105	105	110	105	106	98	104	100	114	106	114	109	110	102
Cr	231		211		217		222		217		213		225	
V	294	238	272	272	277	280	279	293	275	281	258	263	282	274
Zn	84		79		79		82		77		72		79	
Co	45		45		42		43		44		44		44	
Cu	64		56		66		67		59		62		65	

^a P = pillow unit; V = vesicular unit; M = massive unit. See Figures 11 and 12.

^b DRN was run as an unknown with the Leg 109 shipboard samples. Average and one standard deviation (in parentheses) are given along with values from last calibration done on Leg 109.

^c WHOI = S. Humphris at WHOI; Ship = L. K. Autio and M. Loubet, on Leg 109, shipboard XRF.

^d Fe₂O₃* = total Fe analyzed as Fe₂O₃ (Leg 109 shipboard analyses) or recast as Fe₂O₃ (WHOI analyses).

^e Normalized to 100%.

^f Mg'-value = molar MgO/(MgO + FeO), where Fe²⁺/(Fe²⁺ + Fe³⁺) = 0.9.

press). Although the whole rocks and glasses contain similar MgO concentrations, Al₂O₃ is systematically higher in the whole rocks.

Discussion and Summary

Textural variations in Hole 648B basalts are produced by cooling-rate differences (e.g. Bryan, 1972). Glassy margins on samples are pillow-lava exteriors formed when magmatic liquids were rapidly quenched by cold seawater. This process involves the highest cooling rates. Variolitic-textured samples were cooled at a somewhat slower rate that was still sufficiently rapid to cause formation of abundant swallowtail and hopper plagioclase and radiating sheaf-like intergrowths of plagioclase, clinopyroxene, glass, and opaque minerals. Basalts having variolitic textures probably formed in a zone just inside the glassy pillow margins. Intergranular textures formed inward from the variolitic zone, where still slower cooling rates prevailed. This is indicated by the much lower abundance of quench crystal morphologies. The subophitic sample recovered in Core 109-648B-19R formed at the slowest relative cooling rate, probably in the interior of a thick pillow or flow. Here, the cooling time to solidus temperatures was long enough for growth of large clinopyroxene and olivine grains.

Petrographic and chemical data presented above show that the Hole 648B basalts were saturated with olivine and plagioclase at or near the ocean floor. They had not yet achieved clinopyroxene saturation. Experiments in natural basalt systems (Grove and Bryan, 1983) show that basalts constrained to the olivine + plagioclase saturation surface crystallize plagioclase and olivine at a ratio of 70:30. The phenocryst-abundance ratio in the Hole 648B basalts is 75% plagioclase: 25% olivine, nearly

that predicted by experiment. A crystal-fractionation trend calculated assuming the experimentally determined phase proportions is presented in Figure 30. Most of the whole-rock compositions can be generated from mixtures of glass with phenocrysts of 70% plagioclase: 30% olivine. However, some of the whole rock compositions are too anorthite rich to be these types of mixtures. These anorthite-rich samples may have accumulated a small amount of plagioclase. A small amount of plagioclase accumulation can also explain the Al₂O₃-rich compositions of certain whole rocks (Fig. 31).

These effects could equally well be explained by preferential loss of olivine rather than accumulation of plagioclase. However, calculations show that olivine phenocrysts are in iron-magnesium equilibrium with their host lavas. Certain plagioclase phenocrysts, on the other hand, have compositions, morphologies, and zoning patterns that suggest disequilibrium between plagioclase and host liquids. Therefore, evidence supports accumulation of excess plagioclase than redistribution of olivine. Accumulation of excess plagioclase into the Hole 648B lavas might occur during magma mixing (Rhodes et al., 1979).

The diverse morphologies, complex zoning patterns, and disequilibrium compositions present in certain Hole 648B plagioclase phenocrysts are also characteristic of basalts from Sites 395 (Dungan et al., 1978; Natland, 1978) and 396 (Flower et al., 1978; Kirkpatrick, 1978). These features, coupled with geochemical data, have commonly been interpreted as being evidence of mixing of two or more magma batches, one more primitive than the other. Mixing is a direct consequence of the episodic nature and intermittent replenishing of magmatic systems at mid-ocean ridges (e.g., Dungan et al., 1978). Upon mixing, plagioclase that originally formed in the primitive magma may undergo skeletal

Table 5 (continued).

648B V 6R-1 78-81		648B M 6R-1 132-135		648B P 8R-1 68-70	648B V 9R-1 80-82	648B P 13R-1 11-13	648B V 15R-1 111-113	648B M 16R-1 48-50	648B M 16R-1 88-90	648B P 17R-1 22-24	648B M 18R-1 38-40	648B M 19R-1 13-15	648B M 20R-1 48-50	Internal std DRN ^b	
WHOI	Ship	WHOI	Ship	Ship	Ship	Ship	Ship	Ship	Ship	Ship	Ship	Ship	Ship	Ship	Cal
49.30	49.49	49.28	49.96	49.58	49.24	49.19	49.57	48.71	49.19	49.64	48.81	48.68	49.29	52.59 (0.13)	52.60
1.71	1.69	1.65	1.64	1.67	1.67	1.63	1.67	1.61	1.63	1.68	1.65	1.63	1.68	1.07 (0.01)	1.06
15.74	15.83	15.96	16.07	15.90	15.89	16.09	16.02	16.12	16.21	16.02	15.79	15.77	16.12	17.69 (0.05)	17.67
10.96	11.01	10.74	11.18	11.00	10.87	10.70	11.22	10.86	10.85	11.02	10.84	10.82	10.52	9.7 (0.07)	9.71
0.18	0.18	0.18	0.18	0.17	0.18	0.16	0.17	0.17	0.17	0.18	0.17	0.17	0.18	0.21 (0.01)	0.21
7.53	7.74	7.68	7.79	7.56	7.52	7.54	7.64	7.50	7.89	7.71	7.59	7.61	7.70	4.27 (0.03)	4.31
11.14	11.34	11.07	11.51	11.17	11.22	11.26	11.31	11.32	11.32	11.27	11.10	11.17	11.20	6.90 (0.01)	6.88
2.80	2.82	2.83	2.90	2.88	2.86	2.97	2.80	2.88	2.86	2.75	2.66	2.59	2.72	3.11 (0.11)	3.16
0.18	0.21	0.08	0.12	0.25	0.22	0.21	0.24	0.09	0.11	0.23	0.23	0.16	0.17	1.69 (0.01)	1.70
0.17	0.17	0.18	0.15	0.16	0.16	0.16	0.16	0.15	0.15	0.17	0.19	0.16	0.16	0.23 (0.01)	0.23
99.71	100.48	99.65	100.50	100.34	99.83	99.91	100.80	99.41	100.38	100.67	99.03	98.76	99.69	97.48	97.51
0.26		0.09													
0.602	0.607	0.611	0.605	0.602	0.604	0.608	0.600	0.603	0.615	0.606	0.606	0.608	0.617		
4.1	2.5	1.7	1.5	3.0	3.0	2.4	3.2	1.4	1.8	2.8	3.9	3.1	1.4		
144	152	148	163	153	151	153	155	156	156	151	154	153	148		
41	34	40	34	35	34	33	35	34	33	34	34	34	33		
128	132	123	133	132	131	126	134	129	128	130	132	131	127		
3.9	3.5	3.9	3.3	3.3	3.5	3.3	3.5	3.0	3.3	3.5	3.5	3.2	3.5		
104	104	105	103	104	102	107	106	101	102	104	97	98	105		
210		185													
273	259	251	235	273	270	261	272	279	279	263	248	258			
73		69													
43		42													
55		63													

Table 6. Summary of basalt compositions.

wt%	Hole 648B average ^a				AlI92-29 ^b Whole rock	KFZ average ^c		KFZ range ^c	
	Glass		Whole rock			Glass	Whole rock	Min.	Max.
	Average	Sigma	Average	Sigma					
SiO ₂	50.33	0.20	49.78	0.35	50.53	50.72	49.99	47.79	50.63
TiO ₂	1.77	0.05	1.68	0.03	1.76	1.61	1.50	0.87	2.11
Al ₂ O ₃	15.76	0.10	16.15	0.15	15.77	15.46	15.95	14.67	17.88
FeO*	10.02	0.13	9.94	0.17	9.98	10.00	9.62	8.05	11.52
MnO	0.20	0.03	0.17	0.01	0.17		0.17	0.14	0.21
MgO	7.60	0.04	7.74	0.11	7.79	7.34	8.12	7.05	10.35
CaO	11.11	0.15	11.42	0.12	11.12	11.23	11.46	10.12	12.37
Na ₂ O	3.00	0.06	2.84	0.10	2.78	2.97	2.55	2.36	3.01
K ₂ O	0.14	0.01	0.19	0.05	0.12	0.13	0.14	0.07	0.23
P ₂ O ₅	0.16	0.01	0.17	0.02	0.19	0.16	0.16	0.06	0.23
Total	100.09	0.30	100.08	0.54	100.21	99.62	99.66		
LOI			0.23	0.08					
^d Mg'-value	0.600	0.005	0.606	0.007	0.607	0.592	0.626		
CaO/Al ₂ O ₃	0.705	0.010	0.707	0.010	0.705	0.726	0.718		
Normative Ol	11.47	1.36	13.28	1.51	8.38	8.61	9.43		
Ni (ppm)			108	4	103		129	86	245
Sr			144	2	133		131	114	150
Zr			128	3	135		106	50	151

^a Data from Tables 4 and 5, with Fe₂O₃ recalculated to FeO. Major elements: average of 6 MIT glass analyses and 17 shipboard whole-rock analyses. Trace elements: average of 8 WHOI whole-rock analyses. Average LOI calculated from WHOI whole-rock analyses.

^b Contains 4.5% plagioclase and trace olivine phenocrysts. Tables 2 and 8, Bryan et al. (1981).

^c Table 10a, Bryan et al. (1981).

^d Mg'-value = molar MgO/(MgO + FeO), where Fe²⁺/(Fe²⁺ + Fe³⁺) ≅ 0.9.

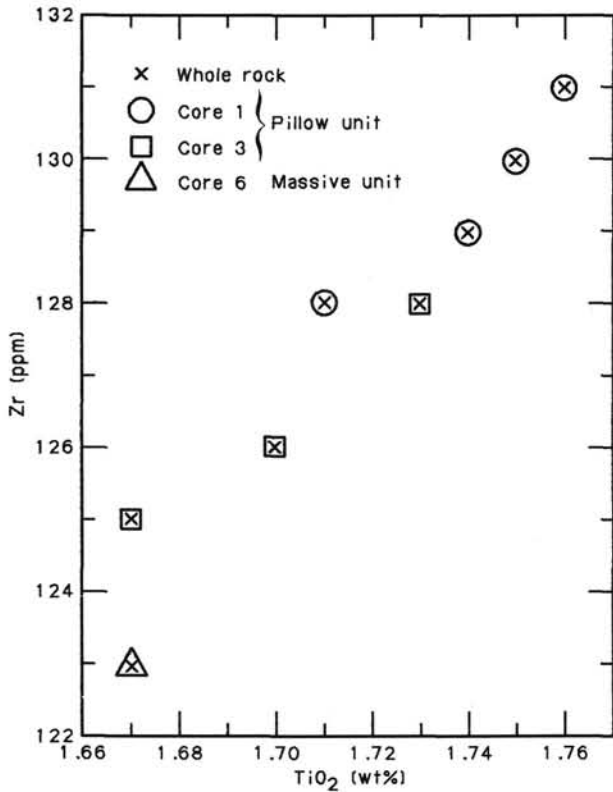


Figure 27. Zr vs. TiO₂ in Hole 648B whole rocks.

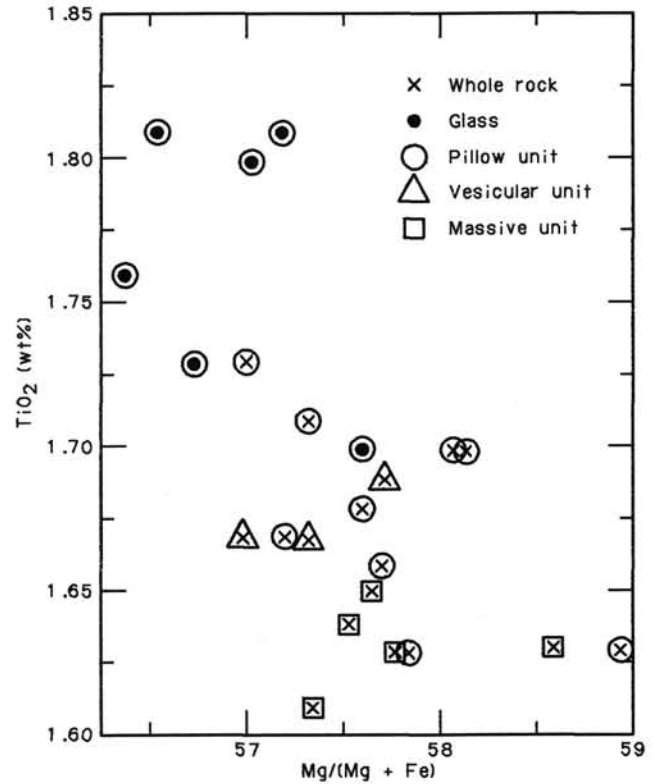


Figure 28. Mg/(Mg + Fe) vs. TiO₂ in Hole 648B whole rocks and glasses.

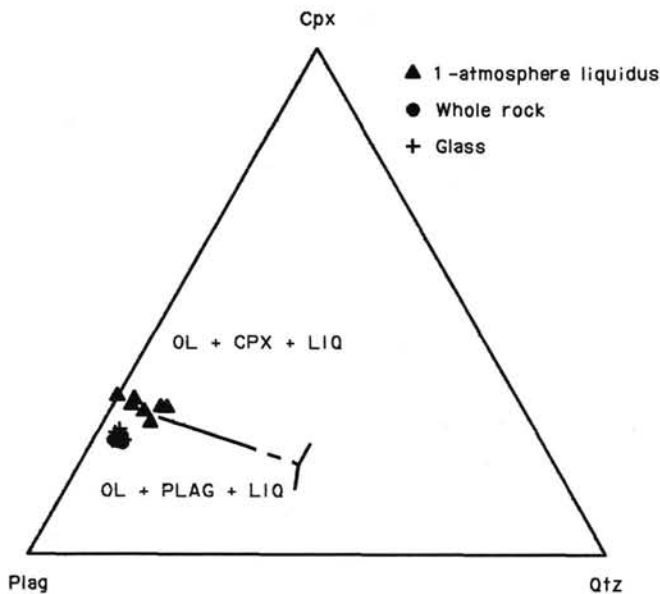


Figure 29. Olivine-saturated pseudoliquidus projection. The triangles show the position of an experimentally determined 1-atmosphere pseudocotectic curve in which olivine (OL) + plagioclase (PL) + clinopyroxene (CPX) + liquid (LIQ) coexist, (WHOI sample AII96-18-1; Torrey et al., 1987). Schematic phase boundaries are shown in a part of the ternary diagram. Crosses and dots show the compositions of Hole 648B glasses and whole rocks.

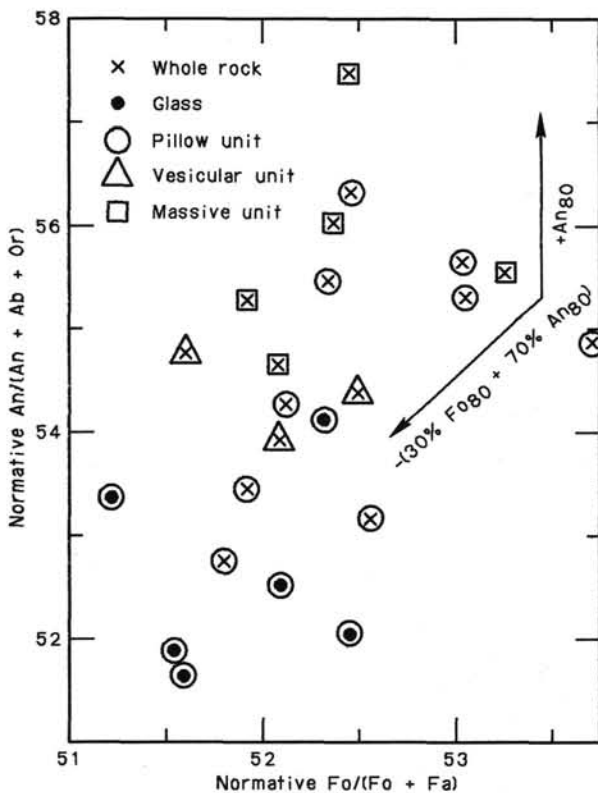


Figure 30. Normative $Fo/(Fo + Fa)$ vs. $An/(An + Ab + Or)$. One vector shows the effects of subtracting Fo_{80} olivine plus An_{80} plagioclase in the proportions 30%/70%, respectively. The vertical vector shows the effects of plagioclase addition. Note that some of the whole-rock compositions are too rich in plagioclase to represent simple addition of 30% olivine/70% plagioclase to the glass compositions. Accumulation of excess plagioclase may have occurred in these samples.

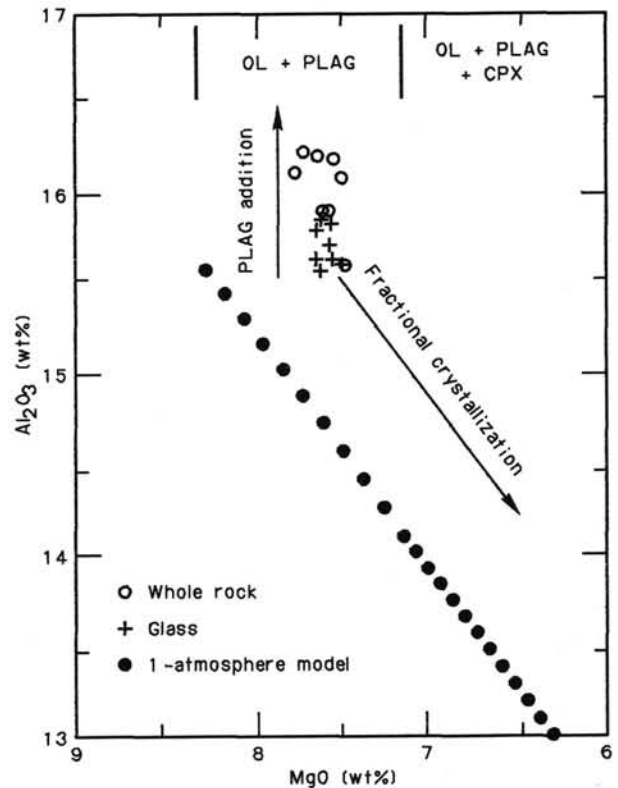


Figure 31. Concentrations of Al_2O_3 vs. MgO in Hole 648B basalts. Compared with glasses, whole rocks have similar MgO contents but higher Al_2O_3 . Shown also is an experimentally determined 1-atmosphere liquid line of descent for WHOI sample AII96-18-1 (dots; Torrey et al., 1987). Fractional crystallization will drive the Hole 648B compositions along a path parallel to the experimental path (lower arrow). Addition to the glasses of plagioclase (PLAG) and olivine (OL) in the proportions of 30% olivine/70% plagioclase produces whole-rock compositions lying above and to the left of the glasses. Accumulation of excess plagioclase into the glasses produces whole-rock compositions directly above the glasses. Across the top of the figure are shown the phases that crystallize along different portions of the experimental liquid line of descent. CPX = clinopyroxene.

growth, while at the same time the plagioclase that formed in the evolved magma may be partly resorbed (Kuo and Kirkpatrick, 1982). Since plagioclase is neutrally buoyant in basaltic magmas and does not reequilibrate rapidly, it records these mixing events in the form of compositional zones. The nature of the zoning patterns depends on the composition, temperature, and storage depths of magmas being mixed, which are partly controlled by the frequency and volume of replenishing magma. If replenishment is infrequent, magma in the shallow reservoir will cool and evolve significantly from the parent magma, leading to mixing of compositionally and thermally diverse magma types and extreme variability in zoning patterns.

Tectonic processes in this area may also have an effect on the types of magmas being mixed. If the rift axis is continuously or periodically shifting position, as suggested by the Sea Beam data, the size and temperature of shallow magma chambers may be significantly reduced, enhancing fractional crystallization and mixing of diverse magma types.

ALTERATION

The rocks recovered from Hole 648B are predominantly fresh, but a few samples are incipiently altered along fractures. Most rock pieces recovered are partly bounded by fracture surfaces, adjacent to which are some well-defined dark alteration halos.

The fractures were filled or lined with secondary minerals, which remain as coatings on the fracture surfaces. Only in a few samples (e.g., Sample 106-648B-3R-1, 73-79 cm; Fig. 32) do both sides of a fracture-controlled halo remain in contact.

Macroscopic Features

Two types of alteration halo can be recognized:

Type 1: 1-4-mm-thick, dark bands are developed adjacent to fracture surfaces (Fig. 33). The fracture surfaces, and any vesicle they intersect, are generally coated with variously colored secondary minerals. In one sample (Sample 106-648B-1R-1, 26-35 cm), a 5-mm vug is lined with iron-hydroxyoxides and surrounded by a 3-mm-thick dark band.

Type 2: 1-4-mm-thick dark bands are contained within the rock fragment. These halos are generally parallel to fracture surfaces or chilled margins. A lighter zone extends from one side of the dark band to the outer surface of the sample, varying in thickness from a few millimeters (Fig. 34) to several centimeters (Figs. 35 and 36). Fracture control of type 2 halos is evident only where the light-grey zone is <1 cm thick (Fig. 34). Dark bands of the type 2 halos are identical to the type 1 halos. In the light zones of some type 2 halos, flecks of yellow to orange alteration products are observed in hand specimen.

Some samples have type 1 halos, which grade into type 2 (Fig. 33), indicating that the penetration of the type 1 inward from the outer margin toward the center of a rock fragment could produce the type 2 halos. Since most of the pieces are rounded, their outer surface may have been partly (or totally) abraded during the coring, and the distance between the dark bands of some type 2 halos and the outer surfaces may have been reduced.

Table 7 summarizes the occurrence of type 1 and 2 halos in Hole 648B. Both halo types occur throughout the drilled sec-

tion. Type 1 halos occur in all textural types of rock apart from glassy chilled margins. Type 2 halos occur in all textural types of rock, but only in very fine grained margins have such halos advanced more than about 1 cm into the rock from a fracture surface. Such well-advanced type 2 halos occur only in the upper part of the hole (Core 106-648B-1R-1 to the top of Core 106-648B-6R-1), where the basalts are mainly fine grained.

Thin Section Petrography

Alteration features of the shipboard thin sections that contain secondary minerals are summarized in Table 8. The only primary phases that are commonly altered are intersertal glass (in the coarser grained basalts) and sulfides. Alteration products occur chiefly as miarolitic cavity linings and fillings (Fig. 37) and as vesicle linings (Figs. 38 and 39). The importance of fillings of microscopic miarolitic cavities was not recognized in the initial petrographic descriptions. This was because of the difficulty of distinguishing microscopic miarolitic cavity fillings from mesostasis glass replacements and also because of the difficulty of establishing the extent of miarolitic porosity (as opposed to artificial holes in the thin sections) in the fresh rock.

Five petrographic types of alteration product were distinguished:

1. Olive-green clay has a low refractive index and is virtually isotropic. Layers of browner and greener clay may be distinguished in vesicle-lining clay of this type.

2. Yellow clay has a low to moderate birefringence, which increases as the color changes from greenish yellow (transitional to olive-green clay) to orangish yellow (Fig. 39). Yellow clay forms more complete fillings of micromiarolitic cavities than does the olive-green clay and also forms vesicle linings as thick as 80 μm . The vesicle linings have a strongly parallel to locally

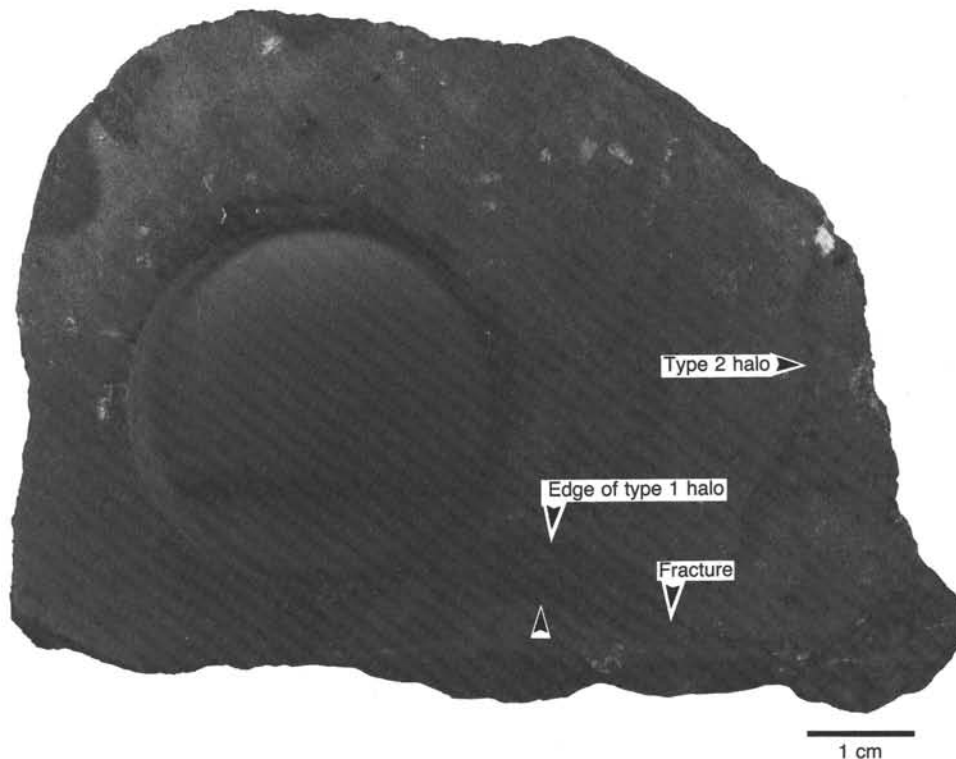


Figure 32. Sample 106-648B-3R-1, 73-79 cm. A type 2 halo passes into a type 1 halo developed along a fracture within a rock sample. See text for definition of halo types.

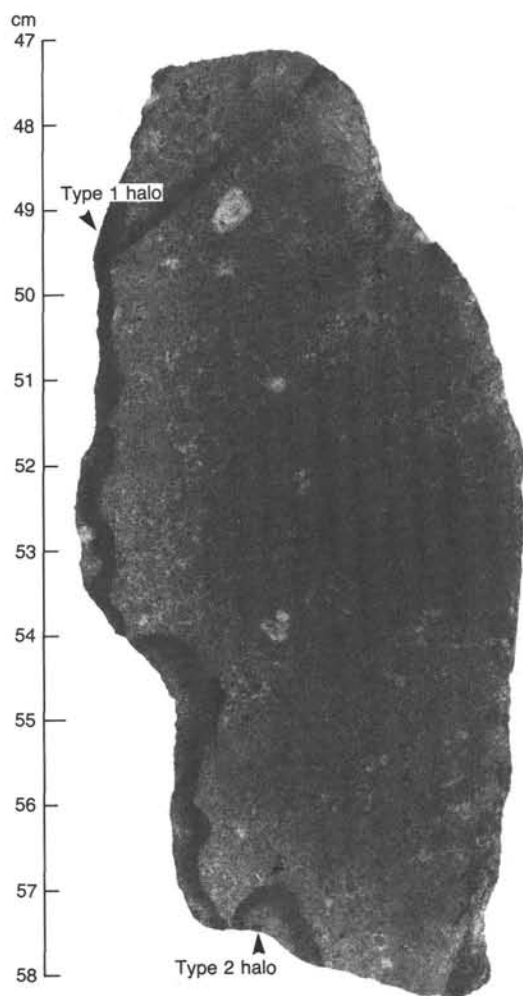


Figure 33. Sample 109-648B-8R-1, 47–58 cm. Type 1 halo passes locally into a type 2 halo. The edge of the sample next to the scale is mainly a fracture surface.

radiate growth structure and appear dull blue in hand specimen. The blue hue results from the dark color of the vesicle wall showing through the yellow clay.

3. Orange-red clay has moderate birefringence and a higher refractive index than do the previously described clays. It probably represents a mixture of clay and iron-hydroxyoxide (commonly referred to as iddingsite).

4. Red iron-hydroxyoxide is isotropic, has a high refractive index, and has a moderate reflectivity (similar to magnetite). It mainly occurs in miarolitic cavities and vesicles but also in fractures and replacing sulfides in some places.

5. Opaque iron-hydroxyoxide is observed only in and around a fracture and as a minor vesicle-lining phase in Sample 109-648B-9R-1, 69–71 cm.

Microprobe analyses of the various alteration products were obtained from four of the shipboard-made thin sections: Samples 109-648B-8R-1, 68–70 cm; 109-648B-9R-1, 69–71 cm; 109-648B-16R-1, 2–5 cm; and 109-648B-18R-1, 0–2 cm. Analyses were done on the energy-dispersive modified Cambridge Geoscan in the Department of Geology, University of Manchester, U.K. Six representative analyses are listed in Table 9. All these are from Sample 109-648B-9R-1, 69–71 cm (Fig. 38), but are compositionally similar to petrographically similar phases in the other samples. Preliminary shipboard X-ray diffractometry of

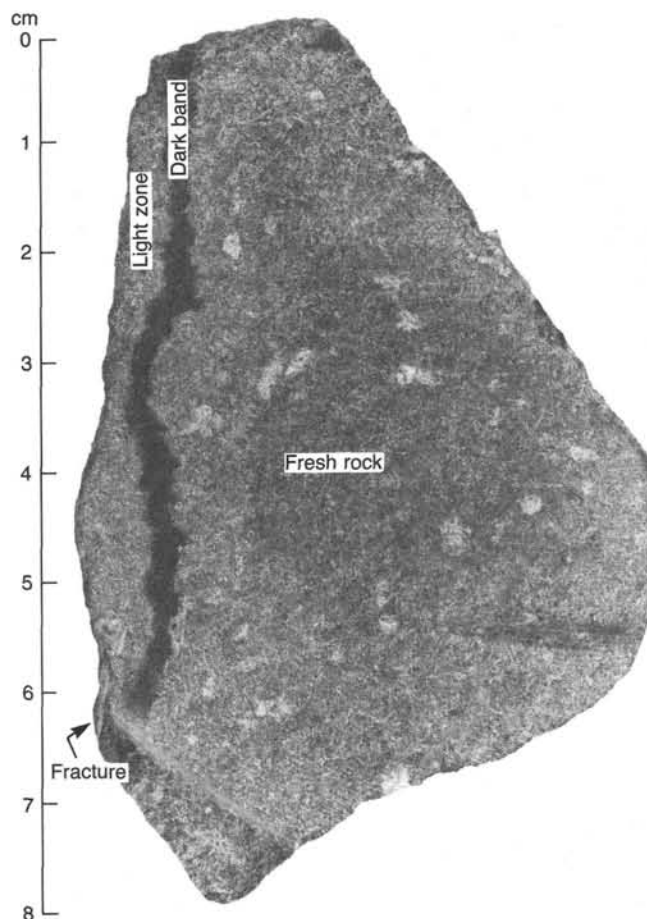


Figure 34. Sample 109-648B-18R-1, 0–8 cm. Type 2 halo (see shading) is adjacent to fracture in medium-grained basalt.

halo samples (see following section) revealed only smectite as a positively identifiable secondary phase. The microprobe analyses of both olive-green and yellow clays, when recalculated to a total anionic charge of 44 (22 oxygens) have higher interlayer cationic charges than do true smectites, but are more iron rich and less potassium and magnesium rich than true celadonites as defined by Buckley et al. (1978). The iron-hydroxyoxides contain substantial amounts of silicon and significant amounts of calcium and potassium, as well as iron. Some darker varieties of iron-hydroxyoxide contain significant amounts of manganese. The aforementioned vesicle-lining opaque iron-hydroxyoxide contains >4% MnO (uncontaminated analyses of this material were not obtained).

A systematic distribution of the alteration products exists within the halos. The olive-green clay occurs in the dark halo areas near the halo/fresh-rock boundaries. At increasing distances within the dark zones from the halo/fresh-rock boundary, the clay becomes increasingly yellow and birefringent and generally more abundant. The clay lining the vesicles has the same color as the clay in the adjacent groundmass. Where the groundmass is very fine grained, clay filling the intergranular microporous areas may impart a greenish to yellowish brown tinge to the groundmass as a whole.

Microfractures, most obvious in the plagioclase, are filled with the same clay (Fig. 40). The orange-red clays and red iron-hydroxyoxides tend to appear farther from the halo/fresh-rock boundary and may overlap with the yellow clay-bearing zone (Fig. 38). Sparse orange-red clays and iron-hydroxyoxides are the only distinguishable alteration products in the light zones of

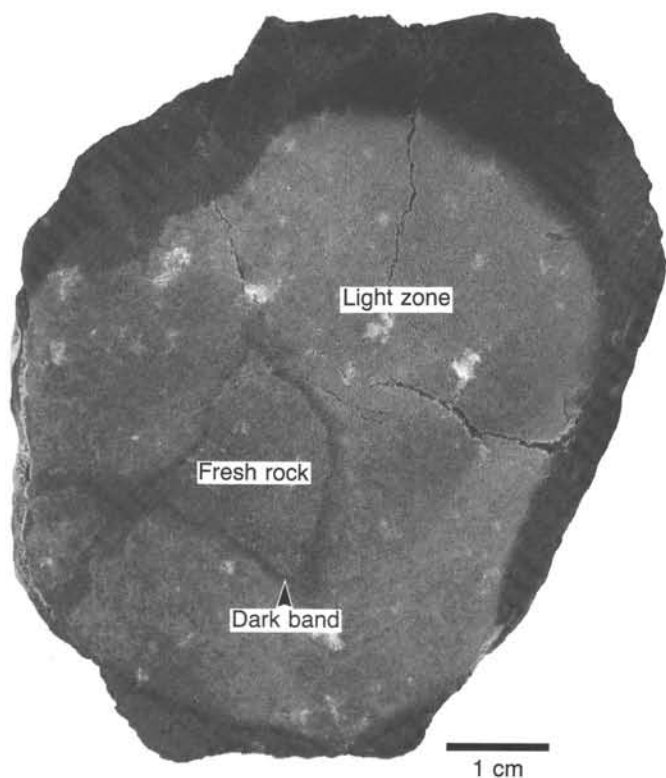


Figure 35. Sample 106-648B-3R-1, 85–90 cm. Type 2 halo is parallel to all the sides of the sample. Note that all the fractures are empty. (The outer dark rim is not a halo but is condensation on the refrigerated sample.)

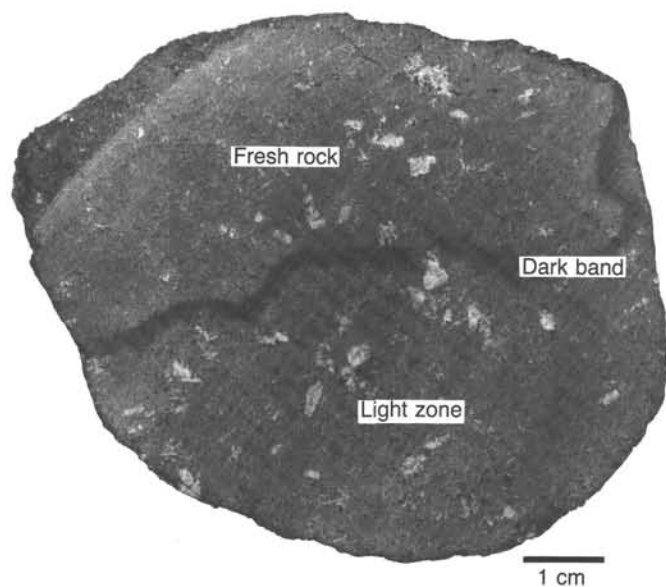


Figure 36. Sample 106-648B-1R-2, 108–111 cm. An example of type 2 halo. A sinuous 1–2-mm-thick dark band rims the inner edge of a light-colored zone that extends from one side of the band to the outer margin of the sample.

the type 2 halos. In the type 2 halo of Sample 109-648B-18R-1, 0–2 cm, sulfide globules (as large as 25 μm in diameter) within the light zone show progressive replacement by red iron-hydroxide, via speckled globular sulfide/hydroxyoxide aggregates. In the dark band of this halo, sulfide globules are incipiently al-

Table 7. Occurrence of alteration halos in Hole 648B basalts.

Core (648B)	Interval (cm)	Piece	Halo type
1R-1	13–17	4	1
	26–35	6	1 (plus type 1 halo surrounding 7 × 4 mm vug)
	22–26	10	1 + 2
	58–65	11	1 (around fracture terminating within rock)
	79–81	14	2
	82–85	15	2
	87–91	16	1
	93–96	17	2
	97–102	18	1
	118–121	21	2
	143–148	26	1
1R-2	6–15	2	2
	30–34	5	2
	43–45	7	2
	45–48	8	1
	50–54	9	2
	55–57	10	1
	61–66	11	1
	72–77	13	1
	108–111	18	2
	112–119	19	1
	121–126	20	1
	128–131	21	1
	134–136	22	1
	1R-3	1–4	1
13–17		3	1
25–26		5	1
28–30		6	2
37–39		8	2
42–47		9	2
49–51		10	2
55–58		11	1
61–65		12	1
67–71		13	2
87–91		16	2 (3.5 cm from glassy margin)
99–101	18	2	
2R-1	1–3	1	1
	5–7	2	1
3R-1	1–8	1	2
	10–14	2	2
	15–18	3	1
	19–25	4	2
	26–34	5	2
	36–44	6	1 + 2
	45–52	7	2
	54–56	8	2
	73–79	12	2 (1 cm from glassy margin)
	82–84	13	2
85–90	14	2	
4R-1	5–7	2	1
	7–13	3	1 + 2
	22–29	5	2 (double halo)
	35–39	7	1 + 2 (plus dark patches, possibly halo cut obliquely)
	42–45	8	2 (irregular)
	46–50	9	2
	51–56	10	2
	62–67	12	2 (3.5 cm from glassy margin)

tered (rougher polish). In some type 1 dark halos, sulfide globules are absent. The thin section from Sample 106-648B-4R-1, 40–42 cm, has sulfide globules about 2 μm in size in the fresh rock and rare irregular angular sulfide aggregates as large as 50 μm (but no primary globules) within the type 1 halo zone. The alteration of the sulfide globules has apparently resulted in local mobilization to form the aggregates. No obvious alteration of the titanomagnetites was observed in any of the halos examined. In the light band of the type 2 halo in Sample 109-648B-18R-1, 0–2 cm, a few of the oxide grains are compound grains

Table 7 (continued).

Core (648B)	Interval (cm)	Piece	Halo type
5R-1	17-22	4	2
	30-36	6	1 + 2
	42-47	8	2
6R-1	8-10	2	2
	32-37	9	1
	41-45	11	1 (not intersected by saw cut)
	46-51	12	1
	53-59	13	1
	62-65	14	1
	67-73	15	1
	74-81	16	1
	82-89	17	1
	90-97	18	1
	98-102	19	1
	110-115	21	1
	120-124	23	1 + 2
8R-1	125-127	24	1
	130-134	25	2
	8-12	2	2
	18-24	4	2
	31-34	6	1 + 2
	42-50	8	1 + 2
	63-73	10	1
	80-83	12	1
	86-95	13	1
	97-101	14	1
9R-1	68-76	10	1
	78-88	11	1
13R-1	1-7	1	1
	10-15	2	1
	17-22	3	?2
	23-28	4	1
	31-35	5	1
15R-1	37-42	6	1
	10-17	2	1 + 2
	38-42	6	1
	45-48	7	1
	66-73	10	2
	75-78	11	1
	82-89	12	1 + 2
	92-99	13	1
	103-107	14	1
	131-138	18	1
16R-1	142-145	19	2
	146-148	20	2
	2-7	1	2
	20-31	3	1 + 2
	33-38	4	1
	41-53	5	1
	55-61	6	1
	78-91	9	2
17R-1	93-99	10	1
	35-40	8	1 + 2
18R-1	1-7	1a	2
	7-15	1b	1
	18-46	2	1
20R-1	1-7	1	1
	10-18	2	1
	21-25	3	1
	37-42	5	1
	45-52	6	1

of titanomagnetite and a smaller grain of a slightly more reflective, apparently isotropic mineral, possibly maghemite.

Apart from the ubiquitous microfractures (Fig. 40), cracks partly or wholly filled with alteration products occur in only two thin sections. In both places, the alteration products in the wall rock adjacent to these veinlets are similar to the veinlet fillings. In Sample 109-648B-16R-1, 2-5 cm, fractures in the light band of a type 2 halo are filled with yellow clay grading into red iron-hydroxyoxide. In Sample 109-648B-9R-1, 69-71 cm, orange clay and opaque iron-hydroxyoxide impregnate the groundmass immediately adjacent to a fracture. This fracture is probably connected to the fracture controlling the halo itself.

In general, the only primary phases that are commonly altered in the halos in Hole 648B basalts are primary sulfides and some intersertal glass in the coarser grained rocks.

X-Ray Diffractometry

"Clay concentrates" were prepared from two thin-section billet residues containing halos. Each rock chip was ground to a fine powder using an agate mortar and pestle, disaggregated in an ultrasonic bath with 100 mL of deionized water and a few drops of Calgon solution, and then centrifuged for 5 min. The resulting suspension of fine-grained material was then decanted and centrifuged for 15 min, resulting in a clear liquid, which was itself decanted. The fine-grained residue was washed with deionized water, recentrifuged, transferred to a glass slide as a dense suspension, and allowed to dry. An additional sample was prepared by scraping alteration products off a fracture coating. The scrapings were simply ground under water to make a dense suspension that was then transferred to a slide. The X-ray diffraction (XRD) was run using a copper tube at 40 kV, 35 mA, with a goniometer step size of $0.02^\circ 2\theta$ and a count time of 2 s. The slides were run from 2° to $50^\circ 2\theta$, then glycolated at 65°C for 2 hr, then rerun from 2° to $20^\circ 2\theta$.

The thin-section billet samples are from a type 1 halo (Sample 109-648B-8R-1, 68-70 cm) and a type 2 halo (109-648B-18R-1, 0-2 cm). The latter sample includes both the light and dark parts of the halo. The fracture coating is a soft, predominantly yellow material from the fracture surface adjoining the same type 2 halo.

The diffractograms are dominated by primary plagioclase (Fig. 41). A summary of the data relevant to the alteration study is given in Table 10. High d-spacing peaks demonstrate the presence of small amounts of clay minerals. Only smectite could be identified with confidence. It occurs in both halo samples, giving well-defined 17 \AA glycolated peaks and broader air-dried peaks indicative of a range of interlayer ions (Fig. 42). The type 2 halo sample also gives a very weak 10 \AA air-dried peak that might be due to celadonite, but this peak is one of several weak, unassignable peaks $>7 \text{ \AA}$, all of which are listed in Table 10. The weak intensity of the smectite peaks obtained from the type 1 halo (Table 10) may reflect the poor crystallinity of the non-birefringent olive-green clay that predominates in the thin section. Traces of smectite were detected by glycolation of the fracture-coating sample. The main component of this coating may be amorphous iron-hydroxyoxides, as in the adjacent light-colored part of the type 2 halo described previously.

Summary and Interpretation

Incipient alteration of basalt in Hole 648B has proceeded by the penetration of water from fractures into the rock. At each alteration front, small amounts of olive-green, poorly crystalline iron- and potassium-rich smectite were produced. As the alteration front worked its way inward, the degree of oxidation of the rock through which the alteration front had passed probably increased, and the earlier clay was replaced by a more oxidized-looking, well-crystallized yellow clay (also a potassium-rich smectite) and subordinate amounts of iron-hydroxyoxides. The alteration products predominantly occur lining or filling miarolitic voids or vesicles. The only primary phases that were altered were sulfides and intersertal glass in coarser grained rocks. The secondary phases in the dark bands could not have been derived by *in-situ* alteration of primary phases.

Once the alteration front had penetrated more than about 4 mm from the fracture, the clays were apparently redissolved, leaving a pale, oxidized zone behind the advancing clay-bearing dark band, containing only sparse iron-hydroxyoxides. The secondary phases in the dark zones were presumably precipitated from solutions containing silicon, iron, and potassium, proba-

Table 8. Thin-section alteration petrology Hole 648B.

Sample no. (648B)	3R-1, 31-34 cm	4R-1, 40-42 cm	6R-1, 129-131 cm	8R-1, 68-70 cm	9R-1, 69-71 cm	16R-1, 2-5 cm	18R-1, 0-2 cm
Grain size	Fine	Fine	Medium	Fine	Fine	Fine to medium	Medium
Vesicles (%)	<1	<1	>1	0	7	10	<0.5
Fractures	—	—	—		+	+	
Halo type	2	1	2	1	1	2	2
Olive-green clay	VS MR F		+	+	+	+	+
Yellow clay	VS MR F			+	+	+	+
Orange-red clay	VS MR F	+	+	+		+	+
Red iron-hydroxy- oxide	VS MR F		+		+	+	+
Opaque iron- hydroxyoxide	VS MR F	+	+		+	+	+

Note: VS = lining vesicles; MR = filling/lining miaroles; F = filling fractures.



Figure 37. Photomicrograph of Sample 106-648B-3R-1, 31-34 cm (plane polarized light) Orange clay (CL) with brown iron-hydroxyoxide(?) (B) in the center, filling a miarolitic cavity in the groundmass.

bly similar to those responsible for the formation of iron, manganese hydroxyoxide, and nontronite deposits of the hydrothermal mounds south of the Galapagos Spreading Center (Honno- rez et al., 1983).

The alteration reported here represents the initial (oxidative) stage of low-temperature alteration of the oceanic crust, probably at near ambient ocean-bottom temperatures. The alteration is similar to that reported by Laverne and Vivier (1983) from < 1-m.y.-old basalts south of the Galapagos Spreading Center. Near the MARK area, the most comparable alteration study is that of Böhlke et al. (1980) at Site 396. The "black halos" they describe are similar to the dark bands in Hole 648B. However, Böhlke et al. (1980) reported low-level oxidative alteration in the gray interiors of their samples, in contrast to the entirely fresh interiors of the Hole 648B samples. Their "gray-interior-zone"

alteration represents an additional alteration stage that does not exist in Site 648 samples. Furthermore, their "brown zone" type of alteration, in which olivine is essentially completely altered to iron-hydroxyoxides, is clearly not developed in the Hole 648B samples. Hole 396B lies to the east of Hole 648B in 9-m.y.-old crust, so that the differences between the alteration at the two sites are presumably due to the difference in crustal age.

PALEOMAGNETICS

One of the purposes of the paleomagnetic study on zero-age crustal rocks is to investigate the acquisition of initial magnetization of the oceanic crust and to clarify the magnetic source layer responsible for the observed magnetic lineations. Natural remanent magnetization (NRM) and magnetizations after stepwise demagnetization up to 600 Oe were measured, and the sta-

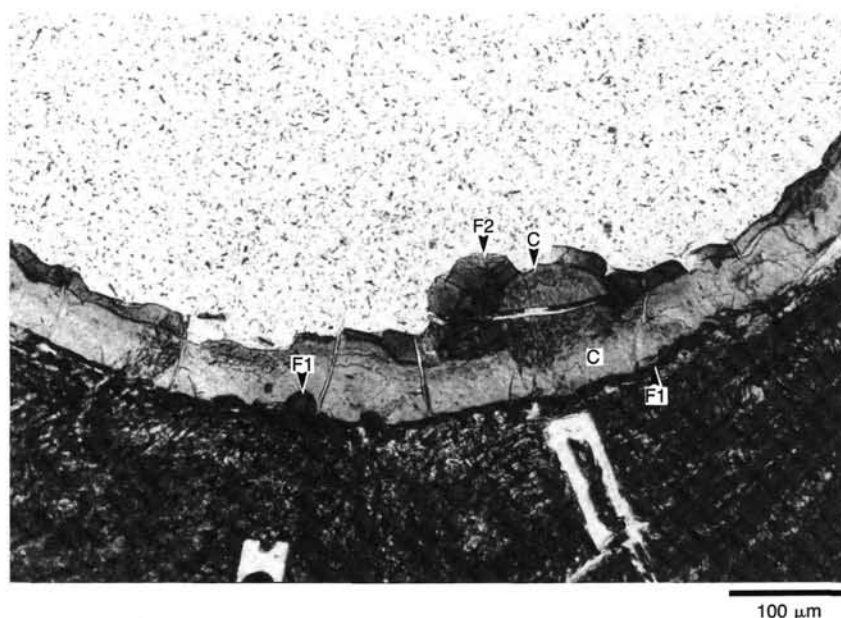


Figure 38. Photomicrograph (plane polarized light) of Sample 109-648B-9R-1, 69-71 cm, showing three-component vesicle lining. Dark-red iron-hydroxyoxide (F1); yellow clay (C); translucent red iron-hydroxyoxide (F2). See Table 9 for microprobe analyses.

Table 9. Representative analyses of secondary phases, Sample 109-648B-9R-1, 69-71 cm.

	1	2	3	4	5	6
SiO ₂	48.79	47.84	48.27	44.90	35.84	26.47
Al ₂ O ₃	1.07	0.49	0.00	0.00	0.00	0.00
Fe ₂ O ₃	34.80	33.12	39.15	40.15	49.82	55.93
MgO	5.02	4.63	4.28	3.85	2.65	1.88
MnO	0.0	0.0	0.0	0.0	0.78	0.0
CaO	0.90	0.62	0.72	0.72	1.77	3.81
Na ₂ O	0.0	0.0	0.0	0.0	0.0	0.76
K ₂ O	4.17	3.72	4.31	4.37	1.96	0.85
TiO ₂	0.0	0.0	0.0	0.0	0.0	0.0
Total	94.75	90.42	96.73	93.99	92.82	89.71
Si	7.16	7.32	7.05	6.84	5.81	4.69
Al	0.19	0.09	0.0	0.0	0.0	0.0
Fe	3.84	3.81	4.30	4.60	6.08	7.45
Mg	1.10	1.06	0.93	0.87	0.64	0.50
Mn	0.0	0.0	0.0	0.0	0.11	0.0
Ca	0.14	0.10	0.11	0.12	0.31	0.72
Na	0.0	0.0	0.0	0.0	0.0	0.26
K	0.78	0.73	0.80	0.85	0.40	0.19
Ti	0.0	0.0	0.0	0.0	0.0	0.0

- Olive-green clay in miarolitic cavity.
 - Olive-green clay lining vesicle.
 - Yellow clay filling miarolitic cavity.
 - Yellow clay lining vesicle (C in Fig. 38).
 - Pale red iron-hydroxyoxide overgrowing (4) (F2 in Fig. 38).
 - Dark red iron-hydroxyoxide overgrown by (4) (F1 in Fig. 38).
- Note: All analyses calculated to 22 "oxygens," Fe assumed to be as Fe₂O₃.

ble inclinations were obtained for these samples. The low field magnetic initial susceptibility of the samples was also measured. Anhyseretic-remnant-magnetization (ARM) acquisition curves were obtained for part of the samples to determine the relative field intensities existing while these rock were erupted.

Samples and Experimental Procedure

NRM intensity, inclination, and declination are shown in Table 11. The samples were taken from the cores after the orienta-

tion of the vertical direction had been marked. Owing to the small size of the recovered sections, the orientations are not entirely reliable. Remanent magnetizations of the basalt samples were measured with a Molspin portable rock magnetometer. The result of stepwise demagnetization is represented by Zijderveld diagrams.

It was necessary to eliminate the secondary magnetizations to establish the original remanence direction. Stepwise alternating-field demagnetization with peak fields as high as 600 Oe was employed. Since the magnetic coercivity of the NRM of the investigated samples is low in most cases, as can be estimated from the median destructive field (MDF), we chose steps of 10, 20, 30, 50, 70, 100, 150, 200, 300, 400, and 600 Oe of the peak field during the alternating-field demagnetizations. A Schonstedt geophysical specimen demagnetizer (model GSD-1) was used for the demagnetization. The stable inclinations and declinations were obtained from the least-squares fit of a line for the high coercive part of the magnetization on the Zijderveld diagram (Fig. 43A). Nearly all the basalt samples have a secondary component of magnetization, which in most cases can be at a peak field of about 50 Oe. MDF's of the samples were determined from the intensity plots as shown in Figure 43B.

Magnetic initial susceptibility of the basalt samples was measured by a Bartington magnetic susceptibility meter (model MS1). From the observed NRM intensity and the susceptibility, the Q-ratio (Königsberger ratio) of the samples was calculated by using the present strength of the geomagnetic field at this position (0.4 Oe based on IGRF80).

$$Q = J_{\text{NRM}} / (X \times H),$$

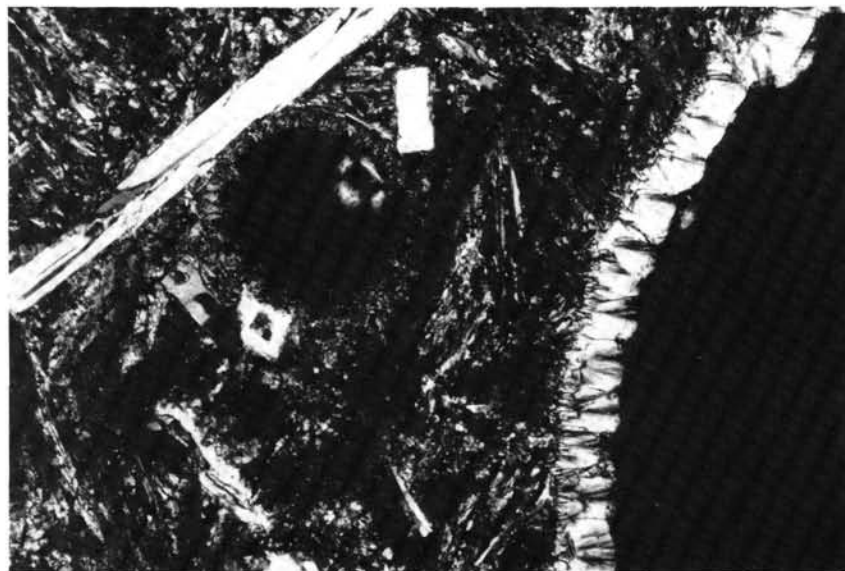
where J_{NRM} is the volumetric NRM intensity, X is the susceptibility, and H is the Earth's magnetic field at this location.

For the ARM measurement, we made a small coil fit inside the Schonstedt demagnetizer. The field inside the coil corresponding to a certain electric current was calibrated by using a Schonstedt fluxgate digital magnetometer (model DM2220) on board. The acquisition of ARM was measured by increasing the alternating field with increments of 10, 20, 30, 50, 70, 100, 150, 200, 300, and 400 Oe of the peak field. Throughout this experi-



A

100 μm



B

100 μm

Figure 39. Photomicrographs of Sample 109-648B-9R-1, 69–71 cm. Two vesicles lined with clay. The large one is lined with well-crystallized, birefringent yellow clay. The small one is lined with less well-crystallized, weakly birefringent greenish yellow clay. A. Plane polarized light. B. Crossed polars.

ment, the DC field applied to the sample was fixed at 0.5 Oe. From the demagnetization of NRM and the acquisition of ARM, the relative strength of the magnetic field can be estimated.

The stable inclination, the susceptibility, the MDF, and the Q-ratio for the samples are listed in Table 12.

Magnetostratigraphy

Fourteen samples from the pillow-basalt unit, three samples from the vesicular unit, and five samples from the massive unit (Fig. 12) were taken for the paleomagnetic measurements. Depth plots of the paleomagnetic parameters for all the samples are given in Figures 44A, 44B, 45A, 45B and 46. (Depth was calculated by assuming proportional distribution of the recovered

core material over the entire respective core length.) Histograms of the magnetic parameters are shown in Figures 47A–47E.

Stable Inclination

Five samples with stable negative inclinations were found between the depths of 14 and 23 mbsf. Three possible explanations of this phenomenon are as follows:

1. Negative inclinations were caused by a field reversal.
2. Pillows rotated or were displaced after their solidification.
3. Drilled samples, because of their small size, rotated inside the core barrel.

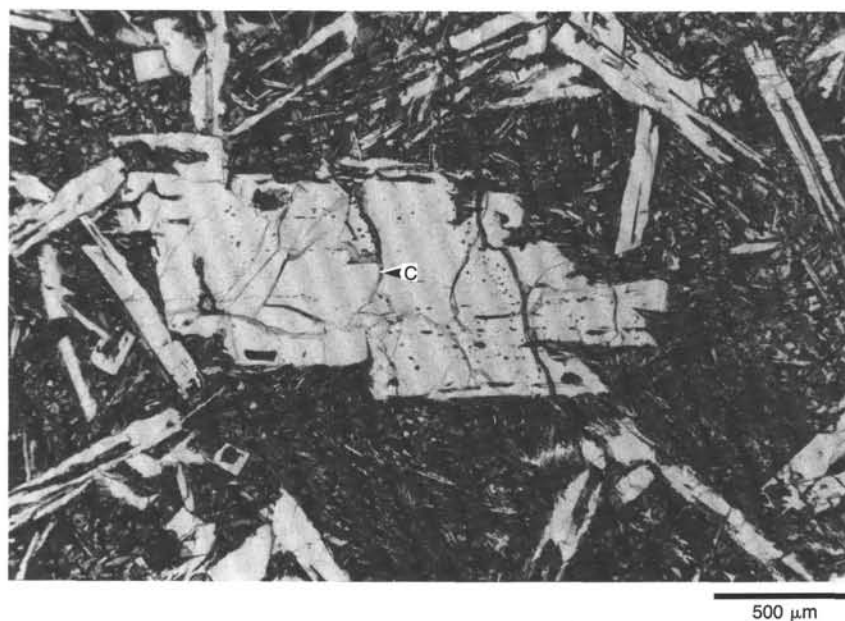


Figure 40. Photomicrograph of Sample 109-648B-9R-1, 69-71 cm. Yellow clay (C) filling microfractures in plagioclase phenocryst. Note also numerous devitrified glass inclusions in the phenocryst. Plane polarized light.

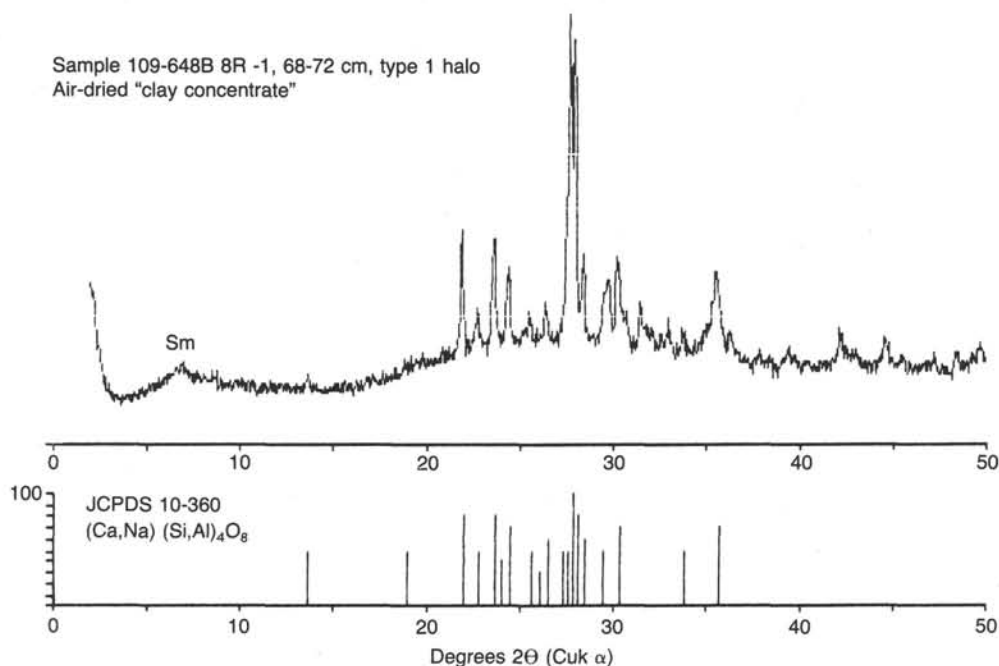


Figure 41. X-ray diffractogram of "clay concentrate" from type 1 halo, with Joint Committee on Powder Diffraction Standards reference pattern for "sodian anorthite (high)." Sm = smectite.

Three samples from the vesicular unit (Samples 106-648B-6R-1, 78-81 cm; 109-648B-9R-1, 80-81 cm; and 109-648B-15R-1, 111-113 cm) have consistently high inclination with the values of 82.0°, 74.6°, and 77.7°, respectively. Five samples from the massive unit (Samples 106-648B-6R-1, 132-135 cm; 109-648B-16R-1, 48-50 cm; 109-648B-16R-1, 88-90 cm; 109-648B-18R-1, 38-40 cm; and 109-648B-19R-1, 13-15 cm) have stable inclinations near 47°. Compared with these two units, samples from the pillow basalts show a wide scatter of the stable inclina-

tion (see Fig. 44B). The high inclination of the vesicular unit may be due to a coherent rotation of the unit, because the geomagnetic inclination of the drill site is only 40°. Only the massive unit has a reasonable mean inclination that comes close to this value.

Median Destructive Field

MDF's are a rough measure of the magnetic coercivity of the magnetic minerals contained in the samples. The coercivity can

Table 10. X-ray diffraction results.

Sample	d-spacing	I/I _(max) %	Peak quality	Assignment
109-648B-8R-1,	41.0	0.8	1.55	Spurious peak
68-70 cm	13.1	7.3	1.26	Smectite
1 halo	6.48	4.2	0.83	Plagioclase
(air)	5.14	4.2	0.81	?
	4.70	8.1	1.23	Plagioclase
	4.05	42.0	4.37	Plagioclase
	3.91	15.3	0.91	Plagioclase
	3.76	38.1	7.08	Plagioclase
	3.65	26.6	1.26	Plagioclase
109-648B-8R-1,	17.0	8.8	1.95	Smectite
68-70 cm	8.62	0.8	0.76	Smectite
1 halo	6.46	4.1	0.89	Plagioclase
(glycol)	4.69	7.7	1.02	Plagioclase
109-648B-18R-1,	14.9	31.9	0.87	Smectite (Mg, Ca)
0-2 cm	12.9	26.2	1.70	Smectite (Na)
2 halos	10.2	1.7	0.98	?Celadonite
(air)	9.61	6.25	0.79	?
	7.24	3.0	0.89	?
	6.48	7.1	1.38	Plagioclase
	4.62	11.2	1.15	Smectite
	4.06	81.6	5.50	Plagioclase
	3.915	20.4	0.93	?Celadonite
	3.77	38.1	2.24	Plagioclase
	3.65	26.6	1.17	Plagioclase
	2.716	58.1	1.00	?
	2.031	19.3	1.95	?
109-648B-18R-1,	40.8	100.0	1.12	Spurious peak
0-2 cm	17.2	91.0	1.00	Smectite
2 halos	9.56	15.0	1.23	?
(glycol)	6.50	16.4	1.15	Plagioclase
109-648B-18R-1,	9.57	2.7	1.29	?
0-2 cm	7.28	0.9	1.89	?
Coating	6.55	1.9	0.95	Plagioclase
(air)	4.72	3.4	0.85	Plagioclase
	4.06	12.8	2.19	Plagioclase
	3.93	12.5	1.45	Plagioclase
	3.78	22.8	4.37	Plagioclase
	3.66	17.5	2.45	Plagioclase
109-648B-18R-1,	17.05	2.8	1.58	Smectite
0-2 cm	9.48	1.3	1.12	?
Coating	7.21	0.7	1.15	?
(glycol)	6.51	1.1	1.41	Plagioclase
	4.70	5.2	0.91	Plagioclase

Note: Listing of all recorded peaks with d-spacings > 3.5 angstroms, plus two strong, unassigned lower d-spacing peaks in Sample 109-648B-18R-1, 0-2 cm. Peak quality (Q) is that given by the Philips APD1700 software and is defined by the relation $P = 1 - 0.0001^Q$, where P is the probability of the peak not being due to noise. If $Q > 1.0$, the peak is definitely significant. The threshold for peaks being "unreliable" is $Q < 0.5$.

give some clue to the grain size of the magnetic minerals. For titanomagnetite grains larger than a few micrometers, an inverse relationship exists between coercivity and grain size. MDF of the present samples varies from 38 to 144 Oe. The mean and the standard deviation are 69 and 28 Oe, respectively. Large variation of the MDF is observed in the pillow-basalt unit. In contrast, MDF's from the vesicular and massive units fall within a small range of values. This may indicate that magnetic minerals contained in these units show little variation in grain size.

Q-Ratio (Königsberger Ratio)

Q-ratio indicates the relative importance of the remanent magnetization with respect to the induced magnetization. The Q-ratios listed here are calculated from the NRM intensity and the susceptibility by using the field strength at this site (0.4 Oe, based on IGRF80). High values are observed in the top pillow-

basalt unit. The samples from the vesicular and massive units show consistently low Q-ratios.

Susceptibility

Susceptibility of the 22 samples ranges from 4.21×10^{-4} G/Oe to 23.94×10^{-4} G/Oe. The mean and the standard deviation are 12.69×10^{-4} G/Oe and 5.61×10^{-4} G/Oe, respectively. Susceptibility of the samples from the vesicular unit is consistently higher than that of the pillow-basalt unit.

Magnetic Grain Size

Two dissimilar samples were selected for reflected-light microscopic observation: Samples 109-648B-19R-1, 13-15 cm (high susceptibility and low MDF and Q-ratio) and 106-648B-3R-1, 74-77 cm (low susceptibility and intermediate MDF and Q-ratio). Only titanomagnetite grains were measured; ilmenite and sulfide were not included in this study. The histograms of the grain diameters are shown in Figures 47F and 47G, respectively. As evident from Figures 47F and 47G, the average grain sizes are different in the two samples. This may indicate that the low susceptibility of Sample 106-648B-3R-1, 74-77 cm, is mainly caused by the small grain size of the magnetic grains.

Anhyseretic Remanent Magnetization Intensity

As mentioned above, ARM acquisition curves were run for eight samples. ARM is an artificial remanence known to have magnetic characteristics that are similar to thermoremanent magnetization (TRM). Hence, ARM has been used as an analog of TRM to determine the intensity of the paleomagnetic field. Compared with Thellier's method (Thellier, 1951), ARM has the advantage of not causing an irreversible change in mineralogy from heating.

Figures 48A and 48B show the acquisition curves of ARM for the selected samples. ARM tends to saturate after some critical value of the alternating field. This critical field gives some information about the grain size of the magnetic minerals that cause the remanence. The acquisition curves for pillow basalts (Fig. 48A) and flows (Fig. 48B) are only slightly different. This indicates that the magnetic grain sizes of the samples that have been selected for the ARM studies are similar.

Some information about the magnetic mineral content can be obtained by plotting the ARM intensity vs. the inverse of the peak alternating field. Extension of the linear part to the vertical axis gives the saturation ARM intensity corresponding to an infinite alternating field. The variation of the ARM intensity is not large and varies parallel with the change in the NRM intensity. This suggests that the acquisition mechanism of the NRMs is similar for the eight basalt samples measured.

NRM-ARM Relation

The best-known method for determining paleointensity is the Thellier-Thellier method (Thellier and Thellier, 1959), where the thermal demagnetization of NRM and the acquisition of TRM in a known magnetic field are compared over successively higher temperature steps. However, because the mineralogy of the investigated samples changes during heating, the Thellier method cannot be used in our study.

Stephenson and Collinson (1974) used ARM instead of TRM for the paleointensity determination. This method was later criticized because, although the coercivity spectrum is similar for TRM and ARM, the scaling factor for these remanences are different, depending on the chemical composition of the magnetic minerals and the grain size. However, for samples that contain magnetic grains of a similar grain size, the Stephenson and Collinson method might be used to determine the relative change in the intensity of the paleomagnetic field.

Sample 109-648B 18R-1, 0-2 cm, type 2 halo "clay concentrate"

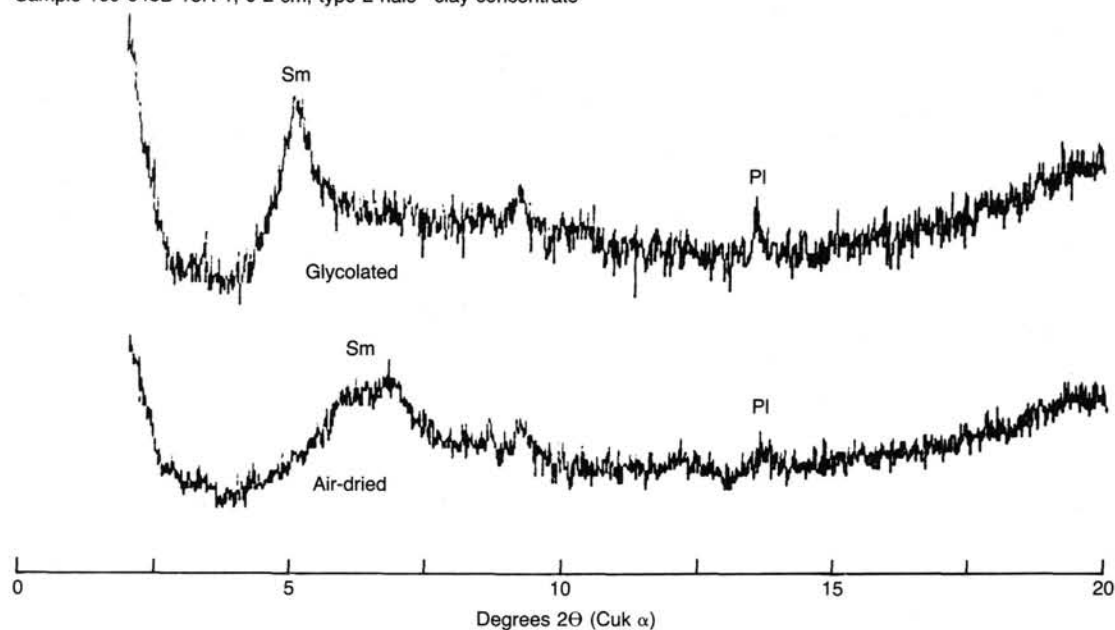


Figure 42. X-ray diffractograms of "clay concentrate" from type 2 halo, showing glycolation peak shift of smectite. Pl = plagioclase; Sm = smectite.

Table 11. Inclination, declination, and intensity of natural remanent magnetization (NRM), Hole 648B.

Core section	Interval (cm)	Depth (mbsf)	NRM			Intensity ($\times 10^{-4}$ emu/cm ³)
			Inclination (degrees)	Declination (degrees)		
106-648B-1R-1	2-4	1.93	-19	348	119	
106-648B-1R-1	17-20	7.35	62	17	190	
106-648B-1R-1	30-33	7.82	82	167	142	
106-648B-1R-1	59-62	8.87	24	230	76	
106-648B-1R-2	37-40	13.50	-52	225	50	
106-648B-3R-1	3-6	14.60	-3	87	68	
106-648B-1R-2	114-117	16.29	-16	245	131	
106-648B-1R-2	117-119	16.40	35	65	91	
106-648B-3R-1	31-34	16.67	-35	306	132	
106-648B-3R-1	74-77	19.84	—	—	53	
106-648B-5R-1	32-35	21.90	62	274	69	
109-648B-13R-1	11-13	25.56	-32	215	120	
109-648B-8R-1	68-70	26.72	44	341	119	
106-648B-6R-1	57-60	28.92	65	225	162	
106-648B-6R-1	78-81	30.08	71	156	166	
109-648B-15R-1	11-113	31.99	82	94	95	
109-648B-9R-1	80-82	32.89	75	236	77	
106-648B-6R-1	132-135	33.08	69	203	198	
109-648B-16R-1	48-50	38.34	56	105	111	
109-648B-16R-1	88-90	42.54	72	12	84	
109-648B-18R-1	88-90	42.73	69	279	74	
109-648B-19R-1	13-15	47.32	81	329	100	

For the present rocks, we plotted the NRM-ARM diagram in Figures 49A and 49B. A least-squares fit of a line was made for the linear portion of the diagram. As evident from Figures 49A and 49B, the slopes for the eight samples are similar. The standard deviation of the slope is about 10% of the mean value. No appreciable difference between pillows and flows was observed. This result indicates that the intensity of the paleomagnetic field during formation of these rocks was relatively constant, possibly varying about 10%.

Since Gauss' first analysis in 1835, the intensity of the Earth's dipole field has decreased by about 5%. Archeomagnetic studies indicate that the intensity of the Earth's magnetic field has changed by more than a factor of 2 within a period of 1000-2000 yr, during the last several thousand years (cf., Merrill and McElhinny, 1983). If we also assume a similar behavior of the Earth's magnetic field for the period when the investigated

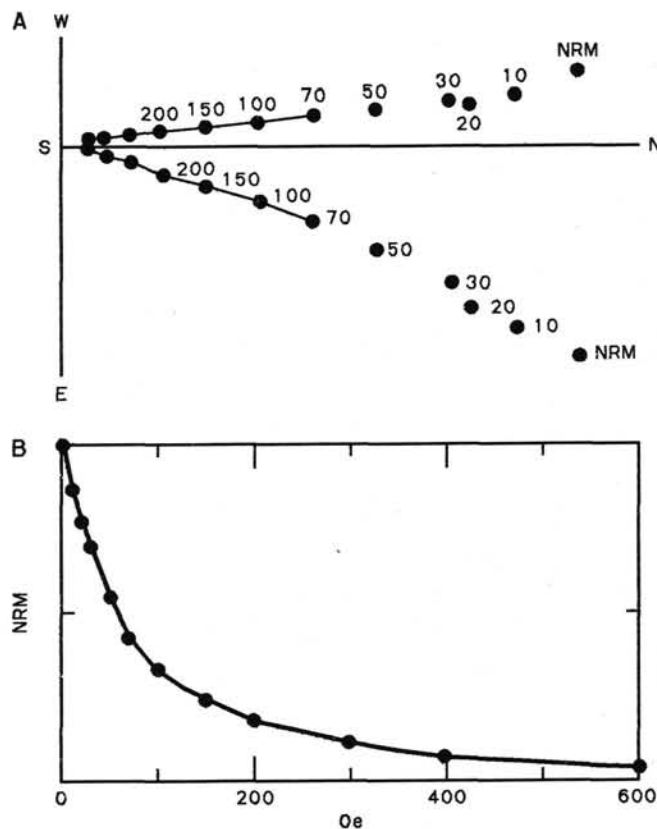


Figure 43. Stepwise alternating-field demagnetization of Sample 109-648B-8R-1, 68-70 cm. A. Zijderveld plot. B. Intensity plot. NRM = natural remanent magnetization.

Table 12. Stable natural remanent magnetization inclination, susceptibility, median destructive field (MDF), and Koenigsberger Q-ratio, Hole 648B.

Core section	Interval (cm)	Depth (m)	Stable inclination (degrees)	Susceptibility ($\times 10^{-4}$ G/Oe)	MDF (Oe)	Q-ratio
106-648B-1R-1	2-5	1.93	—	4.72	57	63
106-648B-1R-1	17-20	7.35	50	10.34	99	46
106-648B-1R-1	30-33	7.82	72	15.07	64	24
106-648B-1R-1	59-62	8.87	31	11.0	82	17
106-648B-1R-2	37-40	13.50	-25	9.83	75	13
106-648B-3R-1	3-6	14.60	0	4.81	45	35
106-648B-1R-3	114-117	16.29	-13	4.21	110	78
106-648B-1R-2	117-120	16.40	15	6.16	109	37
106-648B-3R-1	31-34	16.67	-45	13.12	89	25
106-648B-3R-1	74-77	19.84	-40	6.27	45	21
106-648B-5R-1	32-35	21.90	65	5.59	144	31
109-648B-13R-1	11-13	25.56	-36	14.00	69	21
109-648B-8R-1	68-70	26.72	38	14.14	59	21
106-648B-6R-1	57-60	28.92	38	17.80	56	23
106-648B-6R-1	78-81	30.08	82	18.00	41	23
109-648B-15R-1	111-113	31.99	78	15.78	59	15
109-648B-9R-1	80-82	32.89	75	13.32	86	14
106-648B-6R-1	132-135	33.08	43	23.94	47	21
109-648B-16R-1	48-50	38.34	47	15.52	57	18
109-648B-16R-1	88-90	42.54	46	17.47	38	12
109-648B-18R-1	38-40	42.73	48	18.70	39	10
109-648B-19R-1	13-15	47.32	51	19.36	43	13

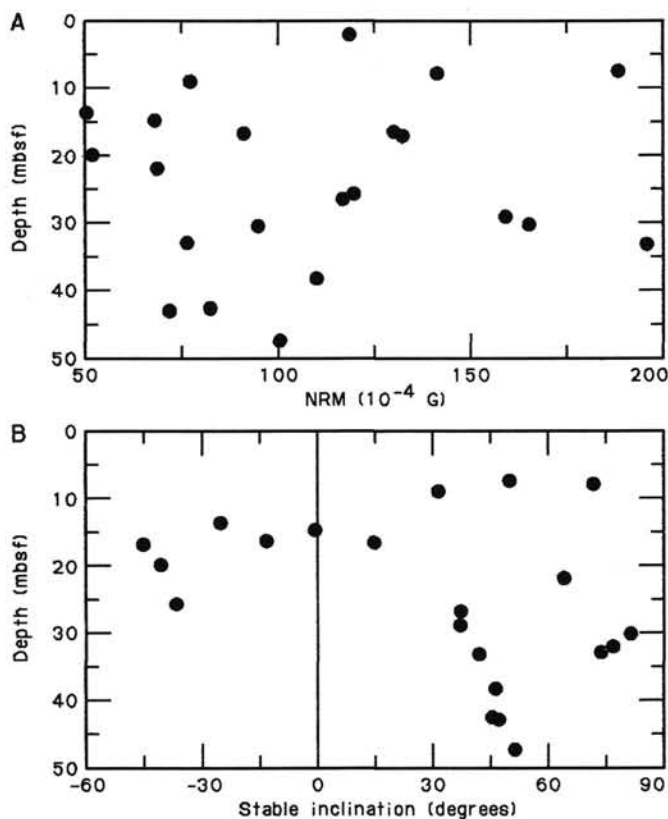


Figure 44. Hole 648B. A. Downhole plot of the NRM intensity. B. Downhole plot of the stable inclination. Expected magnetic inclination at the drill site is 40°.

rocks were emplaced, the NRM/ARM ratio of the present samples implies that these three lithological units were emplaced within a few hundred years. However, the absolute age of the eruption cannot be obtained from the current method.

Comparison with Other Oceanic Basalts

The NRM intensity and the susceptibility of the basalt samples from Hole 648B are compared with other suites of oceanic

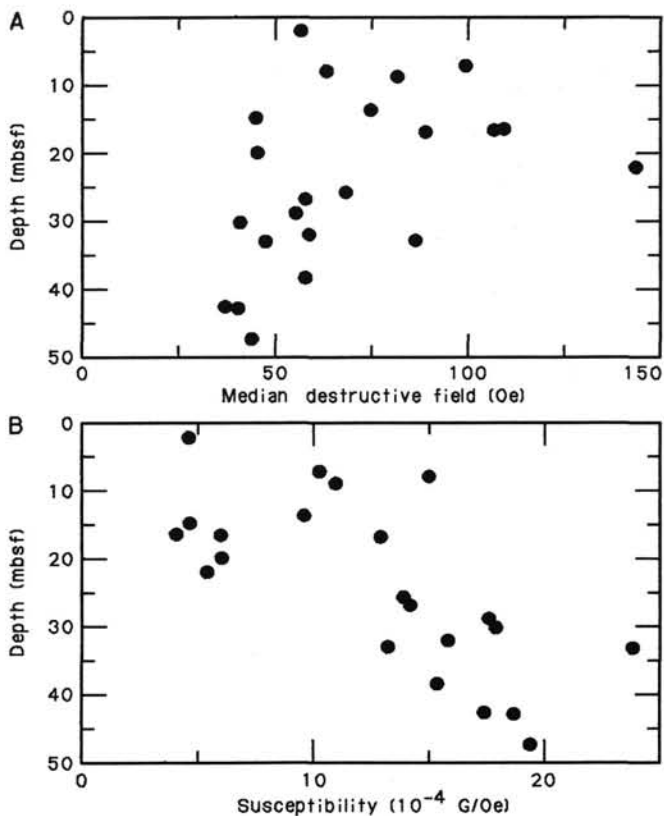


Figure 45. Hole 648B. A. Downhole plot of the median destructive field. B. Downhole plot of low-field susceptibility.

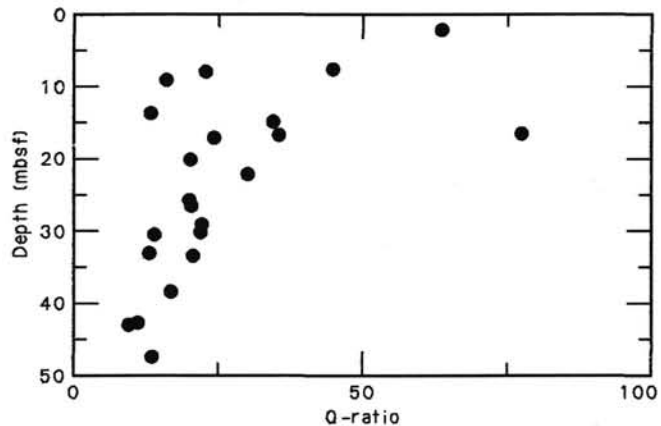


Figure 46. Downhole plot of the Koenigsberger Q-ratio, Hole 648B.

basalts in Table 13. Only the mean and the standard deviation are shown. Q-ratio can be calculated from these values. Among basalt samples compared, magnetic properties of the basalts from Hole 648B are similar to 100 m.y. old basalt recovered on Leg 52 (Holes 417D and 418A; Hamano et al., 1980). Dredged samples from the FAMOUS area (Prévot et al., 1979) and the samples obtained during Leg 37 (Hole 332; Prévot et al., 1979) have small susceptibilities compared with the present basalt, though the NRM intensity of FAMOUS basalts is similar to those from Hole 648B. Leg 45 basalts (Hole 395A; Johnson, 1978) have higher susceptibility and lower NRM intensity than do the samples from Hole 648B; this is an expected tendency if

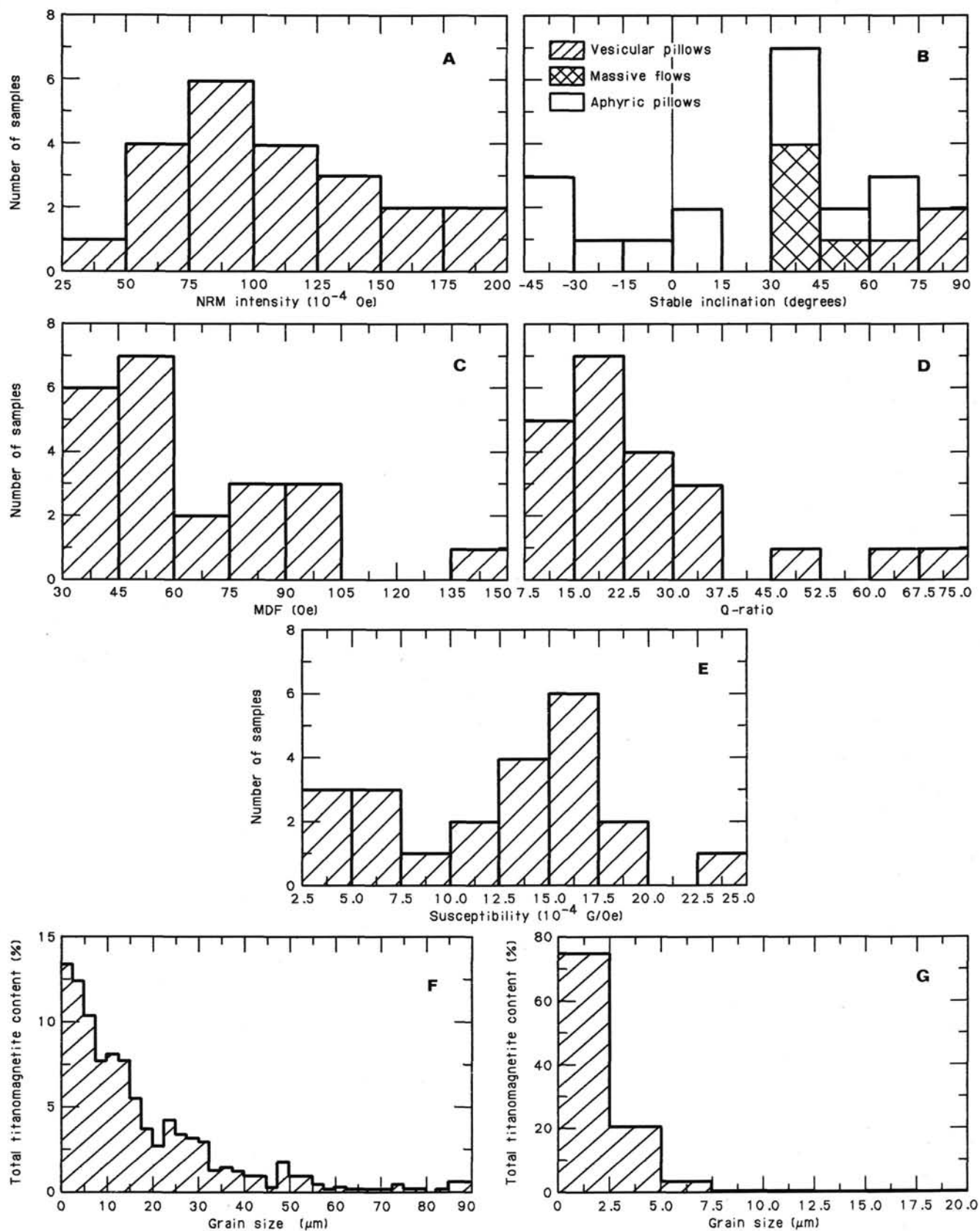


Figure 47. Histograms of different magnetic parameters, Hole 648B. A. Natural remanent magnetization intensity. B. Stable inclination. C. Median destructive field (MDF). D. Koenigsberger Q-ratio. E. Susceptibility. F. Titanomagnetite grain sizes of Sample 109-648B-19R-1, 13-15 cm. G. Titanomagnetite grain sizes of Sample 106-648B-3R-1, 74-77 cm.

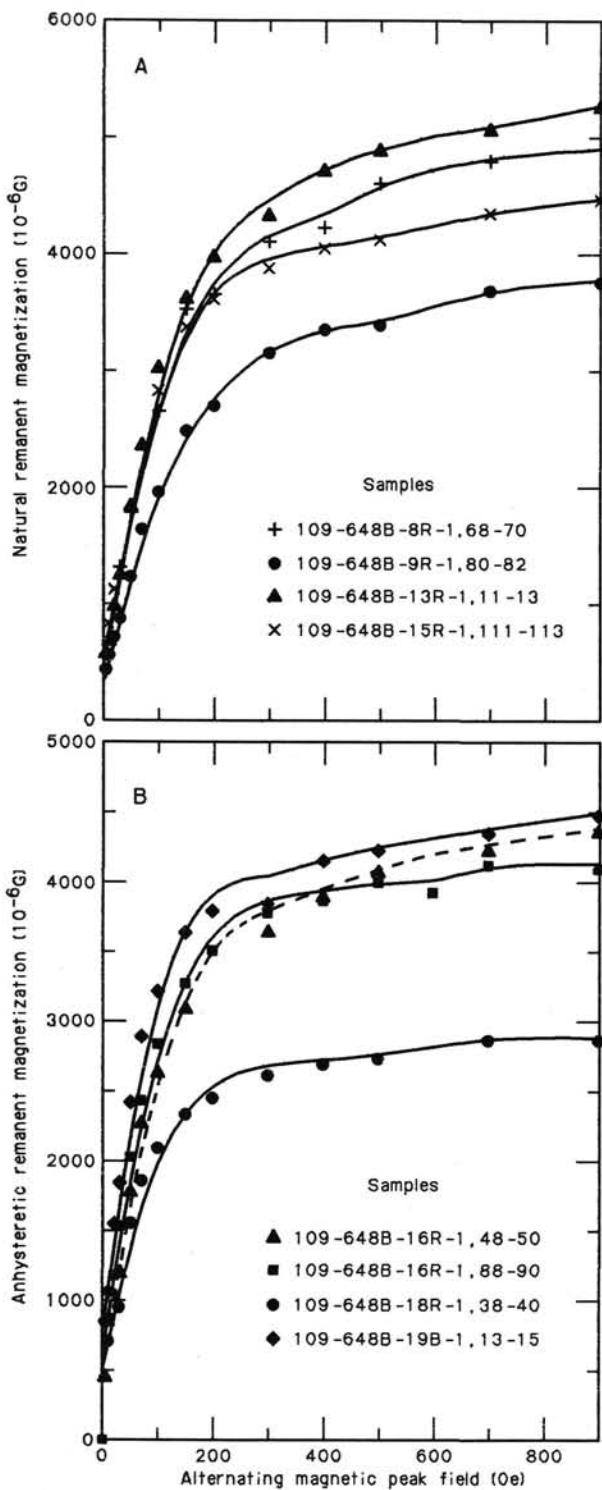


Figure 48. A and B. Anhysteretic remanent magnetization (ARM) vs. alternating magnetic peak field for various samples. Magnetic dc-field 0.5 Oe.

the magnetic grain size of Leg 45 basalts is larger than those from Hole 648B. However, the effect of the low-temperature oxidation should also be considered. Clearly, more information is required to delineate the differences among these basalt samples.

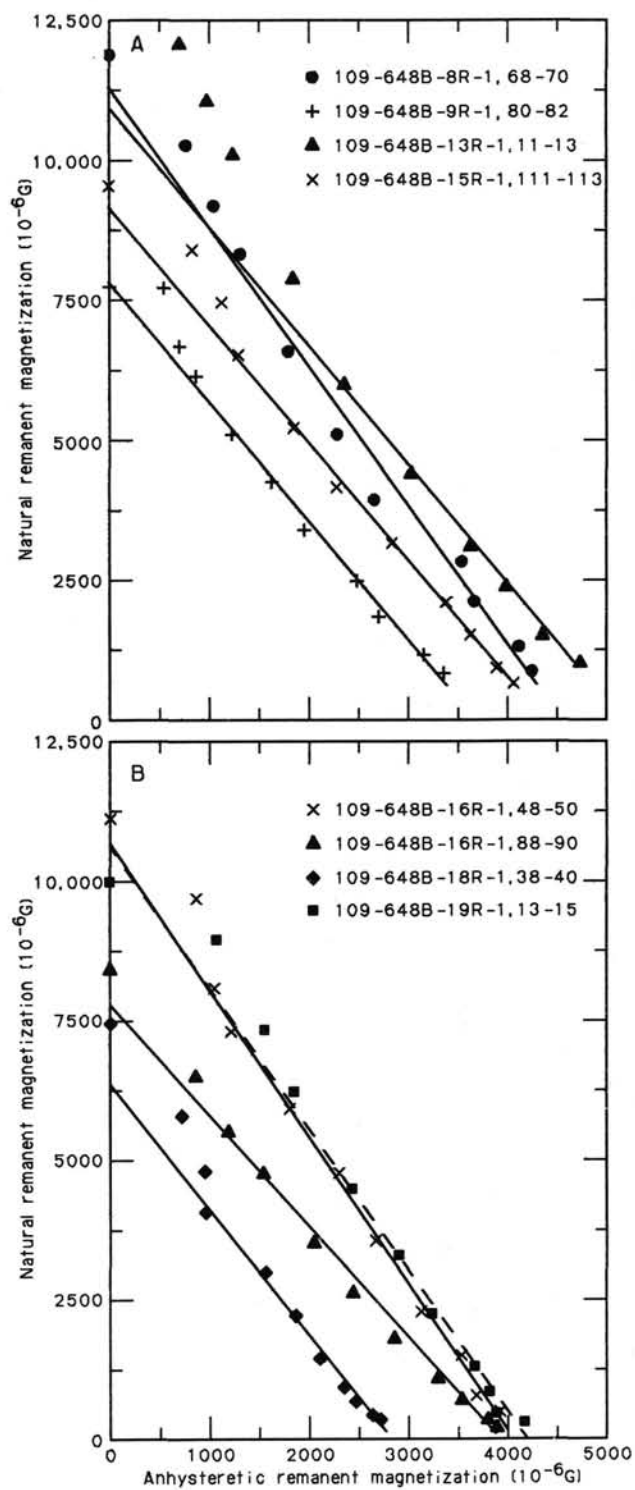


Figure 49. A and B. Natural remanent magnetization vs. anhysteretic remanent magnetization. Determination of the paleomagnetic field for various samples.

PHYSICAL PROPERTIES

The physical properties of crystalline rocks are controlled primarily by porosity (O'Connell and Budiansky, 1974; Toksöz et al., 1976), although both matrix alteration and filling of frac-

Table 13. Comparison of NRM and susceptibility of other oceanic basalts.

	NRM intensity (10^{-4} emu/cm ³)	Susceptibility (10^{-4} G/Oe)
^a Hole 648B	110 ± 42 (22)	12.7 ± 5.6 (22)
^b Famous	144 ± 123 (103)	2.99 ± 0.34 (103)
^b Leg 37	36 ± 31 (85)	2.41 ± 0.23 (84)
^c Leg 52	119 ± 73 (84)	20.0 ± 8.5 (83)
^d Leg 45	34 ± 24 (135)	20.9 ± 30.2 (42)

^aPresent study.^bPrévot et al. (1979).^cHamano et al. (1980).^dJohnson (1978).

Note: Number in parenthesis after the value is the number of samples analyzed.

tures and voids by secondary mineral phases can play an important role (e.g., Moos and Zoback, 1983). Because Hole 648B was drilled on the axis of the MAR, one might expect the materials recovered in this hole to be the least altered and to have the least vein-filling materials of any ocean-floor basalt. Microscopic and other examination of the cores largely confirms this expected result (see the appropriate chapters in this volume). Because physical properties are also controlled by pore structure, accurate measurements of compressional- and shear-wave velocities, porosity, and density characterize the connectivity, aspect ratio, and size of the pore space.

The velocity of a material that has pores can be expressed theoretically in terms of (1) the velocity of the solid part (matrix) of the rock and (2) the velocity of the material in the pores and the porosity, assuming that the shape of the pores is spheroidal or spherical (e.g., Kuster and Toksöz, 1974; Yamamoto et al., 1981). By defining the aspect ratio of pores by the ratio of the length of the shorter axis to that of the longer one in the case of oblate spheroidal pores, we expect the ratio of the *P*-wave velocity of a sample in a wet state to that of the sample in a dry state to be smaller for larger aspect ratio pores at a constant porosity. Therefore, we may obtain information about the shape of pores from sonic velocities in the wet and dry states. Accordingly, we are introducing a new parameter that gives information about the shape of pores by measuring the wet and dry velocity of a sample.

Measurements of wet and dry weight, bulk density, and ultrasonic compressional velocity were made on 22 samples from Hole 648B (12 during Leg 106 and 10 during Leg 109). Porosity and grain density were calculated from the measured weights and the bulk densities using two different methods. Differences in the calculated values can be related to measurement errors and can serve as a check on the results. During Leg 106, a new technique was employed to aid in determination of pore geometry from comparison of wet and dry compressional-wave velocities; compressional-wave velocity was remeasured during Leg 109 after the samples were dried to provide a complementary data set.

Methods

Measurements were made on 1.8–2.0-cm-long, 2.5-cm-diameter cylindrical specimens cut perpendicular to the axis of the recovered cores. The samples were cut as soon as possible after core recovery and were kept saturated in seawater. During Leg 106, paleomagnetic measurements were made after determination of the densities and velocities of the saturated samples. However, paleomagnetic measurements were made on the samples before running physical properties during Leg 109 because we suspected that the physical-properties measurements might introduce a spurious magnetic signature. The sequence for each leg is described in detail below.

Measurement Sequence

The fundamental physical-properties measurements discussed in this section include the compressional velocity (at 500 KHz) of saturated and vacuum-dried samples, made using the Hamilton Frame; bulk density, using the 2-min GRAPE count (Leg 109 only); weight, using the Scitech balance; and volume, made by an automatic penta-pycnometer (Leg 106 only). Samples were selected from each core to be representative of the recovered units, typically this translates to one sample per core. Because paleomagnetic determinations and thermal-conductivity measurements (see the appropriate chapters) are also made on the same sample, the samples were selected in consultation with the other physical-properties investigators. The measurement sequence for each leg is outlined as follows:

Leg 106: (1) Saturated weight, (2) saturated volume, (3) saturated compressional-wave velocity, (4) paleomagnetism, (5) sample dehydration, (6) dry weight, and (7) dry compressional-wave velocity.

Leg 109: (1) paleomagnetism, (2) saturated compressional velocity, (3) saturated weight, (4) saturated bulk density, (5) sample dehydration, (6) dry weight, (7) dry compressional-wave velocity, and (8) dry bulk density.

Experimental Technique

Weight Determination

Sample weights were measured by a gimbaled digital balance. Standard weights were measured both before and after each sample determination to calibrate the balance and to determine measurement errors. The accuracy and repeatability were both <0.02 g, yielding a measurement error of <0.1%.

Volume Determination (Leg 106 only)

The volume of each wet sample was measured by an automatic penta-pycnometer with a purge time of about 1 min. Two aluminum samples were used for calibration. One of them was 25.24 mm in diameter and 19.99 mm in length, and the other was 25.05 mm in diameter and 20.08 mm in length. Their calculated volumes are 10.00 cm³ and 9.90 cm³, respectively. After determination of the parameters of the pycnometer, calibration volumes were measured four times using all five of the pycnometer cells under the same purge-time condition as for the sample measurement. The results are shown in Table 14. The error of the measurement is <0.5%.

To further constrain the measurement, the sample volume was also measured with a 2-min purge time. For this condition, the volume was systematically smaller (by about 0.4%) than for a 1-min purge time. Assuming that this is due to removal of fluid from the pores, which should diminish the volume of the

Table 14. Volumes of two aluminum samples measured by the pycnometer during Leg 106. Values shown were averaged over four measured values.

Cell no.	Measured volume (cm ³)	
	Sample A	Sample B
1	9.995 ± 0.010	9.878 ± 0.037
2	9.975 ± 0.014	9.863 ± 0.030
3	9.968 ± 0.020	9.848 ± 0.029
4	10.018 ± 0.019	9.891 ± 0.023
5	10.026 ± 0.009	9.921 ± 0.024

Sample A: 25.24 mm θ × 19.99 mm; 10.002 cm³.Sample B: 25.05 mm θ × 20.08 mm; 9.896 cm³.

wet sample exponentially with increasing purge time, the measured volume will be about 1.5% ($\pm 0.5\%$) smaller than the actual volume. The sample volumes can be determined to within 1%–2%.

During Leg 109, no volume determinations were made, owing to poor repeatability of the volume measurements.

Traveltime (Compressional Velocity) Determination

The traveltime across the length of each sample of a 500-kHz pulse was measured on the Hamilton Frame, using a pulse detector that yields 1 ns precision. During Leg 109, the zero-path delay time determined before each measurement was subtracted from the apparent time through the sample to arrive at a true traveltime through the sample alone. During Leg 106, the traveltime through the transducers was calculated from data obtained from two aluminum calibration blocks of different lengths. To remove bias from the peak-detection technique, the source power was kept constant and the arrival peak amplitude was adjusted to a fixed value on the oscilloscope screen for each measurement. Owing to small changes in the relative position of the transducers from one measurement to the next and to the lack of plane parallelism of the sample faces, the repeatability of the traveltime measurements is about ± 50 ns.

During Leg 106, the wave velocity of each sample was measured in three mutually perpendicular directions—the axial direction and the two perpendicular radial directions. The path length was about 18–20 mm in the axial direction and about 25 mm in the radial directions.

The total error of the traveltime in a sample thus measured is estimated to be no more than 0.15 μ s. Because the average traveltime is typically about 4 μ s, velocity is thought to have an error of about 6% of the measured values.

GRAPE Bulk Density (Leg 109 only)

The 2-min GRAPE technique yields a measure of wet-bulk density. A reference measurement was made on a 5.08-cm-thick quartz crystal, and the reference was repeated every few measurements. Bulk density was determined repeatedly at several orientations. The scatter in the measurements, therefore, results partly from the statistical nature of the measurement technique and partly from real differences in the integrated density of the beam path. Where the beam intersects a larger number of vesicles, the apparent bulk density will be lower. The true bulk density of the aggregate material is thus an average of all the density measurements on the sample.

Sample Drying

On Legs 106 and 109, the samples were dried for 24 hr in a 110°C oven. On Leg 109, the weight was then measured, and the sample was placed in the vacuum drier for 24 hr before the final dry weight was determined. If the final result was substantially different from the intermediate value, the vacuum-drying process was repeated.

Determination of Grain Density and Porosity

In general, only three independent measurements are needed to determine uniquely bulk and grain density and porosity: the wet and dry weights and the GRAPE bulk density (or the pycnometer volume). A fourth determination, such as dry-bulk density, provides a check on the accuracy of the results.

The calculations proceed as follows. In the absence of accurate pycnometer data, the sample volume is first calculated by dividing the wet weight by the wet-bulk density:

$$\text{Volume} = \frac{\text{wet weight}}{\text{wet-bulk density}} \quad (1)$$

Porosity is then determined using equation 2:

$$\text{Porosity} = \frac{\text{wet weight} - \text{dry weight}}{1.0245 \times \text{sample volume}}, \quad (2)$$

where 1.0245 is the density of the pore fluid (seawater). Finally, grain density can be calculated using equation 3:

$$\text{Grain density} = \frac{\text{dry weight}}{\text{sample volume} \times (1 - \text{porosity})} \quad (3)$$

The grain and dry-bulk densities provide an alternative method for porosity determination:

$$\text{Porosity} = \frac{\text{grain density} - \text{dry density}}{\text{grain density}} \quad (4)$$

The difference between the weight of a sample in the wet and dry states generally is about 0.5 g, and the accuracy of the weight measurement is ± 0.02 g. Sample volume is about 10 cm³ and can be measured to within 1%–2% (see above). On the basis of these estimates, Leg 106 porosity is thought to have been obtained with an error $< 6\%$ of the obtained value.

Differences between the porosities determined by equations 2 and 4 are a further indication of the accuracy of the measurements. Estimates of measurement accuracy can also be made by measuring the weight and density of known materials and by observing the scatter of the repeated measurements. The reference measurements made during Leg 109 are described briefly below.

One further source of error results from incomplete removal of sample pore fluid, both from noninterconnected pore space and from small pore throats. The presence of this residual fluid in the pore space lowers the calculated porosities and grain densities. Finally, small isolated pockets of primordial gas lower the measured grain densities.

Reference Measurements (Leg 109)

The weight and bulk density of reference samples of aluminum and Lucite determined using the aforementioned techniques are summarized in Table 15. The CRC Handbook (Carmichael, 1982) lists the compressional velocity and density of aluminum as being 6.26–6.38 km/s and 2.70 g/cm³ respectively, and the velocity and density of Lucite as being 2.62–2.64 km/s and 1.18 g/cm³.

From calibration measurements and from the repeatability of the sample results, we estimate that the precision of the weight determinations is better than ± 0.02 g. However, the GRAPE density determinations may be systematically biased, reading a few percentage points low for higher densities. On the other hand, the GRAPE calibration instructions use a density for aluminum of 2.60 g/cm³; using this value, these densities are 1.5%

Table 15. Reference measurements on Lucite and aluminum used for calibration.

Sample	GRAPE density (g/cm ³)	Weight (g)	Sonic velocity (km/s)
Aluminum	2.634	27.03	6.291
(repeat)	2.625	27.04	6.365
Lucite	1.279	17.65	2.650
(repeat)	1.273	17.66	2.654
20-g weight		20.00	
(repeat)		20.01	

Table 17. Compressional-wave velocities of saturated and dry samples from Hole 648B, with thickness parameters determined for the Leg 106 data.

Sample Core, section, interval (cm)	Depth (mbsf)	Wet sample			Dry sample			Mean sonic velocity			
		Vp(v) (km/s)	Vp(H1) (km/s)	Vp(2) (km/s)	Vp(V) (km/s)	Vp(H1) (km/s)	Vp(H2) (km/s)	Vpwet (km/s)	Vpdry (km/s)	r	T
106-648B											
1R-1, 20-23	7		5.38			4.74		5.38	4.74	1.14	2.85
1R-1, 29-32	8	5.79	5.51	5.79	5.08	4.89	4.98	5.70	4.98	1.14	3.50
1R-1, 59-62	9	5.78	5.52	5.65				5.65			
1R-2, 37-40	14	6.07	5.97	6.10	5.48	5.50	5.53	6.05	5.50	1.10	2.70
1R-2, 117-120	16	5.78	5.88	5.72				5.79			
3R-1, 3-6	15	5.79	5.84	5.60				5.74			
3R-1, 31-34	17	5.47	5.55	5.47	4.23	4.24	4.20	5.50	4.22	1.30	4.76
3R-1, 74-77	20	5.99	5.98	5.93	5.30	5.35	5.35	5.97	5.33	1.11	3.06
5R-1, 32-35	22	5.85	5.82	5.72	4.46	4.14	4.38	5.80	4.33	1.34	10.0
6R-1, 57-60	29	5.59	5.65	5.59				5.61			
6R-1, 78-81	30	5.57	5.41	5.30	4.49	4.70	4.49	5.43	4.56	1.19	2.60
6R-1, 132-135	33	5.35	5.22	5.29	4.23	4.35	4.41	5.29	4.33	1.22	4.40
109-648B											
Sample Core, section, interval (cm)		Wet velocity (km/s)	Dry velocity (km/s)								
8R-1, 68-70		5.47 (0.02)	4.00 (0.2)								
9R-1, 80-82		5.17 (0.03)	4.40 (0.1)								
13R-1, 11-13		5.10 (0.02)	4.05 (0.03)								
15R-1, 111-113		4.95 (0.02)	4.00 (0.07)								
16R-1, 48-50		5.16 (0.02)	4.02 (0.13)								
16R-1, 88-90		5.21 (0.1)	4.28 (0.1)								
17R-1, 22-24		5.33 (0.04)	4.70 (0.1)								
18R-1, 38-40		5.42 (0.01)	4.21 (0.2)								
19R-1, 13-15		5.16 (0.08)	4.26 (0.1)								
20R-1, 48-50		5.34 (0.12)	4.78 (0.1)								
Average		5.23 (0.05)	4.27 (0.11)								

Note: Parentheses indicate standard deviation.

of the lack of any measurable difference in grain density or porosity. The only difference between the techniques used to determine velocity is the different method by which the zero-path-length delay time was determined. A careful review of the raw data did not shed any additional light on the question.

Discussion

Theoretical considerations suggest that, in crystalline rock, velocity and bulk density are positively correlated, whereas velocity is inversely related to porosity. Figure 50 shows porosity as a function of bulk density. The vesicular samples have the lowest bulk density and define a trend that, if extrapolated to zero porosity, yields a grain density of about 3.0 g/cm³, agreeing well with the average of the individual measurements. This suggests that no pronounced variations occur in rock chemistry in these samples that would cause differences in grain densities.

Figure 51 shows velocity as a function of density. In general, velocity and density are positively correlated, although a fair degree of scatter exists. This is not surprising, as other factors also control velocity. Figure 52 shows the inverse correlation between velocity and porosity.

Velocity is controlled not only by porosity but also by the distribution and geometry of the pores (O'Connell and Buidiansky, 1974; Toksöz et al., 1976). This can be seen clearly by the fact that the high vesicular porosity of Sample 109-648B-9R-1, 80-82 cm, does not reduce the velocity as much as one might expect. Furthermore, grain-size variations also affect velocity—larger grains tend to have more internal cracking, which reduces their elastic moduli without contributing much to the overall porosity. Thus, subtle variations in grain size and microstructure also affect elastic properties.

The bimodal distribution of porosities suggests that two distinct types of pores are contributing to the total. SEM photomicrographs and thin-section descriptions (see appropriate chapters) characterize the groundmass as being microcrystalline with relatively small amounts of interstitial glass. Gaps between these grains equal to or slightly smaller than the average grain size make up the bulk of the porosity in these samples. Small (2-5 mm) vesicles contribute an additional component of as much as 5% of the rock volume for Samples 109-648B-9R-1, 80-82 cm, and 109-648B-15R-1, 111-113 cm.

To analyze the relationship between velocity and pore geometry, we used the NSC method (Yamamoto, et al., 1981), which was developed on the basis of Eshelby's theory (Eshelby, 1957). These theories are applicable to rocks under the following conditions: (1) the wave length used for velocity measurement is sufficiently large compared with grain size and pore size, (2) the transfer of pore water caused by incident waves is negligible, and (3) the frictional properties of grain boundaries are unchanged by the presence of pore water. The first two conditions are presumed to be satisfied because the shortest wave length is about 10 mm and the wave period is < 10 μs. Whether the last condition is satisfied is unclear.

We assume a simple model where pores are oblate spheroids of similar shape and the orientation of the pores is random. Therefore, pore geometry is defined only by the aspect ratio α of the oblate spheroid, defined as the ratio of the length of the shorter axis to that of the longer axis. It is assumed that the ratio of the incompressibility of pore water to that of the matrix is 0.04, and the Poisson's ratio of the matrix is 0.3.

Figure 53 shows the wet to matrix velocity ratio (normalized by the ratio of matrix to wet-bulk density) as a function of po-

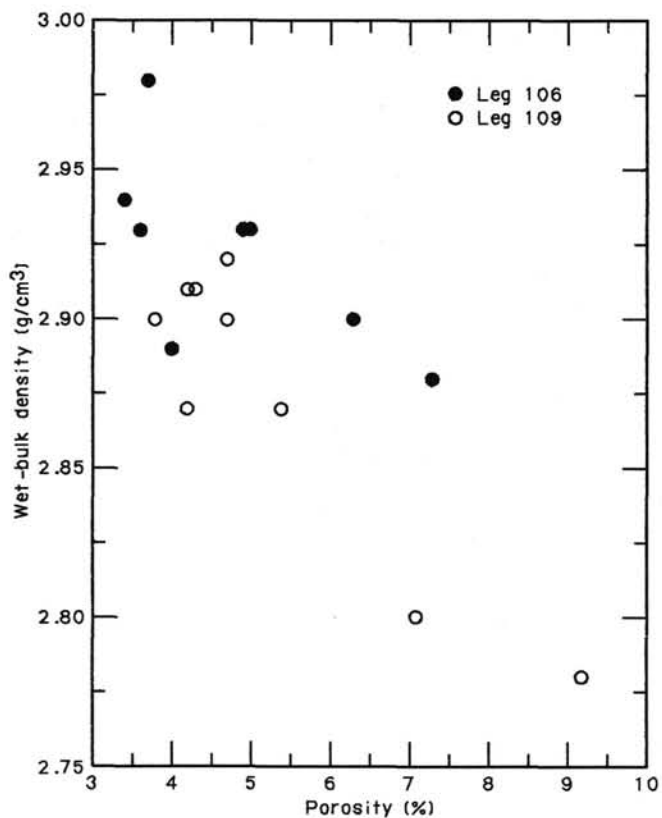


Figure 50. Porosity as a function of density. Porosities for Leg 109 samples are those calculated using equation 2 (see text in "Physical Properties" section, this chapter).

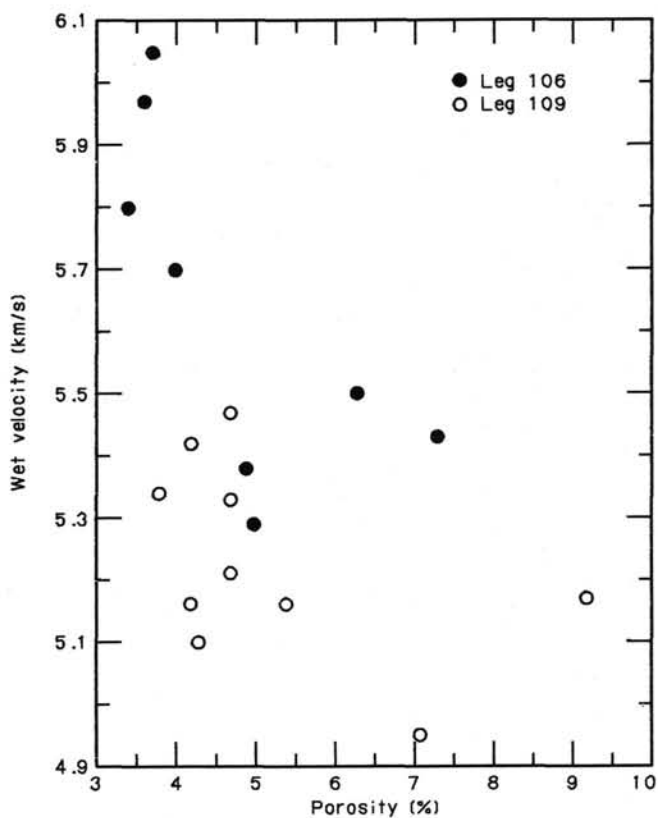


Figure 52. Compressional-wave velocity of the saturated samples as a function of porosity.

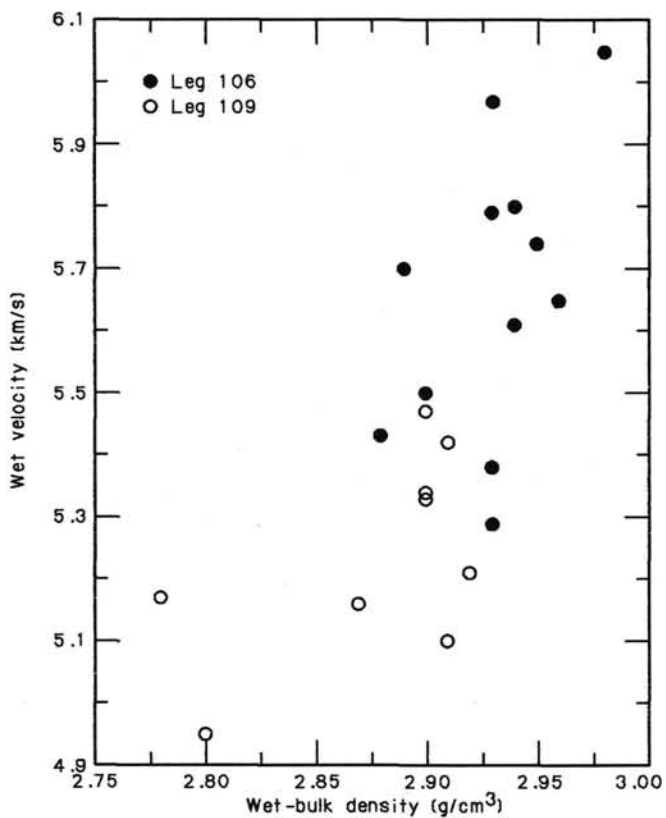


Figure 51. Compressional-wave velocity of the saturated samples as a function of density.

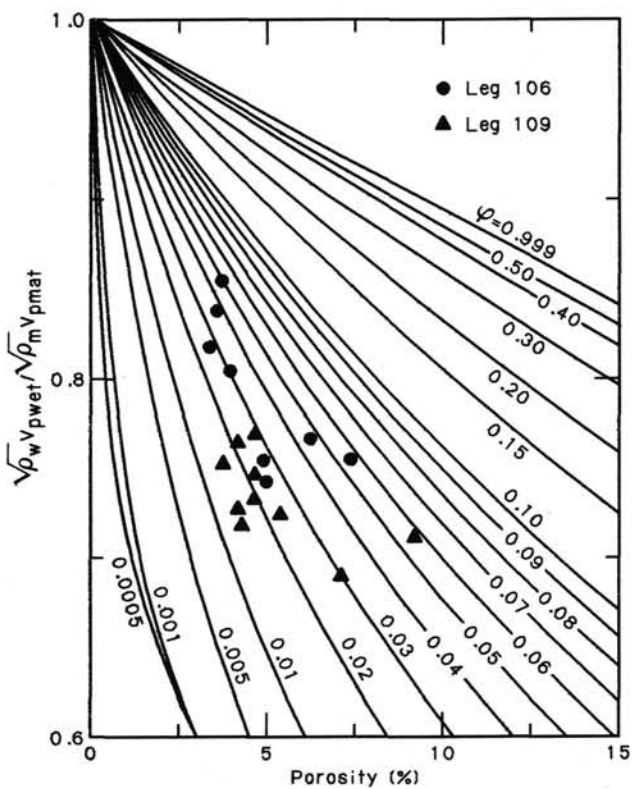


Figure 53. Ratio of the compressional-wave velocity of wet sample to that of matrix vs. porosity for samples from Hole 648B. The velocity of matrix is assumed to be 7.0 km/s.

rosity for the samples from each leg. Superimposed on this data are type curves based on the aforementioned model for different crack-aspect ratios, assuming a zero-porosity velocity of 7 km/s. All the data fall within the range of from $\alpha = 0.015$ to $\alpha = 0.06$. The Leg 109 data somewhat tend to fall at the low end of the spectrum, except for two points at $\alpha = 0.03$ and $\alpha = 0.06$. However, errors in velocity and porosity of 6% tend to blur this distinction slightly.

Figure 54 shows porosities and densities as a function of depth for the samples described here. Because many of the cores were from fill that had fallen into the hole from above the depth at which the cores were taken, variations in these parameters do not necessarily reflect *in-situ* stratigraphy. A more reasonable approach is to treat these measurements as providing a statistical representation of the cored material throughout the uppermost 47 m of Serocki Volcano. However, cores taken during periods when the hole was advanced beyond the previous total depth can be placed unambiguously.

Lithologies in this hole can be subdivided into three distinct units on the basis of these measurements. The uppermost unit is a low-porosity, high-velocity unit extending to 30 mbsf. Below this is a 3-m-thick, highly porous, vesicular, low-velocity unit. The rest of the hole penetrated dense, nonvesicular, high-velocity material. This subdivision agrees with the lithologic interpretation based on thin section and core descriptions. Therefore, these physical properties can be used to infer crystallographic and lithologic variations.

Conclusions

The physical properties of these samples are typical of oceanic basalts. Grain densities of 2.9-3.02 g/cm³ and porosities

from 3% to 10% yield bulk densities from slightly less than 2.8 g/cm³ to somewhat more than 2.9 g/cm³. Velocities range from 4.9 to 5.6 km/s, increasing with decreasing porosity. These properties subdivide the cored interval into three zones. An upper, high-velocity, nonporous unit overlies highly vesicular, low-velocity material, below which the basalts again have uniformly high velocities and are nonvesicular. This subdivision is also seen in the hand specimens; thus, physical properties well characterize the microstructure of these basalts.

THERMAL-CONDUCTIVITY MEASUREMENTS

The thermal conductivities of nine basalt samples from Hole 648B were measured with the modified half-space needle-probe device installed on the ship (THERMCON-85). Before measuring on the drill-core samples, a series of tests with a fused silica standard were performed to verify proper measurement conditions and to calibrate the device. The measurements on the basalt samples yielded mean thermal conductivity and standard deviation of 1.80 ± 0.07 W/m·°C.

Method of Measurement

The measurement method is based on the solution of the equation of heat conduction for an infinite line source (Carslaw and Jaeger, 1959). Its application to thermal-conductivity measurements of rock materials, as given by Von Herzen and Maxwell (1959), makes use of the linear part of the temperature-log time relation, which is valid for heating, at a constant rate, a needle that is in perfect contact with the measurement sample:

$$T = \frac{Q}{4K} (\ln t) + A$$

- K = thermal conductivity
- T = temperature measured with thermistor at needle center
- t = time of heating
- Q = power released at constant rate by heater wire in needle
- A = constant.

According to this equation, thermal conductivity is inversely proportional to the slope of the curve temperature vs. log time. However, this linear relationship is valid only if the measurement readings are taken in the proper range of time and if higher order terms of the solution of the heat-conduction equation are negligible.

Figure 55 shows the increase of temperature and log time measured for a 5-min heating period during a series of test runs on the fused-silica calibration standard and on one of the basalt samples from Hole 648B. There is a significant deviation from linearity, not only for the whole interval of time but also within smaller portions of the curve. As can be seen from Table 18, the slope of the curve at the end portion is about 50% lower than at the beginning. For that reason, the temperature-time dependency obtained with the installed measurement device was carefully checked to find out the best fitting range for the evaluation of the measurements.

The curve-fitting function as typically used with the THERMCON-85 apparatus

$$T = C(\ln t) + B(t) + A$$

(where A, B, and C are constants) includes a term that is linear with respect to time, taking into account small temperature drifts to allow measurements also in a certain range of a disturbed-temperature equilibrium. Therefore, it is assumed that any deviation from the ideal straight line of temperature plotted vs. log time are solely due to a superimposed temperature drift at a constant rate. However, the fitting of the test measurements

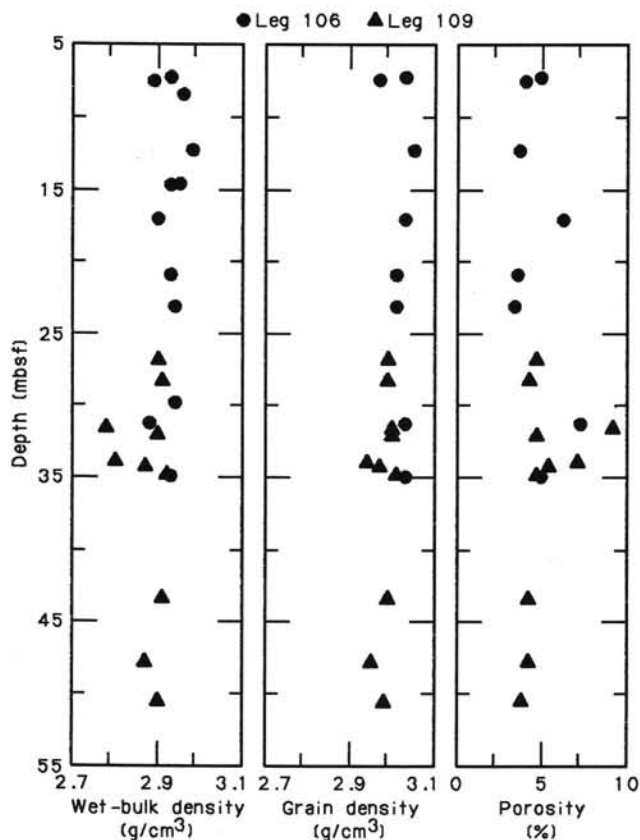


Figure 54. Wet-bulk density, grain density, and porosity as a function of depth.

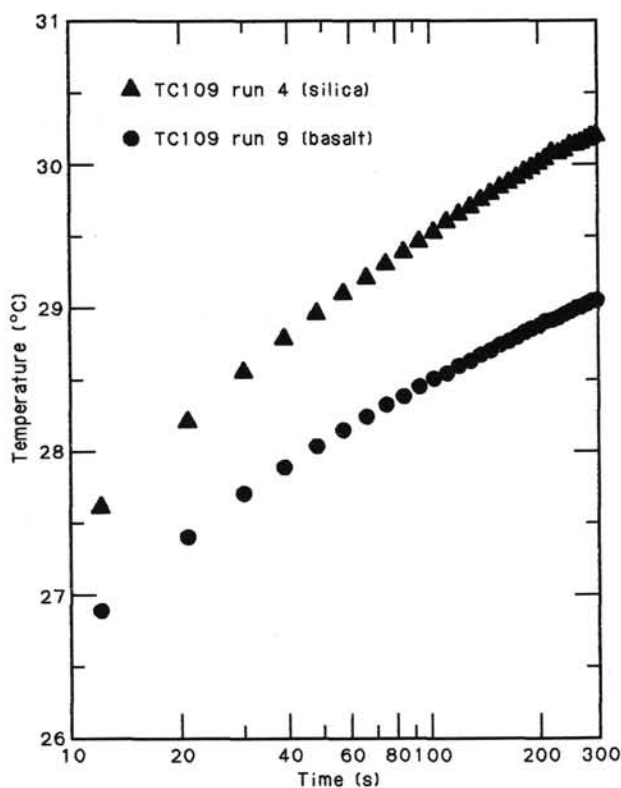


Figure 55. Temperature/log time curves resulting from test runs.

Table 18. Results of temperature vs. log time evaluations of different periods of heating time.

Evaluation range (s)	Constant C	Fitting parameter	Temperature drift rate (°C/min)
Curve fitting: $Y = C \cdot \ln t + B \cdot t + A$			
12-39	1.230	0.0009	-0.614
30-66	1.074	0.0008	-0.327
120-300	0.604	0.0041	-0.038
Curve fitting: $Y = C \cdot \ln t + A$			
12-39	1.001	0.0248	—
30-66	0.829	0.0103	—
120-300	0.611	0.0147	—

to this function yielded drift rates of about 0.01°C/min, although the voltmeter readings before starting the measurements revealed stable outputs (on the order of 0.1 mV corresponding to about 0.001°C) over periods of >10 min. Because the regression routines of the computer program used for the data reduction were carefully checked, we concluded that for the applied half-space needle-probe method, deviations from the ideal linear temperature-log time behavior are governed by factors other than a constant temperature-drift rate (e.g., unsymmetrical heat-flow pattern owing to partial embedment of the needle sensor into the base plate, improper thermal contacts, or finite length of needle and sample). Therefore, a second run was included in the program performing a simple linear regression:

$$T = C(\ln t) + A.$$

This curve fitting proved to be more consistent with the experimental conditions, according to a comparison of the evaluation

of the test measurements using both fittings over a variety of intervals of the measured temperature/log time curve. It yielded values for the constant C with significantly lower variation.

According to the results of the test measurements, a period from 30 to 66 s appeared to be most suitable for the evaluation of the thermal-conductivity measurements of basalt samples. All the measurement results listed in the following text were calculated from temperatures measured during this interval of heating time. However, for data reading and storage, a period of 2 min was chosen to provide an extended data base for a possible recalculation. The curve fitting might be improved by choosing time increments that are equidistant within the logarithmic time scale, thus avoiding a weighting of measurement points with increasing time. (This could be easily done by a slight hardware and software modification of the measurement device.) The recalibration of the measurement device for half-space needle-probe operation was performed with a fused-silica standard having a nominal thermal conductivity of 1.38 W/m·°C. The thermal conductivity of the rock samples is determined from the measurements by using the following formula, which is derivable from the aforementioned relations:

$$K = F \frac{1}{C},$$

where F is the instrumental calibration constant determined from C_0 , which is obtained by the measurement on the reference sample with known thermal conductivity K_0 :

$$F = C_0 K_0.$$

It should be mentioned that the evaluation of the measurements on rock samples, has to be performed only with the same time period as used for the determination of the calibration constant. As the test runs showed, a difference of chosen periods of only one measurement point may yield variations of the evaluated thermal-conductivity values of >10%.

The measurements were performed on seawater-saturated samples. The needle-probe device was installed underwater within a container. To improve the temperature stability, this container was provided a thermal insulation at its outer surfaces. To achieve temperature equilibrium, the measurements were done only after a waiting period of at least several hours.

In some measurements, the sample was slightly moved before repeating a measurement to ensure proper thermal contact. Table 19 shows an example of an outprint from measurement evaluation.

Results

The results of the measurements are shown in Table 20. The values given parenthetically were calculated by including a regression with a temperature-drift term. The thermal-conductivity measurement on the nine basalt samples from Hole 648B yielded the following mean value and standard deviation:

$$K = 1.80 \pm 0.07 (1.86 \pm 0.18) \text{ W/m} \cdot \text{°C}.$$

The value 1.80 W/m·°C agrees well with thermal conductivities measured with a divided bar instrument on 10 basalt samples from Hole 395A (Leg 78B), which yielded mean and standard deviation of 1.77 ± 0.02 W/m·°C (Hyndman et al., 1984). This value is also fully consistent with the results from measurements on about 60 basalt samples from Holes 417D and 418A (Legs 51 through 53) which are reported in a range from about 1.7 to 1.9 W/m·°C (Hamano, 1980).

Measurements performed on basalt samples from Hole 648B in ice water yielded no significant variations of the results

Table 19. Example of listing of results of thermal-conductivity determination modified for half-space needle probe.

Leg TC109			
27 May 1986			
Output for data from Site = Hole 648B			
Thermcon-85 run # 15			
Heater current = 0.1598			
Thermcon-85 position 1			
..... Needle KWH- 118			
Core-Section = 18-1			
Distance from top of section (cm) = 40-48			
Calibration Constant = 2.657			
Curve Fitting $T = C * \text{Int} + B * t + A$			
Time (sec)	Temp (deg C)	Deviation (deg C)	Resistance
30	27.732	1.412E-03	9197.08
39	27.904	-3.816E-03	9136.68
48	28.042	1.852E-03	9088.50
57	28.146	2.102E-03	9052.62
66	28.225	-1.549E-03	9025.38
Curve fit parameter ----- 2.989E-03			
Temp drift rate ----- 2.505E-01 (deg C/Min)			
Conductivity ----- 3.9664E-03 (Cal/cm C/s)			
1.66 (W/m·°C)			
Calibration Constant = 2.238			
Curve Fitting $T = C * \text{Int} + B * t + A$			
Time (sec)	Temp (deg C)	Deviation (deg C)	Resistance
30	27.732	-5.401E-03	9197.08
39	27.904	1.514E-03	9136.68
48	28.042	8.954E-03	9088.50
57	28.146	4.191E-03	9052.62
66	28.225	-9.257E-03	9025.38
Curve fit parameter ----- 8.464E-03			
Conductivity ----- 4.3457E-03 (Cal/cm C/s)			
1.82 (W/m·°C)			

within the tolerance of the present measurements. Therefore, we conclude that temperature dependency of the thermal conductivity of basalt is negligible in the temperature range from room temperature to about 0°C. It was not possible to perform a correlation with the data obtained from density and porosity measurements owing to the small variation of the results and the limited number of samples.

SUMMARY AND CONCLUSIONS

The establishment of the first bare-rock crustal drill hole in the rift valley of the Mid-Atlantic Ridge at Site 648 represents a major technological achievement. The utilization of the hard-rock guidebase and drilling-motor technology proved to be an effective means of spudding a hole on hard rock, providing adequate support for the bottom-hole assembly. The most limiting factor in drilling young fractured basalt, according to the results from Legs 106 and 109, is the lack of hole stability. An effective solution to this problem will require a major engineering effort to design new drilling systems specifically adapted to this difficult drilling environment.

Despite the limited penetration and core recovery at Hole 648B, the combined drilling results from Legs 106 and 109 provide a unique view of the internal structure of a small axial volcano on the MAR. The uppermost 30 m of the hole consists of plagioclase and olivine phyric pillow lava, erupted during the growth of the volcano. Below this there is a layer of fine-grained to glassy basalt <1 m thick, which grades downward into a coarsely vesicular aphyric basalt about 3 m thick. Below this, the basalt becomes massive and holocrystalline with some plagioclase phyric intervals. Major- and trace-element analyses through

Table 20. Results of thermal-conductivity measurements on basalt samples from Hole 648B.

Core section	Distance from top of section (cm)	Thermal conductivity (W/m·°C)	
109-648B-9R-1	77-90	1.69	(1.51)
		1.70	(1.68)
		1.72	(1.66)
		1.70	(1.61)
15R-1	30-37	1.79	(1.80)
		1.74	(1.76)
		1.77	(1.78)
16R-1	39-53	1.82	(1.66)
		1.81	(1.79)
		1.82	(1.73)
16R-1	77-92	1.87	(1.93)
		1.91	(1.74)
		1.88	(1.98)
		1.89	(1.88)
17R-1	20-25	1.88	(1.88)
		1.90	(2.00)
		1.89	(1.94)
18R-1	16-40	1.89	(2.05)
		1.69	(1.97)
		1.79	(2.01)
18R-1	40-48	1.83	(2.41)
		1.91	(1.88)
		1.87	(2.15)
19R-1	8-12	1.77	(2.16)
		1.79	(1.84)
		1.78	(2.00)
20R-1	44-54	1.72	(1.71)
		1.72	(1.61)
		1.72	(1.66)

these lithologically distinct units show, in contrast, a monotonous compositional uniformity, indicative of moderately evolved MORB.

The magnetic properties of the basalts from Hole 648B are similar to 100-m.y.-old basalt recovered on Leg 52 from DSDP Holes 417D and 418A. Dredged samples from the FAMOUS area and the samples obtained during Leg 37 (DSDP Hole 332) have small susceptibilities compared with the Hole 648B basalts, although the NRM intensities of the FAMOUS basalts are similar.

Physical properties of the samples from Hole 648B are typical of fresh, young oceanic basalts. Grain densities of 2.9–3.02 g/cm³ and porosities of 3%–10% yield bulk densities of 2.8–2.9 g/cm³. Sample compressional velocities range from 4.9 to 5.6 km/s, increasing with decreasing porosity. These porosities subdivide the cored interval into three zones: an upper, high-velocity, nonporous unit overlies highly vesicular, low-velocity material. Beneath this, the basalts again are nonvesicular and have uniformly high velocities.

The aforementioned drilling results combined with site-survey data indicate the following evolution of Serocki Volcano: (1) Eruptions of olivine-plagioclase phyric pillow lava constructed a small volcanic edifice on the floor of the rift valley. The thin, glassy zone recovered in Hole 648B probably represents the quenched top of a lava pond within the cone, which served as a holding tank for lava being fed to flows erupting at the seafloor.

Rising gas trapped beneath the quenched surface accounts for the vesicular unit, whereas the deeper holocrystalline basalts probably represent the more slowly cooled interior of the pond. (2) Additional eruptive pulses built a broad cone of pillow lavas above this pond. (3) Post-eruptive tectonism extensively fissured and faulted the flanks of the volcano. The relatively thick pelagic sediment that accumulated on the summit plateau suggests an age of at least few tens of thousands of years for Serocki Volcano.

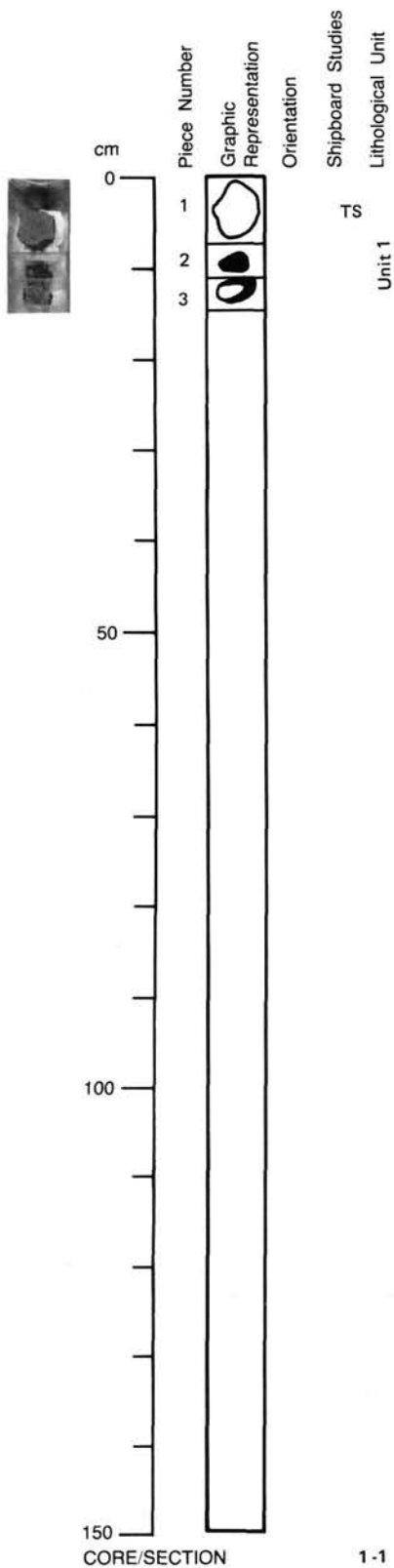
REFERENCES

- Baragar, W.R.A., Plant, A. G., Pringle, G. J., and Schau, M., 1977. Petrology and alteration of selected units of Mid-Atlantic Ridge basalt samples from Sites 332 and 335, DSDP. *Can. J. Earth Sci.*, 14:837-874.
- Böhlke, J. K., Honnorez, J., and Honnorez-Guerstein, B.-M., 1980. Alteration of basalts from Site 396B, DSDP: Petrographic and mineralogic studies. *Contrib. Mineral. Petrol.*, 73:341-364.
- Buckley, H. A., Bevan, J. C., Brown, K. M., and Johnson, L. R., 1978. Glauconite and celadonite: two separate mineral species. *Mineral. Mag.*, 42:373-382.
- Bryan, W. B., 1972. Morphology of quench crystals in submarine basalts. *J. Geophys. Res.*, 29:5812-5819.
- , 1974. Fe-Mg relationships in sector-zoned submarine basalt plagioclase. *Earth Planet. Sci. Lett.*, 24:157-165.
- Bryan, W. B., Thompson, G., and Ludden, J. N., 1981. Compositional variation in normal MORB from 22°-24°N, Mid-Atlantic Ridge and Kane Fracture Zone. *J. Geophys. Res.*, 86:11815-11836.
- Carmichael, R. S., 1982. *CRC Handbook of Physical Properties of Rocks*, Vol. 2: Boca Raton, FL (CRC Press).
- Carlsaw, H. S., and Jaeger, J. C., 1959. *Conduction of Heat in Solids* (2nd ed.): London (Oxford Univ. Press).
- Delaney, J. R., Muenow, D. W., and Graham, D. G., 1978. Abundance and distribution of water, carbon and sulfur in the glassy rims of pillow basalts. *Geochim. Cosmochim. Acta*, 42:581-594.
- Detrick, R. S., Ryan, W.B.F., Mayer, L., Fox, P. J., Kong, L., Manchester, K., Kastens, K., Karson, J., and Pockalny, R., 1985. *Mid-Atlantic Ridge/Kane Fracture Zone Final Site Survey Report*: Prepared for Joint Oceanogr. Inst., Inc
- Dungan, M. A., Long, P. E., and Rhodes, J. M., 1978. The petrography, mineral chemistry, and one-atmosphere phase relations of basalts from Site 395. In Melson, W. G., Rabinowitz, P. D., et al., *Init. Repts. DSDP*, 45: Washington (U.S. Govt. Printing Office), 461-478.
- Eshelby, J. D., 1957. The determination of the elastic field of an ellipsoidal inclusion and related problems. *Proc. R. Soc. London*, A241: 376-396.
- Flower, M.F.J., Ohnmacht, W., Schmincke, H.-U., Gibson, I. L., Robinson, P. T., and Parker, R., 1978. Petrology and geochemistry of basalts from Hole 396B, Leg 46. In Dmitriev, L., Heirtzler, J., et al., *Init. Repts. DSDP*, 46: Washington (U.S. Govt. Printing Office), 179-213.
- Grove, T. L., Bryan, W. B., 1983. Fractionation of pyroxene-phyric MORB at low pressure: An experimental study. *Contrib. Mineral. Petrol.*, 84:293-309.
- Hamano, Y., 1980. Physical properties of basalts from Holes 417D and 418A. In Donnelly, T., Francheteau, F., Robinson, P., Flower, M., Salisbury, M., et al., *Init. Repts. DSDP*, 51-53, Pt. 2: Washington (U.S. Govt. Printing Office), 1457-1466.
- Hamano, Y., Nishitani, T., and Kono, M., 1980. Magnetic properties of basalt samples from Deep Sea Drilling Project Holes 417D and 418A. In Donnelly, T., Francheteau, J., Bryan, W., Robinson, P., Flower, M., Salisbury, M., et al., *Init. Repts. DSDP*, 51-53, Pt. 2: Washington (U.S. Govt. Printing Office), 1391-1405.
- Honnorez, J., Karpoff, A. M., and Trauth-Badaut, D., 1983. Sedimentology, mineralogy, and geochemistry of green clay samples from the Galapagos hydrothermal mounds, Holes 506, 506C, and 507D, Deep Sea Drilling Project Leg 70 (preliminary data). In Honnorez, J., Von Herzen, R. P., et al., *Init. Repts. DSDP*, 70: Washington (U.S. Govt. Printing Office), 211-224.
- Hyndman, R. D., Christensen, N. I., and Drury, M. J., 1984. The physical properties of basalt core samples from Deep Sea Drilling Project Leg 78B, Hole 395A. In Hyndman, R. D., Salisbury, M. H., et al., *Init. Repts. DSDP*, 78B: Washington (U.S. Govt. Printing Office), 801-810.
- Jarosewich, E., Nelson, J. A., and Norberg, J. A., 1979. Reference samples for electron microprobe analysis. *Smithson. Contrib. Earth Sci.*, 22:68-72.
- Johnson, H. P., 1978. Rock magnetic properties of igneous rock samples—Leg 45. In Melson, W. G., Rabinowitz, P. D., et al., *Init. Repts. DSDP*, 45: Washington (U.S. Govt. Printing Office), 397-406.
- Kirkpatrick, R. J., 1978. Petrology of basalts: Hole 396B, DSDP Leg 46. In Dmitriev, L., Heirtzler, J., et al., *Init. Repts. DSDP*, 46: Washington (U.S. Govt. Printing Office), 165-178.
- Kuo, L. C., and Kirkpatrick, R. J., 1982. Pre-eruption history of phyrlic basalts from DSDP Legs 45 and 46: Evidence from morphology and zoning patterns in plagioclase. *Contrib. Mineral. Petrol.* 79:13-27.
- Kuster, G. T., and Toksöz, M. N., 1974. Velocity and attenuation of seismic wave in two-phase media: Part I. Theoretical formulation. *Geophysics*, 39:587-606.
- Laverne, C., and Vivier, G., 1983. Petrographical and chemical study of basement basalts from the Galapagos Spreading Center, Leg 70. In Honnorez, J., Von Herzen, R. P., et al., *Init. Repts. DSDP*, 70: Washington (U.S. Govt. Printing Office), 375-389.
- Merrill, R. T., and McElhinny, M. W., 1983. *The Earth's Magnetic Field*: London (Academic Press).
- Moos, D., and Zoback, M. D., 1983. In situ measurements of the properties of fractured crystalline rocks. *J. Geophys. Res.*, 80:2345-2354.
- Natland, J. H., 1978. Crystal morphologies in basalts from DSDP Site 395, 23°N, 46°W, Mid-Atlantic Ridge. In Melson, W. G., Rabinowitz, P. D., et al., 1978. *Init. Repts. DSDP*, 45: Washington (U.S. Govt. Printing Office), 423-446.
- O'Connell, R. J., and Budiasky, B., 1974. Seismic velocities in dry and saturated cracked solids. *J. Geophys. Res.*, 79:5412-5426.
- Prévoit, M., Lecaille, A., and Hekinian, R., 1979. Magnetism of the Mid-Atlantic Ridge crest near 37°N from FAMOUS and DSDP results: A review. In *Deep Drilling Results in the Atlantic Ocean: Ocean Crust*: Am. Geophys. Union, Maurice Ewing ser., 2,210-229.
- Rhodes, J. M., Dungan, M. A., Blanchard, D. P., and Long, P. E., 1979. Magma mixing at mid-ocean ridges: Evidence from basalts drilled near 22°N on the Mid-Atlantic Ridge. *Tectonophysics*, 55: 35-61.
- Roeder, P. L., and Emslie, R. F., 1970. Olivine-liquid equilibrium. *Contrib. Mineral. Petrol.*, 29:275-289.
- Sato, H., 1978. Segregation vesicles and immiscible liquid droplets in ocean-floor basalt of Hole 396B, IPOD/DSDP Leg 46. In Dmitriev, L., Heirtzler, J., et al., *Init. Repts. DSDP*, 46: Washington (U.S. Govt. Printing Office), 283-292.
- Smith, R. E., 1968. Segregation vesicles in basaltic lava. *Am. J. Sci.*, 265:696-713.
- Stephenson, A., and Collinson, D. W., 1974. Lunar magnetic field paleointensities determined by anhysteretic remanent magnetization method. *Earth Planet. Sci. Lett.*, 23:220.
- Thellier, E., 1951. Propriétés magnétiques des terres cuites et de roches. *J. Phys. Radium*, 12:205-218.
- Thellier, E., and Thellier, O., 1959. Sur l'intensité du champ magnétique terrestre dans le passé historique et géologique. *Ann. Geophys.*, 15:285-376.
- Toksöz, N., Cheng, C. H., and Timur, A., 1976. Velocities of seismic waves in porous rocks. *Geophysics*, 41:621-645.
- Tormey, D. T., Grove, T. L., and Bryan, W. B., 1987. Experimental petrology of normal MORB from the Kane Fracture Zone, 22°-25°N, Mid-Atlantic Ridge. *Contrib. Mineral. Petrol.*
- Von Herzen, R. P., and Maxwell, A. E., 1959. The measurement of thermal conductivity of deep sea sediments by a needle-probe method. *J. Geophys. Res.*, 64:1557-1563.
- Yamamoto, K., Kosuga, M., and Hirawawa, T., 1981. A theoretical method for determination of effective elastic constants of isotropic composites. *Sci. Rept. Tohoku Univ., ser. 5, Geophys.*, 28:47-67.
- Yoder, H. S., and Sahama, Th. G., 1957. Olivine x-ray determinative curve. *Am. Mineral.*, 42:475-491.

106-648A-1R-1

UNIT 1: SPARSELY PLAGIOCLASE PHYRIC-PILLOW BASALT

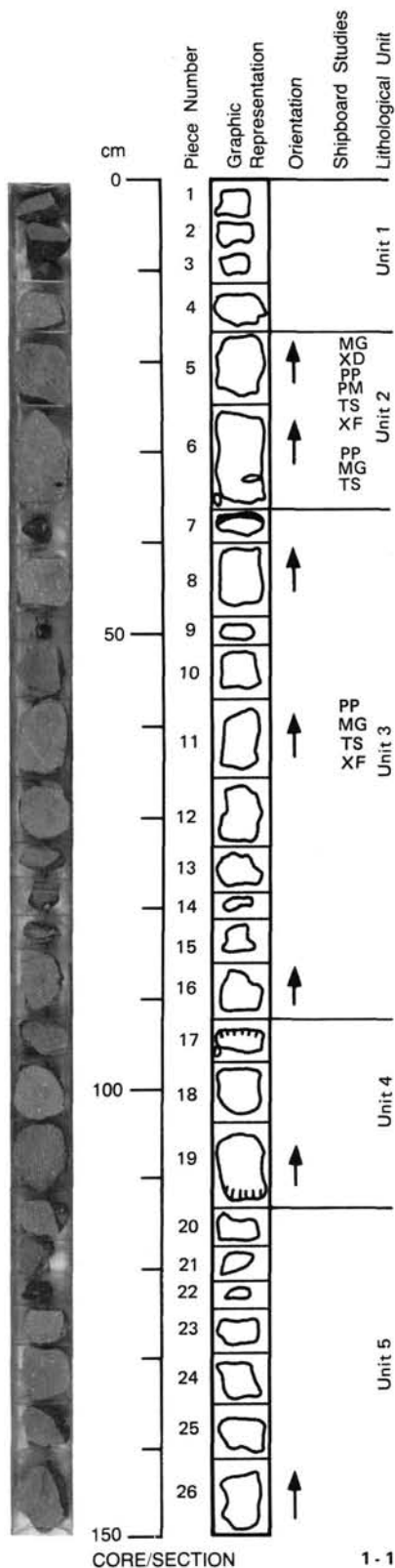
Pieces 1-3



GLASS: fresh; forms 70% of Piece 2, 50% of Piece 3.
PHENOCRYSTS: inhomogeneous distribution of plagioclase, approximately 1-2 mm, euhedral-subhedral, fresh.
 Piece 1: $\leq 1\%$.
 Piece 2: 2-4%.
 Piece 3: approximately 1%.
GROUNDMASS: Piece 1: microcrystalline ($\leq 100 \mu\text{m}$).
 Pieces 2 and 3: glassy variolitic.
COLOR: dark gray.
VESICLES: $< 1\%$, approximately 0.1 mm, round, unevenly distributed, dark smectite linings $< 5\%$.
ALTERATION: fresh, medium brown smectite surface coating, $< 2\%$ secondary phases in rock.
VEINS/FRACTURES: none.

Information on Core Description Forms, for ALL sites, represents field notes taken aboard ship. Some of this information has been refined in accord with post-cruise findings, but production schedules prohibit definitive correlation of these forms with subsequent findings. Thus the reader should be alerted to the occasional ambiguity or discrepancy.

106-648B-1R-1



UNIT 1: ASSORTED RUBBLE

Pieces 1-4

PIECE 1: SPARSELY PLAGIOCLASE PHYRIC BASALT

GLASS: none, no contacts.
PHENOCRYSTS: homogeneous distribution, plagioclase, 2%, approximately 2 mm, euhedral, fresh.
GROUNDMASS: uniformly fine grained.
COLOR: gray.
VESICLES: <1%, <1 mm, round, empty, clustered near phenocrysts.
ALTERATION: fresh.
VEINS/FRACTURES: none.

PIECE 2: SPARSELY PLAGIOCLASE PHYRIC BASALT

GLASS: none, no contacts.
PHENOCRYSTS: homogeneous distribution, plagioclase, 2%, 1-3 mm, euhedral, fresh.
GROUNDMASS: uniformly microcrystalline.
COLOR: gray.
VESICLES: <1%, <1 mm, round, empty.
ALTERATION: fresh.
VEINS/FRACTURES: none.

PIECE 3: APHYRIC BASALT

GLASS: none, no contacts.
PHENOCRYSTS: <1% plagioclase.
GROUNDMASS: very fine grained.
COLOR: gray.
VESICLES: <1%, <1 mm, round, empty.
ALTERATION: fresh.
VEINS/FRACTURES: none.

PIECE 4: MODERATELY PLAGIOCLASE PHYRIC BASALT

GLASS: none, no contacts.
PHENOCRYSTS: homogeneous distribution, plagioclase, 5%, <5 mm, euhedral, fresh.
GROUNDMASS: fine-grained, visible plagioclase laths.
COLOR: gray.
VESICLES: 1%, <1 mm, round, empty.
ALTERATION: fresh.
VEINS/FRACTURES: none.

UNIT 2: MODERATELY PLAGIOCLASE PHYRIC BASALT

Pieces 5 and 6

GLASS: none, no contacts.
PHENOCRYSTS: homogeneous distribution throughout unit of plagioclase, 3%, 2-5 mm, euhedral, fresh.
GROUNDMASS: microcrystalline (Piece 5) to fine grained (Piece 6), coarsening downward.
COLOR: gray.
VESICLES: Piece 5: 4%, <2 mm, round, empty.
 Piece 6: vug, approximately 10 mm diameter, lined with orange brown iron mineral; vesicles on outer surface lined with green clay mineral; black line and light halo 3 mm wide.
ALTERATION: fresh.
 Piece 6: 1 mm halo on top edge.
VEINS/FRACTURES: none.

CORE/SECTION

1 - 1

106-648B-1R-1 (continued)

UNIT 3: SPARSELY TO MODERATELY PLAGIOCLASE PHYRIC BASALT**Pieces 7-16**

GLASS: Piece 7: glassy margin with little glass, fresh, no contacts.

PHENOCRYSTS: irregular distribution of plagioclase throughout unit.

Pieces 7-10 and 13-16: approximately 2%, 2-5 mm, euhedral, fresh.

Pieces 11 and 12: 4%, 2-5 mm, euhedral, fresh.

GROUNDMASS: microcrystalline (Piece 7) to fine grained (Piece 16), coarsening downward.

COLOR: gray.

VESICLES: Tr-1%, <1-2 mm, round, empty, even distribution.

Piece 7: vug approximately 10 mm long lined with yellow orange iron mineral with 3 mm-wide halo.

Piece 14: vesicles concentrated along dark alteration zone.

ALTERATION: fresh.

Pieces 11 and 14: black line and light alteration halo around edge.

Piece 16: dark alteration halo around plagioclase phenocrysts at bottom of piece.

VEINS/FRACTURES: Piece 10: empty crack.

UNIT 4: MODERATELY PLAGIOCLASE PHYRIC BASALT**Pieces 17-19**

GLASS: none, cooling margin on Pieces 17 and 19, no contacts.

PHENOCRYSTS: homogeneous distribution throughout unit, plagioclase, 4%, 2-5 mm, euhedral, fresh.

GROUNDMASS: microcrystalline (Pieces 17 and 19) to fine grained in center (Piece 18).

COLOR: gray.

VESICLES: Piece 17: <7%, 1 mm, round, vesicles concentrated.

Piece 18: Tr-1%, <1 mm, round, empty, even distribution.

Piece 19: 2%, some 2 mm, most <1 mm, round, concentrated.

ALTERATION: fresh.

Piece 17: light alteration halo <2 cm wide with thin black line parallel to cooling margin.

VEINS/FRACTURES: several fine fractures with very thin green clay coating on broken surfaces.

UNIT 5: SPARSELY PLAGIOCLASE PHYRIC BASALT**1R-1, Piece 20, to 1R-2, Piece 1**

GLASS: none, no contacts.

PHENOCRYSTS: homogeneous distribution throughout unit, plagioclase, 2%, 2-5 mm, euhedral, fresh.

Piece 26: glomerocrysts, 2 mm across.

GROUNDMASS: microcrystalline margins with fine-grained center (Piece 24)

COLOR: gray.

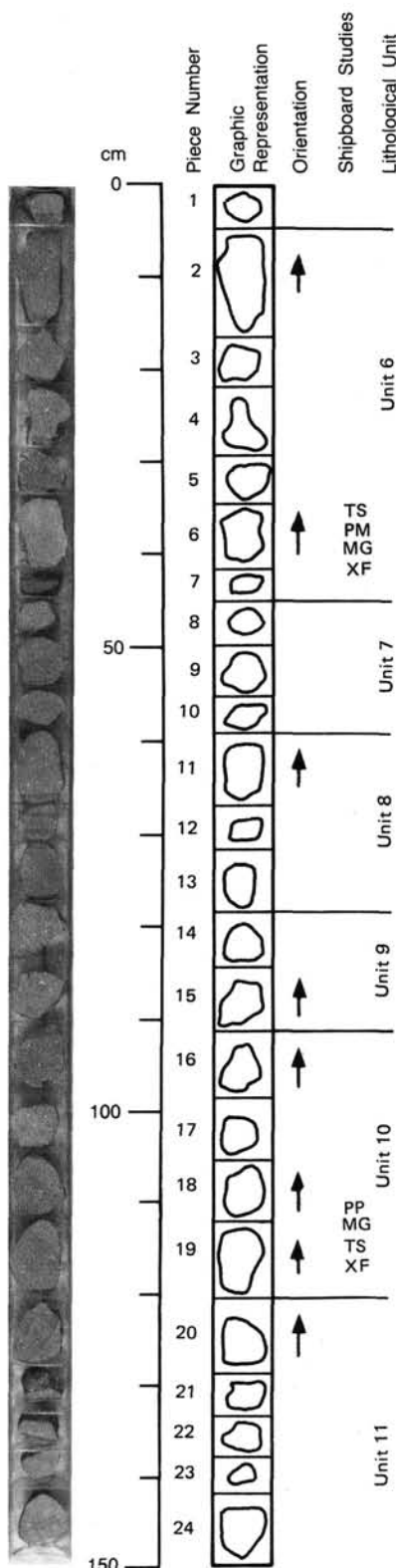
VESICLES: Tr-1%, <1-2 mm, round, empty, even distribution.

ALTERATION: fresh.

Piece 26: 3 mm light alteration halo along top with thin black line.

VEINS/FRACTURES: none.

106-648B-1R-2



UNIT 6: SPARSELY TO MODERATELY PLAGIOCLASE PHYRIC BASALT

Pieces 2-7

GLASS: none, no contacts.
PHENOCRYSTS: variable distribution throughout unit, plagioclase.
 Piece 2: 3%, 2-5 mm, euhedral, fresh.
 Pieces 3 and 4: 1%, 2-5 mm, euhedral, fresh.
 Piece 5: 2%, 2-5 mm, euhedral, fresh.
 Pieces 6 and 7: <1%, 2-5 mm, euhedral, fresh.
GROUNDMASS: uniformly microcrystalline except Piece 5, which is fine grained.
COLOR: gray.
VESICLES: Tr-1%, <1-2 mm, round, empty, even distribution.
ALTERATION: fresh.
 Piece 2: 4 cm-wide light alteration halo at top with thin black line.
VEINS/FRACTURES: Piece 4: minor empty cracks.

UNIT 7: SPARSELY PLAGIOCLASE PHYRIC BASALT

Pieces 8-10

GLASS: none, no contacts.
PHENOCRYSTS: homogeneous distribution throughout unit, plagioclase.
 Pieces 8 and 9: <2%, 2-5 mm, euhedral, fresh, including glomerocrysts.
 Piece 10: <1%, 2-5 mm, euhedral, fresh.
GROUNDMASS: microcrystalline (Pieces 8 and 10) to fine grained (Piece 9), coarsening to center.
COLOR: gray.
VESICLES: <1%, <1 mm, round, empty, even distribution.
ALTERATION: fresh.
 Piece 9: light alteration halos running irregularly across piece with thin black line.
 Piece 10: 2 mm black halo along edge.
VEINS/FRACTURES: none.

UNIT 8: SPARSELY TO MODERATELY PLAGIOCLASE PHYRIC BASALT

Pieces 11-13

GLASS: none, no contacts.
PHENOCRYSTS: variable distribution throughout unit, plagioclase.
 Piece 11: 4%, 2-5 mm, euhedral, fresh, glomerocrysts <3 mm across.
 Piece 12: 1%, 2-5 mm, euhedral, fresh.
 Piece 13: <1%, 2-5 mm, euhedral, fresh.
GROUNDMASS: microcrystalline (Piece 13) to fine grained (Piece 11), coarsening upward.
COLOR: gray.
VESICLES: Piece 11: 1%, <1 mm, round, empty, associated with phenocrysts.
 Pieces 12 and 13: <1%, <1 mm, round, empty, associated with phenocrysts.
ALTERATION: fresh.
 Piece 11: 2 mm black alteration halo along edge.
VEINS/FRACTURES: Piece 11: two empty hairline cracks.

CORE/SECTION

1 - 2

106-648B-1R-2 (continued)

UNIT 9: SPARSELY PLAGIOCLASE PHYRIC BASALT

Pieces 14 and 15

GLASS: none, no contacts.

PHENOCRYSTS: homogeneous distribution throughout unit, plagioclase.

Piece 14: 1-2%, 3 mm, euhedral, fresh, glomerocrysts 4 mm across.

Piece 15: 1-2%, 4 mm, euhedral, fresh, no glomerocrysts.

GROUNDMASS: fine grained (Piece 14) to microcrystalline (Piece 15), coarsening upward.

COLOR: gray.

VESICLES: <1%, <1 mm, round, empty, even distribution.

ALTERATION: fresh.

VEINS/FRACTURES: one very thin empty crack.

UNIT 10: SPARSELY TO MODERATELY PLAGIOCLASE PHYRIC BASALT

Pieces 16-19

GLASS: none, no contacts.

PHENOCRYSTS: irregular distribution throughout unit, plagioclase.

Pieces 16 and 18: 2%, 2-5 mm, euhedral, fresh.

Piece 17: 1%, 2-5 mm, euhedral, fresh.

Piece 19: 4%, 2-5 mm, euhedral, fresh.

GROUNDMASS: microcrystalline (Piece 19) to fine grained (Pieces 16-18), coarsening downward.

COLOR: gray.

VESICLES: <1%, <1 mm, round, empty, even distribution.

ALTERATION: fresh.

Piece 18: light alteration halo with black line, yellow-stained plagioclase.

Piece 19: black halo.

VEINS/FRACTURES: Pieces 16, 19, and 20: single open fracture without lining.

UNIT 11: SPARSELY TO MODERATELY PLAGIOCLASE PHYRIC BASALT

1R-2, Piece 20, to 1R-3, Piece 1

GLASS: none, no contacts.

PHENOCRYSTS: irregular distribution throughout unit, plagioclase.

Piece 20: 2%, 2-5 mm, euhedral, fresh.

Pieces 21-23: 1%, 2-5 mm, euhedral, fresh.

Piece 21: glomerocryst 10 mm across.

Piece 24: 4%, 2-5 mm, euhedral, fresh.

GROUNDMASS: microcrystalline (Piece 24) to fine grained (Piece 20), coarsening upward.

COLOR: gray.

VESICLES: <1%, <1 mm, round, empty, even distribution.

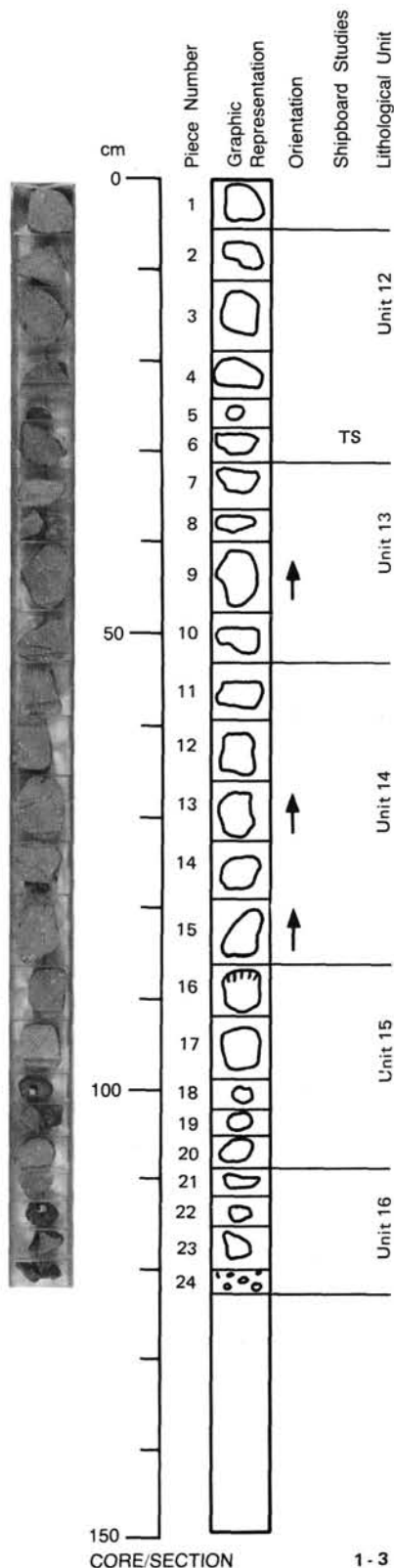
Pieces 21 and 22: associated with phenocrysts.

ALTERATION: fresh.

Piece 1: light alteration halo with black line.

VEINS/FRACTURES: none.

106-648B-1R-3



UNIT 12: SPARSELY TO MODERATELY PLAGIOCLASE PHYRIC BASALT

Pieces 2-6

GLASS: none, no contacts.
PHENOCRYSTS: irregular distribution throughout unit, plagioclase.
 Piece 2: 2%, 2-5 mm, euhedral, fresh.
 Pieces 3-6: 4%, 2-5 mm, euhedral, fresh.
GROUNDMASS: microcrystalline (Piece 6) to fine grained (Piece 2), coarsening upward.
COLOR: gray.
VESICLES: <1%, <2 mm, round, empty, even distribution.
ALTERATION: fresh.
VEINS/FRACTURES: none.

UNIT 13: SPARSELY TO MODERATELY PLAGIOCLASE PHYRIC BASALT

Pieces 7-10

GLASS: none, no contacts.
PHENOCRYSTS: homogeneous distribution throughout unit, plagioclase, 2-4%, 2-5 mm, euhedral, fresh.
GROUNDMASS: microcrystalline (Pieces 9 and 10) to fine grained (Pieces 7 and 8), coarsening upward.
COLOR: gray.
VESICLES: <1%, <1 mm, round, empty, associated with phenocrysts.
ALTERATION: fresh.
 Piece 8: light alteration halo with black line and yellow stained plagioclase.
 Pieces 9 and 10: light alteration halo with black line.
VEINS/FRACTURES: Piece 8: empty crack.

UNIT 14: SPARSELY TO MODERATELY PLAGIOCLASE PHYRIC BASALT

Pieces 11-15

GLASS: none, no contacts.
PHENOCRYSTS: homogeneous distribution throughout unit, plagioclase, 2-4%, 2-5 mm, euhedral, fresh.
 Pieces 11 and 14: glomerocrysts <3 mm across.
GROUNDMASS: uniformly fine grained.
COLOR: gray.
VESICLES: Tr-1%, <1 mm, round, empty, associated with phenocrysts and glomerocrysts.
 Piece 11: 2-3% vesicles and microlites, <0.5 mm, round, empty, concentrated in lines, not parallel.
ALTERATION: fresh.
 Piece 13: light alteration halo with black line.
VEINS/FRACTURES: none.

UNIT 15: SPARSELY TO MODERATELY PLAGIOCLASE PHYRIC BASALT

Pieces 16-20

GLASS: none.
 Piece 16: cooling margin without glass, no contacts.
PHENOCRYSTS: homogeneous distribution throughout unit, plagioclase, 2-4%, 2-5 mm, euhedral, fresh, glomerocrysts.
GROUNDMASS: microcrystalline (Pieces 17-20) to glassy (Piece 16), coarsening downward.
COLOR: gray.
VESICLES: Tr-1%, <1 mm, round, empty, often associated with phenocrysts.
 Piece 16: vesicles concentrated near margin (1%) <1% away from margin.
ALTERATION: fresh.
 Piece 16: light alteration halo with black line 35 mm from glassy margin edge.
 Pieces 18 and 19: light alteration halo with black line.
VEINS/FRACTURES: Piece 16: some open cracks extending from glass margin into sample.

UNIT 16: SPARSELY PLAGIOCLASE PHYRIC BASALT

Pieces 21-24

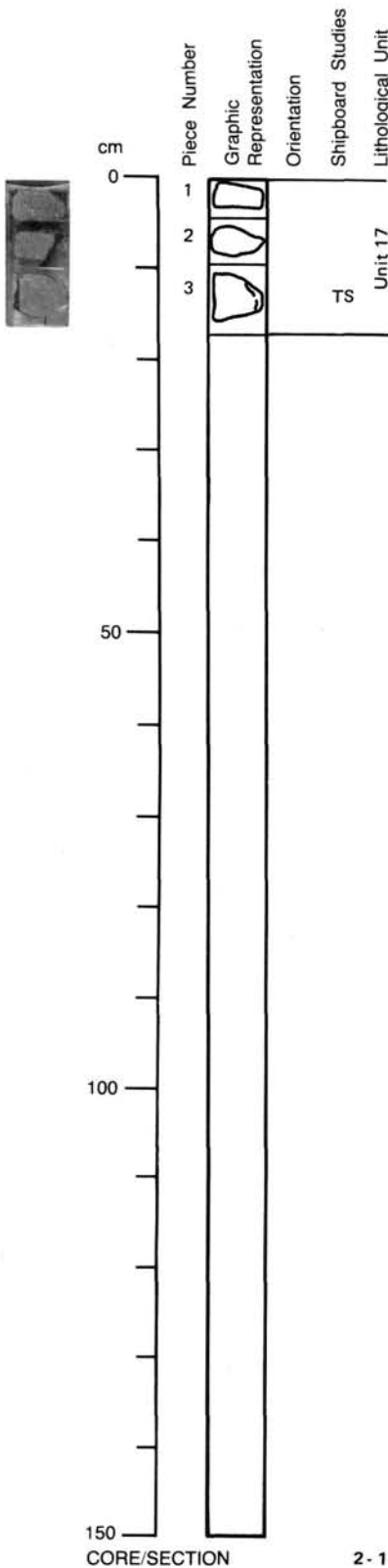
GLASS: none, no contacts.
PHENOCRYSTS: homogeneous distribution throughout unit, plagioclase, 2%, 2-5 mm, euhedral, fresh.
GROUNDMASS: microcrystalline (Piece 23) to fine grained (Piece 21), coarsening upward.
COLOR: gray.
VESICLES: <1%, <1 mm, round, empty, even distribution.
ALTERATION: fresh.
VEINS/FRACTURES: Piece 23: empty hairline crack.

CORE/SECTION

1-3

UNIT 17: ASSORTED RUBBLE

Pieces 1-3



PIECE 1: SPARSELY PLAGIOCLASE PHYRIC BASALT

GLASS: none, no contacts.
PHENOCRYSTS: homogeneous distribution, plagioclase, 2%, <4 mm, euhedral, fresh.
GROUNDMASS: uniformly fine grained.
COLOR: gray.
VESICLES: <1%, <1 mm, round, empty, even distribution.
ALTERATION: fresh, dark alteration halo on one edge.
VEINS/FRACTURES: none.

PIECE 2: SPARSELY PLAGIOCLASE PHYRIC BASALT

GLASS: none, no contacts.
PHENOCRYSTS: homogeneous distribution, plagioclase, 2%, <4 mm, euhedral, fresh.
GROUNDMASS: uniformly fine grained.
COLOR: gray.
VESICLES: <1%, <1 mm, round, empty, even distribution.
ALTERATION: fresh, 2 mm dark alteration halo along one edge.
VEINS/FRACTURES: none.

PIECE 3: SPARSELY PLAGIOCLASE PHYRIC BASALT

GLASS: none, no contacts.
PHENOCRYSTS: homogeneous distribution, plagioclase, 2%, <4 mm, euhedral, fresh.
GROUNDMASS: uniformly fine grained.
COLOR: gray.
VESICLES: <1%, <1 mm, round, empty, concentrated along some margins.
ALTERATION: fresh, light alteration halo with black line.
VEINS/FRACTURES: several hairline cracks, all empty; no preferred orientation.

106-648B-3R-1

UNIT 18: SPARSELY TO MODERATELY OLIVINE-PLAGIOCLASE PHYRIC BASALT

Pieces 1-4

GLASS: none, cooling margin on Piece 4, no contacts.

PHENOCRYSTS: irregular distribution throughout unit.

Plagioclase -

Piece 1: 2%, 2 mm, euhedral, fresh.

Piece 2: 2%, <6 mm, euhedral, fresh.

Piece 3: 4%, <6 mm, euhedral, fresh.

Piece 4: 3%, <6 mm, euhedral, fresh.

Pieces 1-4: approximately 20% of phenocrysts are glomerocrysts.

Olivine -

Piece 4: 1%, <0.5 mm, subhedral, in glomerocryst, fresh.

GROUNDMASS: microcrystalline (Piece 4) to fine grained (Piece 1), coarsening upward.

COLOR: gray.

VESICLES: Piece 1: <1%, <1 mm, round, empty, approximately 33% as miaroles, vesicles concentrated at lower margin.

Pieces 2 and 3: as in Piece 1, but even distribution.

Piece 4: 2%, <2 mm, round, most empty some with lining, even distribution, approximately 33% as miaroles.

ALTERATION: fresh.

Pieces 2 and 4: light alteration halo with black line.

VEINS/FRACTURES: Piece 4: several open cracks.

UNIT 19: SPARSELY TO MODERATELY OLIVINE-PLAGIOCLASE PHYRIC BASALT

Pieces 5-12

GLASS: Piece 12: glassy margin, fresh, no contacts.

PHENOCRYSTS: irregular distribution throughout unit.

Plagioclase -

Pieces 5-8: 3%, 2-4 mm, euhedral, fresh; approximately 33% of phenocrysts are glomerocrysts.

Pieces 9-12: 2%, 2-4 mm, euhedral, fresh.

Olivine - <1%, <1 mm, euhedral, in glomerocrysts, fresh.

GROUNDMASS: fine grained, with acicular groundmass plagioclase as large as 1 mm (Piece 5) to microcrystalline (Piece 12), coarsening upward.

COLOR: dark gray.

VESICLES: Pieces 5-8, 10, and 12: 3%, <1 mm, round, 5-10% with clay lining, others empty, even distribution, approximately 33% as miaroles.

Piece 8: 10% of vesicles lined with brown clay.

Pieces 9 and 11: <1%, <1 mm, round, empty.

Piece 12: concentrated at bottom.

ALTERATION: fresh.

Piece 5: 10-mm-thick light alteration halo with black line.

Pieces 6-8: light alteration halo on margin with black line.

Piece 12: light alteration halo with black line 10 mm from glassy margin, penetrating further inside along a fracture.

VEINS/FRACTURES: Piece 10: several fractures, void.

Piece 12: several fractures coated with greenish brown clay.

UNIT 20: SPARSELY TO MODERATELY OLIVINE-PLAGIOCLASE PHYRIC BASALT

3R-1, Piece 13, to 4R-1, Piece 1

GLASS: none, no contacts.

PHENOCRYSTS: irregular distribution throughout unit.

Plagioclase -

Piece 13: 2%, 1-2 mm, euhedral, fresh, some glomerocrysts.

Pieces 1 and 14: 3%, <5 mm, euhedral, fresh, some glomerocrysts.

Olivine - <1%, <1 mm, euhedral, fresh, some glomerocrysts.

GROUNDMASS: uniformly fine grained.

COLOR: dark gray.

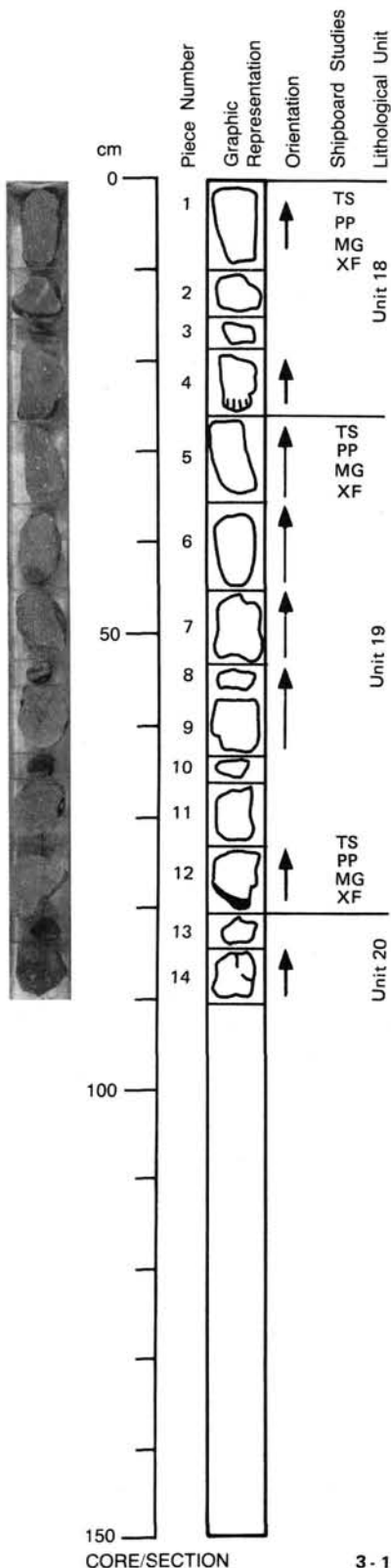
VESICLES: Pieces 1 and 14: 1%, <1 mm, round, empty, even distribution.

Piece 13: concentrated at one margin.

ALTERATION: fresh.

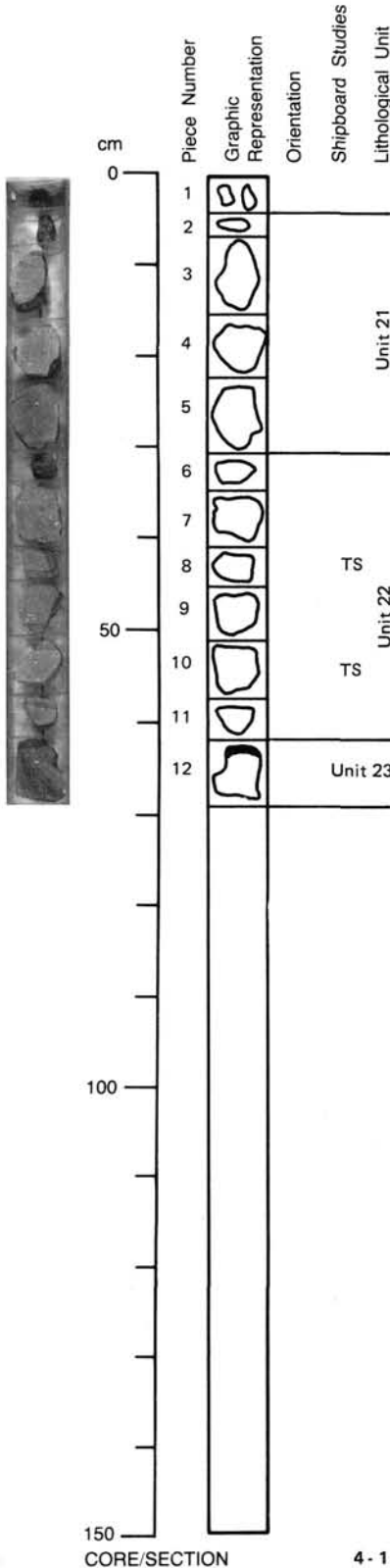
Piece 14: 20-30-mm light alteration halo with black line on all sides.

VEINS/FRACTURES: Piece 14: several empty cracks.



CORE/SECTION

3 - 1



UNIT 21: MODERATELY PLAGIOCLASE PHYRIC BASALT

Pieces 2-5

GLASS: none, no contacts.
PHENOCRYSTS: homogeneous distribution throughout unit, plagioclase, 3%, <5 mm, euhedral, fresh.
 Piece 4: 1-7 mm.
GROUNDMASS: uniformly fine grained.
COLOR: gray.
VESICLES: <1%, <1 mm, round, empty, even distribution.
 Piece 4: concentrated along two margins.
ALTERATION: fresh.
 Pieces 2 and 3: Light alteration halo with black line approximately 2 mm in from edge.
 Piece 3: orange clay coating on some surfaces.
 Piece 5: light alteration halo with two black lines approximately 4 mm and 10 mm from edge.
VEINS/FRACTURES: Piece 5: empty fracture.

UNIT 22: SPARSELY PLAGIOCLASE PHYRIC BASALT

Pieces 6-11

GLASS: none, no contacts.
PHENOCRYSTS: homogeneous distribution throughout unit, plagioclase, 2%, 2-5 mm (average 3 mm), euhedral, fresh.
 Piece 7: 3%.
GROUNDMASS: fine grained, coarsening toward Piece 10.
COLOR: gray.
VESICLES: Piece 6: 1%, <2 mm, irregular, empty, aligned throughout center of piece.
 Pieces 7-9 and 11: <1%, <1 mm, irregular, empty, even distribution.
 Piece 8: occasionally lined with orange brown mineral.
 Piece 10: 2%, <2 mm, mostly round, empty, even distribution.
ALTERATION: fresh.
 Piece 7: light alteration halo with black line approximately 3 mm from edge; three dark, irregularly shaped patches approximately 7 mm across.
 Piece 8: complex and irregular halo, structure similar to Piece 7, clay on outer surface.
 Piece 9: light alteration halo with black line approximately 10 mm from edge
 Piece 10: small, light alteration halo with black line approximately 2-5 mm from edge.
 Piece 11: minor clay on surface.
VEINS/FRACTURES: Pieces 7 and 8: one small fracture, empty.

UNIT 23: SPARSELY PLAGIOCLASE PHYRIC BASALT

Piece 12

GLASS: glassy margin (pillow?), incipient weathering, no contacts.
PHENOCRYSTS: homogeneous distribution throughout unit, plagioclase, 1%, 3-6 mm, average 3 mm, euhedral, fresh.
GROUNDMASS: very fine grained to microcrystalline.
COLOR: dark gray.
VESICLES: <1%, generally <1 mm but some 3 mm, round and elongate, empty, concentrated toward glassy margins.
ALTERATION: fresh, light alteration halo with 1-2 mm black line 35 mm from glassy margin, incipient weathering of glass.
VEINS/FRACTURES: none.

106-648B-5R-1

UNIT 24: ASSORTED RUBBLE

Pieces 1-8

PIECE 1: SPARSELY PLAGIOCLASE-OLIVINE PHYRIC BASALT

GLASS: very little, maybe tachylite, no contacts.
PHENOCRYSTS: homogeneous distribution.
 Plagioclase - 1-2%, 1.5 mm, euhedral, fresh, 20% as glomerocrysts with olivine.
 Olivine - <1%, 0.5 mm, euhedral, fresh, in glomerocrysts with plagioclase.
GROUNDMASS: microcrystalline to fine grained.

COLOR: dark gray.
VESICLES: none.
ALTERATION: fresh.
VEINS/FRACTURES: none.

PIECE 2: SPARSELY PLAGIOCLASE PHYRIC BASALT

GLASS: none, no contacts.
PHENOCRYSTS: homogeneous distribution, plagioclase, 1-2%, 1.5 mm, euhedral, fresh.
GROUNDMASS: uniformly fine grained.

COLOR: dark gray.
VESICLES: 2%, 0.5 mm average, round, empty, 80% as miaroles.
ALTERATION: fresh.
VEINS/FRACTURES: none.

PIECE 3: SPARSELY PLAGIOCLASE PHYRIC BASALT

GLASS: none, no contacts.
PHENOCRYSTS: homogeneous distribution, plagioclase, 1-2%, approximately 2 mm, euhedral, fresh.
GROUNDMASS: uniformly fine grained.

COLOR: dark gray.
VESICLES: 1%, 0.5 mm average, round, empty, 10% as miaroles.
ALTERATION: fresh.
VEINS/FRACTURES: none.

PIECE 4: SPARSELY PLAGIOCLASE PHYRIC BASALT

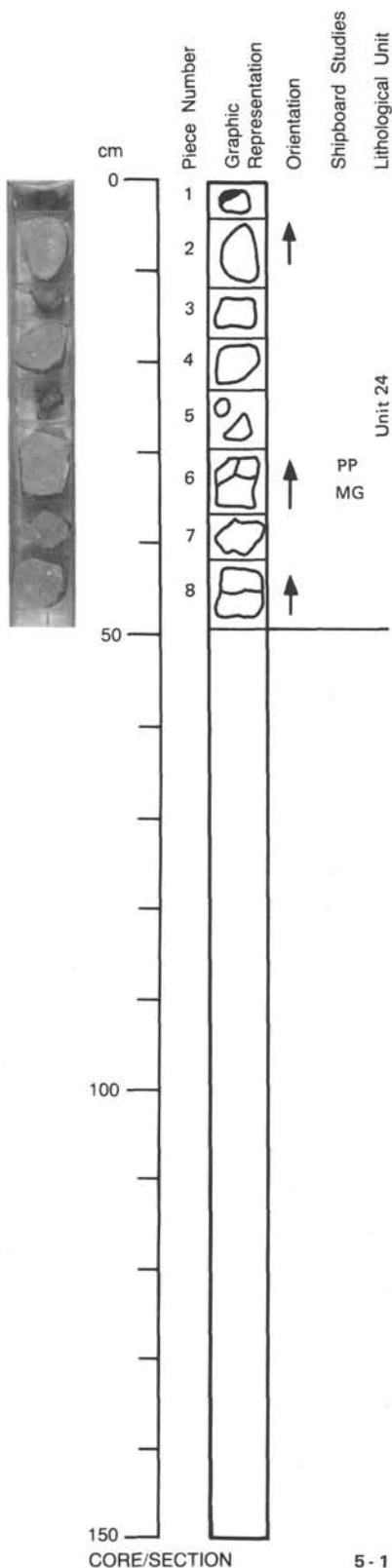
GLASS: none, no contacts.
PHENOCRYSTS: homogeneous distribution, plagioclase, 1-2%, approximately 2 mm, euhedral, fresh.
GROUNDMASS: uniformly fine grained.

COLOR: dark gray.
VESICLES: 3%, 0.1-0.5 mm average, round, 90% empty 10% with brown lining at edge of piece.
ALTERATION: fresh, 6 mm light alteration halo with black line, brown lining in vesicles.
VEINS/FRACTURES: none.

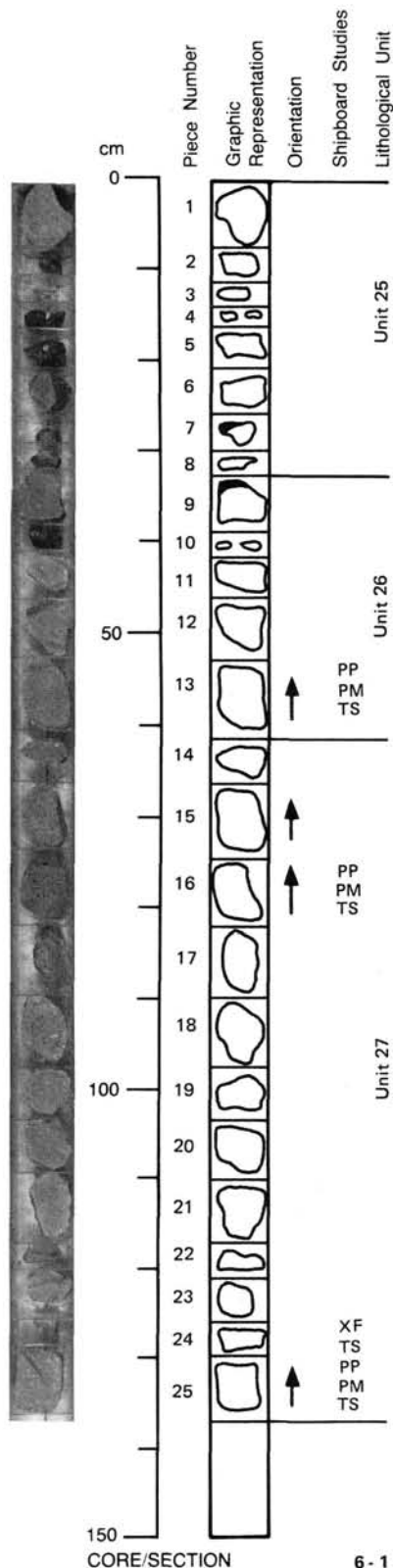
PIECE 5: SPARSELY PLAGIOCLASE-OLIVINE PHYRIC BASALT

GLASS: none, no contacts.
PHENOCRYSTS: homogeneous distribution.
 Plagioclase - 1-2%, 1.5 mm, euhedral, fresh, in glomerocrysts with olivine.
 Olivine - <1%, 0.5 mm, euhedral, fresh, in glomerocrysts with plagioclase.

GROUNDMASS: very fine grained.
COLOR: dark gray.
VESICLES: approximately 1%, 0.5 mm, round, minor lining to vesicles at edge of piece.
ALTERATION: fresh, surface coating.
VEINS/FRACTURES: none.



5 - 1



UNIT 25: SPARSELY TO MODERATELY PLAGIOCLASE PHYRIC BASALT

Pieces 1-8

GLASS: Piece 7: two glass fragments <5 mm, fresh, no contacts.
PHENOCRYSTS: irregular distribution throughout unit, plagioclase.
 Pieces 1-4, 6, and 7: 3%, <4 mm, euhedral, fresh.
 Pieces 5 and 8: 2%, <4 mm, euhedral, fresh.
GROUNDMASS: uniformly fine grained, glass fragments (Piece 7).
COLOR: gray.
VESICLES: Pieces 1-3, 6, and 7: rare, <1 mm, round, empty, even distribution.
 Piece 4: 1%, <1-2 mm, round, empty, even distribution.
 Pieces 5 and 8: <1%, 1 mm, round, minor clay on surface.
ALTERATION: fresh.
 Piece 2: small, light alteration halo with black line.
 Pieces 4, 5, and 8: minor yellow green clay on surfaces.
VEINS/FRACTURES: none.

UNIT 26: SPARSELY PLAGIOCLASE-OLIVINE PHYRIC BASALT

Pieces 9-13

GLASS: Piece 9: fresh glassy margin, no contacts.
PHENOCRYSTS: homogeneous distribution throughout unit.
 Plagioclase - <2%, 1-4 mm, euhedral, fresh.
 Olivine - Piece 9: rare, <1 mm, euhedral to subhedral, fresh.
GROUNDMASS: microcrystalline (Piece 9) to fine grained (Piece 13), coarsening downward.
COLOR: gray.
VESICLES: <1%, <1 mm, round, empty, even distribution.
ALTERATION: fresh.
 Piece 9: 2 mm-wide dark alteration halo on one margin, minor clay on surface.
 Piece 11: minor yellow green clay on surface.
 Piece 12: 5 mm-wide dark alteration halo on one margin.
 Piece 13: 2-4 mm-wide dark alteration halo on one margin.
VEINS/FRACTURES: empty hairline fractures void.

UNIT 27: SPARSELY TO MODERATELY PLAGIOCLASE-OLIVINE PHYRIC BASALT

Pieces 14-25

GLASS: none, no contacts.
PHENOCRYSTS: irregular distribution throughout unit.
 Plagioclase - 2%, 1-5 mm, euhedral, fresh.
 Piece 18: one phenocryst 8 mm long.
 Piece 25: 3%, 1-5 mm, euhedral, fresh.
 Olivine - trace, 1 mm, subhedral to euhedral, fresh.
GROUNDMASS: fine grained, coarsening toward Piece 25.
COLOR: gray.
VESICLES: vesicle distribution distinct in this unit.
 Pieces 14-18: 5%, 1-3 mm, mostly round, some irregular, even distribution, some filled with orange brown clay or lined with bluish green mineral in halos.
 Pieces 19-25: <1%, <1 mm, round, empty, even distribution.
ALTERATION: fresh, but with alteration halos.
 Pieces 14, 15, 17, and 21-24: light alteration halo with 1 mm-wide black line 2 mm from margin.
 Piece 16: light alteration halo with black line 4 mm from margin, minor orange brown clay on surface.
 Piece 18: light alteration halo with black line 1-4 mm from surface, clay on surface, vesicles in halo filled or lined by clay.
 Piece 25: incipient light alteration halo with black line 5 mm from upper margin, clay on upper surface.
VEINS/FRACTURES: Piece 15: empty hairline fracture.

106-648B-6R-1 (continued)

PIECE 6: SPARSELY PLAGIOCLASE-OLIVINE PHYRIC BASALT**GLASS:** none, no contacts.**PHENOCRYSTS:** homogeneous distribution.

Plagioclase - 1-2%, 1.5 mm, euhedral, fresh.

Olivine - <1%, 0.5-1.0 mm, euhedral, fresh, as isolated crystals.

GROUNDMASS: fine grained.**COLOR:** dark gray.**VESICLES:** 1%, 1 mm, round, some elongate, empty, 20% as miaroles.**ALTERATION:** fresh, 25-mm light alteration halo near open crack with black line.**VEINS/FRACTURES:** several empty cracks.**PIECE 7: SPARSELY PLAGIOCLASE-OLIVINE PHYRIC BASALT****GLASS:** none, no contacts.**PHENOCRYSTS:** homogeneous distribution.

Plagioclase - 1-2%, 2 mm, euhedral, fresh, as glomerocrysts with olivine.

Olivine - <1%, 0.5 mm, euhedral, fresh, in glomerocrysts with plagioclase.

GROUNDMASS: fine grained.**COLOR:** dark gray.**VESICLES:** <1%, 1 mm, few 3-4 mm on outer surface, round, lined by brownish yellow clay.**ALTERATION:** fresh, except outer surfaces.**VEINS/FRACTURES:** several empty cracks.**PIECE 8: SPARSELY PLAGIOCLASE-OLIVINE PHYRIC BASALT****GLASS:** none, no contacts.**PHENOCRYSTS:** homogeneous distribution.

Plagioclase - 1-2%, 2 mm (one 5 mm), euhedral, fresh, as glomerocrysts with olivine.

Olivine - <1%, 0.5 mm, euhedral, fresh, in glomerocrysts with plagioclase.

GROUNDMASS: fine grained.**COLOR:** dark gray.**VESICLES:** 2%, 0.2-0.5 mm, round, empty, approximately 20% as miaroles.**ALTERATION:** fresh, light alteration halo with black line on outer surface.**VEINS/FRACTURES:** one crack partially lined with brown smectite.

THIN SECTION DESCRIPTION

106-648A-1R-1 (Piece 1, 2-4 cm)

ROCK NAME: Sparsely olivine plagioclase phyric basalt

WHERE SAMPLED: Unit 1

TEXTURE: Subvolcanic

GRAIN SIZE: Fine to cryptocrystalline

PRIMARY MINERALOGY	PERCENT PRESENT	PERCENT ORIGINAL	SIZE RANGE (mm)	APPROX. COMPOSITION	MORPHOLOGY	COMMENTS
PHENOCRYSTS						
Olivine	<1	<1	0.3		Euhedral-subhedral	
Plagioclase	<1	<1	0.5-1.5		Euhedral	Normally zoned.
GROUNDMASS						
Plagioclase	50	50	0.05-0.30		Acicular	Also belt buckle, swallowtail, and radiate.
Olivine	1	1	0.05-0.30		Acicular	
Clinopyroxene	38	38	0.02-0.30		Acicular, sheaths	
Mesostasis	10	10				Cryptocrystalline. Percentage includes opaques.
SECONDARY MINERALOGY						
SECONDARY MINERALOGY	PERCENT	REPLACING/FILLING				COMMENTS
Clays	Tr	Mesostasis				Rare reddish brown and yellow-green clays occur in the groundmass.

VESICLES/CAVITIES	PERCENT	LOCATION	SIZE RANGE (mm)	FILLING	SHAPE
Vesicles	<1		0.1	None	Round

THIN SECTION DESCRIPTION

106-648B-1R-1 (Piece 5, 20-23 cm)

ROCK NAME: Moderately plagioclase olivine phyric basalt

WHERE SAMPLED: Unit 2

TEXTURE: Glomeroporphyritic, intersertal to intergranular

GRAIN SIZE: Fine to cryptocrystalline

PRIMARY MINERALOGY	PERCENT PRESENT	PERCENT ORIGINAL	SIZE RANGE (mm)	APPROX. COMPOSITION	MORPHOLOGY	COMMENTS
PHENOCRYSTS						
Olivine	<1	<1	0.4		Subhedral	In glomerocrysts with plag.
Plagioclase	1	1	≤ 2	An 75	Acicular	In glomerocrysts with ol.
Plagioclase	2	2	≤ 2.4	An 79	Euhedral	Equant to prismatic. Discrete crystals. Often patchy zoning.
GROUNDMASS						
Plagioclase	50	50	0.04-0.60		Acicular, belt buckle	
Olivine	2	2	0.04		Acicular	Radiate ol-cpx-plag.
Clinopyroxene	40	40	0.04		Acicular	
Opaques	3	3				
Mesostasis	1	1				Cryptocrystalline.

VESICLES/CAVITIES	PERCENT	LOCATION	SIZE RANGE (mm)	FILLING	SHAPE
Vesicles	<1		<0.1	None	Round

COMMENTS: Similar to 106-648B-1R-1 (Piece 6, 30-33 cm). Possible microlites. Possible segregation vesicles with diffuse boundaries (<1% of the section).

THIN SECTION DESCRIPTION

106-648B-1R-1 (Piece 6, 30-33 cm)

ROCK NAME: Moderately plagioclase olivine phyric basalt

WHERE SAMPLED: Unit 2

TEXTURE: Glomeroporphyritic, intersertal to intergranular

GRAIN SIZE: Fine to cryptocrystalline

PRIMARY MINERALOGY	PERCENT PRESENT	PERCENT ORIGINAL	SIZE RANGE (mm)	APPROX. COMPOSITION	MORPHOLOGY	COMMENTS
PHENOCRYSTS						
Olivine	1	1	0.4		Subhedral	In glomerocrysts with plag.
Plagioclase	3	3	≤2		Acicular	In glomerocrysts with ol.
Plagioclase	2	2	≤2	An 77	Euhedral	Equant to prismatic. Discrete crystals, often zoned.
GROUNDMASS						
Plagioclase	50	50	0.06-0.16		Acicular, belt buckle, swallowtail	
Olivine	2	2	0.06-0.12		Acicular	Radiate ol-plag-cpx.
Clinopyroxene	38	38	0.06-0.12		Subhedral, acicular	
Opaques	2	2				
Mesostasis	2	2				Cryptocrystalline

COMMENTS: One plag phenocryst is composed of elongated, interfingering of plag and groundmass. One plag phenocryst is sector zoned. Some plag phenocrysts have partially resorbed cores with cryptocrystalline melt inclusions.

THIN SECTION DESCRIPTION

106-648B-1R-1 (Piece 11, 59-62 cm)

ROCK NAME: Moderately plagioclase olivine phyric basalt

WHERE SAMPLED: Unit 3

TEXTURE: Glomeroporphyritic, subvolcanic to intersertal

GRAIN SIZE: Fine to cryptocrystalline

PRIMARY MINERALOGY	PERCENT PRESENT	PERCENT ORIGINAL	SIZE RANGE (mm)	APPROX. COMPOSITION	MORPHOLOGY	COMMENTS
PHENOCRYSTS						
Olivine	1	1	≤1		Subhedral	In glomerocrysts with plag.
Plagioclase	1	1	≤2	An 75	Euhedral	Prismatic. In glomerocrysts with olivine.
Plagioclase	3	3	≤2	An 79	Euhedral, rounded	Isolated crystals. Some strongly, normally zoned. Some oscillatory zoned.
GROUNDMASS						
Plagioclase	50	50	0.06-2.00		Acicular	Belt buckle and swallowtail forms also.
Olivine	2	2	0.01-0.06		Acicular	
Clinopyroxene	38	38	0.03		Acicular	
Opaques	3	3		Ilmenite, Fe sulfide, titanomagnetite		Fe sulfide occurs as blebs.
Mesostasis	2	2				Cryptocrystalline.

VESICLES / CAVITIES	PERCENT	LOCATION	SIZE RANGE (mm)	FILLING	SHAPE
Vesicles	< 1		0.25	None	Round

THIN SECTION DESCRIPTION

106-648B-1R-2 (Piece 6, 37-40 cm)

ROCK NAME: Moderately plagioclase olivine phyric basalt

WHERE SAMPLED: Unit 6

TEXTURE: Glomeroporphyritic, subvariolithic

GRAIN SIZE: Fine to cryptocrystalline

PRIMARY MINERALOGY	PERCENT PRESENT	PERCENT ORIGINAL	SIZE RANGE (mm)	APPROX. COMPOSITION	MORPHOLOGY	COMMENTS
PHENOCRYSTS						
Olivine	0.2	0.2	0.2-0.3		Anhedral	Isolated crystals.
Olivine	0.8	0.8	0.1-0.3		Subhedral	In glomerocrysts.
Plagioclase	3	3	≤ 4	An 79	Laths, equant	Isolated crystals. Narrow normally-zoned rims. Some sector zoning.
Plagioclase	1	1	1-3	An 75	Tabular	In glomerocrysts.
Clinopyroxene	Tr	Tr	0.35		Anhedral	In glomerocrysts.
GROUNDMASS						
Plagioclase	50	50	< 0.1		Acicular	Belt buckle and swallowtail forms also present.
Olivine	1	1	< 0.1		Acicular	Radiate ol-plag-cpx.
Clinopyroxene	38	38	< 0.1		Acicular	
Opaques	4	4	0.01			
Mesostasis	2	2				Cryptocrystalline.

COMMENTS: Melt inclusions in larger plag and ol phenocrysts are cryptocrystalline.

THIN SECTION DESCRIPTION

106-648B-1R-2 (Piece 19, 114-117 cm)

ROCK NAME: Moderately plagioclase olivine phyric basalt

WHERE SAMPLED: Unit 10

TEXTURE: Glomeroporphyritic, intersertal to intergranular

GRAIN SIZE: Fine to cryptocrystalline

PRIMARY MINERALOGY	PERCENT PRESENT	PERCENT ORIGINAL	SIZE RANGE (mm)	APPROX. COMPOSITION	MORPHOLOGY	COMMENTS
PHENOCRYSTS						
Olivine	0.8	0.8	≤ 1		Subhedral-euhedral	In glomerocrysts with plag.
Olivine	0.2	0.2	0.6		Subhedral	Isolated crystals.
Plagioclase	2	2	≤ 1.5		Laths	In glomerocrysts with ol.
Plagioclase	2	2	≤ 2	An 79	Euhedral, rounded	Isolated crystals. Normally zoned rims.
GROUNDMASS						
Plagioclase	50	50	< 0.1		Acicular	Belt buckle and swallowtail forms also present.
Olivine	1	1	< 0.1		Acicular	Radiate plag-ol-cpx.
Clinopyroxene	40	40	< 0.1		Acicular	
Opaques	2	2	< 0.1			
Mesostasis	2	2				Cryptocrystalline.

VESICLES/CAVITIES	PERCENT	LOCATION	SIZE RANGE (mm)	FILLING	SHAPE
Vesicles	< 1		< 0.3	None	Round

COMMENTS: Finer grained than 106-648B-1R-2 (Piece 6, 37-40 cm). Round segregation vesicles (< 1% of the section), 1 mm in diameter, are completely filled. Cryptocrystalline melt inclusions in some large plag phenocrysts.

THIN SECTION DESCRIPTION

106-648B-1R-2 (Piece 19, 117-120 cm)

ROCK NAME: Moderately plagioclase olivine phyric basalt

WHERE SAMPLED: Unit 10

TEXTURE: Glomeroporphyritic, subvolcanitic

GRAIN SIZE: Fine to cryptocrystalline

PRIMARY MINERALOGY	PERCENT PRESENT	PERCENT ORIGINAL	SIZE RANGE (mm)	APPROX. COMPOSITION	MORPHOLOGY	COMMENTS
PHENOCRYSTS						
Olivine	1.5	1.5	≤ 1		Euhedral-subhedral	In glomerocrysts with plag.
Olivine	0.5	0.5	≤ 1		Euhedral	Isolated crystals.
Plagioclase	1	1	≤ 1.5		Euhedral	In glomerocrysts with ol.
Plagioclase	3	3	≤ 2	An 79	Euhedral, rounded	Isolated crystals. Some normally zoned.
GROUNDMASS						
Plagioclase	50	50	< 0.1		Acicular	Belt buckle and swallowtail forms also present.
Olivine	2	2	< 0.1		Acicular	Radiate ol-plag-cpx.
Opaques	3	3	< 0.1			
Mesostasis	7	7				Cryptocrystalline.
Clinopyroxene	32	32	< 0.1		Acicular	Radiating

VESICLES/CAVITIES	PERCENT	LOCATION	SIZE RANGE (mm)	FILLING	SHAPE	COMMENTS
Vesicles	< 0.1		< 0.1	None	Round	

COMMENTS: Similar to 106-648B-1R-2 (Piece 19, 114-117 cm), except more ol in glomerocrysts. Round segregation vesicles (< 1% of the section), 0.4 - 1.0 mm in diameter, are completely filled. Rare cryptocrystalline inclusions in plag and ol phenocrysts.

THIN SECTION DESCRIPTION

106-648B-1R-3 (Piece 6, 26-29 cm)

ROCK NAME: Moderately plagioclase olivine phyric basalt

WHERE SAMPLED: Unit 12

TEXTURE: Glomeroporphyritic, subvolcanitic

GRAIN SIZE: Fine to cryptocrystalline

PRIMARY MINERALOGY	PERCENT PRESENT	PERCENT ORIGINAL	SIZE RANGE (mm)	APPROX. COMPOSITION	MORPHOLOGY	COMMENTS
PHENOCRYSTS						
Olivine	1	1	≤ 0.5		Subhedral	In glomerocrysts with plag.
Olivine	Tr	Tr	≤ 0.5		Subhedral	Isolated crystals.
Plagioclase	3	3	1.0		Euhedral-subhedral	Equant to prismatic. In glomerocrysts with olivine. Some resorbed cores. Some oscillatory zoning. Cryptocrystalline melt inclusions.
Plagioclase	2	2	2-3		Euhedral	Equant. Isolated crystals with melt inclusions.
GROUNDMASS						
Plagioclase	45	45	0.25		Acicular	Belt buckle and swallowtail forms also present.
Olivine	1	1	< 0.1		Acicular	
Clinopyroxene	35	35	< 0.1		Acicular	Plumose. Radiate.
Opaques	1	1				
Mesostasis	10	12				Cryptocrystalline.
SECONDARY MINERALOGY	PERCENT	REPLACING/FILLING				COMMENTS
Clays	2	Mesostasis				Yellow-brown clays in groundmass. Concentrated in central zone of slide.

VESICLES/CAVITIES	PERCENT	LOCATION	SIZE RANGE (mm)	FILLING	SHAPE	COMMENTS
Vesicles	< 1		0.8-1.1	Clay	Round	Partially filled with yellow-brown clay.

COMMENTS: Round segregation vesicles (< 1% of the section), 0.3-1.2 mm, are partially to completely filled. One contains yellow clays.

THIN SECTION DESCRIPTION

106-648B-2R-1 (Piece 3, 14-16 cm)

ROCK NAME: Moderately plagioclase olivine phyric basalt

WHERE SAMPLED: Unit 17

TEXTURE: Glomeroporphyritic, subvolcanic

GRAIN SIZE: Fine to cryptocrystalline

PRIMARY MINERALOGY	PERCENT PRESENT	PERCENT ORIGINAL	SIZE RANGE (mm)	APPROX. COMPOSITION	MORPHOLOGY	COMMENTS
PHENOCRYSTS						
Olivine	1	1	0.5-1.0		Subhedral	In glomerocrysts with plag.
Plagioclase	2	2	0.5-1.5		Euhedral, prismatic	In glomerocrysts with ol. Normal and patchy zoning. Some resorbed cores.
Plagioclase	1	1	1.6		Euhedral	Isolated crystals. Zoned.
GROUNDMASS						
Plagioclase	50	50	0.05-0.30		Acicular	Belt buckle and swallowtail forms also present.
Olivine	Tr	Tr	0.1		Acicular	
Clinopyroxene	43	43	< 0.05		Acicular	Plumose. Radiate.
Opakes	1	1				
Mesostasis	2	2				Cryptocrystalline.

COMMENTS: Plag phenocrysts contain some cryptocrystalline melt inclusions. Round segregation vesicles (< 1% of the section), 0.75 mm, are partially filled. Some possibly with reddish-brown clays.

THIN SECTION DESCRIPTION

106-648B-3R-1 (Piece 1, 3-6 cm)

ROCK NAME: Moderately plagioclase olivine phyric basalt

WHERE SAMPLED: Unit 18

TEXTURE: Glomeroporphyritic, subvolcanic

GRAIN SIZE: Fine to cryptocrystalline

PRIMARY MINERALOGY	PERCENT PRESENT	PERCENT ORIGINAL	SIZE RANGE (mm)	APPROX. COMPOSITION	MORPHOLOGY	COMMENTS
PHENOCRYSTS						
Olivine	1	1	0.5		Subhedral	In glomerocrysts with plag.
Plagioclase	2	2	0.5-1.0		Euhedral	Equant to prismatic. In glomerocrysts with ol. Some oscillatory and patchy zoning.
Plagioclase	2	2	1-3		Euhedral	Isolated crystals. Zoned.
GROUNDMASS						
Plagioclase	50	50	0.25		Acicular	Belt buckle and swallowtail forms also present.
Olivine	Tr	Tr	< 0.1		Anhedral	
Clinopyroxene	42	42	< 0.05		Acicular	Plumose. Radiate.
Opakes	1	1				
Mesostasis	2	2				Cryptocrystalline.
SECONDARY MINERALOGY	PERCENT	REPLACING/FILLING				COMMENTS
Clays	Tr	Mesostasis				Rare orange-brown clay in groundmass.
VESICLES / CAVITIES	PERCENT	LOCATION	SIZE RANGE (mm)	FILLING	SHAPE	
Vesicles	< 1		0.15-0.75	None	Round	

COMMENTS: Cryptocrystalline melt inclusions in plag and ol phenocrysts.

THIN SECTION DESCRIPTION

106-648B-3R-1 (Piece 5, 31-34 cm)

ROCK NAME: Moderately plagioclase olivine phyric basalt

WHERE SAMPLED: Unit 19

TEXTURE: Glomeroporphyritic, intergranular

GRAIN SIZE: Fine

PRIMARY MINERALOGY	PERCENT PRESENT	PERCENT ORIGINAL	SIZE RANGE (mm)	APPROX. COMPOSITION	MORPHOLOGY	COMMENTS
PHENOCRYSTS						
Olivine	3	3	0.6-0.8		Subhedral	In glomerocrysts with plag.
Plagioclase	5	5	1.0-1.8		Euhedral	Equant to prismatic. In glomerocrysts with ol. Normal and patchy zoning. Some resorbed cores.
Plagioclase	1	1	1.5-4.0		Euhedral	Isolated crystals. Zoned.
GROUNDMASS						
Plagioclase	20	20	1.0		Acicular	Belt buckle and swallowtail forms also present.
Plagioclase	25	25	<0.05		Acicular	Belt buckle and swallowtail forms also present.
Olivine	10	10	<0.2		Anhedral acicular	Two size groups for ol and plag in groundmass. Ol crystals <0.2 mm are anhedral. Ol crystals <0.05 mm are acicular.
Clinopyroxene	34	34	<0.2		Subhedral, acicular	Radiate
Opaques	2	2				
Mesostasis	<1	<1				Cryptocrystalline.
SECONDARY MINERALOGY						
Clays	Tr	Mesostasis				Rare orange-brown clays in groundmass.
VESICLES/CAVITIES						
Vesicles	<1	Even	SIZE RANGE (mm) <0.1	FILLING None	SHAPE Round	

COMMENTS: Groundmass is coarse compared to 106-648B-3R-1 (Piece 1, 3-6 cm).
Cryptocrystalline melt inclusions in plag.

THIN SECTION DESCRIPTION

106-648B-3R-1 (Piece 12, 74-77 cm)

ROCK NAME: Moderately plagioclase olivine phyric basalt

WHERE SAMPLED: Unit 19

TEXTURE: Porphyritic, subvolcanitic

GRAIN SIZE: Fine to cryptocrystalline

PRIMARY MINERALOGY	PERCENT PRESENT	PERCENT ORIGINAL	SIZE RANGE (mm)	APPROX. COMPOSITION	MORPHOLOGY	COMMENTS
PHENOCRYSTS						
Olivine	1	1	0.2-0.7		Euhedral-subhedral	
Plagioclase	2	2	0.3-3.0		Euhedral	One prismatic crystal, 6 mm long. Some patchy zoning. Some resorbed cores.
GROUNDMASS						
Plagioclase	50	50	0.02-0.15		Acicular	Belt buckle and swallowtail forms also present.
Olivine	1	1	0.01-0.05		Acicular	
Clinopyroxene	40	40	0.01-0.05		Acicular	Plumose. Radiate.
Opaques	3	3				
Mesostasis	3	3				Cryptocrystalline.
SECONDARY MINERALOGY						
Clays	Tr	Mesostasis				Yellow-brown clays in groundmass.
VESICLES/CAVITIES						
Vesicles	<1		SIZE RANGE (mm) 0.1	FILLING None	SHAPE Round	

COMMENTS: Some plag crystals have a cloudy appearance. Large plag phenocrysts have cryptocrystalline melt inclusions.

THIN SECTION DESCRIPTION

106-648B-4R-1 (Piece 8, 40-42 cm)

ROCK NAME: Moderately plagioclase olivine phyric basalt

WHERE SAMPLED: Unit 22

TEXTURE: Glomeroporphyritic, subvariolithic

GRAIN SIZE: Fine to cryptocrystalline

PRIMARY MINERALOGY	PERCENT PRESENT	PERCENT ORIGINAL	SIZE RANGE (mm)	APPROX. COMPOSITION	MORPHOLOGY	COMMENTS
PHENOCRYSTS						
Olivine	0.5	0.5	0.1-0.4		Subhedral	In glomerocrysts with plag.
Olivine	0.5	0.5	0.2-0.7		Euhedral	Isolated crystals.
Plagioclase	0.5	0.5	0.2-0.6		Subhedral	In glomerocrysts with ol.
Plagioclase	2.5	2.5	0.4-3.0		Euhedral	Isolated crystals. Narrow rim normally zoned. Some patchy zoning. Some resorbed cores.
GROUNDMASS						
Plagioclase	50	50	0.03-0.30		Acicular	Belt buckles and swallowtail forms also present. Rarely up to 0.75 mm.
Olivine	1	1	0.05		Acicular	
Clinopyroxene	38	38	0.05		Acicular	Radiate.
Opakes	2	2				
Mesostasis	5	5				Cryptocrystalline.
SECONDARY MINERALOGY	PERCENT	REPLACING/FILLING				COMMENTS
Clays	Tr	Mesostasis				Rare yellow-brown and reddish brown clays in groundmass, concentrated on one side of slide in halo area.

VESICLES/CAVITIES	PERCENT	LOCATION	SIZE RANGE (mm)	FILLING	SHAPE
Vesicles	< 1		0.15-0.30	None	Round

COMMENTS: Segregation vesicles (<1% of the section), 0.75 mm, $\frac{2}{3}$ filled. Cryptocrystalline melt inclusions in plag phenocrysts.

THIN SECTION DESCRIPTION

106-648B-4R-1 (Piece 10, 53-55 cm)

ROCK NAME: Moderately plagioclase olivine phyric basalt

WHERE SAMPLED: Unit 22

TEXTURE: Intersertal to intergranular

GRAIN SIZE: Fine to cryptocrystalline

PRIMARY MINERALOGY	PERCENT PRESENT	PERCENT ORIGINAL	SIZE RANGE (mm)	APPROX. COMPOSITION	MORPHOLOGY	COMMENTS
PHENOCRYSTS						
Olivine	1	1	0.25		Subhedral	
Plagioclase	3	3	1-3		Subhedral, prismatic	Narrow normally zoned rims. Patchy zoning around enclosed groundmass.
GROUNDMASS						
Plagioclase	45	45	0.1-0.3		Acicular	Belt buckle and swallowtail forms also present.
Olivine	2	2	0.10-0.15		Acicular	Hollow crystal.
Clinopyroxene	32	32	0.15			Radiate.
Opakes	2	2	< 0.1			
Mesostasis	15	15				
VESICLES/CAVITIES	PERCENT	LOCATION	SIZE RANGE (mm)	FILLING	SHAPE	
Vesicles	< 1		0.3	None	Round	

COMMENTS: Possible miaroles (or plucked part of slide), = 1%.

THIN SECTION DESCRIPTION

106-648B-6R-1 (Piece 13, 57-60 cm)

ROCK NAME: Moderately plagioclase olivine phyric basalt

WHERE SAMPLED: Unit 26

TEXTURE: Intergranular, holocrystalline, glomeroporphyritic

GRAIN SIZE: Fine

PRIMARY MINERALOGY	PERCENT PRESENT	PERCENT ORIGINAL	SIZE RANGE (mm)	APPROX. COMPOSITION	MORPHOLOGY	COMMENTS
PHENOCRYSTS						
Olivine	1	1	1.5		Subhedral	In glomerocrysts with plag.
Plagioclase	2	2	1.5		Euhedral	In glomerocrysts with ol.
Plagioclase	3	3	1.5-3.0		Euhedral	Isolated crystals. Normal and patchy zoning. Some melt inclusions in cores. Narrow rim. Resorbed cores.
GROUNDMASS						
Plagioclase	48	48	0.1-1.0		Acicular, prismatic	Belt buckle forms also present.
Olivine	2	2	≤ 1		Acicular	
Clinopyroxene	40	40	0.1-0.5		Subhedral, prismatic	
Opaques	4	4	0.1		Radiate.	

THIN SECTION DESCRIPTION

106-648B-6R-1 (Piece 16, 78-81 cm)

ROCK NAME: Sparsely plagioclase olivine phyric basalt

WHERE SAMPLED: Unit 26

TEXTURE: Holocrystalline, intergranular

GRAIN SIZE: Fine

PRIMARY MINERALOGY	PERCENT PRESENT	PERCENT ORIGINAL	SIZE RANGE (mm)	APPROX. COMPOSITION	MORPHOLOGY	COMMENTS
PHENOCRYSTS						
Olivine	< 1	< 1	0.3		Euhedral	
Plagioclase	1	1	1.5-3.0	An 74-82	Euhedral, prismatic	Normally zoned. Some patchy zoning. Cores enclose lenticular patches of groundmass.
GROUNDMASS						
Plagioclase	54	54	0.1-1.5		Acicular	Belt buckle forms also present.
Olivine	1	1	0.1		Acicular	
Clinopyroxene	40	40	0.1-0.3		Acicular	Radiate.
Opaques	3	3				

VESICLES/CAVITIES	PERCENT	LOCATION	SIZE RANGE (mm)	FILLING	SHAPE
Vesicles	4	Even	1-2	None	Round

COMMENTS: Segregation vesicles (<1% of the section), 1 mm, are filled.

THIN SECTION DESCRIPTION

106-648B-6R-1 (Piece 25, 132-135 cm)

ROCK NAME: Moderately plagioclase olivine phyric basalt

WHERE SAMPLED: Unit 27

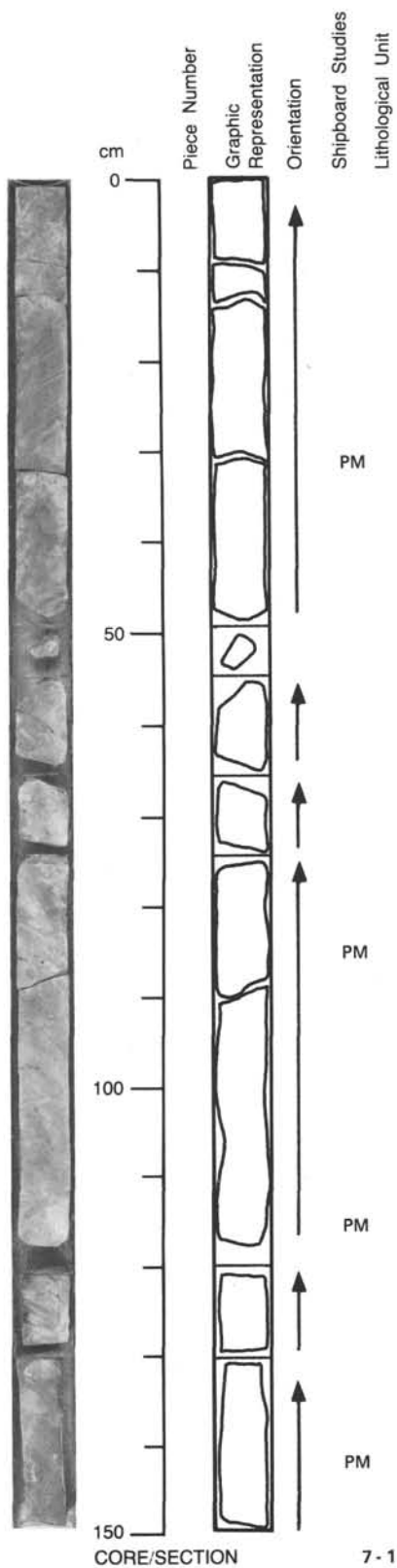
TEXTURE: Intergranular

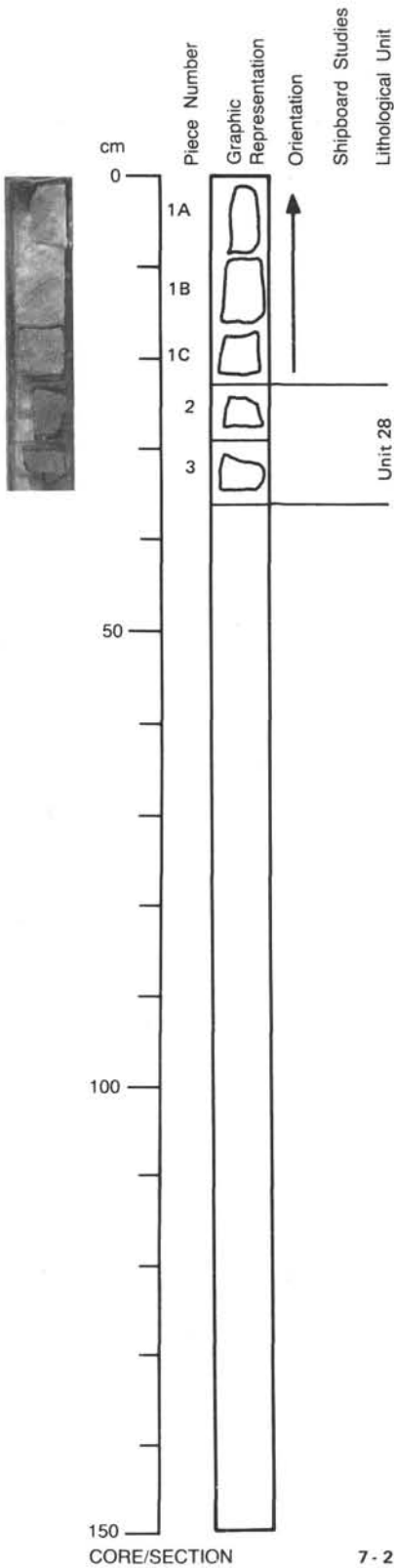
GRAIN SIZE: Fine

PRIMARY MINERALOGY	PERCENT PRESENT	PERCENT ORIGINAL	SIZE RANGE (mm)	APPROX. COMPOSITION	MORPHOLOGY	COMMENTS
PHENOCRYSTS						
Olivine	2	2	1.0-2.5		Euhedral	Similar to subophitic texture, ol enclosing plag. Seriate in size to groundmass.
Plagioclase	2.5	2.5	1-3		Subhedral-euhedral	Normal and patchy zoning. Resorbed cores. Seriate in size to groundmass. Narrow rim strongly zoned (normal).
GROUNDMASS						
Plagioclase	50	50	0.3-2.0		Laths	Hollow structure.
Olivine	3.5	3.5	0.3		Subhedral	
Clinopyroxene	36	36	0.3-1.5		Subhedral	Slightly colored, pale brown.
Opakes	4	4				
Mesostasis	2	2				Cryptocrystalline.

109-648B-7R-1

0-150 cms: CEMENT WITH <1% BASALT FRAGMENTS





Pieces 1A-1C: CEMENT

UNIT 28: SPARSELY PLAGIOCLASE-OLIVINE PHYRIC BASALT

Pieces 2 and 3

GLASS: None, no contacts.

PHENOCRYSTS: Homogeneous distribution throughout unit.

Plagioclase - 1-2%, 2-4 mm, euhedral, fresh; includes plagioclase-olivine glomerocrysts.

Olivine - <1%, <1 mm, round, fresh.

GROUNDMASS: Uniformly fine grained.

COLOR: Gray.

VESICLES: <1%, <1 mm, round, empty, concentrated near edge, some as miaroles.

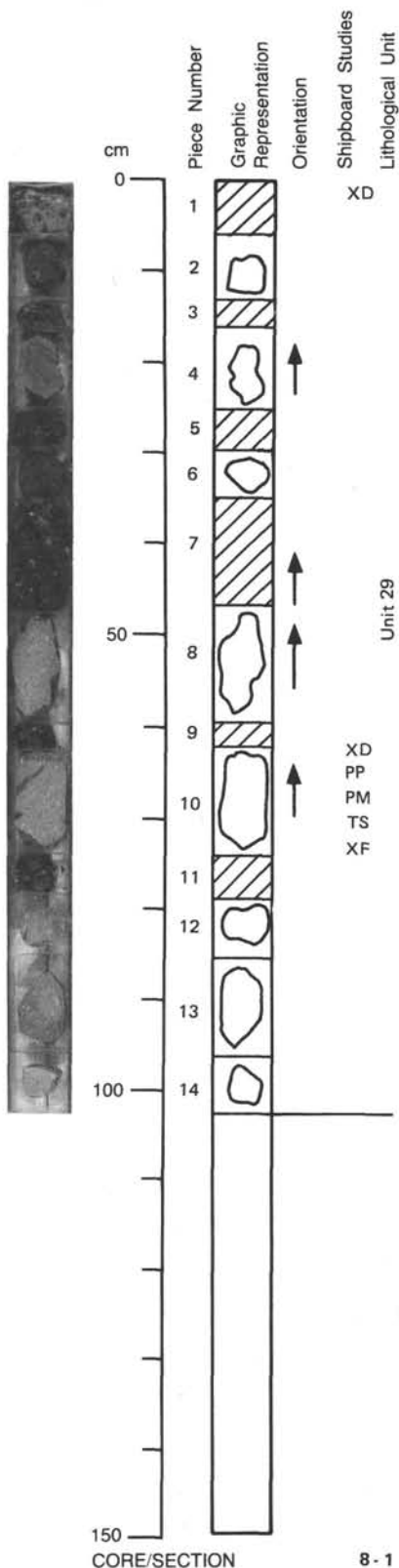
ALTERATION: Fresh.

VEINS/FRACTURES: None.

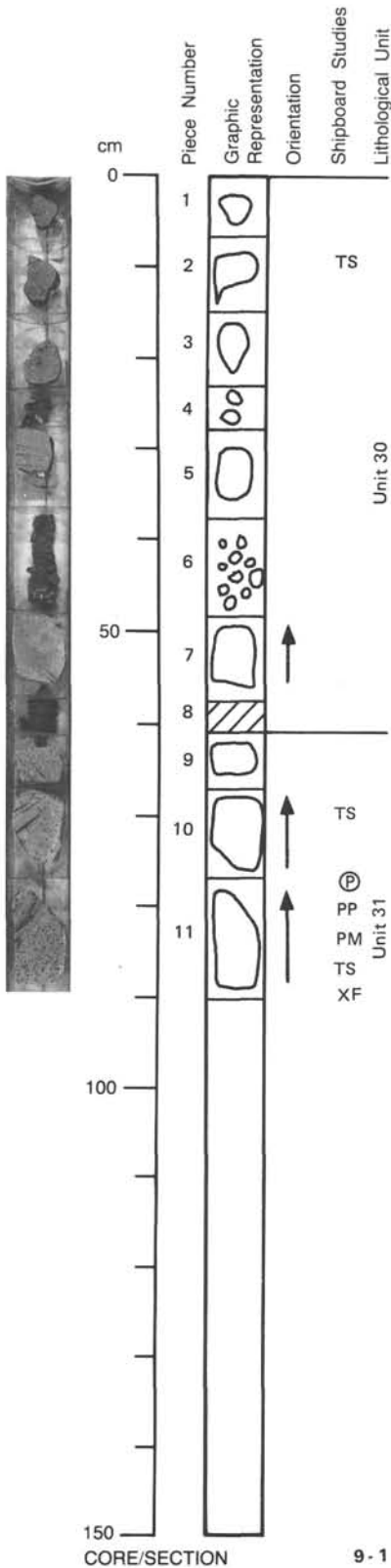
109-648B-8R-1

UNIT 29: SPARSELY PLAGIOCLASE PHYRIC BASALT

Pieces 1-14



GLASS: None, no contacts.
PHENOCRYSTS: Homogeneous distribution throughout unit.
 Plagioclase - 1-2%, 1-6 mm, euhedral-subhedral, fresh.
 Olivine - Rare, <1 mm, rounded, fresh, associated with plagioclase phenocrysts.
GROUNDMASS: Fine grained (Pieces 2, 4, and 6) to fine to medium grained (Pieces 8, 10, and 12-14), coarsening downward.
COLOR: Gray.
VESICLES: Pieces 2 and 6: 2%, 1-5 mm, round, some elongate, empty, homogeneous distribution, some as miaroles.
 Pieces 4, 10, and 12-14: <1%, <1 mm, mostly round, empty, homogeneous distribution.
 Pieces 8 and 13: Miaroles <1%, 1-5 mm, elongate, concentrated near edge.
ALTERATION: Fresh.
 Pieces 4 and 8: Alteration halo 4-5 mm wide composed of 2-3 mm-wide pale band adjacent to vein and 2 mm wide outer black line with sharp alteration front.
 Pieces 2, 6, 10, and 12-14: Dark alteration halo 2-4 mm wide with sharp alteration front.
 Pieces 6 and 13: Black halos, irregular thickness.
VEINS/FRACTURES: Alteration halos indicate position of fractures, no clay on fracture surfaces.
 Piece 14: Small empty fracture in dark alteration halo.
NOTE: Pieces 1, 3, 5, 7, 9, and 11 are drill cuttings composed of:
 Basalt - Microcrystalline basalt with <1% plagioclase phenocrysts, some broken.
 Glass - Exhibiting conchoidal fracturing with fractures commonly filled by "sugary," microcrystalline, pale orange mineral; some plagioclase phenocrysts embedded in glass.
 Cement - Irregular and rounded fragments.



UNIT 30: SPARSELY TO MODERATELY PLAGIOCLASE-OLIVINE PHYRIC BASALT

Pieces 1-8

GLASS: None, no contacts.
PHENOCRYSTS: Homogeneous distribution throughout unit; occur singly and in glomerocrysts.
 Plagioclase - 1-2%, 2-4 mm, euhedral, fresh.
 Olivine - <1%, <1 mm, rounded, fresh.
GROUNDMASS: Fine grained (Piece 1) to fine to medium grained (Piece 7), coarsening downward.
COLOR: Gray.
VESICLES: Pieces 1-3: <1%, <0.5 mm, round, empty, homogeneous distribution.
 Pieces 5 and 7: Miaroles <1%, <1 mm, round to elongate, empty, homogeneous distribution.
ALTERATION: Fresh.
VEINS/FRACTURES: Piece 2: Small empty fracture.

UNIT 31: SPARSELY TO MODERATELY PLAGIOCLASE-OLIVINE PHYRIC BASALT

Pieces 9-11

GLASS: None, no contacts.
PHENOCRYSTS: Heterogeneous distribution; concentrated in isolated patches.
 Plagioclase - 1-2%, 1-4 mm, euhedral, fresh, occur singly and in glomerocrysts.
 Olivine - <1%, <1 mm, rounded, fresh, occur primarily in glomerocrysts, rarely as isolated phenocrysts.
GROUNDMASS: Uniformly fine grained.
COLOR: Gray.
VESICLES: Pieces 9 and 10: 5%, 0.5-2.0 mm, round, most empty, some lined with orange or bluish smectite, concentrated in local areas.
 Piece 11: 10%, 0.5-2.0 mm, round, most empty, some lined with orange clay or bluish smectite, homogeneous distribution.
 Pieces 9-11 <5% of vesicles as miaroles.
ALTERATION: Fresh.
 Pieces 10 and 11: Dark alteration halo 2 mm wide parallel to fracture surfaces bounding sample, smectite and orange clay confined to vesicles within halos.
VEINS/FRACTURES: Bounding margins of samples, none within samples.

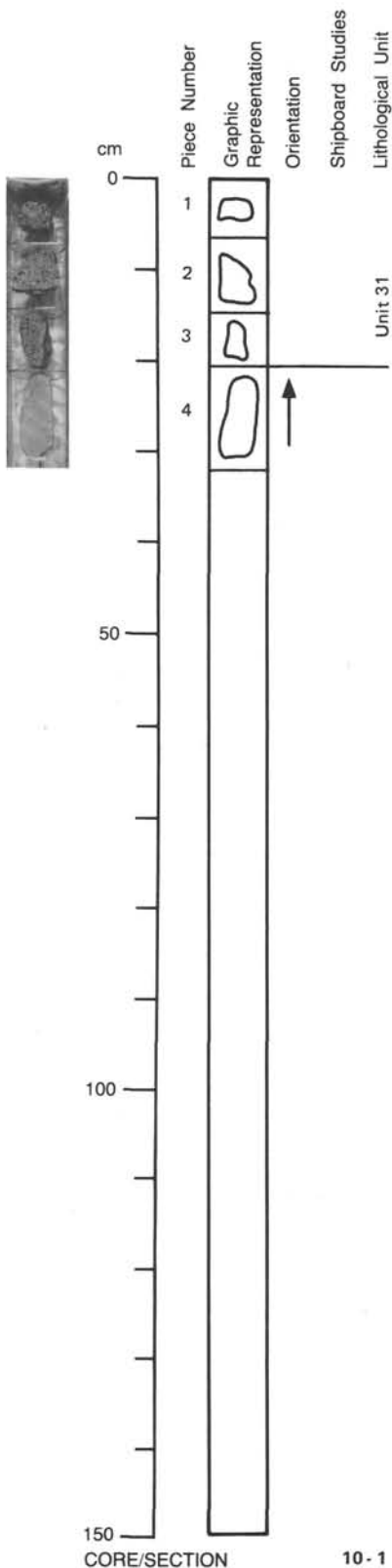
109-648B-10R-1

UNIT 31 (continued): SPARSELY TO MODERATELY PLAGIOCLASE-OLIVINE PHYRIC BASALT

Pieces 1-3

- GLASS:** None, no contacts.
- PHENOCRYSTS:** Homogeneous distribution throughout unit; mostly as glomerocrysts but also singly.
 Plagioclase - 1-2%, 2-4 mm, euhedral, fresh.
 Olivine - Rare, <1 mm, round, fresh.
- GROUNDMASS:** Uniformly fine grained.
- COLOR:** Gray.
- VESICLES:** 5%, 0.5-2.5 mm, round, empty, homogeneous distribution.
 Piece 2: Miaroles <1%, 1-2 mm, irregular shapes, empty, concentrated in band through center.
 Pieces 1 and 3: Miaroles, <1%, 1-2 mm, irregular shapes, empty, occur near or next to vesicles.
 Piece 1: Orange clay in vesicle near rim.
- ALTERATION:** Fresh.
 Piece 1: Dark alteration halo 2 mm wide.
- VEINS/FRACTURES:** Piece 2: Empty crack.

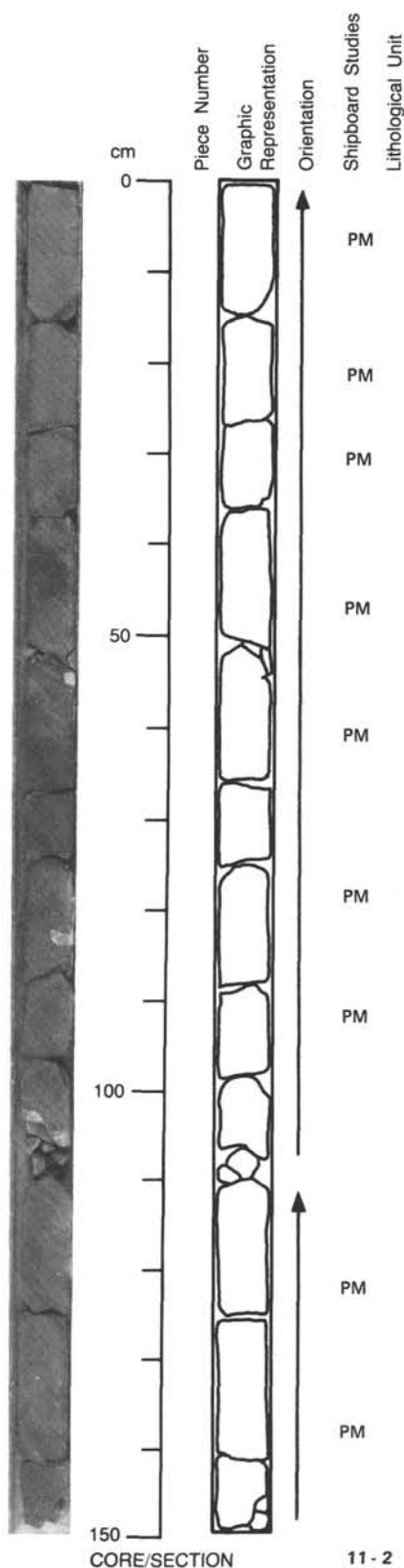
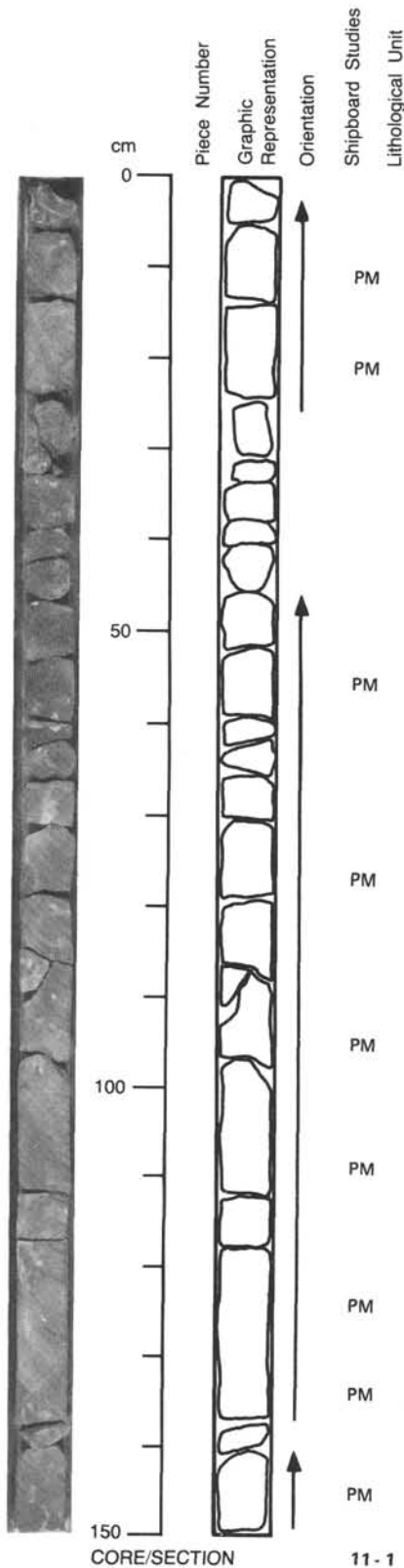
Piece 4: CEMENT



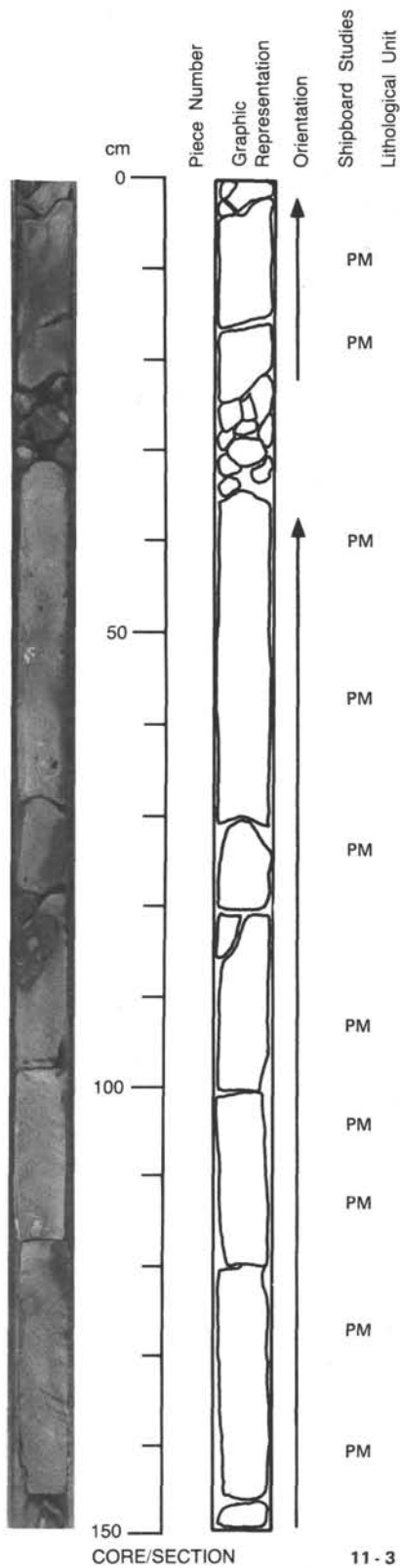
10-1

109-648B-11R-1 0-150 cm: CEMENT

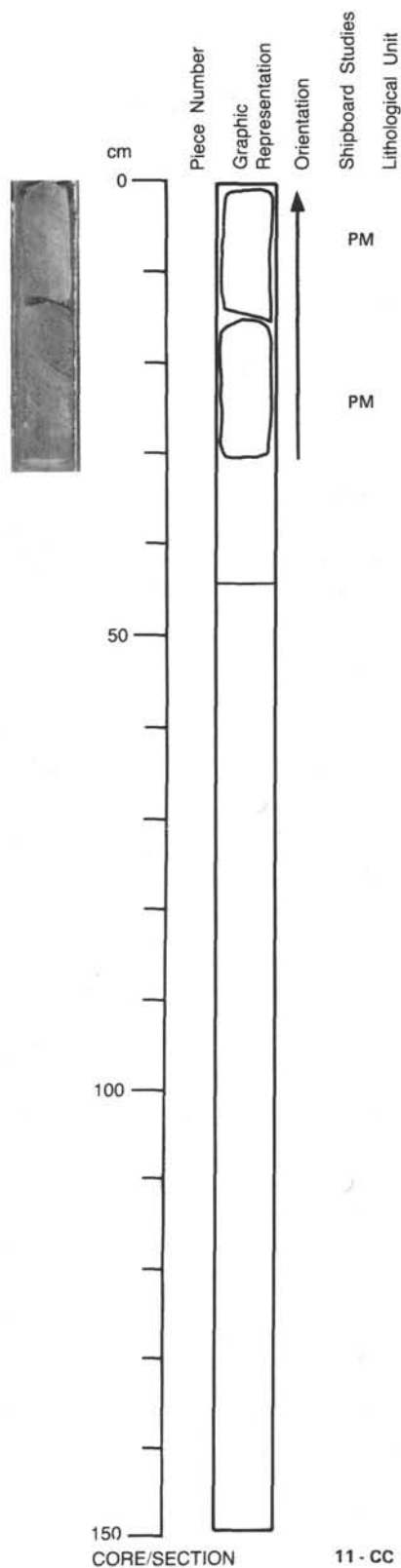
109-648B-11R-2 0-150 cm: CEMENT



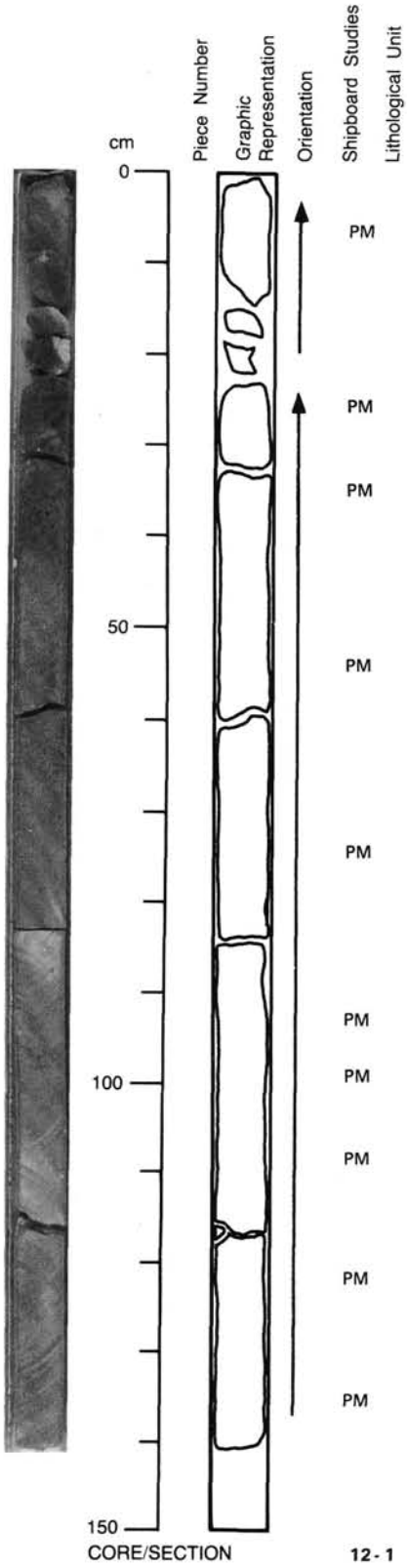
109-648B-11R-3 0-150 cm: CEMENT



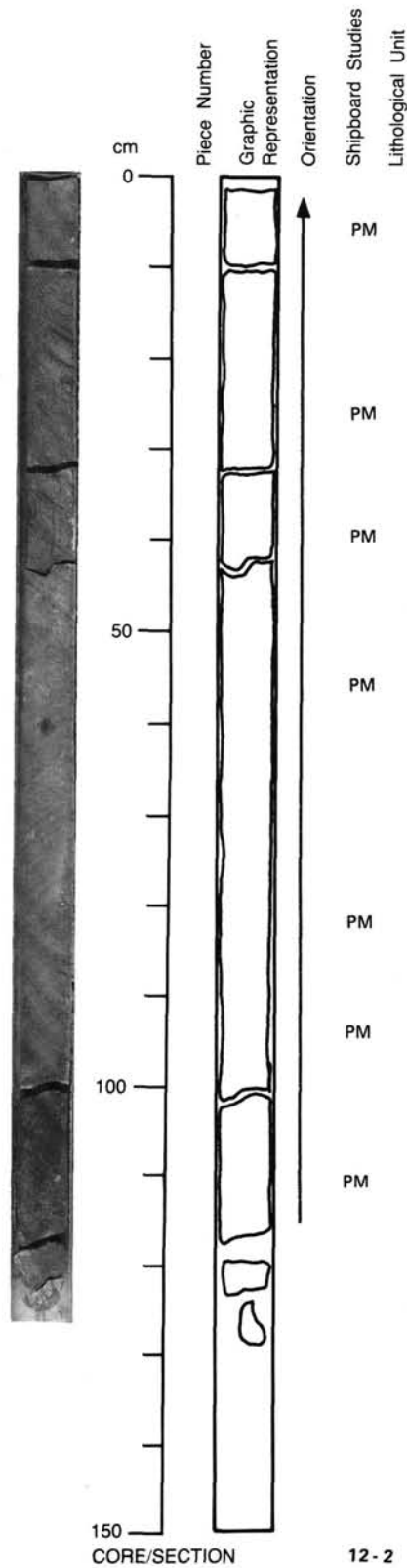
109-648B-11R-CC 0-30 cm: CEMENT



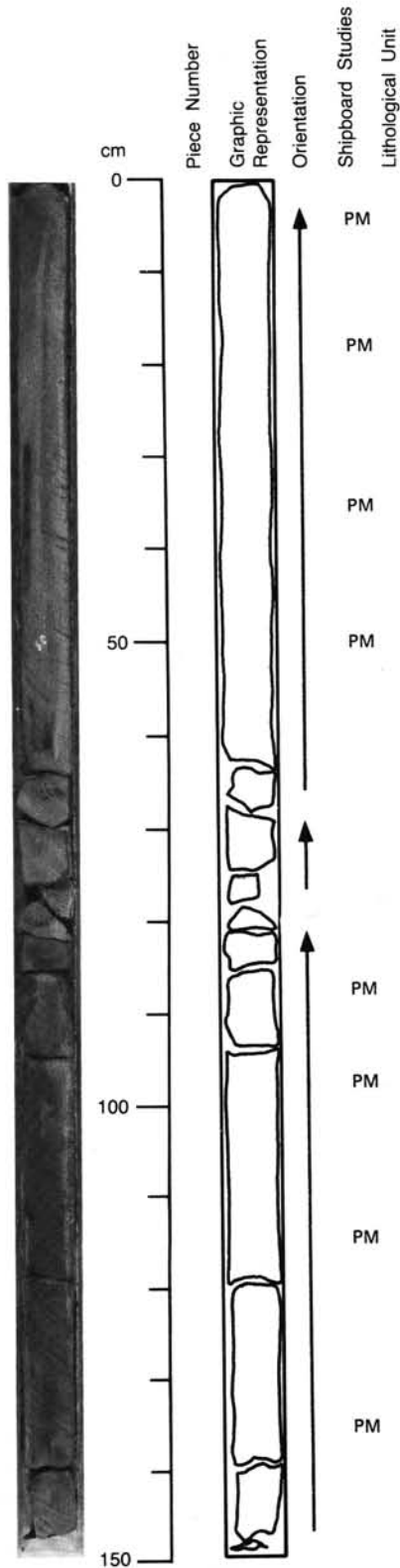
109-648B-12R-1 0-140 cm: CEMENT



109-648B-12R-2 0-130 cm: CEMENT



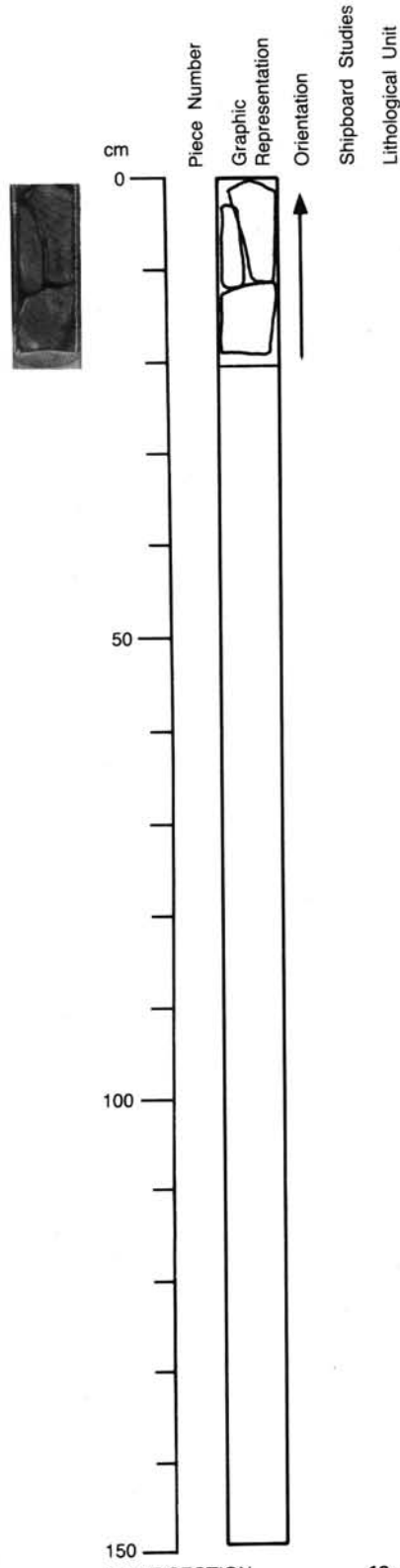
109-648B-12R-3 0-148 cm: CEMENT



CORE/SECTION

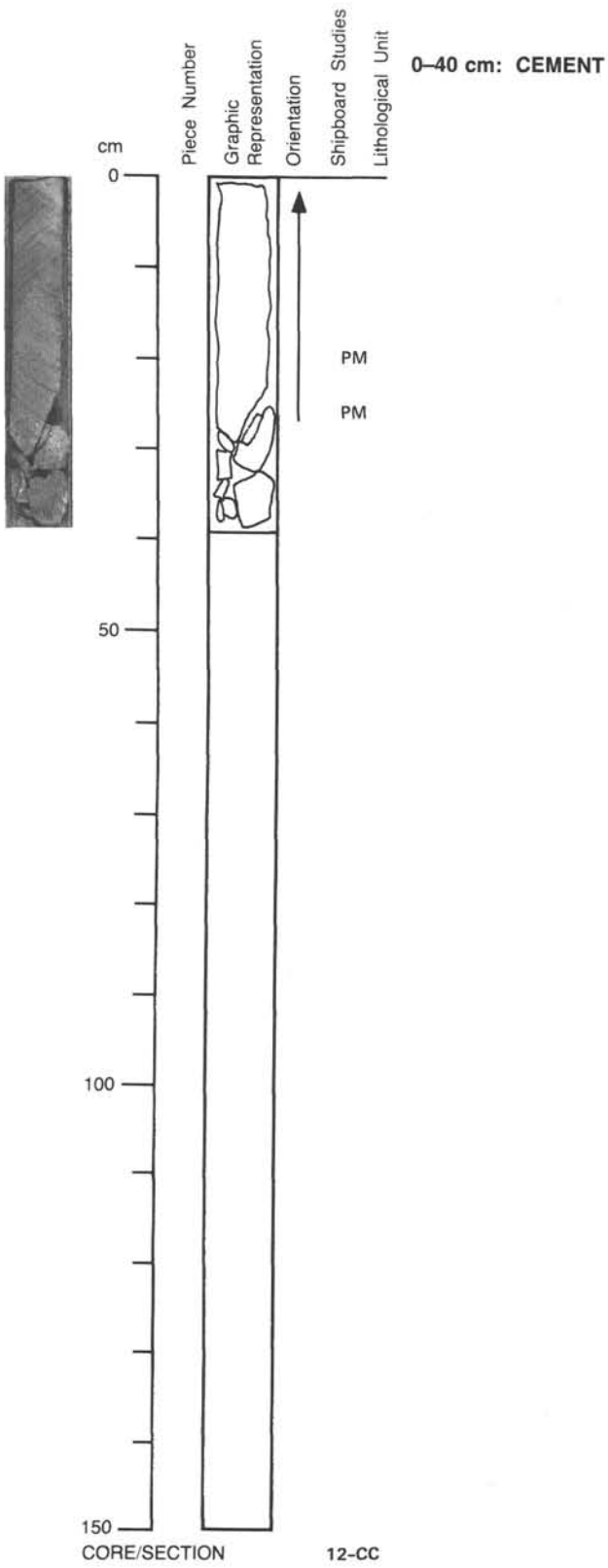
12 - 3

109-648B-12R-4 0-19 cm: CEMENT



CORE/SECTION

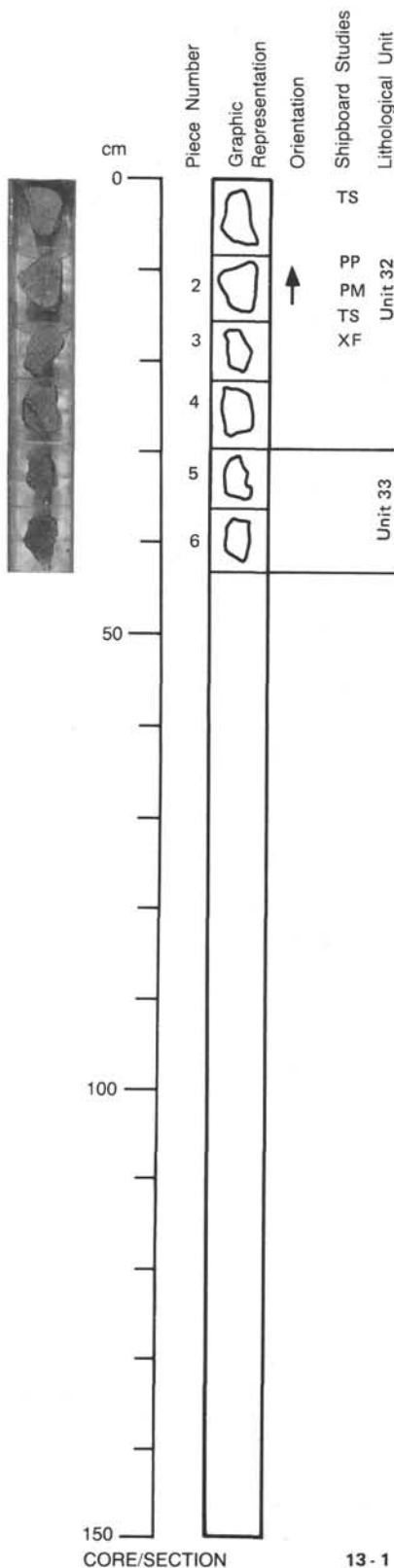
12 - 4



109-648B-13R-1

UNIT 32: SPARSELY TO MODERATELY PLAGIOCLASE-OLIVINE PHYRIC BASALT

Pieces 1-4



GLASS: Pieces 1, 3, and 4: Possible glass-infilling vesicles.

Piece 2: None.

Pieces 1-4: No contacts.

PHENOCRYSTS: Heterogeneous distribution; concentrated in patches, especially in Piece 3; occur singly and in glomerocrysts.

Plagioclase - <1-3%, 0.5-3.0 mm, euhedral, fresh.

Olivine - <1%, <0.5 mm, rounded, fresh.

GROUNDMASS: Fine grained (Pieces 1, 3, and 4) to fine to medium grained (Piece 2).

COLOR: Gray.

VESICLES: Pieces 1 and 3-4: <1%, <1 mm, round, empty or glass(?) - filled, homogeneous distribution.

Piece 2: Approximately 1%, <1 mm, round, empty, patchy distribution.

Piece 3: Bluish smectite-lined vesicles in dark alteration halo.

Miaroles: <1%, <1 mm, irregular shape, bounded by crystal faces, patchy distribution; approximately 50% of all voids are miaroles.

ALTERATION: Fresh.

Pieces 1-2 and 4: Dark alteration halos approximately 2 mm wide parallel to fracture surfaces bounding samples.

Piece 3: Bisected by alteration front, bluish smectite occurs as vesicle lining within the dark zone.

VEINS/FRACTURES: Piece 1: Small crack.

UNIT 33: SPARSELY TO MODERATELY PLAGIOCLASE-OLIVINE PHYRIC BASALT

Pieces 5 and 6

GLASS: None, no contacts.

PHENOCRYSTS: Homogeneous distribution throughout unit; occur singly and in glomerocrysts.

Plagioclase - 1-2%, 1-4 mm, euhedral, fresh.

Olivine - <1%, <1 mm, rounded, fresh, rarely as isolated phenocrysts, mainly in glomerocrysts.

GROUNDMASS: Uniformly fine grained.

COLOR: Gray.

VESICLES: 5%, 0.5-2.0 mm, round, most empty, lined by bluish smectite in dark halos, homogeneous distribution.

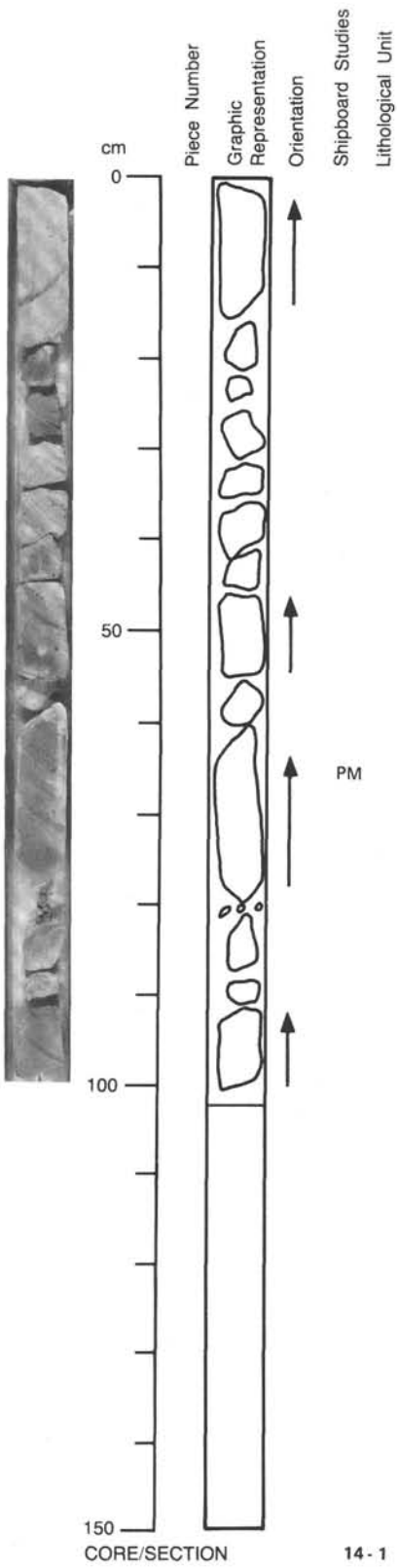
Miaroles: <5% of all voids, <0.5 mm, empty, patchy distribution.

ALTERATION: Fresh. Dark alteration halos 1-2 mm wide, developed parallel to fractures bounding samples, lobate edge; bluish smectite-lined vesicles in halos.

CORE/SECTION

13 - 1

0-101 cm: CEMENT WITH APPROXIMATELY 2% BASALT FRAGMENTS <4 mm



109-648B-15R-1

UNIT 34: MODERATELY PLAGIOCLASE-OLIVINE PHYRIC BASALT

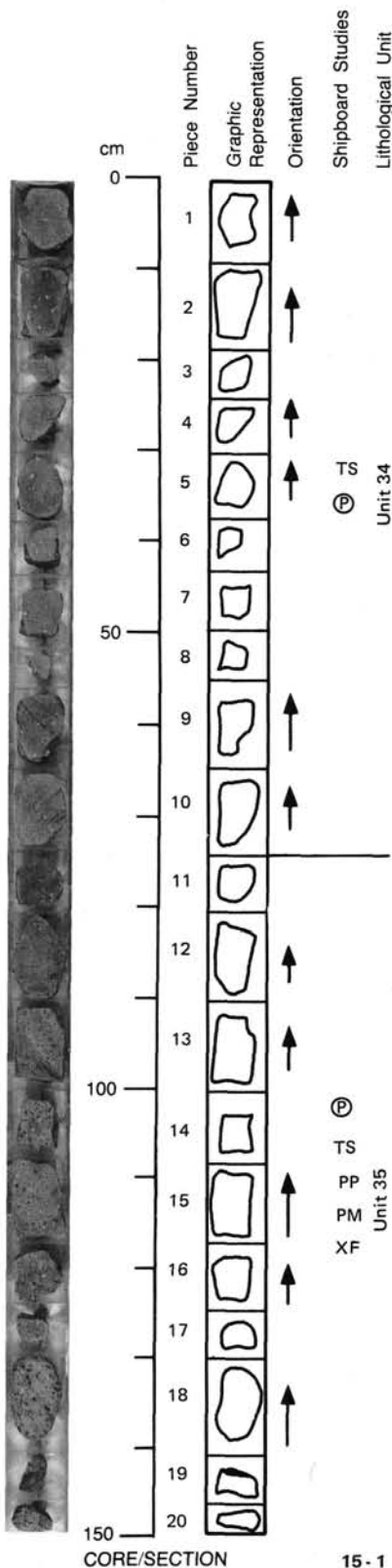
Pieces 1-10

GLASS: None, no contacts.
PHENOCRYSTS: Homogeneous distribution throughout unit; occur singly and in glomerocrysts.
 Plagioclase - 2-3%, 0.5-3.0 mm, euhedral, fresh.
 Olivine - <1%, <0.5 mm, subhedral, fresh.
 Pieces 2, 5, and 9: Glomerocrysts as large as 6 mm.
GROUNDMASS: Uniformly fine grained.
COLOR: Gray.
VESICLES: Pieces 2 and 5: 2%, <1.5 mm, round, empty away from alteration halos, concentrated around edges and adjacent to plagioclase phenocryst in Piece 5.
 Pieces 1, 3-4, and 6-10: <1%, <0.5 mm, round, empty, homogeneous distribution.
 Miaroles: <20% of all voids, <0.5 mm, irregular shape, empty, patchy distribution.
ALTERATION: Fresh.
 Piece 2: Bluish smectite in one vesicle.
 Pieces 2, 6, and 10: Dark alteration halos as wide as 8 mm, parallel to cracks.
 Piece 7: Yellow and orange clay lining vesicles and replacing mesostasis, especially along cracks; sharp boundary between altered and fresh parts of sample.
VEINS/FRACTURES: Pieces 2, 6, and 10: Fracture bounded, surfaces coated by thin layer of light orange green clay.

UNIT 35: MODERATELY PLAGIOCLASE-OLIVINE PHYRIC BASALT

Pieces 11-20

GLASS: None, no contacts.
PHENOCRYSTS: Homogeneous distribution throughout unit; occur singly and in glomerocrysts as large as 6 mm.
 Plagioclase - 1-3%, 0.5-3.0 mm, euhedral, fresh.
 Olivine - <<0.5%, <0.5 mm, euhedral, fresh.
GROUNDMASS: Microcrystalline to fine grained (Piece 11) to fine grained (Piece 12-20), coarsening downward.
COLOR: Gray.
VESICLES: Pieces 11-15 and 19: 2-5%, <2 mm, round, empty away from alteration halos, homogeneous distribution.
 Pieces 16-18, 20, and 21: 5-10%, 0.5-3.0 mm, round, often interconnected, empty away from alteration halos, homogeneous distribution.
 Miaroles: <10% of all voids, <0.5 mm, irregular and elongate shape, empty, patchy distribution.
ALTERATION: Fresh.
 Pieces 12-14 and 18-20: Dark alteration halo 2-5 mm wide parallel to fractures bounding samples; boundaries lobate in places; yellow orange clay/iron hydroxide mixtures along fractures, especially in Piece 14; vesicles unusually free of alteration minerals; uneven lining of iron hydroxide(?) and clay in a few vesicles directly adjoining fractures.
VEINS/FRACTURES: Pieces 12-14: Fractures with orange yellow clay coating, often banded.



CORE/SECTION

UNIT 35 (continued): MODERATELY PLAGIOCLASE-OLIVINE PHYRIC BASALT

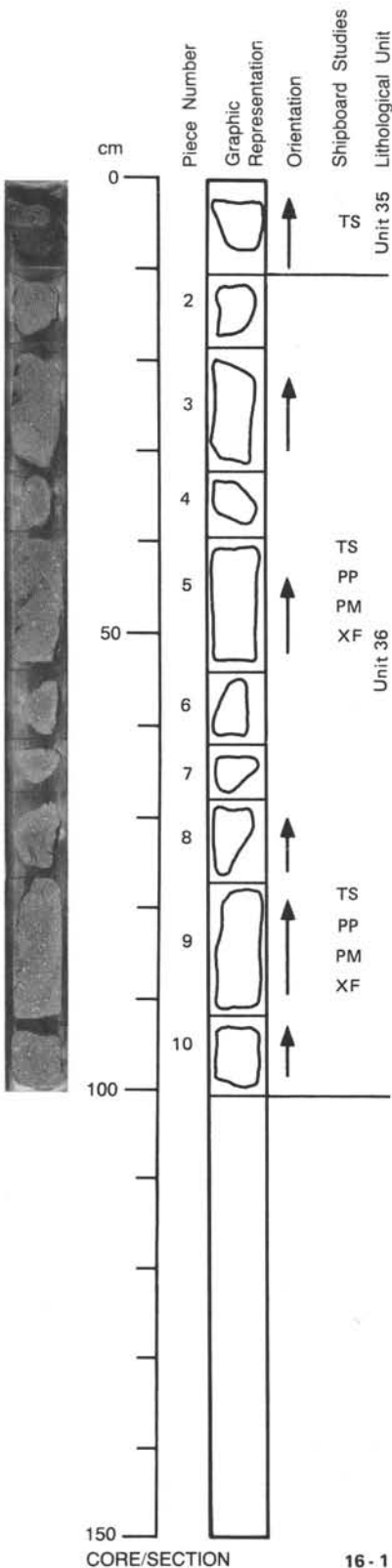
Piece 1

GLASS: None, no contacts.
PHENOCRYSTS: Homogeneous distribution; occur singly and in glomerocrysts as large as 6 mm.
 Plagioclase - 1-3%, 0.5-3.0 mm, euhedral, fresh.
 Olivine - <<0.5%, <0.5 mm, euhedral, fresh.
GROUNDMASS: Fine grained.
COLOR: Gray.
VESICLES: 10%, 0.5-3.0 mm, round, often interconnected, empty away from alteration halos, homogeneous distribution.
 Miaroles: <10% of all voids, <0.5 mm, irregular and elongate shape, empty, patchy distribution.
ALTERATION: Fresh, dark alteration halo as wide as 11 mm along one side; intense development of green yellow orange iron hydroxide clay in almost all vesicles with dark alteration halo.
VEINS/FRACTURES: Within and parallel to alteration halo, lined with iron hydroxide clay.

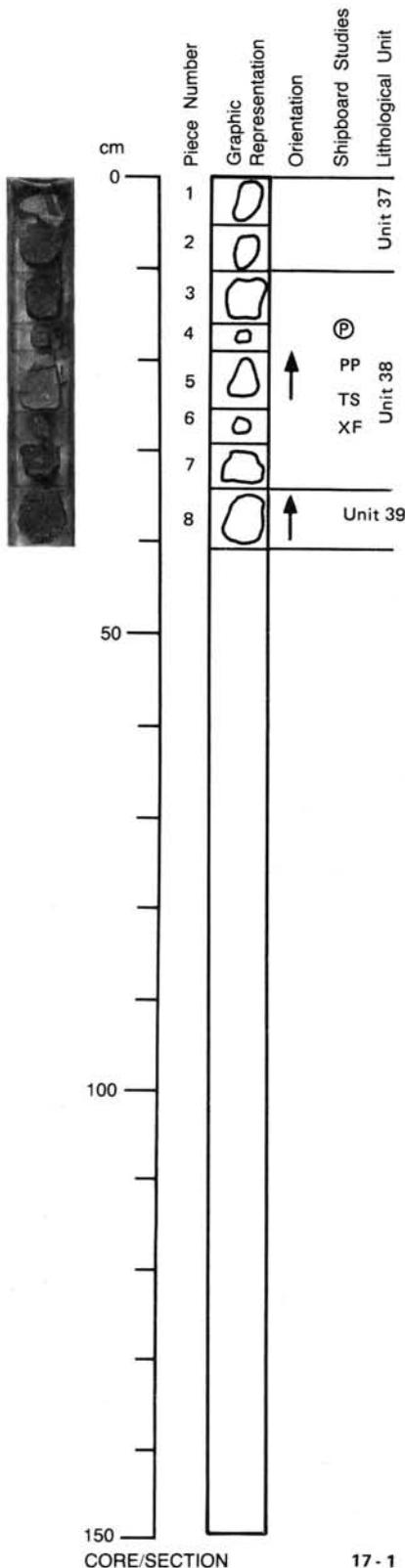
UNIT 36: MODERATELY PLAGIOCLASE-OLIVINE PHYRIC BASALT

Pieces 2-10

GLASS: None, no contacts.
PHENOCRYSTS: Homogeneous distribution throughout unit; occur singly and in glomerocrysts as large as 5 mm.
 Plagioclase - Approximately 3%, 0.5-4.0 mm, euhedral, fresh.
 Olivine - <0.5%, <0.5 mm, euhedral, fresh.
GROUNDMASS: Patchy, fine grained to microcrystalline throughout unit, particularly in Piece 9.
COLOR: Gray.
VESICLES: <1%, <1 mm, round, empty, randomly distributed.
 Piece 3: Bright red iron hydroxide(?) lining part of vesicle in alteration halo.
 Miaroles: <30% of all voids, <0.5 mm, irregular shape, empty, patchy distribution.
ALTERATION: Fresh.
 Pieces 3-6 and 9: Dark alteration halos parallel to fractures bounding samples, yellow green clay on surface(?).
 Piece 3: Bright red iron hydroxide(?) lining part of vesicle in halo zone.
VEINS/FRACTURES: Fractured surfaces bounding pieces with dark alteration halos.



109-648B-17R-1



PIECE 1: CEMENT

UNIT 37: SPARSELY PLAGIOCLASE-OLIVINE PHYRIC BASALT

Piece 2

GLASS: None, no contacts.
PHENOCRYSTS: Homogeneous distribution; occur singly and in glomerocrysts.
 Plagioclase - 1-2%, 1-3 mm, euhedral, fresh.
 Olivine - <1%, 0.5 mm, round, fresh.
GROUNDMASS: Fine grained.
COLOR: Gray.
VESICLES: <1%, <1 mm, irregular shapes, empty or coated with orange clay, concentrated near one edge.
 Miaroles: <10% of all voids, <0.5 mm, irregular shape, empty, concentrated in horizontal bands.
ALTERATION: Fresh, patchy orange clay coating on exterior of sample, filling some vesicles.
VEINS/FRACTURES: None.

UNIT 38: SPARSELY TO MODERATELY PLAGIOCLASE-OLIVINE PHYRIC BASALT

Pieces 3-7

GLASS: Pieces 3 and 7: Glassy margins as thick as 3 mm, fresh, no contacts.
PHENOCRYSTS: Homogeneous distribution throughout unit; occur singly and in glomerocrysts.
 Plagioclase - 2%, 0.5-4.0 mm, subhedral to euhedral, fresh.
 Olivine - <1%, 0.5-1.0 mm, subhedral to euhedral, fresh.
GROUNDMASS: Microcrystalline (Pieces 3 and 7) to fine grained (Piece 5), coarsening toward center.
COLOR: Gray, glass is black.
VESICLES: Pieces 3-5 and 7: <1%, <0.5 mm, irregular shapes, empty in interior of unit, can be filled near glass margins, irregular distribution.
 Pieces 3 and 7: Concentrated near glassy margins, can be partially to completely filled by glass near glassy margins, yellow orange clay lines some vesicles.
 Piece 6: 1-3%, 1-2 mm, irregular shapes, empty, irregular distribution.
 Miaroles: In Pieces 3, 4, 6, and 7 are <10% of all voids, 0.5-2.0 mm, irregular shapes, empty, and concentrated in bands; in Piece 5 are approximately 75% of all voids, 0.5-3.0 mm, irregular shape, empty, and with homogeneous distribution.
ALTERATION: Fresh.
 Piece 3: Olive green clay coating on portions of glassy margin, yellow orange clay lining in some vesicles.
VEINS/FRACTURES: None.

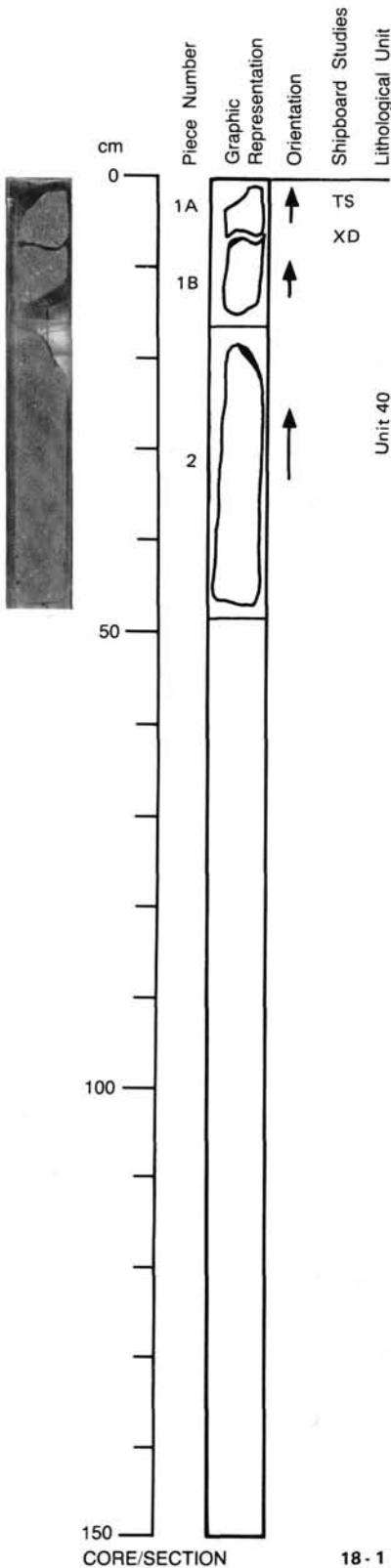
UNIT 39: SPARSELY TO MODERATELY PLAGIOCLASE-OLIVINE PHYRIC BASALT

Piece 8

GLASS: None, no contacts.
PHENOCRYSTS: Homogeneous distribution; occur singly and in glomerocrysts.
 Plagioclase - 2%, 0.5-3.0 mm, euhedral to subhedral, fresh.
 Olivine - <1%, <0.5 mm, round to subhedral, fresh.
GROUNDMASS: Microcrystalline to fine grained.
COLOR: Dark gray.
VESICLES: 8%, 0.5-5.0 mm, most round, some irregularly shaped, empty, homogeneous distribution.
 Miaroles: 15%? of all voids, <1.0 mm, irregular shapes, empty, homogeneous distribution.
ALTERATION: Fresh, dark alteration halo 2-3 mm wide along one side of piece, side coated by yellow orange clay.
VEINS/FRACTURES: None.

UNIT 40: SPARSELY PLAGIOCLASE-OLIVINE PHYRIC BASALT

Pieces 1-2



GLASS: None, no contacts.

PHENOCRYSTS: Heterogeneous distribution.

Pieces 1A and 1B: Concentrated in patches.

Piece 2: Concentrated near top and bottom.

Plagioclase - 1-2%, 1-5 mm, euhedral-subhedral, fresh.

Olivine - <1%, as large as 0.5 mm (Pieces 1A and 1B), as large as 1.0 mm (Piece 2), round, fresh, associated with plagioclase in glomerocrysts, also singly.

GROUNDMASS: Uniformly fine grained, with patchy microcrystalline regions in Piece 2.

COLOR: Gray.

VESICLES: Rare, <1 mm, round, empty, concentrated in Pieces 1A and 1B.

Miaroles: 75% of all voids, <0.5 mm, irregular shape, long, bounded by crystal faces, empty, homogeneous distribution.

ALTERATION: Fresh, all pieces have alteration halos parallel to fractured surfaces, yellow green (locally orange) clay/iron hydroxides coat fractures.

Piece 1A: Layered alteration halo 9 mm wide at top of sample, 2 mm-wide dark green band farthest from fracture (same type as in Pieces 1B and 2), 7 mm-wide band adjacent to fracture, speckled yellow orange appearance, intense clay/iron hydroxide alteration.

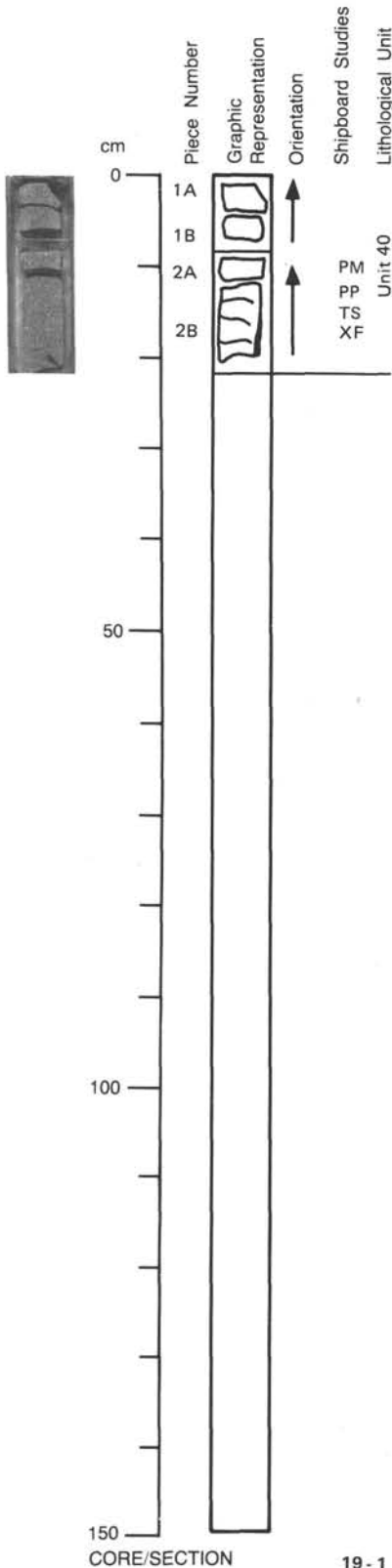
Pieces 1B and 2: 3-4 mm-thick dark alteration halos (homogeneous dark green color) on bottom of Piece 1A and top of Piece 2.

VEINS/FRACTURES: Fractures with alteration halos, as above.

109-648B-19R-1

UNIT 40 (continued): SPARSELY PLAGIOCLASE-OLIVINE PHYRIC BASALT

Pieces 1-2



GLASS: None, no contacts.

PHENOCRYSTS: Heterogeneous distribution.

Pieces 1A and 1B: Concentrated near sides, few phenocrysts.

Pieces 2A and 2B: Concentrated near centers.

Plagioclase - Occur singly and in glomerocrysts, 1-2%, 1-4 mm, euhedral-subhedral, fresh.

Olivine - Occur primarily in glomerocrysts with plagioclase, <1%, 0.5-2.0 mm, rounded, fresh.

GROUNDMASS: Fine grained with patchy microcrystalline regions.

COLOR: Gray.

VESICLES: <<1%, <1 mm, round, empty, homogeneous distribution.

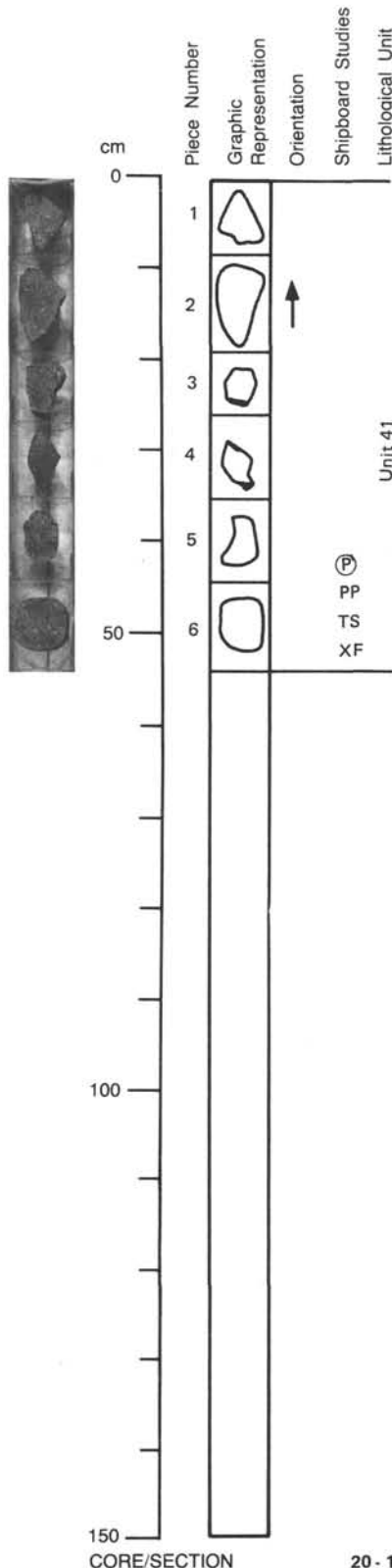
Miroleles: None.

ALTERATION: Fresh.

VEINS/FRACTURES: Series of horizontal fractures with spacing of 2-3 cm on cut surface of core; fracture surfaces are fresh, no alteration.

UNIT 41: ASSORTED RUBBLE

Pieces 1-6



PIECES 1, 3, and 5: SPARSELY PLAGIOCLASE-OLIVINE PHYRIC BASALT

GLASS: None, no contacts.

PHENOCRYSTS: Homogeneous distribution; occur singly and in glomerocrysts.

Plagioclase – 1-2%, 1-4 mm, euhedral, fresh.

Olivine – <1%, <1 mm, rounded, fresh, mainly as glomerocrysts.

GROUNDMASS: Uniformly fine grained.

COLOR: Gray.

VESICLES: Piece 1: 2-3%, 0.2-2.0 mm, round, empty or lined by bluish smectite in alteration halos, concentrated in bands.

Pieces 3 and 5: 7%, 0.5-2.5 mm, round, empty or lined by bluish smectite in alteration halos, concentrated around edges.

Miaroles: <10% of all voids, <0.5 mm, round, look like vesicles with crystals projecting toward interior, empty, homogeneous distribution.

ALTERATION: Fresh, dark alteration halos 1-2 mm wide developed parallel to edges, bluish smectite-lined vesicles within halos.

VEINS/FRACTURES: Piece 5: Contains fresh crack on edge.

PIECES 2, 4, and 6: SPARSELY PLAGIOCLASE-OLIVINE PHYRIC BASALT

GLASS: Piece 4: Small amount of glass on edge, fresh, no contacts.

Pieces 2 and 6: None, no contacts.

PHENOCRYSTS: Homogeneous distribution throughout unit; occur singly and in glomerocrysts.

Plagioclase – 1-2%, 1-3 mm, euhedral, fresh.

Olivine – <1%, <0.5 mm, euhedral, fresh.

GROUNDMASS: Pieces 2 and 6: Uniformly fine grained.

Piece 4: Glassy to microcrystalline.

COLOR: Gray, glass is black.

VESICLES: 1%, <1 mm, round to irregular, empty, homogeneous distribution.

Miaroles: 25% of all voids, <0.5 mm, irregular, empty, homogeneous distribution.

ALTERATION: Fresh.

Piece 2: Dark alteration halo 1-2 mm wide on part of margin.

Pieces 4 and 6: Green coating on outer surface.

VEINS/FRACTURES: Piece 6: Fracture through part of sample.

THIN SECTION DESCRIPTION

109-648B-8R-1 (Piece 10, 68-70 cm)

ROCK NAME: Moderately plagioclase olivine phyric basalt.
WHERE SAMPLED: Unit 29, pillow or flow interior; intersects alteration halo
TEXTURE: Intergranular, glomeroporphyritic
GRAIN SIZE: Fine grained

PRIMARY MINERALOGY	PERCENT PRESENT	PERCENT ORIGINAL	SIZE RANGE (mm)	APPROX. COMPOSITION	MORPHOLOGY	COMMENTS
PHENOCRYSTS						
Olivine	<1	<1	0.2-0.8		Anhedra- euhedral	
Plagioclase	3	3	0.8-2.0	C = An 85 R = An 77	Euhedral	Some hopper and swallowtail. Margins embayed and/or fractured. Yellow alteration material lines cracks in plag.
GROUNDMASS						
Plagioclase	42	42	0.1	An 65	Subhedral- euhedral	
Clinopyroxene	45	45				
Opakes	8	8	0.03		Skeletal- euhedral	
Mesostasis	<1	1				Commonly altered.
SECONDARY MINERALOGY						
Clays	PERCENT	REPLACING/ FILLING				COMMENTS
	<1	Mesostasis				Mesostasis altered to olive green clay with perceptible birefringence. Affects 75% of mesostasis within halo area. Bright red and transitional brown-orange types of alteration (Fe hydroxides) also present.

COMMENTS: Plag compositions determined using A-normal method.

THIN SECTION DESCRIPTION

109-648B-9R-1 (Piece 3, 17-22 cm)

ROCK NAME: Sparsely plagioclase olivine phyric basalt
WHERE SAMPLED: Unit 30, pillow or flow interior
TEXTURE: Variolitic with some intersertal and intergranular
GRAIN SIZE: Fine

PRIMARY MINERALOGY	PERCENT PRESENT	PERCENT ORIGINAL	SIZE RANGE (mm)	APPROX. COMPOSITION	MORPHOLOGY	COMMENTS
PHENOCRYSTS						
Olivine	<1	<1	0.15-0.30		Subhedral- euhedral	Rare trapped melt inclusions.
Plagioclase	1	1	0.10-1.50		Euhedral	
Spinel	Tr	Tr	0.06		Euhedral	Included in plag phenocrysts.
GROUNDMASS						
Plagioclase	46	46	<0.01-0.05			Elongate with hopper and swallowtail terminations.
Clinopyroxene	42	42	<0.01-0.05		Acicular, dendritic	Variolitic. Acicular. Intergrown with plag.
Opakes	5	5	≤0.01			Ulvospinel, ilmenite, sulfide.
Mesostasis	5	5				
VESICLES/ CAVITIES						
Vesicles	PERCENT	LOCATION	SIZE RANGE (mm)	FILLING	SHAPE	
	<1	With glomero- crysts	0.1-0.2	None	Round	

COMMENTS: Mesostasis consists of mixture of acicular plag, plumose cpx, glass and opakes.

THIN SECTION DESCRIPTION

109-648B-9R-1 (Piece 10, 69-71 cm)

ROCK NAME: Plagioclase olivine phyric basalt

WHERE SAMPLED: Unit 31, cut at shallow angle to halo.

TEXTURE: Variolitic/glomeroporphyritic, plumose-microlitic

GRAIN SIZE: Fine-medium

PRIMARY MINERALOGY	PERCENT PRESENT	PERCENT ORIGINAL	SIZE RANGE (mm)	APPROX. COMPOSITION	MORPHOLOGY	COMMENTS
PHENOCRYSTS						
Olivine	<1	<1	0.15-0.50		Subhedral	Occurs only in glomerocrysts. Fresh.
Plagioclase	2	2	0.50-3.00	An > 65	Subhedral-euhedral	Mostly as glomerocrysts. Fresh except as below. One large plag glomerocryst 4 mm across, with a small aggregate of olivines. Plag glomerocrysts otherwise olivine-free.
GROUNDMASS						
Plagioclase	35	35	0.5-3.0		Euhedral	Acicular to lath-shaped. Hollow and hopper types.
Clinopyroxene	19	19			Anhedral	Intergranular.
Plumose cpx	39	40	< 1 μ		Subhedral	Plumose aggregates of microlites.
Mesostasis	1	2			Anhedral	Clear, near colorless.
Ilmenite(?)	1	1	5 μ		Subhedral	Mainly occurs within plumose cpx, perpendicular to cpx.
Spinel/magnetite	1	1	5 μ		Euhedral	Mainly in non-plumose textured areas.
SECONDARY MINERALOGY						
Clays	<2	REPLACING/FILLING Mesostasis plumose cpx				COMMENTS Leading edge of dark halo shows alteration of mesostasis to olive-green clay (probably corresponds to thin dark line seen on dry sawn surfaces). Clay is non-birefringent. 2 mm from edge of halo, clay changes gradationally from olive-green through yellow-green to orange-yellow, birefringent clay over a distance of about 2 mm. (N.B., distances not perpendicular to halo boundary.) 3 mm further in, patches of monomineralic clay 0-2 mm across, replaces both mesostasis and plumose cpx. This sequence holds good for the half of the slide opposite the large plag glomerocryst. In the other half, alteration is generally of the olive-green clay type, interrupted by a crack, along which intense orange-yellow clay + darker brown to opaque Fe hydroxide alteration replaces mesostasis, cpx, and in the center of the zone, plag and parts of ol. This alteration passes out via yellow clay into olive-green clay replacing mesostasis only. Yellow clay infills fractures in the large plag glomerocryst.

VESICLES/CAVITIES	PERCENT	LOCATION	SIZE RANGE (mm)	FILLING	SHAPE	COMMENTS
Vesicles	7		0.1-2.0	Clay linings	Round	Vesicles were usually impregnated with resin before sectioning. Three types of vesicle linings: 1) Olive-green/brown clay lining. Non-birefringent. Occurs in two vesicles at/near edge of the slide near a large glomerocryst. Browner band overgrown by pale green band. Thickness 0.05 mm. 2) Simple yellow clay shows parallel and radiating growth structures. Thickness 0.01-0.08 mm, variable between vesicles. Some small vesicles are filled. 3) Celadonite/iron hydroxide linings. Shown by one large vesicle and one small one adjacent to a large glomerocryst. Sequence is (a) discontinuous thin lining of dark red to opaque "iron hydroxide" with some bulbous protrusions; (b) normal parallel to radiating yellow celadonite; (c) discontinuous layer of translucent isotropic "iron hydroxide". The colors of the clay components of the vesicle linings are the same as the clay replacing the adjacent groundmass mesostasis. Vesicle clays of types (1) and (2) occur within 1 mm of each other.

COMMENTS: Section is half altered, half fresh. Modal % estimated for fresh part.

THIN SECTION DESCRIPTION

109-648B-9R-1 (Piece 11, 80-82 cm)

ROCK NAME: Sparsely olivine plagioclase phyric basalt

WHERE SAMPLED: Unit 31, pillow or flow interior

TEXTURE: Intersertal to intergranular, variolitic

GRAIN SIZE: Fine

PRIMARY MINERALOGY	PERCENT PRESENT	PERCENT ORIGINAL	SIZE RANGE (mm)	APPROX. COMPOSITION	MORPHOLOGY	COMMENTS
PHENOCRYSTS						
Olivine	<1	<1	0.05-0.10		Subhedral	Fresh.
Plagioclase	<1	<1	0.40-1.40		Subhedral	Fresh.
GROUNDMASS						
Plagioclase	40	40	0.1-0.3		Elongate, hopper, swallowtail	
Clinopyroxene	47	47				Intergranular
Opaques	8	8	0.01-0.11		Anhedral-euhedral	Some skeletal crystals.
Mesostasis	4	4				
VESICLES/CAVITIES						
Vesicles	4	Even	0.5-2.5	None	Round	

THIN SECTION DESCRIPTION

109-648B-13R-1 (Piece 1, 0-3 cm)

ROCK NAME: Moderately plagioclase olivine phyric basalt

WHERE SAMPLED: Unit 32, pillow or flow interior

TEXTURE: Variolitic

GRAIN SIZE: Fine

PRIMARY MINERALOGY	PERCENT PRESENT	PERCENT ORIGINAL	SIZE RANGE (mm)	APPROX. COMPOSITION	MORPHOLOGY	COMMENTS
PHENOCRYSTS						
Olivine	1	1	0.1-0.5		Anhedral-euhedral	Some melt inclusions.
Plagioclase	3	3	0.5-1.4		Rounded, euhedral	Margins commonly fractured and/or embayed. Complex zoning patterns. Common intergrowths of two or more plag phenocrysts. Ol and plag phenocrysts form glomerocrysts.
GROUNDMASS						
Plagioclase	20	20	0.01-0.2		Acicular to tabular, hopper, swallowtail	
Mesostasis	76	76				Microcrystalline intergrowth of acicular plag microlites, dendritic cpx, small pools of reddish glass, and small granular opaque minerals. Opaques include ulvospinel, and ilmenite. Plumose pattern developed in mesostasis.
VESICLES/CAVITIES						
Vesicles	<1%	Even	0.2-0.5	Some glass	Round	May be partially to completely glass-filled. Mesostasis and plag microphenocrysts wrap around vesicles.

COMMENTS: Groundmass plag described above are microphenocrysts. These are significantly larger than the plag microlites in the mesostasis.

THIN SECTION DESCRIPTION

109-648B-13R-1 (Piece 2, 11-13 cm)

ROCK NAME: Moderately olivine plagioclase phyric basalt

WHERE SAMPLED: Unit 32, pillow or flow interior

TEXTURE: Intergranular, variolitic

GRAIN SIZE: Fine to medium

PRIMARY MINERALOGY	PERCENT PRESENT	PERCENT ORIGINAL	SIZE RANGE (mm)	APPROX. COMPOSITION	MORPHOLOGY	COMMENTS
PHENOCRYSTS						
Olivine	2	2	0.2-0.6		Anhedra-subhedra	Also skeletal and fresh crystals.
Plagioclase	2	2	0.4-1.2		Subhedra-euhedra	Some very irregular crystals with embayed and/or fractured margins. Zoning common. Occasional hopper crystals. Occasional intergrowths of two or more phenocrysts.
GROUNDMASS						
Plagioclase	40	40	0.04-0.25		Subhedra-euhedra	Common swallowtail. Some hopper.
Clinopyroxene	46	46			Elongate	Intergranular. Microcrystalline
Olivine	Tr	Tr				Sinuuous grains associated with plag glomerocrysts.
Opauques	10	10				
Mesostasis	Tr	Tr			Cryptocrystalline	
VESICLES/CAVITIES						
Vesicles	Tr	Even	0.04-0.20	None	Round	

THIN SECTION DESCRIPTION

109-648B-15R-1 (Piece 5, 33-37 cm)

ROCK NAME: Sparsely plagioclase olivine phyric basalt

WHERE SAMPLED: Unit 34, pillow or flow interior

TEXTURE: Variolitic, glomeroporphyritic

GRAIN SIZE: Microcrystalline

PRIMARY MINERALOGY	PERCENT PRESENT	PERCENT ORIGINAL	SIZE RANGE (mm)	APPROX. COMPOSITION	MORPHOLOGY	COMMENTS
PHENOCRYSTS						
Olivine	< 1	< 1	0.4-0.5		Subhedra-euhedra	
Plagioclase	1	1	0.5-1.5		Euhedra-subhedra	Some crystals are skeletal including cryptocrystalline materials.
GROUNDMASS						
Plagioclase	45	45	0.01-0.03		Elongated	Some crystals are skeletal.
Clinopyroxene (+ glass)	45	45	0.03 ≤ 2μ			Cryptocrystalline-microcrystalline. Forms variolitic texture with groundmass plag and opaques.
Opauques	8	8	1-3μ	Titano-magnetite, ilmenite	Euhedra-subhedra	
VESICLES/CAVITIES						
Vesicles	< 1	Even	0.5-1.2	None	Round	Partially coated by cryptocrystalline materials (originally glass).

THIN SECTION DESCRIPTION

109-648B-15R-1 (Piece 15, 111-113 cm)

ROCK NAME: Moderately plagioclase olivine phyric basalt

WHERE SAMPLED: Unit 35, pillow or flow interior

TEXTURE: Intergranular, variolitic

GRAIN SIZE: Fine

PRIMARY MINERALOGY	PERCENT PRESENT	PERCENT ORIGINAL	SIZE RANGE (mm)	APPROX. COMPOSITION	MORPHOLOGY	COMMENTS
PHENOCRYSTS						
Olivine	1	1	≈ 0.5		Round	Intergrown with plag in glomerocrysts Some glass inclusions (5 μ round blebs), crystallographically oriented parallel to plag crystal faces.
Plagioclase	3	3	1-2.5		Euhedral	
GROUNDMASS						
Plagioclase	46	46			Euhedral	Some hopper shaped crystals, intergrown with cpx. Internally skeletal to dendritic. Some radiate textures. Spinel, ilmenite, Fe sulfides. Spinel is euhedral to internally skeletal. Ilmenite is elongated. Fe sulfides occur as spheres. as spheres. Rare patches.
Pyroxene	44	44		Spinel, ilmenite, Fe sulfides	Euhedral	
Opaques	5	5				
Mesostasis	1	1				
VESICLES/CAVITIES						
VESICLES/CAVITIES	PERCENT	LOCATION	SIZE RANGE (mm)	FILLING	SHAPE	COMMENTS
Vesicles	5	Even		None	Round	Contain dark fine-grained partial linings. May be a filling by late stage residual liquid. In all vesicles, the partial lining is on the same side.

THIN SECTION DESCRIPTION

109-648B-15R-1 (Piece 16, 120-123 cm)

ROCK NAME: Sparse olivine plagioclase phyric basalt

WHERE SAMPLED: Unit 35, pillow or flow interior

TEXTURE: Intergranular, variolitic

GRAIN SIZE: Fine

PRIMARY MINERALOGY	PERCENT PRESENT	PERCENT ORIGINAL	SIZE RANGE (mm)	APPROX. COMPOSITION	MORPHOLOGY	COMMENTS
PHENOCRYSTS						
Olivine	<1	<1	0.2-0.3		Euhedral-subhedral	Some glass inclusions.
Plagioclase	<1	<1	0.8-1.0		Euhedral	Fractured margins. Concentric zoning.
GROUNDMASS						
Plagioclase	45	45	0.05-0.50		Subhedral-euhedral	Also acicular, hopper, and swallowtail crystal forms.
Clinopyroxene	48	48			Acicular, dendritic	
Olivine	1	1	0.04-0.08		Anhedral	Ulvospinel crystals are anhedral to euhedral. Ilmenite crystals are bladed.
Opaques	5	5	0.01-0.07	Ulvospinel, ilmenite		
VESICLES/CAVITIES						
VESICLES/CAVITIES	PERCENT	LOCATION	SIZE RANGE (mm)	FILLING	SHAPE	COMMENTS
Vesicles	5	Even	0.8-3.2	None	Round	Spinel(?) crystallized on the edge of one vesicle.

THIN SECTION DESCRIPTION

109-648B-16R-1 (Piece 1, 2-5 cm)

ROCK NAME: Moderately plagioclase olivine phyric basalt
WHERE SAMPLED: Unit 35, cut perpendicular to alteration halo
TEXTURE: Glomeroporphyritic, intersertal and intergranular
GRAIN SIZE: Fine-medium

PRIMARY MINERALOGY	PERCENT PRESENT	PERCENT ORIGINAL	SIZE RANGE (mm)	APPROX. COMPOSITION	MORPHOLOGY	COMMENTS
PHENOCRYSTS						
Olivine	1.5	1.5	0.1-0.6		Subhedral	Occur in ol-plag glomerocrysts. Resorption indicated by deep embayment of largest phenocryst, which also has numerous crystallographically oriented trapped melt inclusions. Most phenocrysts have ragged edges which are overgrown by optically continuous hollow plag (resembling groundmass plag).
Plagioclase	2	2	0.6-3.0	C = An > 65	Subhedral	
GROUNDMASS						
Plagioclase	33	33	0.1-1.0		Euhedral	Mainly hollow lath-shaped to acicular. Occurs as equant or prismatic grains in mesostasis, as radiating plumose aggregates (some intergrown with plag), or intergranular to plag.
Clinopyroxene	37	37	< 0.1			
Titanomagnetite	1	1	< 0.05		Euhedral-subhedral	Intersertal. Dark to opaque, with acicular opaques.
Mesostasis	24	25.5				
SECONDARY MINERALOGY						
Clays	1.5	REPLACING/FILLING				<p>Within the halo area, intersertal mesostasis is partially to completely replaced by yellow clay or orange-red Fe hydroxide. This alteration is confined to a few patches. Most of the mesostasis appears fresh but the pervasive yellowish-green tinge to the halo when viewed with the naked eye indicates that there is probably a more pervasive incipient alteration of the mesostasis which has no obvious optical manifestation.</p> <p>Two 0.1 mm fractures run through the halo area, subparallel to the halo boundary. There is a very incomplete filling of red Fe hydroxide in the longer fracture, and a more complete filling in the shorter fracture. Fe hydroxide replacing the mesostasis usually occurs near these fractures, as does much of the replaceive clay.</p>
		Mesostasis				
		Fracture filling				

VESICLES/CAVITIES	PERCENT	LOCATION	SIZE RANGE (mm)	FILLING	SHAPE	COMMENTS
Vesicles	10		0.3-3.0	± clay	Round	Vesicles generally empty. The two that are connected by the shorter fracture mentioned above, however are lined with Fe hydroxide, ± thin clay. Some plucking of vesicle linings from the section may have occurred. Three vesicles have a near-opaque glass lining on one side.

COMMENTS: Vesicle and phenocryst abundances visually estimated.

THIN SECTION DESCRIPTION

109-648B-16R-1 (Piece 5, 48-50 cm)

ROCK NAME: Moderately plagioclase olivine phyric basalt
WHERE SAMPLED: Unit 36, pillow or flow interior
TEXTURE: Intergranular
GRAIN SIZE: Fine-medium

PRIMARY MINERALOGY	PERCENT PRESENT	PERCENT ORIGINAL	SIZE RANGE (mm)	APPROX. COMPOSITION	MORPHOLOGY	COMMENTS
PHENOCRYSTS						
Olivine	2	2	0.05-0.07		Euhedral-anhedral	Forms glomerocrysts with plag. Various skeletal shapes.
Plagioclase	3	3	0.50-1.20		Euhedral-subhedral	Albite and carlsbad twinning. Well developed zoning at the outer margins of the grains.
GROUNDMASS						
Olivine	1	1	0.01-0.05		Euhedral-anhedral	Blade-like intergrowth with plag or isolated.
Plagioclase	55	55	0.01-0.30		Acicular, laths	Microlites with some hollow cores.
Clinopyroxene	31	31	0.05-0.30		Plumose	Prismatic in intergranular spaces.
Titanomagnetite	8	8	0.01-0.03		Anhedral-acicular	May be found as inclusions in plag crystals.
VESICLES/CAVITIES						
Vesicles	0.6		< 1	None	Round	

COMMENTS: Point count: 1000 points, 0.5 mm grid. Some glomerocrysts show a radial pattern. Generally, plag is the dominant phase in glomerocrysts, forming sub-ophitic-like intergrowths with or wrapping around ol grains.

THIN SECTION DESCRIPTION

109-648B-16R-1 (Piece 9, 88-90 cm)

ROCK NAME: Highly olivine plagioclase phyrlic basalt

WHERE SAMPLED: Unit 36, pillow or flow interior

TEXTURE: Intergranular, glomeroporphyritic

GRAIN SIZE: Fine-medium

PRIMARY MINERALOGY	PERCENT PRESENT	PERCENT ORIGINAL	SIZE RANGE (mm)	APPROX. COMPOSITION	MORPHOLOGY	COMMENTS
PHENOCRYSTS						
Olivine	5	5	0.1-0.8	Fo 79	Anhedra-subhedra	Occurs mostly in plag-olivine glomerocrysts. Melt inclusions.
Plagioclase	5	5	0.4-1.4		Euhedral	Common embayed and fractured margins. Complex zoning patterns. Common intergrowths between two or more plag crystals. Melt inclusions.
GROUNDMASS						
Plagioclase	35	35	0.01-0.20		Subhedra-euhedra	Hopper and swallowtail forms also present.
Clinopyroxene	46	46			Acicular, dendritic	
Opaques	8	8	0.04-0.08	Ilmenite, magnetite	Anhedra-euhedra	
Olivine	1	1			Anhedra-subhedra	

VESICLES/CAVITIES	PERCENT	LOCATION	SIZE RANGE (mm)	FILLING	SHAPE
Vesicles	< 1	Even	0.2-0.6	None	Round

COMMENTS: Plag has seriate grain size distribution. Range of grain sizes quoted above for "groundmass" plag includes both small, acicular plag in groundmass, and larger plag microphenocrysts. Ol composition determined by XRD.

THIN SECTION DESCRIPTION

109-648B-17R-1 (Piece 5, 22-24 cm)

ROCK NAME: Moderately plagioclase olivine phyrlic basalt

WHERE SAMPLED: Unit 38, pillow or flow interior

TEXTURE: Intergranular, glomeroporphyritic

GRAIN SIZE: Fine

PRIMARY MINERALOGY	PERCENT PRESENT	PERCENT ORIGINAL	SIZE RANGE (mm)	APPROX. COMPOSITION	MORPHOLOGY	COMMENTS
PHENOCRYSTS						
Olivine	2	2	0.1-0.4	Fo 80	Subhedra-anhedra	In glomerocrysts with plag.
Plagioclase	4	4	0.2-1.0	C = An 60 R = An 75	Euhedral	Core and rim compositions were taken on two separate crystals. Complex zoning. Fractured margins. Discrete crystals and glomerocrysts.
GROUNDMASS						
Plagioclase	42	42	0.02-0.15		Subhedra-euhedra	Also acicular, swallowtail, and hopper forms present.
Clinopyroxene	46	46			Dendritic, bladed	Cpx is intergranular to plag laths.
Olivine	1	1	0.05		Anhedra	
Opaques	5	5	0.01-0.02	Titanomagnetite, ilmenite, sulfides	Anhedra-euhedra	Titanomagnetite is euhedral, skeletal. Ilmenite is bladed, lath-like. Sulfides are bleb-like.

THIN SECTION DESCRIPTION

109-648B-18R-1 (Piece 1A, 0-2 cm)

ROCK NAME: Sparsely plagioclase olivine phyric basalt
 WHERE SAMPLED: Unit 40, alteration halo
 TEXTURE: Seriate, sub-ophitic
 GRAIN SIZE: Medium

PRIMARY MINERALOGY	PERCENT PRESENT	PERCENT ORIGINAL	SIZE RANGE (mm)	APPROX. COMPOSITION	MORPHOLOGY	COMMENTS
PHENOCRYSTS						
Olivine	0.5	0.5	0.5-1.0		Equant, anhedral	In poorly defined glomerocrysts.
Plagioclase	1	1	1.0-3.0		Subhedral	Six crystals are large enough to be called phenocrysts. Various crystals have different features, listed below. 1) Inclusion-free, almost unzoned core. Normally zoned rim with intricate intergrowth with groundmass sized cpx, ol, and mesostasis. 2) Similar to (1), but lacking distinct zonation. 3) Composite crystal: rounded, almost unzoned plag and small anhedral olivine enclosed in unzoned core. Ol inclusion acts as a nucleus for one of several aggregates of quenched-looking ol(?) growths. 4) Elongate, weakly zoned, with abundant cpx, magnetite, and mesostasis inclusions oriented parallel to length. 5) Elongate, zoned glomerocrysts with few inclusions. (two examples.)
GROUNDMASS						
Olivine	5	5	0.2-1.5		Anhedral	Equant to sub-poikilitic, elongated parallel to C axis.
Plagioclase	47.5	54	0.1-2.0		Subhedral	
Clinopyroxene	26	30	0.1-2.0		Anhedral	Equant intergrowths or sub-poikilitic.
Titanomagnetite	12	12	0.02-0.10		Euhedral, skeletal	
Mesostasis	8	8				Intersertal, partially crystallized.

SECONDARY MINERALOGY

COMMENTS

Alteration minerals, from edge of halo inward toward site of fracture:
 1) Small amounts of olive-green, low-birefringent clay. Partially replaces mesostasis, with an associated more general brown discoloration of the mesostasis.
 2) A variety of yellow to orange birefringent clays. Commonly forms fringes on scarce vesicles, replacing mesostasis. Also fills microfractures. Associated red-orange, non-birefringent "Fe hydroxide" ± birefringent clay forms globular masses up to 0.2 mm (gives gray reflective polished surface) and irregular replacements of mesostasis.
 3) A zone at least 2-3 mm wide along the edge of the section nearest the fracture has relatively little distinctive alteration material (very sparse, mainly Fe hydroxide). Reflected light shows that the mesostasis is in fact pervasively altered to a soft (hydrated) material.

VESICLES/CAVITIES	PERCENT	LOCATION	SIZE RANGE (mm)	FILLING	SHAPE
Vesicles	<0.5		<0.2	Clay linings	Round

COMMENTS:

Interesting groundmass textures:
 1) Elongate ol in optical continuity extend for up to 3 mm parallel to the c-axis, forming sub-poikilitic relationship to plag. Locally overgrown by intergranular cpx in near optical continuity with ol. Similar elongate ol extends in continuity from the 1 mm equant ol phenocryst, with rods of the same crystal extending 0.1 mm into enclosing cpx and plag (cpx is not in optical relation to ol). Some of oikocrysts partially enclose and interpenetrate a plag lath oriented parallel to the c-axis of ol. More equant, sub-poikilitic to intergranular ol is common in the vicinity of the 1-mm sized ol phenocryst.
 2) "Bow-tie" structures: rare occurrence defined by intersecting plag laths and by a gap in plag enclosed in ol oikocryst.
 3) Rare hollow subhedral olivine crystals enclosing plag and mesostasis.

THIN SECTION DESCRIPTION

109-648B-18R-1 (Piece 2, 38-40 cm)

ROCK NAME: Sparsely plagioclase olivine phyric basalt

WHERE SAMPLED: Unit 40, pillow or flow interior

TEXTURE: Intergranular, intersertal, hypocrySTALLINE

GRAIN SIZE: Fine

PRIMARY MINERALOGY	PERCENT PRESENT	PERCENT ORIGINAL	SIZE RANGE (mm)	APPROX. COMPOSITION	MORPHOLOGY	COMMENTS
PHENOCRYSTS						
Olivine	<1	<1	0.1-0.6		AnhedraL-subhedraL	
Plagioclase	1	1	0.8-1.0		EuhedraL-subhedraL	Complex zoning. Embayed margins.
GROUNDMASS						
Plagioclase	43	43	0.01-0.04		SubhedraL-euhedraL	Tabular.
Clinopyroxene	40	40	0.02-0.20		AnhedraL	Most anhedraL. Intergranular. Some bladed, dendritic.
Olivine	5	5	0.03-0.08		AnhedraL	
Glass	3	3				Brown patches 0.03-0.05 mm. Fills interstice between plag laths.
Opagues	7	7	0.02-0.20	Magnetite, ilmenite, sulfides		Magnetite, subhedraL. Ilmenite, bladed. Sulfide, blebs.
Spinel	<<1	<<1	0.05		EuhedraL	

COMMENTS: Needles of plag and cpx are enclosed in pools of glass.

THIN SECTION DESCRIPTION

109-648B-19R-1 (Piece 26, 13-15 cm)

ROCK NAME: Sparsely plagioclase olivine phyric basalt

WHERE SAMPLED: Unit 40, pillow or flow interior

TEXTURE: Intergranular

GRAIN SIZE: Fine

PRIMARY MINERALOGY	PERCENT PRESENT	PERCENT ORIGINAL	SIZE RANGE (mm)	APPROX. COMPOSITION	MORPHOLOGY	COMMENTS
PHENOCRYSTS						
Olivine	<1	<1	<0.5		Rounded, skeletal	
Plagioclase	1	1	2.0-4.0			≈ 1 mm wide perpendicular to (010).
GROUNDMASS						
Plagioclase	44	44	0.02-0.10		Tabular, euhedraL-subhedraL	Grains measured perpendicular to (010).
Clinopyroxene	50	50	0.02-0.10		Acicular	Measurements represent needle widths.
Mesostasis	1	1				
Opagues	3	3				
Olivine	<1	<1	0.10		Equant	

COMMENTS: Point count: 1000 points, 0.5 mm grid.

THIN SECTION DESCRIPTION

109-648B-20R-1 (Piece 6, 48-50 cm)

ROCK NAME: Sparsely plagioclase olivine phyric basalt

WHERE SAMPLED: Unit 41, pillow or flow interior

TEXTURE: Trachytic, pilotaxitic

GRAIN SIZE: Fine

PRIMARY MINERALOGY	PERCENT PRESENT	PERCENT ORIGINAL	SIZE RANGE (mm)	APPROX. COMPOSITION	MORPHOLOGY	COMMENTS
PHENOCRYSTS						
Olivine	< 1	< 1	0.1-0.3		Subhedral-anhedral	In glomerocrysts with plag.
Plagioclase	1	1	0.2-1.0		Euhedral	Some skeletal with embayed margins and cracks. Some plag has oscillatory or sweeping extinction.
GROUNDMASS						
Plagioclase	45	45	0.01-0.07		Elongate,	Length:width = 1:10 to 1:40. Subparallel alignment.
Clinopyroxene	20	20	< 4 μ		acicular	Comb-like needles.
Olivine	1	1	0.01-0.04		dendritic	Some hollow, swallowtail.
Mesostasis	33	33			Anhedral-euhedral	Consists of microcrystalline to cryptocrystalline mixture of plag, cpx, opaques and minor glass.